https://ntrs.nasa.gov/search.jsp?R=19650023155 2020-03-17T00:56:21+00:00Z

FACILITY FORM 602

N65-32756
(ACCESSION NUMBER)

(THRU)

252
(PAGES)

1
(CODE)

CR 64465
(NASA CR OR TMX OR AD NUMBER)

33
(CATEGORY)

HEAT TRANSFER CHARACTERISTICS OF BOILING NEON AND NITROGEN IN NARROW ANNULI

FINAL REPORT

February 1965

National Aeronautics and Space Administration
Lewis Research Center
Cleveland, Ohio

Prepared under Contract No. NASr-107 by
Air Products and Chemicals, Inc., Allentown, Pennsylvania,
A. Lapin and H. Totten, Authors

GPO PRICE $

CSFTI PRICE(S) $

Hard copy (HC) 6.00

Microfiche (MF) 1.50

ff 653 July 65

HEAT TRANSFER CHARACTERISTICS OF BOILING NEON AND NITROGEN IN NARROW ANNULI

FINAL REPORT

February 1965

National Aeronautics and Space Administration
Lewis Research Center
Cleveland, Ohio

Prepared under Contract No. NASr-107 by
Air Products and Chemicals, Inc., Allentown, Pennsylvania,
A. Lapin and H. Totten, Authors

FOREWORD

This report was prepared by Air Products and Chemicals, Inc. under NASA Contract NASr-107.

This report covers work conducted from April 1962 to September 1963 in the R&D Laboratory in Emmaus, Pennsylvania.

The report is issued in accordance to Article V, Paragraph (d) of the contract dated April 1, 1962 and Revision 1 dated January 6, 1965.

The work performed under this contract was the basis of a Doctoral Dissertation presented to the Graduate Faculty of Lehigh University by A. Lapin in September 1963.

The authors wish to thank the following individuals whose help and advice made the successful completion of the contract possible: Dr. J. M. Geist; Dr. C. McKinley; Prof. L. Wenzel, Chairman Chemical Engineering Department, Lehigh University; Messrs. L. Binder, G. Freeby, A. Palencar, J. Simpson; Mrs. J. Meagher and Mrs. K. David; and Mr. F. Kocon.

TABLE OF CONTENTS

Page

I ABSTRACT 1

II INTRODUCTION 3

III LITERATURE 5

- General Description of Boiling 5
- Literature Surveys 8
- Nucleate Boiling 9
- Film Boiling 11
- Specialized Studies 13
  - Effect of Pressure 13
  - Effect of Forced Circulation 14
  - Boiling Burnout 14
  - Boiling Studies for Oxygen and Nitrogen 15
  - Effect of Material and Surface Roughness on Nucleate Boiling 16
  - Effect of Active Sites on Nucleate Boiling 19
  - Heat Transfer to Boiling Liquids Flowing in Narrow Channels 20

IV THEORY OF BOILING 24

- Rohsenow's Theory 27
- Forster and Zuber's Theory 30
- McNelly's Correlation 35
- Levy's Generalized Equation 36

Cryder and Gilliland's Generalized Equation 38

Hughmark's Statistical Approach 38

Chen's Theory of Additive Mechanisms 39

Sydoriak and Roberts' Derivation for Boiling N_2 and H_2 in Narrow Channels 41

V EXPERIMENTAL INVESTIGATION 42

Apparatus for Cryogenic Confined Space Boiling 42

Introduction 42

Experimental Test Section 42

Geometric Configuration Considerations in Design of Test Section 43

Thermodynamic and Hydrodynamic Considerations in Design of Test Section 45

Experimental Data Collection Consideration in Test Section Design 49

Composite Design, Fabrication and Assembly of Test Section 60

Auxiliary Equipment 62

Experimental Procedure 64

Liquid Nitrogen Boiling Study 64

Liquid Neon Boiling Study 66

Experimental Data 67

Experimental Observations 98

VI TREATMENT OF EXPERIMENTAL DATA 106

Pool Boiling 106

Annular Gap Boiling 106

Experimental Data - Run A-6-5 111

Gap Size 111

Heat Input 112

Wetted Area 112

Heat Flux 112

Overall Temperature Driving Force 113

Boiling Temperature Driving Force 113

Boiling Heat Transfer Coefficient 122

Nitrogen Boil-Off 123

Annular Gap Flow Area 123

Mass Velocity 126

Equivalent Diameter 126

Nusselt Number 126

Reynolds Number 126

Length to Diameter Ratio 126

VII RESULTS AND DISCUSSION 128

Nitrogen Pool Boiling 128

Neon Pool Boiling 146

Annular Gap Boiling - Nitrogen and Neon 149

1. Surface Roughness and Finish 199
2. Back Pressure Created by Rotameter 200
3. Entrainment 200
4. Length to Diameter Ratio 201
5. Comparison Between Neon and Nitrogen Boiling 202

6. Maximum Heat Flux 202

7. Evaluation of the Sydoriak and Roberts Equation 203

VIII CONCLUSIONS 205

IX NOMENCLATURE 207

X BIBLIOGRAPHY 216

XI APPENDIXES 222

A. Calculation of Neon Boil-Off Rate for Preliminary Design of Test Section 223

B. Calculation for Invar Pressure Vessel in Test Section Design 225

C. Calculations for OFHC Copper Pressure Vessels in Test Section 227

D. Calculation of Contraction Characteristic of Test Section Materials 229

E. Test Section Auxiliary Equipment 234

F. Examination of Test Heater Surfaces 237

LIST OF FIGURES

Figure No.	Title	Page
1	Variation of Heat Flux with Temperature Difference	6
2	Effect of Roughness on Temperature Driving Force to Support a Coefficient of 1000	18
3	The Six Steps of Boiling	25
4	Picture of Heater Components	50
5	Picture of Assembled Heater	51
6	Picture of Assembled Test Section	51
7	Sketch of Assembled Test Section	52
8	Schematic Diagram of Test Section	53
9	Wiring Diagram of Thermocouples	56
10	Wiring Diagram of Electric Heating Element	57
11	Picture of Dewars' Assembly	63
12	Picture of Gas Recovery Bag	63
13	Heater Pressure Versus Temperature Difference for Neon and Nitrogen Filled Heaters (psi vs. ^{o}F)	114
14	Heater Pressure Versus Temperature Difference (for neon filled heaters, "Hg vs. ^{o}F)	115
15	Heater Pressure Versus Temperature Difference (for nitrogen filled heaters, "Hg vs. ^{o}F)	116
16	EMF Versus Temperature Difference for Copper-Constantan Thermocouples (0-28°F)	118
17	EMF Versus Temperature Difference for Copper-Constantan Thermocouples (24-48°F)	119
18	Typical Heater Wall Temperature Boiling Driving Force Profile	120

Figure No.	Title	Page
19	Comparison Between Measured and Calculated Nitrogen Boil-Off	125
20	Heat Flux Versus Temperature Driving Force Nitrogen Pool Boiling, Copper Heater 12b	137
21	Heat Flux Versus Temperature Driving Force Nitrogen Pool Boiling, Copper Heater 6	138
22	Heat Flux Versus Temperature Driving Force Nitrogen Pool Boiling, Ni Plated Copper Heater 9	139
23	Heat Flux Versus Temperature Driving Force Nitrogen Pool Boiling, Cd Plated Copper Heater 10	140
24	Heat Flux Versus Temperature Driving Force Nitrogen Pool Boiling, Copper Heater 7b	141
25	Heat Flux Versus Temperature Driving Force Nitrogen Pool Boiling, Copper Heater 8	142
26	Heat Flux Versus Temperature Driving Force Nitrogen Pool Boiling, Comparison Between All Heaters at 7 1/2-Inch Submergence	143
26a	Nitrogen Pool Boiling Full Submergence	147
26b	Nitrogen Pool Boiling Half Submergence	148
27	Heat Flux Versus Temperature Driving Force Nitrogen Annular Gap Boiling, Copper Heater 12b	173
28	Heat Flux Versus Temperature Driving Force Nitrogen Annular Gap Boiling, Copper Heater 6	174
29	Heat Flux Versus Temperature Driving Force Nitrogen Annular Gap Boiling, Nickel Plated Copper Heater 9	175
30	Heat Flux Versus Temperature Driving Force Nitrogen Annular Gap Boiling, Cadmium Plated Copper Heater 10	176
31	Heat Flux Versus Temperature Driving Force Nitrogen Annular Gap Boiling, Copper Heater 7b	177

Figure No.	Title	Page
32	Heat Flux Versus Temperature Driving Force Nitrogen Annular Gap Boiling, Copper Heater 8	178
33	Heat Flux Versus Temperature Driving Force Nitrogen Annular Gap Boiling, Comparison Between All Heaters	179
34	Comparison Between Neon and Nitrogen Pool Boiling Heat Flux Versus Overall Temperature Driving Force, Heater 12b	180
35	Heat Flux Versus Temperature Driving Force Neon Annular Gap Boiling, Copper Heater 12b	181
36	Heat Flux Versus Temperature Driving Force Neon Annular Gap Boiling, Copper Heater 6	182
37	Heat Flux Versus Temperature Driving Force Neon Annular Gap Boiling, Nickel Plated Copper Heater 9	183
38	Heat Flux Versus Temperature Driving Force Neon Annular Gap Boiling, Copper Heater 7b	184
39	Heat Flux Versus Temperature Driving Force Neon Annular Gap Boiling, Copper Heater 8	185
40	Heat Flux Versus Temperature Driving Force Neon Annular Gap Boiling, Comparison Between All Heaters	186
41	Nusselt Number Versus Reynolds Number Nitrogen Annular Gap Boiling, Copper Heater 12b, 6 Mil Gap	187
42	Nusselt Number Versus Reynolds Number Nitrogen Annular Gap Boiling, Copper Heater 6, 20 Mil Gap	188
43	Nusselt Number Versus Reynolds Number Nitrogen Annular Gap Boiling, Nickel Plated Copper Heater 9, 21 Mil Gap	189
44	Nusselt Number Versus Reynolds Number Nitrogen Annular Gap Boiling, Cadmium Plated Copper Heater 10, 22 Mil Gap	190
45	Nusselt Number Versus Reynolds Number Nitrogen Annular Gap Boiling, Copper Heater 7b, 53 Mil Gap	191

Figure No.	Title	Page
46	Nusselt Number Versus Reynolds Number Nitrogen Annular Gap Boiling, Copper Heater 8, 80 Mil Gap	192
47	Nusselt Number Versus Reynolds Number Neon Annular Gap Boiling, Copper Heater 12b, 6 Mil Gap	193
48	Nusselt Number Versus Reynolds Number Neon Annular Gap Boiling, Copper Heater 6, 20 Mil Gap	194
49	Nusselt Number Versus Reynolds Number Neon Annular Gap Boiling, Nickel Plated Copper Heater 9, 21 Mil Gap	195
50	Nusselt Number Versus Reynolds Number Neon Annular Gap Boiling Copper Heater 7b, 53 Mil Gap	196
51	Nusselt Number Versus Reynolds Number Neon Annular Gap Boiling, Copper Heater 8, 80 Mil Gap	197
52	Comparison Between Measured and Calculated Nusselt Number for All Neon and Nitrogen Annular Flow Boiling Data	198
D1	Coefficient of Linear Thermal Expansion for Copper and Pyrex	231

LIST OF TABLES

Table No.	Title	Page
I	Characteristic Dimensions of Test Sections	68
II	Properties of Nitrogen	70
III	Properties of Neon	71
IV through IX	Experimental Temperature Data - Nitrogen Pool Boiling, Heaters 12b, 6, 9, 10, 7b, and 8 respectively	72 through 78
X through XV	Experimental Temperature Data - Nitrogen Annular Gap Boiling, 0.006, 0.020, 0.021, 0.022, 0.053 and 0.080 inch gaps respectively	79 through 91
XVI through XX	Experimental Temperature Data, Neon Annular Gap Boiling, 0.006, 0.020, 0.021, 0.053, and 0.080 inch gaps respectively	92 through 96
XXI	Experimental Data, Neon Pool Boiling, Heater 12b	97
XXII	Comparison Between Calculated and Measured Nitrogen Boil-Off	124
XXIII	Calculation Constants for Nitrogen Runs	127
XXIV	Calculation Constants for Neon Runs	127
XXV through XXX	Calculated Data - Nitrogen Pool Boiling, Heaters 12b, 6, 9, 10, 7b, and 8 respectively	129 through 136
XXXI	Correlation for Nitrogen Pool Boiling	144
XXXII	Comparison Between Nitrogen and Neon Pool Boiling	148
XXXIII through XXXVIII	Calculated Data - Nitrogen Annular Gap Boiling 0.006, 0.020, 0.021, 0.022, 0.053, and 0.080 inch gaps respectively	150 through 167
XXXIX through XLIII	Calculated Data - Neon Annular Gap Boiling 0.006, 0.020, 0.021, 0.053, and 0.080 inch gaps respectively	168 through 172
XLIV	Evaluation of Sydoriak and Roberts Equation	204

I. ABSTRACT

The purpose of this investigation was to determine the boiling characteristics of liquid nitrogen and neon in narrow annuli.

The basic concept for the experimental study consisted of three major parts.

1. Design and construction of test equipment consisting of the main test section and auxiliary equipment. The design of the test section incorporated the capability of visual observation of the boiling mechanism during operation.
2. Experimental evaluation of the test heaters under pool boiling conditions in order to establish a basis for the evaluation of the annular gap boiling.
3. Investigation of boiling characteristics in narrow annuli.

The test section consisted of precision machined heaters having different diameters, which were centered in a precision Pyrex pipe. The gap between the Pyrex sleeve and the heater ranged in size between 0.006-inches and 0.080-inches at liquid nitrogen and neon temperatures.

The nitrogen pool boiling data were correlated by $Q/A_w = 87.2\ (\Delta T_b)^{1.20}$ with an average percent deviation of ±16%, except for the cadmium plated heater. $Q/A_w = 30.0\ (\Delta T_b)^{1.20}$ correlated the data obtained with the cadmium plated heater.

Observation of the annular gap boiling suggested a convective type heat transfer. A generalized equation was thus derived on the basis of this observation.

The data obtained with nitrogen and neon in the six annuli, with varying submergences, were correlated with an average percent deviation of ±23% by the following equation:

$$\frac{h_b D_e}{k_L} = 150 \left(\frac{D_e G}{\mu_L}\right)^{0.18} \left(\frac{L}{D_e}\right)^{-0.82} \left(\frac{Cp_L \mu_L}{k_L}\right)^{0.95}$$

The ability of this equation to correlate data obtained under a wide range of operating conditions covering: gap size range of 0.006 inch to 0.080 inch ; length to equivalent diameter ratio of about 310 to 10; copper, nickel plated and cadmium plated surfaces; and two fluids substantiates the assumptions made in deriving the equation.

Visual observation of both pool boiling and annular gap boiling with neon and nitrogen, showed several types of behavior which were observed by other investigators. These consisted of patch-by-patch boiling, nuclei sites remaining active even with decreasing heat flux, superheating of the surface resulting in sudden explosive boiling with generation of active sites covering the whole surface.

Maximum heat fluxes resulting from gap size limitation were obtained in only four cases: with nitrogen in a 6 mil gap heater, and with neon in 6, 20, and 21 mil gap heaters.

II. INTRODUCTION

Magnets with field strength of the order of 10^5 oersteds or higher are required for research in such areas as controlled nuclear fusion and high energy nuclear physics. The field strength of an electromagnet depends upon its configuration and the current flowing in the coil, which in turn depends upon the voltage applied to the coil, the geometry of the coil, and the resistivity of the coil material. Compactness and lowest possible resistivity are necessary to obtain very high field strengths.

Many pure materials have very low resistivities at low temperatures. It is possible to incorporate this property in the design of compact high field magnets. Several cryogenically cooled magnets have been designed to optimize energy consumption and instantaneous power demand.

The optimum operating temperature for cryogenically cooled magnets depends upon conductor material, field strength, refrigeration efficiency, and magnet design. For example, optimum operating temperatures are about 30°K for copper and about 10°K for sodium.

Magnets may be maintained at their desired temperatures by removing the required energy input as sensible heat in a fluid or as latent heat. Air, water, or kerosene are used for magnets operating at ambient temperatures. Removal of the heat generated in cryogenic magnets by means of a boiling liquid offers two major advantages over the use of a fluid utilizing sensible heat transfer: (1) a lower temperature difference can be maintained between the boiling liquid and the magnet surface, and (2) a much smaller volume of coolant is required.

At 30°K the only fluid refrigerants are helium, hydrogen and neon. Hydrogen and neon are more suitable from the heat transfer point of view, but safety considerations preclude the use of liquid hydrogen until more operating experience with cryomagnets is obtained. Other refrigerants are available for operation at higher cryogenic temperatures. Some cryogenically cooled magnets have been operated at 78°K by using liquid nitrogen as a coolant.

In general, information on boiling heat transfer in narrow annuli is scarce and is almost completely lacking in the case of cryogenic fluids. Since the mechanical design of magnets includes narrow annuli and confined spaces between conductors, it is necessary to develop the necessary design information concerning the cooling characteristics under such conditions.

This research study was undertaken to investigate the various factors affecting the boiling performance of neon and nitrogen in narrow annuli.

III. LITERATURE

The technical literature contains many studies and analyses of heat transfer to boiling liquids.

General Description of Boiling

General descriptions of the various types of boiling are given in textbooks such as McAdams - Heat Transmission (47), and in papers by Asch (4), Kutateladze (38) and (39) and many others.

Boiling involves change of phase from liquid to vapor and usually depends on some form of natural circulation to replenish the vaporized liquid in the vicinity of the heating surface. As early as 1756 Leidenfrost (44) and in 1888 Lang (40) recognized the existence of minimum and maximum heat flux in a boiling liquid. It was Nukiyama (53), however, as late as 1934, who discussed and identified several regimes of boiling, which depend upon different heat transfer mechanisms.

Although there are serious inconsistencies in boiling data which are difficult to explain, the general features and characteristics of the different types of boiling are well known. If boiling data are represented by the logarithm of the heat flux as a function of the logarithm of the temperature difference between the heating surface and the bulk of the liquid, a general type of curve is obtained. The general shape of this curve (Figure 1) is characteristic of boiling for all liquids, although the numerical values of the heat flux or temperature difference

FIGURE I , VARIATION OF HEAT FLUX WITH TEMPERATURE DIFFERENCE

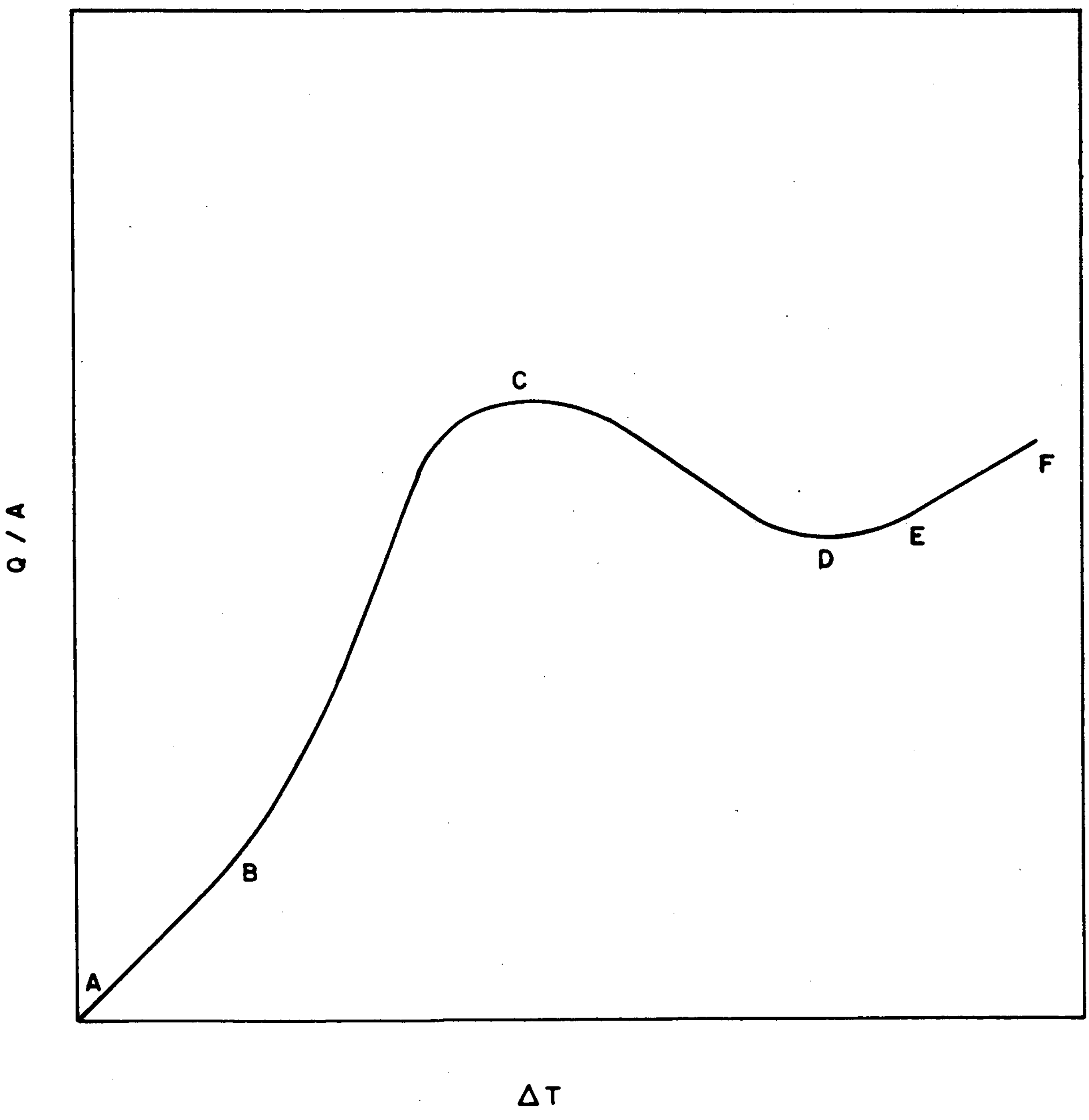

differs from system to system. It is possible to identify several boiling regions in Figure 1. For instance, the first part of the curve AB represents the natural convection heat transfer for the liquid. In this zone the liquid is superheated and evaporation occurs only at the free surface. In the region BC bubbles are generated on the heated surface and rise to the surface. This bubble movement through the pool of liquid sets up natural circulation currents. In this range, called nucleate boiling, the heat flux, q/A varies as the temperature driving force, ΔT to the nth power where n varies from system to system. Bubbles are generated as the result of irregularities in the surface where small quantities of trapped liquid act as nuclei for the bubbles. The heat flux reaches a maximum or peak heat flux at the point C on the curve of Figure 1 and the temperature driving force corresponding to this maximum is called the critical ΔT.

As the temperature driving force increases beyond the critical ΔT, the liquid vaporizes rapidly and in many places. A vapor blanket covers the surface which leads to the reduction of heat flux, to point D on the curve. This boiling region is very unstable and is referred to as the transition regime. This region is limited by a maximum, the maximum heat flux C, and a minimum, D, called the Leidenfrost point. These two critical points represent the conditions at which nucleate boiling ceases and at which destruction of the vapor film takes place. For example, if the temperature driving force rises beyond that of the maximum heat flux, the heat flux is lowered and the vapor film tends to decrease for a while. It is possible to have both nucleate and film boiling alternately on the same surface. The continuous shifting from nucleate to film boiling is the main reason for instability.

At high temperature differences, EF, film boiling is obtained in which heat is transferred through the vapor film by conduction and radiation. At point F the driving force ΔT is such that the temperature at the surface of the metal corresponds to the metal melting point and any tendency of further increase in driving force results in the metal "burning out."

Literature Surveys

Comprehensive surveys of heat transfer to boiling cryogenic liquids have been presented by several authors such as Class, et.al. (11), Richards, et.al (61), and Drayer and Timmerhaus (18). Class briefly examined the work of Haselden and Peters (29), Weil and Lacaze (67 and 68) as well as of many other authors. Most of the review relates to cryogenic fluids. The conclusions reached by Class are that:

> "The results of the several investigators do not agree, there being as much as twenty-fold variations in the value of heat flux for a given value of temperature difference. The theoretical curves are bracketed by the experimental data in the nucleate boiling range. In the film boiling range, the theoretical curve for one atmosphere was made to agree with the experimental curve by selection of the proper value for the constant. In neither case is the theory sufficiently well developed to justify its use in the absence of adequate supporting experimental data."

Richards, et.al. reviewed 156 references on heat transfer from solid surfaces to fluids, and related phenomena. They present the heat transfer data obtained from experimental work on cryogenic fluids in graphical form and compare the theoretical equations to the experimental data. The formulations are also presented graphically to permit comparison with the results of the experimental work. In this case, again, the literature survey is limited to the cryogenic fluids. Richards conclusions are quite similar to the ones reached by Class. These are as follows:

a. "The existing experimental data on heat transfer between solid surfaces and cryogenic liquids (helium, hydrogen, nitrogen, and oxygen) vary appreciably between experimenters, even when heater geometries and orientations, pressures, etc. are comparable. The variations are both in the magnitude of the heat flux and in the shape of the heat-flux-versus-temperature-difference curves, and are possibly due to uncontrolled parameters such as surface roughness and contamination.

b. Existing theoretical and empirical formulations are in qualitative agreement with some of the experimental data. More carefully controlled experiments are needed, and formulations which account for parameters such as surface condition should be developed."

Nucleate Boiling

Forster, Kurt, and Greif (20), Forster and Zuber (21), Zuber (70), Zuber and Fried (71, 72), Rohsenow (62, 63, Reeber (59), and Drayer and Timmerhaus (18) studied the nucleate boiling region. Zuber and Rohsenow presented several general equations to cover nucleate boiling while Drayer and Timmerhaus, and Reeber offered experimental data for hydrogen boiling and helium boiling respectively.

Zuber and Fried (72) conclude that

> "The proposed correlations for nucleate pool boiling do not take into account the conditions of the heating surface. Consequently, these equations are not general and cannot predict the heat transfer rates for any solid-liquid combination.
>
> For a 'smooth' surface and for a given solid-liquid combination, the equation proposed by Rohsenow can be used for predicting the heat transfer rates to liquid hydrogen at various pressures when the value of a constant is determined from one set of experimental conditions. An equally satisfactory agreement was obtained using the equation proposed by Labountzov."

Drayer and Timmerhaus established that the Forster and Zuber equation

$$\frac{Q/A}{(T_w - T_l)k} \left[\left(\frac{\Delta T\, c_p \rho_L (\pi \alpha)^{1/2}}{L \rho_V} \right) \left(\frac{2\sigma}{\Delta P} \right)^{1/2} \left(\frac{\rho_L}{\Delta P} \right)^{1/4} \right] =$$

$$\left[\frac{\rho_L}{\mu} \left(\frac{\Delta T\, c_p\, \rho_L\, (\pi \alpha)^{1/2}}{L_V} \right)^2 \right]^m \left[\frac{c_p}{k} \right] \qquad (1)$$

agrees within 12% with their data on hydrogen boiling with a temperature driving force of 1.17°F. The agreement is poorer at lower values of ΔT_b.

Reeber measured the coefficient of heat transfer between a smooth vertical silver surface and boiling liquid helium to be about 388 Btu/hr-ft^2-°F for a temperature difference of 0.040°K at the 4.0°K level. He determined that the heat transfer rate for pool boiling decreases with decreasing temperature between 4.0° and 2.5°K in proportion to the latent heat of vaporization and inversely as the molar volume of the vapor at the pressure and temperature of the experiment. He also states that the heat transfer curves in the boiling range have a definite hysteritic nature. This suggests a nucleation mechanism which is dependent on the thermal history of the surface. It can be explained by associating an activation energy with initiation of a nucleation site. Once a site is activated, it remains active even if the heat flow is decreased below the one required to initiate it.

Film Boiling

Film boiling has received much less attention than pool boiling in theoretical treatment and experimental work. Bromley (7) was the first to present a formal equation on film boiling in 1950. His theory is based on the following assumptions:

"(1) The liquid is separated from the hot tube by a continuous vapor blanket.
(2) Heat travels through vapor film by conduction and radiation.
(3) Vapor rises under the action of buoyant forces.
(4) Vapor-liquid interface is smooth in that section of tube where most of the heat is transferred.
(5) Rise of the vapor is retarded by the viscous drag on the tube and more or less on the liquid.
(6) Latent heat of vaporization is the major item in the heat supplied to the vapor film.
(7) The kinetic energy of vapor in film is negligible.
(8) Vapor-liquid interface is smooth and continuous and is not affected by a variation in the vapor-liquid interfacial tension.
(9) It is permissible to use an average value for the temperature difference between the hot tube and the boiling liquid and treat it as a constant value around the tube in the integrations. This approach to the problem is essentially that used by Nusselt for condenser problems....

(10) The boiling liquid is at its boiling point at the vapor-liquid interface.
(11) For engineering calculations it will be satisfactory to evaluate all physical properties of the vapor at the arithmetic average temperature of the hot surface and the boiling liquid.
(12) The combined effect of most of the errors in the foregoing assumptions may be corrected by evaluating a suitable 'constant' factor to be determined from the experimental data."

The derived equation is:

$$h_{co} = (\text{constant}) \left[\frac{k^2 \rho (\rho_L - \rho)\, g\, \lambda'\, C_p}{D\, \Delta t\, Pr} \right]^{1/4} \qquad (2)$$

where the constant should theoretically have the value 0.512 if the liquid surrounding the tube is assumed stagnant and 0.724 if the liquid moves completely freely with the vapor.

Corrections, for the kinetic energy of the vapor in the film, and for radiation, should be made if either effect is appreciable.

Hanson and Richards (28) investigated heat transfer coefficients for large Δ t's measured for a stainless steel surface in a liquid nitrogen bath. They correlated their experimental data in the Δt range of 36° to 540°F, to within 5% by the following equation:

$$h = 5120\ \Delta t^{-0.583}\ \text{Btu/hr-ft}^2\text{-}^\circ\text{F}. \qquad (3)$$

They found that measurements were difficult to make for Δt smaller than 110°F, as the tube would tend to wet and return to nucleate boiling.

Hendricks, et.al. (32) established that heat transfer in the convective film boiling regime for liquid hydrogen, can be predicted by correlating the ratio of experimental to predicted Nusselt numbers with the Martinelli two-phase parameter:

$$\left(\frac{Nu_{calc.}}{Nu_{exp.}}\right)_f = 0.611 + 1.93\,\chi_{tt,f} \qquad (4)$$

Specialized Studies

Many of the investigators restricted their work to some specific aspect of nucleate boiling behavior. The following is a brief summary of their conclusions.

Effect of Pressure

Weil and Lacaze (67 and 68) observed in their nucleate boiling experiments with nitrogen at 120 and 755 mm. Hg that the heat flux at the higher pressure was about 2 times greater than the one at the lower pressure. Similarly, Cichelli and Bonilla (8) found that the coefficient of heat transfer in nucleate boiling continues to rise as the pressure is increased. The boiling surface usually becomes vapor bound near the critical pressure, and nucleate boiling ceases to be stable. They reached their conclusion from studies with water, ethanol, benzene, propane, normal pentane, normal hexane, 50 mol% water-ethanol, and 33-67% propane-pentane mixtures, at pressures ranging from atmospheric pressure to the vicinity of the critical pressure of the system.

Effect of Forced Circulation

Schweppe and Foust (65) measured boiling-film heat-transfer coefficients for streams of boiling water at incipient boiling conditions in about a 10-inch section of three different diameters. Their results indicate an influence of agitation even with increasing velocity up to the highest velocity measured in the test which was approximately 40 ft/sec. Their conclusion is that the boiling-film heat-transfer coefficient increases with an increase in ΔT even at high velocities.

Boiling Burnout

It was stated earlier that burnout occurs whenever the ΔT is large enough so that the melting point of the surface is reached. This point is represented by point F on Figure 1. A change of regime from nucleate to film boiling in any boiler, will result in a sudden sharp increase in ΔT. The abrupt rise in temperature may be sufficient to melt the boiler material. The understanding of boiling burnout is therefore of great industrial interest. Gambill (23) made a thorough survey of this phenomenon. He considers eight possible conditions for regimes of burnout; subcooled and saturated liquid conditions for each one of the following: unconfined natural convection, confined natural convection, forced convection in axial flow, and forced convection with swirl flow. He reviews the various factors affecting burnout and suggests several correlations for burnout prediction. He states however, "it is apparent that a considerable amount of work remains to be done in this area before good predictions for the general case can be made."

Boiling Studies for Oxygen and Nitrogen

Many studies of the boiling behavior of liquid oxygen and nitrogen have been made in the past twenty to thirty years, probably many more than for any one of the other cryogenic fluids. This is probably because of the importance of these two liquids in air separation processes, and because of their extensive use industrially and in military applications. In general these studies were made under conditions similar to the ones found in air separation plants and related applications. Guter (27), Haselden and Peters (29), Haselden and Prosad (30), Monroe, Bristow and Newell (51) have studied heat transfer to boiling liquid oxygen and nitrogen. In general, they have considered the effect of such factors as non-condensible, tube diameter, length to diameter ratio, and pressure effect on boiling coefficients. The experimental technique generally consisted of a boiling-condensing system. Overall and individual heat transfer coefficients were measured and usually reported in graph form.

Ruzicka (64) obtained data for heat transfer to boiling nitrogen by means of electric resistance heating. He derived the following equations for nucleate boiling on the surface of a copper tube, and platinum and copper wires:

$$Nu = 0.1292 \, Pr^{-0.45} \left[\frac{(\gamma' - \gamma'')\delta^2 p'}{\gamma' \, \sigma'} \right]^{0.63} \left[\frac{\gamma' \, c_p \, \sigma'}{(\gamma' - \gamma'') \, \gamma'' \, r p' \delta} \right]^{1/3} \qquad (5)$$

or $$\alpha = 0.00701 \left[\frac{\lambda^{0.82}\, \gamma^{1/3}\, (\gamma' - \gamma'')^{0.0365}\, q^{0.63}}{C_p^{0.117}\, \eta^{0.45}\, b^{1/3}\, (r\gamma'')^{0.036}\, T_s^{0.297}} \right] \text{k-cal/m}^2\text{-hr-}^\circ\text{C} \qquad (6)$$

Effect of Material and Surface Roughness on Nucleate Boiling

Since it was postulated that surface irregularities where small quantities of trapped liquid act as nuclei for the build-up of bubbles, it is reasonable to postulate that the surface material and roughness have a pronounced effect on boiling behavior. Berenson (5) studied the characteristics of pool boiling for n-pentane at atmospheric pressure as a function of surface roughness, material, and cleanliness. He has shown that changes in surface roughness can result in variations of 500 to 600% in nucleate boiling heat transfer coefficient but that surface roughness has no effect on film boiling coefficient. This is reasonable since a vapor blanket completely covers the wall in film boiling and therefore the hot surface has no direct contact with the liquid. He has also concluded that the maximum nucleate boiling burn-out heat flux is essentially independent of surface material, roughness and cleanliness. Berenson listed the effects of the surface material on the nucleate boiling coefficients and has shown that the temperature difference required to produce a given heat flux for the same surface-finishing technique depends on the surface material. This may be explained by the fact that differences in surface hardness may result in surface irregularities and cavity sizes which would differ even though the surface received the same finishing treatment. It is also possible that the thermal conductivity of the material has a direct effect on nucleate boiling performance. Corty and Foust (13) studied the effect of micro-roughness of a surface on the ΔT necessary to sustain nucleate boiling at a given heat flux. Figure 2 represents their results which indicates the effect of micro-roughness in the range of 0 to 24 micro inch RMS on ΔT. It can be seen from this curve that the lower the roughness, the higher the ΔT required to maintain the same heat flux. They also showed that the position of boiling curves (h versus ΔT) and their slopes vary with roughness.

Cryder and Finalborgo (14) studied the effect of metal surfaces on boiling liquids such as water, methanol, CCl_4, n-butanol, kerosene and other systems. They found that the boiling coefficients decreased when the tubes were allowed to remain in the boiling liquid even though the character of the metal surface did not appear to have changed. Danilova and Belsky (16) obtained experimental heat transfer coefficients for boiling refrigerant 22 using nickel and brass tubes. They determined that the coefficients of heat transfer were different for the nickel and brass tubes especially at the low heat loads. This difference was caused by the greater roughness of the brass tube surface. Their experimental data fit the equations of Kutateladze and Kruzhilina well, except for the coefficients which differ from those recommended by the authors of the two equations. Equations 7 and 8 are the Kutateladze equation with a modified coefficient to fit the experimental data.

$$Nu = 0.25 \times 10^{-2} (Re)^{0.75} (Pr)^{0.35} K_p^{0.65} \text{ for nickel tubes} \quad (7)$$

and $$Nu = 0.46 \times 10^{-2} (Re)^{0.70} (Pr)^{0.35} K_p^{0.65} \text{ for brass tubes} \quad (8)$$

FIGURE 2, EFFECT OF ROUGHNESS ON TEMPERATURE DRIVING FORCE TO SUPPORT A COEFFICIENT OF 1000

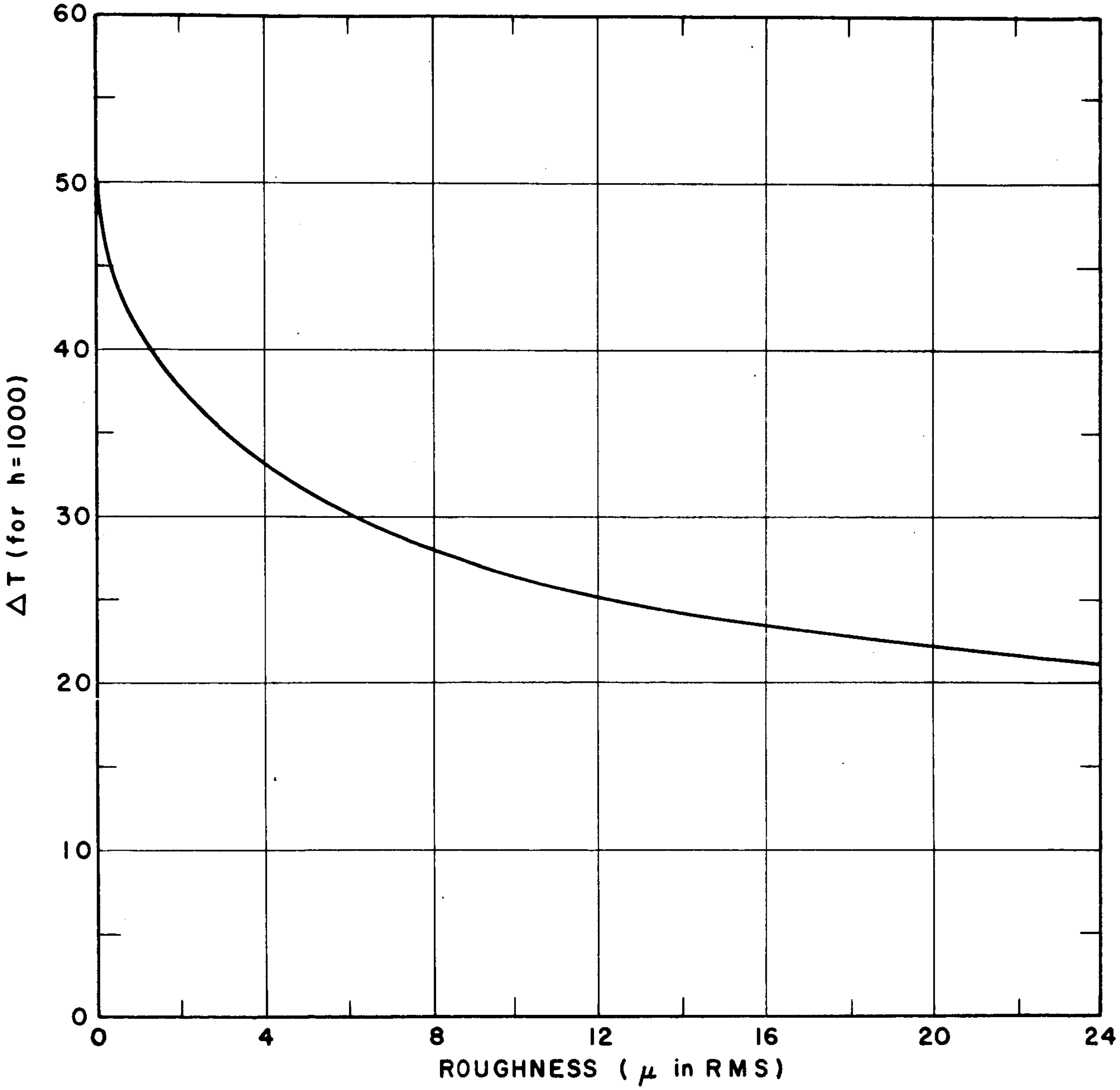

Equation 9 is the Kruzhilina equation similarly modified to fit the data.

$$Nu = 0.194\ (Re)^{0.70}\ (Pr)^{0.25}\ K_t^{\ 0.367} \text{ for the nickel tube} \qquad (9)$$

Since it is extremely difficult to duplicate surface finish, it is believed that the effect of surface on boiling is the main factor causing the very large variations in the experimentally obtained boiling heat transfer coefficients. Even though experimental conditions were described as "identical", undetected differences in surface finish may have been sufficiently large to have an appreciable effect on the boiling behavior.

Effect of Active Sites on Nucleate Boiling

The distribution of active sites on the surface is an important factor in determining the thermodynamic and hydrodynamic characteristics of nucleate boiling. Gaertner (22) treats statistically the subject of distribution of active sites. He determined that the local density of nucleation sites for boiling water containing dissolved metal salts at heat fluxes of 200,000; 294,000; and 317,000 Btu/hr-ft^2 fit a Poisson distribution quite well. The fraction of the surface having a local active site population N in the local area a is given by the equation:

$$Pu_{(Na)} = \frac{e^{-\overline{N}a}\ (\overline{N}a)^{Na}}{(Na)\ !} \qquad (10)$$

He has also established from cursory examination of published data for five liquids boiling from three different surfaces, that the nucleation of active sites depends on surface temperature in accordance with the equation:

$$\overline{N} = N_o \exp \left\{ - \left[\frac{16 \pi \sigma^3 M^2 N^*}{3 \rho_L^2 R^3 \ln \frac{P_\infty}{P_v}^2} \right] \phi \left(\frac{1}{T_w^3} \right) \right\} = N_o e^{-K/T_w^3} \tag{11}$$

The author also offers an explanation for the patch-by-patch boiling which has been observed by many experimenters. The patch-by-patch boiling is the apparent tendency of nucleation sites to cluster on the heat transfer surface. An increase in the surface temperature results in a larger number and size of active site patches. This phenomenon was also observed in the present nitrogen and neon boiling study. Corty and Foust (13) advanced two theories to explain how patch-by-patch boiling can occur. The first one postulates that oscillations and pressure surges created by bubbles growing at an active site may increase the supersaturation at neighboring potential active site cavities on the surface thereby creating new centers for nucleation. The second theory suggests that bubbles from one original site expand and fill many adjacent cavities which were previously wetted with vapor. These cavities will then create new centers for nucleation causing a patch of bubbles to form in the vicinity of the parent active site.

Heat Transfer to Boiling Liquids Flowing in Narrow Channels

The study of heat transfer to boiling liquids flowing in narrow channels is limited. Neusen, Kangas and Sher (52) studied heat transfer and pressure drop for superheated steam flowing in thin annular passages at 600 psia. The test section consisted of annuli formed by an 0.878-inch OD tube inside of an 0.997-inch ID tube, giving a gap of 59.5 mils. The authors determined that the Heineman's correlation of Nusselt number for L/De greater than 60 correlated their data for superheated steam in the thin annulus with both walls heated. Heineman derived the following correlation:

$$Nu_f = 0.0133\ (Re_f)^{0.84}\ (Pr_f)^{1/3} \text{ for } L/De \geqslant 60 \tag{12}$$

when he investigated short round tubes and rectangular channels having an equivalent diameter of 0.332 inch and 0.091 inch respectively at high pressures and temperatures.

Polomik, Levy and Sawochka (56) investigated the heat transfer coefficients at elevated pressures for annular flow with water boiling to 100% quality. The study was made in a 0.625-inch OD tube with two annuli 0.060 inch and 0.120 inch. The surface finish of their stainless steel surface was 50 micro-inches or better. The experimental data were correlated within ±20% by using a Colburn type equation modified by steam quality and steam void groupings. The correlation applied only to the film boiling data. The authors however, discussed the three boiling regimes:

a. Nucleate boiling

b. Transition region

c. Film boiling region

The data obtained in the nucleate boiling region and transition zone were not correlated but are tabulated in their paper.

Kapinos and Nikitenko (37) correlated the data obtained in their study of heat transfer in channels by means of an equation of the type Nu = f (Re). They modified the characteristic length of both the Nusselt and Reynolds number by the introduction of a size factor correction.

Only two references related to the investigation of cryogenic fluids boiling in narrow passages were found. The first one by Sydoriak and Roberts (66) determined experimentally the critical heat input to liquid hydrogen and nitrogen boiling in an annular gap. They derived the following equation:

$$Q = AL \left(\rho_{v_2} \rho_L Z_e \, g \, f_2 \right)^{1/2} \tag{13}$$

on the assumption of a homogeneous and frictionless two-phase flow. This work was duplicated by Richards, Robbins, Jacobs and Holten (60). The heat transfer test section which was identical to the one used by Sydoriak and Roberts simulated the design of an electromagnet operable at a low temperature of 20°K. It consisted of a 7-inch long stainless steel plug which was accurately centered in a 5-inch long stainless steel tube. Various sizes of plugs were used in order to obtain different size annular spaces in the test section. Gap sizes between 7 and 20 mils were tested. The authors concluded that a prediction of the maximum operating power of an electromagnet by theoretical analysis is not reliable at this time. The ratio of Q observed to Q calculated by the Sydoriak-Roberts correlation varied from 1 to 1.8 for the hydrogen runs and from 1.3 to 2.4 for the nitrogen runs.

IV. THEORY OF BOILING

Heat transfer in nucleate boiling is a combination of liquid free convection and agitation caused by the bubble movement in the liquid. The mechanism of nucleate boiling is therefore dependent on the generation of small bubbles on the heated surface. At a given temperature the vapor pressure from a very small concave liquid surface is less than the vapor pressure from a flat liquid surface. Hence, for a given pressure, a liquid must be hotter to evaporate into a small bubble of vapor than into the vapor space above the liquid. The relationship between the two pressures, that is, the vapor pressure inside the bubble and the vapor pressure of the free liquid is as follows:

$$P_c = P_s - \frac{2\sigma}{R} \tag{14}$$

where P_c is the pressure inside the bubble, P_s is the saturation pressure of the liquid, σ is the surface tension of the liquid and R is the radius of the bubble (11).

The six steps sketched in Figure 3 can explain the mechanism of bubble formation which is a major factor in nucleate boiling.

Step 1. Heat is transferred from the hot surface to the surrounding liquid through a thin film and superheats it.

Step 2. As a result of the superheat, several small bubbles form in the hot surface defects such as crevices.

FIGURE 3, THE SIX STEPS OF BOILING

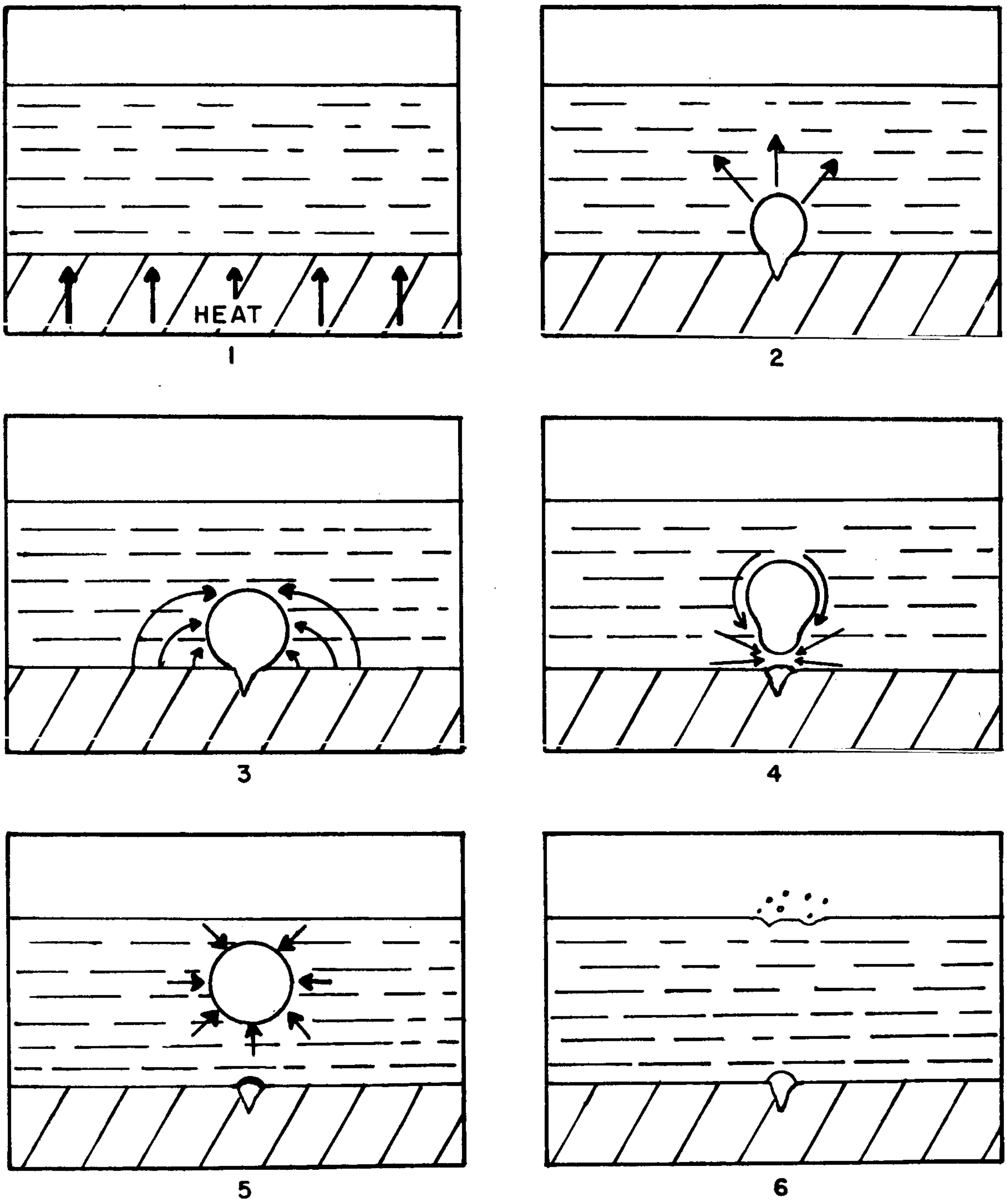
HEAT
1
2
3
4
5
6

Step 3. Heat transferred to the attached bubbles through the liquid causes the superheated liquid to flash at the vapor-liquid interface which results in a gradual growth of the bubbles.

Step 4. Upon reaching a certain size, the bubbles break away from the surface and disturb the surrounding film of superheated liquid.

Step 5. The freed bubbles continue to grow as they rise through the bulk of the liquid.

Step 6. Fresh liquid rushes into the newly vacated nucleation sites on the heating surface. These sites, having been blanketed by the vapor of the previous bubbles, are slightly overheated. New bubbles are generated and the cycle repeated.

The bubbles break away from the heated surface, when they reach a characteristic diameter D_h. The escape of the bubbles is governed by the dynamics of the surrounding liquid as well as by the buoyant and adhesion forces of the bubble.

Since nucleate boiling is a combination of free convection, bubble formation, and behavior in liquid, the various theoretical and empirical approaches to the study of boiling covered several methods such as empirical correlations, dimensional analysis, study of bubbles, study of surfaces, statistical analysis, etc.

In most of the nucleate boiling studies, it was assumed that heat flows from the hot surface into the liquid and from the liquid to the vapor bubbles, the controlling resistance to heat transfer being a stagnant film around the vapor bubbles.

Rohsenow's Theory

Rohsenow (62) assumed that the movement of the bubbles at the instant of break-off from the hot surface is the major factor in providing good agitation to the liquid and therefore improving the convection currents and decreasing the resistance of the stagnant film through which the heat must flow. The form of his equation was influenced by the traditional equation for non-boiling liquids.

This equation

$$Nu = \alpha (Re)^a (Pr)^b \tag{15}$$

is obtained from dimensional analysis and has its coefficient and exponents established by correlating experimental data. Rohsenow modified this equation for boiling. The Reynolds number was taken to be the Reynolds number of a bubble just after breaking away from the hot solid surface. Previous workers found experimentally that the velocity of a released bubble is constant for a short time. Furthermore the following relation between the frequency of emission of bubbles and diameter has also been established:

$$f D_b = C_1 \tag{16}$$

A correlation for the average diameter of a bubble at the instant of break-off derived by others, is also used by Rohsenow for his correlation.

$$D_b = C_2 \beta \left[\frac{2 g_o \sigma}{g (\rho_L - \rho_V)} \right]^{1/2} \tag{17}$$

And now assuming that the bubbles are spheres leaving the solid from n points per unit area the estimated bubble velocity becomes

$$V = f n \pi D_b^3/6 \tag{18}$$

and the bubble Reynold number is then

$$Re = \frac{D_b V \rho_L}{\mu_L} = \frac{C_3 \beta f n \rho_L D_b^3}{\mu_L} \left[\frac{2 g_o \sigma}{g (\rho_L - \rho_V)} \right]^{1/2} \tag{19}$$

Using the relationship that the product of the mass of vapor formed per unit time and the latent heat of vaporization must equal the heat transfer rate

$$q = w \lambda \tag{20}$$

the bubble diameter can be eliminated from the Reynolds number which becomes

$$Re = \frac{C_4 \beta q/A}{\mu_L \lambda} \left[\frac{g_o \sigma}{g (\rho_L - \rho_V)} \right]^{1/2} \tag{21}$$

The Nusselt number is treated in a similar manner, that is, the characteristic length D is replaced by the bubble diameter D_b and

$$Nu = \frac{h\ D_b}{k_L} \tag{22}$$

In substituting the experimental expression for the bubble diameter, the modified Nusselt number becomes

$$Nu = \frac{h\beta}{k_L}\left[\frac{g_o\ \sigma}{g\ (\rho_L - \rho_V)}\right]^{1/2} \tag{23}$$

Since it was assumed that the heat is transferred from the surface of the bubble through a stagnant film of liquid, the Prandtl number is based on liquid properties.

$$Pr_L = \frac{C_L\,\mu_L}{k_L} \tag{24}$$

Rohsenow's final correlation becomes

$$Nu = \text{const.}\ (Re)^{2/3}\ (Pr_L)^{-0.7} \tag{25}$$

or

$$\frac{h\beta}{k_L}\left[\frac{g_o\ \sigma}{g\ (\rho_L - \rho_V)}\right]^{1/2} = \text{const.}\left[\left(\frac{\beta q/A}{\mu_L \lambda}\right)\left(\frac{g_o\,\sigma}{g\ (\rho_L - \rho_V)}\right)^{1/2}\right]^{2/3} \times \left[\frac{C_L\,\mu_L}{k_L}\right]^{-0.7} \tag{26}$$

The coefficient and the two exponents of the equation were obtained experimentally from data of five systems. The exponents were quite constant for all the experimental data tested however the coefficient varied from 0.006 to 0.015 from system to system. Arithmetic modification of the Nusselt form equation results in the new equation relating the heat transfer coefficient of boiling to the temperature driving force and the physical properties of the liquid as follows:

$$h = \text{const.} \; \frac{(\Delta T)^2 \, k_L^{5.1} \, g^{1/2} \, (\rho_L - \rho_V)^{1/2}}{\beta \, \sigma^{1/2} \, C_L^{2.1} \, \lambda^2 \, \mu_L^{4.1}} \tag{27}$$

Forster and Zuber's Theory

Forster and Zuber (21) also approached the problem of nucleate boiling theoretically. They assumed that the movement of well developed bubbles is of little importance in nucleate boiling. The important movement is imagined to be that of the vapor-liquid interface of a growing bubble while the bubble is still attached to the surface. Westwater (69) compares the two approaches of Rohsenow and Forster and Zuber and points out that the linear velocity of the Forster-Zuber interface is much greater than the velocity described by Rohsenow. For example, values of 10 ft/sec were obtained for the Forster-Zuber model as compared with 0.3 ft/sec for Rohsenow small bubbles.

The starting point for the Forster-Zuber theory is the Rayleigh equation for a bubble growing in a liquid medium.

$$R \, \frac{d^2 R}{d \, \theta^2} + \frac{3}{2} \left(\frac{d \, R}{d \, \theta} \right)^2 + \frac{2 \sigma}{\rho_L \, R} = \frac{p_V - p_\infty}{\rho_L} \tag{28}$$

In this case it is assumed that the bubble is spherical, the liquid is incompressible, the viscosity effects are negligible and that the Joule-

Thomson equation is applicable during the growth period (time from the appearance of a nucleus of size R_o, $R_o = 2\sigma/(p_V - p_\infty)$ to some later time). It is possible to obtain a theoretical expression for a vapor growing in a superheated liquid, by combining **Equation** (28) with the Clausius-Clapeyron equation which relates vapor pressure to temperature. The basic Clausius-Clapeyron equation

$$\frac{d\,P_V}{d\,T} = \frac{L}{T \Delta V} \qquad (29)$$

can be approximated as follows:

$$\frac{d\,P_V}{d\,T} = \frac{L\,P_V}{R\,T^2} \qquad (30)$$

The derived equation which is a second order differential equation, is so complex that it has a very limited usefulness. It becomes enormously simpler if the inertia of the liquid can be ignored during bubble growth. Forster and Zuber discuss this point and define the physical requirements for neglecting inertia of a liquid. These are that either the bubble must be very small or the temperature of the bubble must be nearly equal to the saturation temperature. Both requirements are met in boiling at different times, the first one when the bubble is first growing from the nucleus and the second one when the bubble becomes large. For intermediate conditions it is assumed that both requirements are met in part and that the liquid inertia is negligible for these cases also. The growing bubble equation becomes

$$r + \ln\left(\frac{r - 1}{r_1 - 1}\right) = \frac{\Delta T\, C_L\, \rho_L \sqrt{\pi \alpha_L \theta}}{\lambda\, \rho_V\, R_o} \qquad (31)$$

In this equation θ is the time for the bubble to grow from radius R_1 to R_2. The symbol r is the generalized dimensionless radius = R/R_o. The temperature of a bubble growing in a superheated liquid is a function of the bubble size and assuming liquid inertia to be negligible the Forster-Zuber derivation gives the following expression.

$$\frac{T_o - T_v}{T_o - T_\infty} = 1 - \frac{R_o}{R} \qquad (32)$$

This equation states that as a bubble grows from a nucleus to double the radius of a nucleus it will lose 1/2 its temperature of superheat. After the bubble has grown by several orders of magnitude it will have practically no superheat and will be at the saturation temperature. Differentiation of Equation (31) results in an equation giving the velocity of the wall of a growing bubble. The logarithmic term of the equation 31 can be neglected since a growing bubble is considerably larger than a nucleus during most of its life and the following wall radial velocity is obtained.

$$\frac{d\,R}{d\,\theta} = \frac{\Delta T\, C_L\, \rho_L}{2\lambda\rho_V} \left(\frac{\pi \alpha_L}{\theta}\right)^{1/2} \qquad (33)$$

It is seen that the radial velocity is directly proportional to the temperature driving force and inversely proportional to the square root of the elapsed time of growth. It is also noted that the bubble radius is proportional to the temperature driving force and to the direct square root of the time. This results in an independence of time for the product of the bubble radius and its radial velocity

$$R \frac{d\,R}{d\,\theta} = \left[\frac{C_L \, \rho_L \, \Delta T \, \sqrt{\pi \alpha_L}}{\lambda \rho_V} \right]^2 \tag{34}$$

The meaning of this equation is that small bubbles grow rapidly and large ones grow slowly but that the agitation in the surrounding liquid caused by the growth of either bubbles remains uniform.

The correlation derived by Forster and Zuber is also in the form of the Nusselt equation

$$Nu = \text{const.} \; (Re)^a \; (Pr)^b \tag{35}$$

where the Reynolds number is based on the bubble radius and is defined as follows:

$$Re = \frac{R \, (dR/d\theta) \, \rho_L}{\mu_L} = \frac{\rho_L}{\mu_L} \left[\frac{C_L \, \rho_L \, \Delta T \, \sqrt{\pi \alpha_L}}{\lambda \, \rho_V} \right]^2 \tag{36}$$

and the Nusselt number as follows:

$$Nu = \frac{R \; q/A}{k \, \Delta T} \tag{37}$$

Since the bubble radius is usually not known it is convenient to eliminate it by solving for its value in the equation describing bubble dynamics:

$$R = \left(\frac{C_L \rho_L \Delta T \sqrt{\pi \alpha_L}}{\lambda p_V}\right)\left(\frac{2\sigma}{p_V - p_\infty}\right)^{1/2}\left(\frac{\rho_L}{p_V - p_\infty}\right)^{1/4} \qquad (38)$$

The final Forster-Zuber correlation is

$$Nu = 0.0015\ (Re)^{0.62}\ (Pr)^{1/3} \qquad (39)$$

or
$$\left(\frac{C_L \rho_L \sqrt{\pi \alpha_L}\ q/A}{k_L \lambda \rho_V}\right)\left(\frac{2\sigma}{\Delta p}\right)^{1/2}\left(\frac{\rho_L}{\Delta p}\right)^{1/4} = 0.0015\left[\frac{\rho_L}{\mu_L}\left(\frac{C_L \rho_L \Delta T \sqrt{\pi \alpha_L}}{\lambda \rho_V}\right)^2\right]^{0.62} \times \left[\frac{C_L \mu_L}{k_L}\right]^{1/3} \qquad (40)$$

This equation can be written to show the dependence of the heat transfer coefficient on the other variables:

$$h = 0.0012\ \frac{(\Delta T)^{0.24}\ (p_V - p_\infty)^{0.75}\ k_L^{0.79}\ C_L^{0.45}\ \rho_L^{0.49}}{\sigma^{0.5}\ \lambda^{0.24}\ \mu_L^{0.29}\ \rho_V^{0.24}} \qquad (41)$$

A comparison between the Forster-Zuber and Rohsenow equations, Equations (40) and (26) respectively, shows that the Reynolds number is raised to about the same exponent in both cases but that the exponent for the Prandtl number varies greatly.

It should be noted however that the Reynolds numbers in both expressions are completely different both in meaning and in numerical values.

Furthermore a comparison between the Equations (27) and (41) shows that the prediction of the effects of variables on h is quite different for both equations, even though both are derived from theories which are based on the assumptions of single bubble formations departing from the heated surface. Zuber (70) also considers other models of boiling in which bubbles leave the hot surface either in conjunction with several other bubbles or in columns. The analysis for each case requires basic modifications to the derivations based on the single bubble concept.

McNelly's Correlation

Several semi-empirical and empirical correlations have also been derived to describe nucleate boiling. McNelly (49) offers the following equation to cover the entire range of nucleate boiling.

$$\frac{h_b\, d}{k} = 0.225 \left(\frac{C\mu}{k}\right)^{0.69} \left(\frac{H\, d}{L\mu}\right)^{0.69} \left(\frac{\rho d}{\sigma}\right)^{0.31} \left(\frac{\rho_L}{\rho_V} - 1\right)^{0.31} \qquad (42)$$

This equation similarly to the ones obtained by Rohsenow, and Forster and Zuber is based on the assumption that the main transfer resistance is in the thin liquid layer adjacent to the heat surface. Turbulence in the liquid layer is caused by the rapid formation of vapor bubbles. The dimensionless terms of Equation (42) were obtained by dimensional analysis. The constant and the exponents of the equation have been calculated from data obtained with different configurations of heating surfaces. These configurations have been found to have no effect on heat transfer coefficients so long as the bubble formation was not upset by external agitation or by confined space. The author points out that the condition of the heating surface has a great influence on bubble generation and therefore on the overall rate of heat transfer. McNelly uses available boiling data to test the validity of his equation and to establish the constant and exponents. He explains the importance of the surface by pointing out that the pressure difference to initiate a bubble in a very still liquid will be infinite as per Lord Kelvin equation

$$\pi r^2 P = 2 \pi r \sigma \tag{43}$$

and therefore a considerable amount of superheat must be attained before boiling commences. However, if small crevices and irregularities appear on the surface they will promote bubble formation and therefore will have an important effect on the boiling performance.

Levy's Generalized Equation

Levy (45) offers the following generalized equation to describe surface boiling.

$$\frac{Q}{A} = \frac{k_L C_L \rho_L^2}{\sigma T_s (\rho_L - \rho_V)} \frac{1}{B_L} (\Delta T)^3 \tag{44}$$

The starting point for the derivation of this equation is the original equations of Forster and Zuber describing bubble growth.

$$R_i = \frac{2 \sigma T_s (\rho_L - \rho_V)}{\rho_V \rho_L h_{f_g} (T_w - T_s)} \tag{45}$$

and

$$\frac{d\,R}{d\,t} = \frac{(T - T_s)^2 \, C_L^{\,2} \, \rho_L^{\,2} \, \pi \, \alpha}{R \, h_{f_g}^{\,2} \, \rho_V^{\,2}} \tag{46}$$

Equation 46 can be rewritten to give the rate of heat transfer from the liquid to the bubble per unit bubble area.

$$\frac{q_b}{A_b} = h_{f_g} \, \rho_V \, \frac{d\,R}{d\,t} = \frac{(T - T_s)^2 \, C_L \, \rho_L \, \pi \, k_L}{R \, h_{f_g} \, \rho_V} \tag{47}$$

All the heat transferred at the heated surface must be carried by the bubbles as they reach their maximum size R_s,

$$Q = n \, f \, \frac{4}{3} \, \pi \, R_s^{\,3} \, h_{f_g} \, A \, \rho_V \tag{48}$$

The heat carried by bubbles of radius R is

$$Q_b = n \, f \, \frac{4}{3} \, \pi R^3 \, \rho_V \, A \, h_{f_g} \tag{49}$$

By putting $T = T_w$, $q_b/Q_b = 1$, $A_b = A_{b,i}$, $R = R_i$, combining Equations (47), (48), and (49), and substituting the original bubble Equation (45), the following equation is obtained

$$\frac{Q}{A} = \frac{k_L \, C_L \, \rho_L^{\,2}}{\sigma T_s \, (\rho_L - \rho_V)} \; \frac{\pi}{2} \left(\frac{R_s}{R_i}\right)^3 \frac{A_{b,i}}{A} \, (T_w - T_s)^3 \tag{50}$$

which can be simplified to the following form

$$\frac{Q}{A} = \frac{k_L \, C_L \, \rho_L^{\,2}}{\sigma T_s \, (\rho_L - \rho_V)} \; \frac{1}{B_L} \, (\Delta T)^3 \tag{51}$$

It should be noted that

$$\frac{Q}{A} = \frac{1}{B_L} \frac{q_b}{A_b} \tag{52}$$

and that according to Rohsenow, and Forster and Zuber, Q/A is proportional to q_b/A_b and therefore B_L must be a constant. The value of the coefficient B_L must be obtained from experimental data. Levy offers a curve relating $1/B_L$ to $\rho_V \times h_{fg}$ which has to be used in conjunction with his general correlation.

There are several other similar empirical correlations for nucleate boiling in which the heat transfer coefficient is a function of temperature driving force and physical properties of the fluids.

Cryder and Gilliland's Generalized Equation

The generalized equation of Cryder and Gilliland (15) is interesting since it is one of the few equations that incorporate the diameter of the tube where boiling takes place. The equation was derived from tests made with water, salt solutions, and five organic liquids boiling on the outside of a 1.04-inch brass tube.

$$h = \text{const.} \frac{(\Delta T)^{2.39} k_L^{2.97} C_L^{0.43} \rho_L^{3.1} D^{2.1}}{\sigma^{1.65} \mu_L^{3.45}} \tag{53}$$

Hughmark's Statistical Approach

Hughmark (33) statistically analyzed nucleate pool boiling experimental data and derived the following eight-variable equation for heat flux:

$$\bar{q} = 2.67 \times 10^{-9} \frac{\Delta P^{1.867} (\rho_L - \rho_V)_w^{2.27} (C_L)_w^{0.945} T_w^{1.618}}{(\rho_V)_w^{1.385} L_w^{1.15} (\mu_L)_w^{1.630} P_R^{0.202}} \tag{54}$$

This equation which describes experimentally measured heat flux with an average absolute deviation of 40% considers only the thermodynamic properties of the liquid and vapor. It neglects the effects of the condition, geometry, and orientation of the surface. The author states that the equation has no theoretical justification but that it gives the best attainable agreement with experimental data when only thermodynamic properties are considered as products of powers.

Chen's Theory of Additive Mechanisms

Chen (9) using a different approach to solve the problem, postulated an additive mechanism of micro and macro convective heat transfer to represent boiling heat transfer with net vapor generation to saturated non-metallic fluids in convective flow. He defined two dimensionless functions, S and F, to account for the suppression of bubble growth due to flow and for the increase in convective turbulence due to the presence of vapor. Both S and F are functions of a two-phase Reynolds number and a Martinelli parameter respectively. The derivation of Chen's equation is based on the assumption that

$$h = h_{mic} + h_{mac} \tag{55}$$

The micro-convective heat transfer in convective boiling is derived from the Forster-Zuber equation

$$h_{mic} = 0.00122 \; \frac{k_L^{0.79} \; Cp_L^{0.45} \; \rho_L^{0.49} \; g_c^{0.25}}{\sigma^{0.5} \; \mu_L^{0.29} \; \lambda^{0.24} \; \rho_V^{0.24}} \times (\Delta T_e)^{0.24} (\Delta P_e)^{0.75} \qquad (56)$$

By the use of the Clausius and Clapeyron equation and the simplification resulting from $\Delta T/T << 1$ a final suppression term is derived

$$S = \left(\frac{\Delta T_e}{\Delta T}\right)^{0.24} \left(\frac{\Delta P_e}{\Delta P}\right)^{0.75} \qquad (57)$$

Combining this suppression factor with equation 56 a final expression for the micro-convective coefficient in terms of the suppression factor and total superheat is obtained.

$$h_{mic} = 0.00122 \; \frac{k_L^{0.79} \; Cp_L^{0.45} \; \rho_L^{0.49} \; g_c^{0.25}}{\sigma^{0.5} \; \mu_L^{0.29} \; \lambda^{0.24} \; \rho_V^{0.24}} \; (\Delta T)^{0.24} \; (\Delta P)^{0.75} \; S \qquad (58)$$

The Dittus-Boelter equation

$$h_{mac} = 0.023 \; (Re)^{0.8} \; (Pr)^{0.4} \left(\frac{k}{D}\right) \qquad (59)$$

is modified by Chen to represent effective values associated with the two-phase fluid as follows:

$$\beta = Pr/Pr_L \qquad (60)$$

$$\gamma = k/k_L \qquad (61)$$

$$F = (Re/Re_L)^{0.8} = \left(Re \times \frac{\mu L}{DGz}\right)^{0.8} \qquad (62)$$

In the case of ordinary fluids the Prandtl numbers of the liquid and the vapor are normally of the same magnitude and therefore the term β is equal to 1. Furthermore since the heat is transferred through an annular film of liquid it is expected that the liquid properties would be dominant and that γ should also be close to unity. Therefore the Dittus-Boelter modified equation is

$$h_{mac} = 0.023 \, (Re_L)^{0.8} \, (Pr_L)^{0.4} \left(\frac{k_L}{D}\right) F \tag{63}$$

and the total heat transfer coefficient is then the summation of both the micro and the macro convective heat transfer coefficients. Chen verified the validity of his equation with nine experimental cases. An average deviation between calculated and measured boiling coefficient of ±11% was obtained.

Sydoriak and Roberts' Derivation for Boiling N_2 and H_2 in Narrow Channels

Sydoriak and Roberts (66) derived the following equation relating heat flux to annular area and physical properties of the fluid based on their experimental work with nitrogen and hydrogen. They assumed a homogeneous frictionless two-phase flow in the annulus.

$$Q = \hat{A}\bar{L} \left(\rho_V{}^2 \quad \rho_L \, Z_e \, \bar{g} \, f_2 \right)^{1/2} \tag{13}$$

V. EXPERIMENTAL INVESTIGATION

The following discussion of the experimental work consists of a description of the test equipment and of the experimental procedure, a tabulation of the data, and a review of the important experimental observations.

Apparatus for Cryogenic Confined Space Boiling Studies

Introduction

Design, construction, and operation of the apparatus used in the boiling studies incorporated one main objective: the simulation of boiling conditions experienced in the operation of confined space boiling devices, such as cryomagnets (42). The design of the test equipment allowed for either liquid nitrogen or liquid neon testing. A detailed description of the design and construction of the test apparatus follows. The neon liquefier built as a part of this project was described at the semi-annual meeting of ASHRAE in 1963 (41).

For purposes of discussion, the study apparatus has been classified into two groups, namely, experimental test section, and auxiliary equipment. These equipment groups will be considered separately.

Experimental Test Section

A major effort in the overall program was that of design and construction of an experimental test section. The test section design incorporated three major objectives:

a. geometric simulation of confined space boiling channels,

b. thermodynamic and hydrodynamic simulation of confined space boiling mechanisms, and

c. obtaining significant experimental information through use of suitable instrumentation.

Geometric Configuration Considerations in Design of Test Section

As noted, simulation of confined space boiling channels was a major requirement in the test section design. The channels to be simulated, the cooling channels of a cryomagnet for example, have the following typical dimensions:

10 inches - 30 inches vertical length
3 inches - 10 feet circumferential length
0.005 inches - 0.060 inches gap dimension.

The devices incorporating the narrow channels are fully submerged in a cryogenic fluid in normal operation. Boiling then occurs in these vertically oriented channels.

In the boiling test section design, the narrow channel simulation could have been accomplished in either of two ways: (a) by accurately spacing apart two flat plates, or,(b) by accurately spacing apart two concentric cylinders to form an annular gap. It was felt that the concentric cylinders would be preferable, so the annular gap as a simulation of the narrow thickness channels was used.

At the outset it was decided that capability for visual observation of the annular boiling mechanisms during operation would be incorporated in the test section design. To accomplish this, the outer cylinder forming the annular gap was specified as precision formed Pyrex glass pipe, and the inner cylinder as the heating surface which would cause boiling when the pair of concentric cylinders were submerged in liquid nitrogen or liquid neon. To permit studies with various gap widths, it was decided that a single size of precision bore glass tube would be used with six different sized heaters. The heaters would differ from each other only in respective outside diameter dimensions. The outside diameter variation would affect the variation in gap size.

Availability of liquid neon was an important factor in sizing the test section. An average neon boil off rate equivalent to about 6 liquid lt/hr was acceptable. Based on calculation of boil off rate included in the appendix, a test heater nominally 3-inch OD x 7 1/2-inch long was specified as an insertion in a nominal 3 ±0.0003-inch precision Pyrex pipe.* Channel gap sizes of 0.005-inch to 0.080-inch were also specified.

The preliminary design dimensions and the annular space between a glass outer tube and an inner heater element were taken as the basis of geometric simulation of the narrow thickness channels. Heat transfer and fluid flow considerations now were to be incorporated in the test section design

---

*Commercially available - G. K. Porter, Hatfield, Pennsylvania

Thermodynamic and Hydrodynamic Consideration in Design of Test Section

The thermodynamic considerations associated with the test section design were those of simulating the mode of heating found in the narrow thickness channels of cryomagnets. In those situations one surface of the channel was effectively insulated while the other surface was heated by electric resistance heating. That is, while the field producing electric current passed through the conductor which formed one face of the channel, I^2R heating occurred, resulting in a uniform heat generation.

To simulate this heating method in the test section, a resistance element of nominal 3-inch OD was considered. Electrical characteristics of suitable resistance materials at low temperatures indicated that the resistance heating scheme was impractical. Instead, a concept of a boiler-condenser heater was instituted. The boiler condenser heat transfer scheme would involve a small electric heating element to boil liquid nitrogen or liquid neon inside of a pressure vessel having a nominal 3-inch outside diameter. The outer surface of the pressure vessel would form the heating face of the annular gap. A simple thermosyphon pump, (vapor lift pump), installed inside the pressure vessel would pump liquid nitrogen or liquid neon in a fashion so that the inner wall of the pressure vessel would be "splashed," that is, completely washed by the "percolating" fluid and therefore maintained at a constant temperature. Under test conditions, the test heater is submerged in either liquid nitrogen or liquid neon. Resistance heating by means of the partially immersed electric element would result in simultaneous vapor generation and condensation inside the 3-inch vessel, and boiling on its outer wall. At a given electric power input, the heater pressure will rise until the temperature driving force resulting from the difference between the saturation temperature of the boiling-condensing liquid inside the heater at the heater pressure, and the saturation temperature of the boiling liquid outside the heater, is sufficient to dissipate the heat input.

In this fashion, the power input to the resistance element would effectively result in heat transfer from the vessel's outer surface to the fluid in the narrow thickness channel. The thermosyphon pumping insured that the inner surface of the vessel wall would be continuously wetted with a fluid at a higher saturation temperature. The wetting in turn assured the existence of a uniform temperature potential through the vessel wall, thus resulting in the uniform heat generation simulation desired. Having decided on the boiler-condenser heat transfer scheme, various design problems became apparent. At the outset, it was deemed desirable to maintain little contraction of the vessel diameter when cooled from ambient temperature to liquid nitrogen and neon temperatures. For this reason, a pressure vessel made from invar material (36% Ni, 69% Fe) was considered. A.S.M.E. Boiler and Pressure Vessel code (2) calculations showed a wall of 0.0407-inch thickness to be sufficient from the standpoint of internal pressure, however a wall thickness of 0.250-inch was considered more practical. Unfortunately, heat transfer calculations showed that an unreasonably high temperature difference of 40°F across the 0.250-inch thick wall would exist at the higher heat flux value anticipated in this study.

Because of the heat transfer problem posed, it was decided that the desirable contraction characteristics of the pressure vessel material would be compromised for high thermal conductivity. For this reason OFHC (oxygen free high conductivity) copper pipe would be specified as the pressure vessel wall material. At liquid neon temperatures, the OFHC material, certified ASTM Specification B-75 (3), has a thermal conductivity value of 695 Btu/hr-ft-°F which compares with 1.5 Btu/hr-ft-°F for invar (35). The higher thermal conductivity copper would reduce the 40°F temperature difference across the 0.250-inch wall to approximately 0.2°F, at the higher heat fluxes.

A.S.M.E. Boiler and Pressure Vessel Code calculations showed that an OFHC copper wall thickness of 0.102-inches would be sufficient for 400 psia vessel pressure. Deflection consideration, however, indicated that a wall thickness of 0.125 would provide a 6.4% error between gap sizes for a given geometric configuration with 0 psia and 400 psia vessel pressures respectively. To minimize the error in gap under various vessel pressures, a heavier nominal wall thickness of 3/8-inch was specified. (Calculations noted above are included in Appendixes B and C.)

In order to minimize thermal end effects, end closures were specified as 1/4 - 5/16 nominal thickness stainless steel plates. The plates would be soldered into appropriately machined recesses at the respective ends of the OFHC copper pipe length. One plate would have a centrally located access hole while the remaining closure was solid. Each end plate would have a short length of stainless steel rod attached to it, this making the pressure vessel much like a rolling pin in appearance. One of the rods would be bored out to provide access to the pressure vessel cavity through the respective end plate.

The heating element, a Watlow Fire Rod Heater, had a nominal heating capacity of 550 watts at 120 volts AC when operated in liquid nitrogen or liquid neon, and sized 1/2-inch outside diameter, 2 1/8-inch length. The element was mounted inside a 5/8-inch outside diameter, thin wall stainless steel tube. The heater element-tube assembly inserted into the pressure vessel cavity through the access tube constituted the thermosyphon pump.

Figures 4, 5, 6, and 7 show the parts of the test heater and the assembled test section.

Experimental Data Collection Consideration in Test Section Design

Data collection, or instrumentation, considerations in the test section design were directly related to the desired observations to be made, based on the experimental concept shown in the schematic diagram of the test section, Figure 8. The observations deemed necessary were as follows:

a. Saturation pressure of fluid in heater cavity (pressure vessel cavity). Saturation pressure in the pressure vessel cavity would be measured on a bank of manometers and a precision pressure gauge. The various manometers and pressure gauge were specified so as to allow accurate

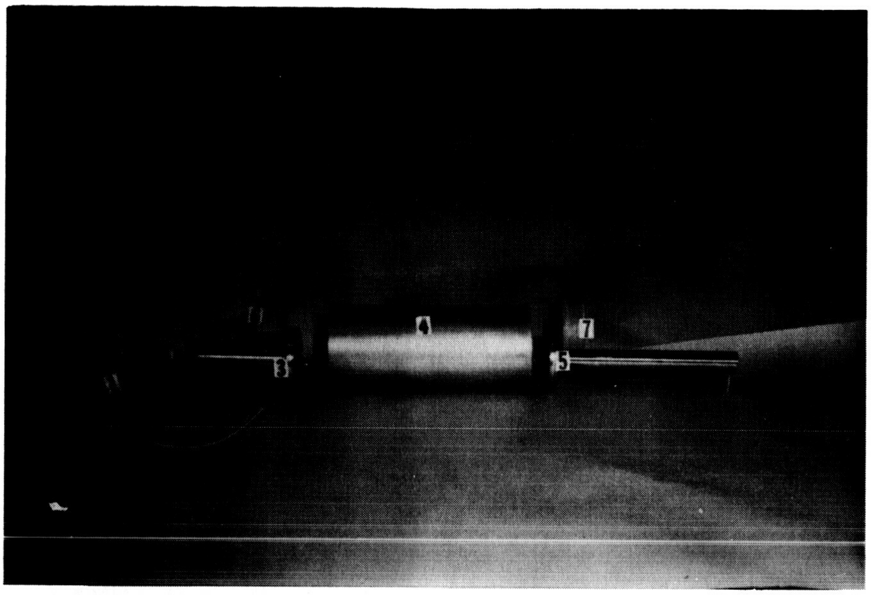

FIGURE 4. PICTURE OF HEATER COMPONENTS

LEGEND

(Figures 4 and 5)

1. Thermocouple Leads
2. Electric Element Wires
3. Top End Plate
4. Heater Body
5. Bottom End Plate
6. Insulation End Piece
7. Insulation End Piece

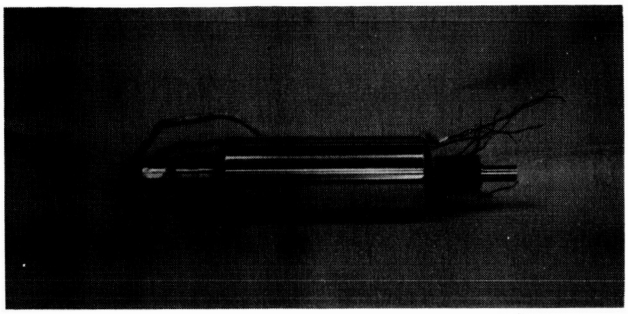

FIGURE 5. PICTURE OF ASSEMBLED HEATER

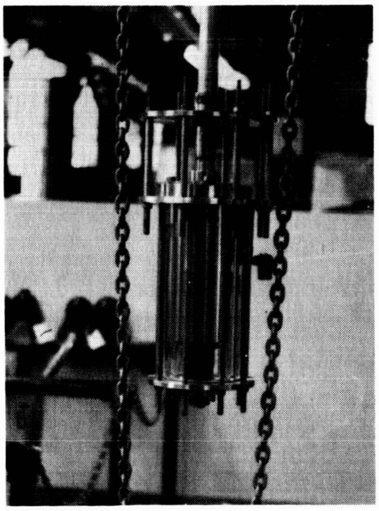

FIGURE 6. PICTURE OF ASSEMBLED TEST SECTION

FIGURE 7, SKETCH OF ASSEMBLED TEST SECTION

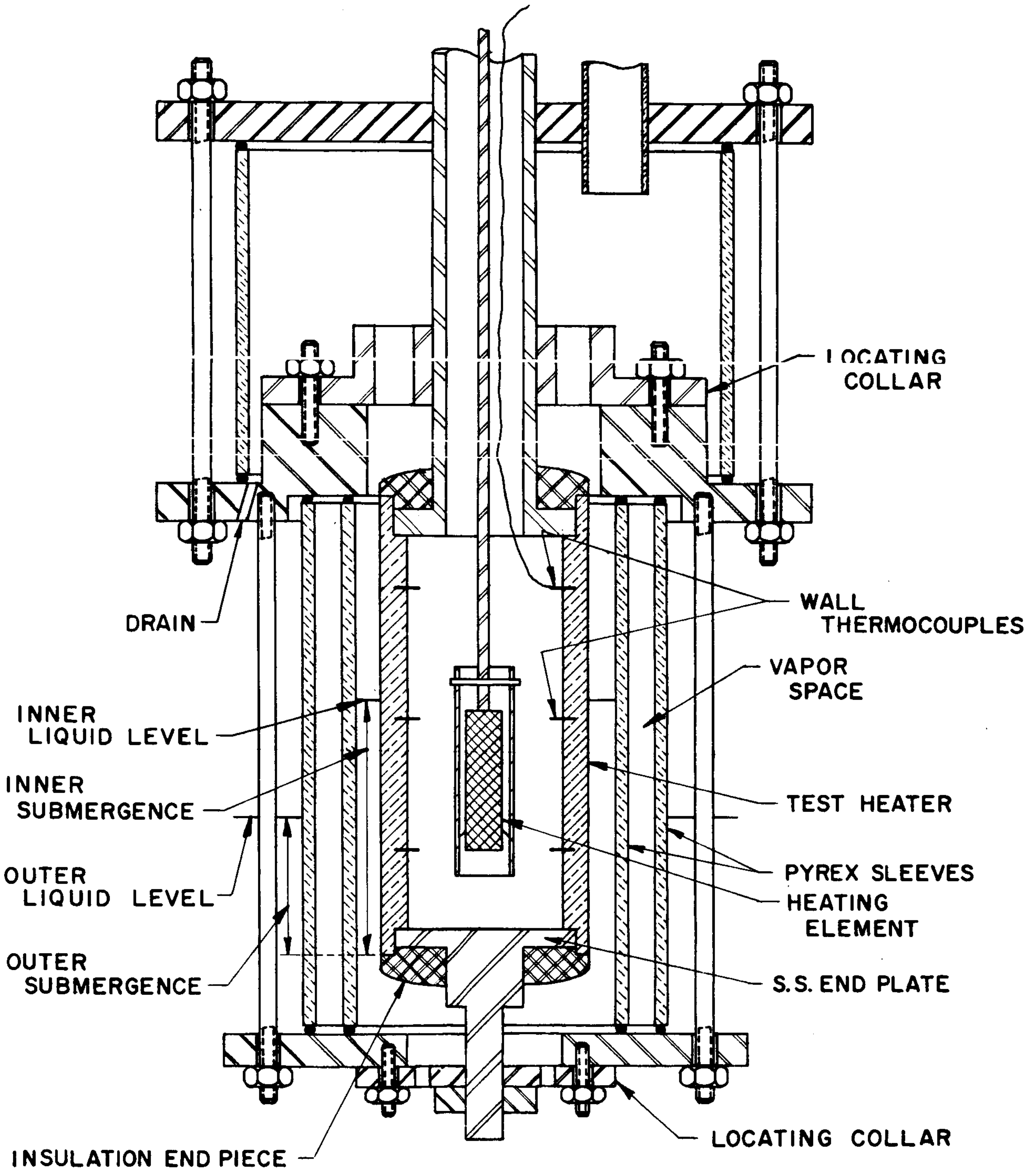
LOCATING COLLAR
DRAIN
WALL THERMOCOUPLES
VAPOR SPACE
INNER LIQUID LEVEL
INNER SUBMERGENCE
TEST HEATER
OUTER LIQUID LEVEL
PYREX SLEEVES
HEATING ELEMENT
OUTER SUBMERGENCE
S.S. END PLATE
LOCATING COLLAR
INSULATION END PIECE

FIGURE 8, SCHEMATIC DIAGRAM OF TEST SECTION

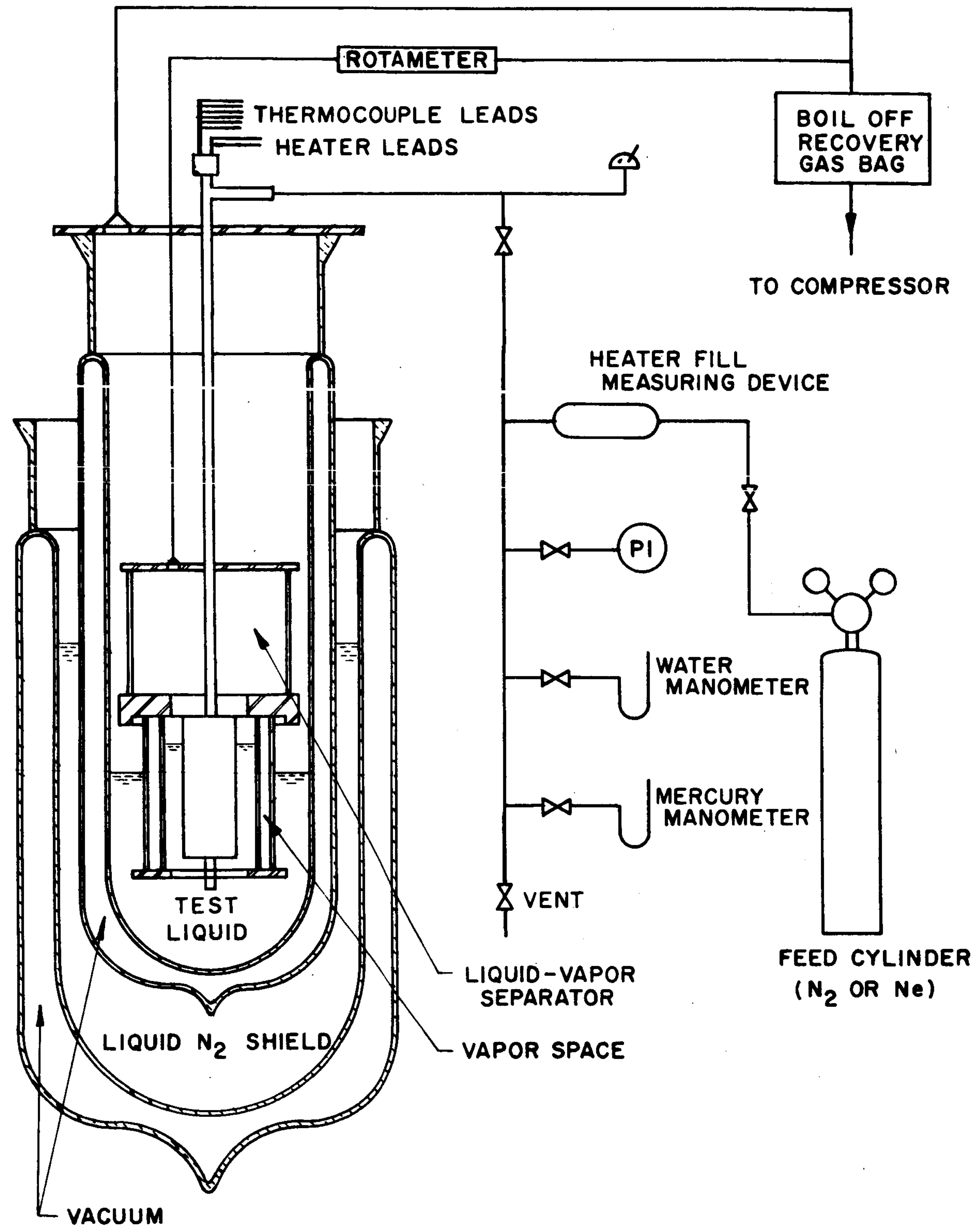
ROTAMETER
THERMOCOUPLE LEADS
HEATER LEADS
BOIL OFF RECOVERY GAS BAG
TO COMPRESSOR
HEATER FILL MEASURING DEVICE
PI
WATER MANOMETER
MERCURY MANOMETER
VENT
TEST LIQUID
LIQUID-VAPOR SEPARATOR
VAPOR SPACE
FEED CYLINDER (N_2 OR Ne)
LIQUID N_2 SHIELD
VACUUM

pressure readout from 0.02 psig to 600 psig. The pressure measurement bank would tap into the gas fill line of the heater and would allow continuous monitoring of the cavity saturation pressure. An auxiliary piping circuit employing the precision high pressure gauge was specified to permit metering of the gas introduced into the vessel cavity.

b. Temperature of heater surface (pressure vessel wall) and of liquid bath into which test section is immersed. Measurement of temperature indicated posed problems since the measurements were to be made at temperatures as low as liquid neon temperature. At this temperature level, $50^{\circ}R$, elaborate sensing equipment is generally employed, e.g., platinum resistance thermometers. Copper-constantan thermocouples, frequently used in cryogenic research, exhibit a very low ratio of electromotive force to temperature change at liquid neon conditions. At $50^{\circ}R$, a copper-constantan thermocouple has a response ratio of approximately 4 μ volts per $^{\circ}R$ temperature change.

Space limitations and practicality of instrumentation eliminated all but copper-constantan thermocouples for temperature measurement considerations. It was also decided that the measurement of the boiling liquid temperature was of secondary importance since boiling occurred at atmospheric pressure. The primary measurement would be, therefore, a direct measurement of the temperature difference between the wall and boiling liquid. Copper-constantan thermocouples mounted in the wall of the pressure vessel and referenced to a copper-constantan junction submerged in the liquid nitrogen or neon bath would yield the desired electromotive force output corresponding to the temperature difference between the pressure vessel wall and the liquid bath. The small signal obtained from the thermocouples would require amplification to provide the desired accuracy for temperature measurements of ±0.1°F. The temperature measurement instrumentation shown in Figure 9 was therefore specified:

1. Copper-constantan differential thermocouple circuit
2. Sanborn 86-1500 PA preamplifier unit
3. Brown Electrick multiple point recorder 0-1 mv full scale
4. Precision Rubicon box potentiometer for suppression voltage.

c. Rate of heat input to the heater, this in turn being heat transferred in annular gap boiling. As shown in Figure 10, the power input to the electric heating element was measured by means of a multiple range precision wattmeter. The assumption was made that all power indicated by the wattmeter was transferred through

FIGURE 16, WIRING DIAGRAM OF THERMOCOUPLES

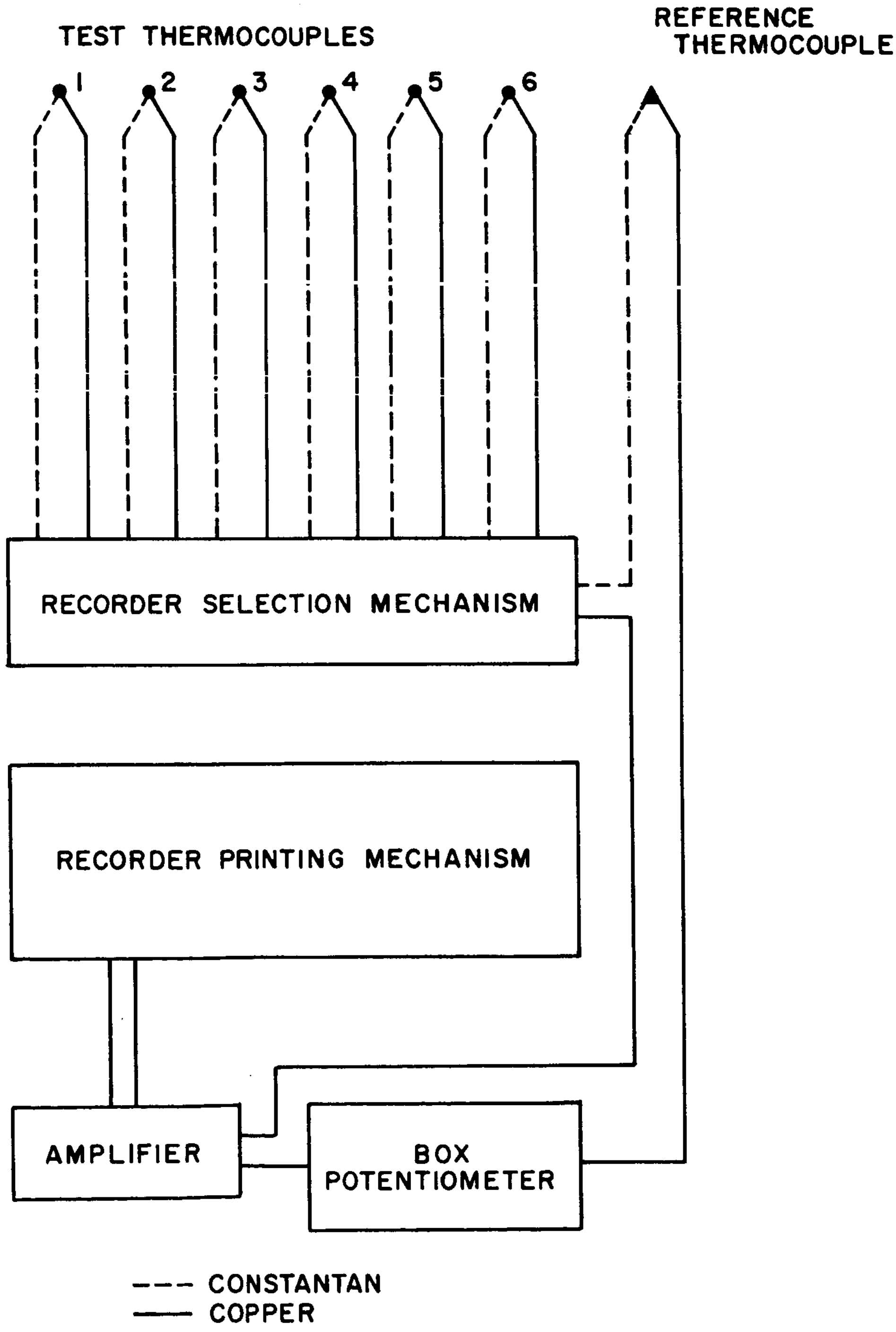
TEST THERMOCOUPLES
1
2
3
4
5
6
REFERENCE THERMOCOUPLE
RECORDER SELECTION MECHANISM
RECORDER PRINTING MECHANISM
AMPLIFIER
BOX POTENTIOMETER
--- CONSTANTAN
—— COPPER

FIGURE 7 , WIRING DIAGRAM OF ELECTRIC HEATING ELEMENT

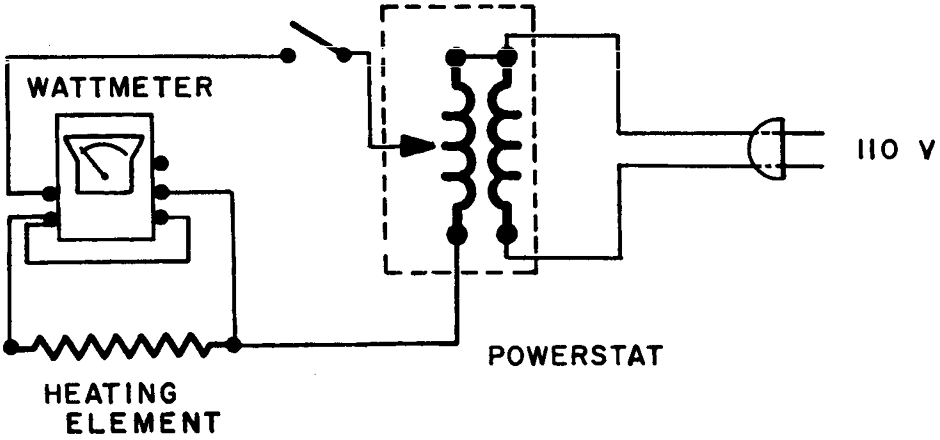
WATTMETER
110 V
POWERSTAT
HEATING ELEMENT

the walls of the pressure vessel. This implied that a negligible amount of heat would be lost through the vessel end plates and in I^2R heating of the heater element lead-in wires.

d. Rate of gas generation or gas flow rate out of annular gap channel. Vapor generation rate or vapor flow rate out of the channel could be measured in two independent ways. The separation chamber above the test heater which would separate vapor and entrained liquid, would also collect and channel the vapor through an access tube to a rotameter for direct measurement. Secondly, the wattmeter employed in measurement of power input would also serve as a rate of vapor generation monitor. That is, if the assumption that all heat input to the test section were consumed in vaporization of channel fluid, the vapor generation rate, then, would be directly proportional to the power consumption; the constant of proportionality being the latent heat of the liquid.

Trial operations of the test section yielded a very good agreement between vapor flow rate measurements by the two independent methods. It was then decided that the wattmeter measurement of vapor flow would suffice since the flowmeter method introduced an undesirable back pressure on the boiling fluid.

e. Liquid entrainment, mass of liquid moving with generated vapor, at exit end of annular channel. Measurement of liquid entrainment at the channel exit posed a major problem because of space limitation in the glass dewars. Ideally, the entrained liquid collected in the phase separator located on top of the test heater, would drain by gravity into a graduated glass container and would therefore be easily measured. However, reduction to practice of this idea was not feasible. The graduated container would have had to be located 2 to 3 inches below the top of the heater, thus submerging it completely. A sealed line between the phase separator and the container would be required. In order to allow for gravity flow a vent would also be needed. The main complication, however, resulted from the need of piping and appropriate valves to regulate the liquid flow to the graduated container and to allow emptying it prior to each run. It was impossible to physically fit the graduated container, all this piping and valves, and the test section in the glass dewars containing the liquid bath. Therefore measurement of liquid entrainment was not carried out, but visual observations regarding the type of entrainment and estimating its amount were made for each run.

f. Wetted area, wetted by liquid gas mixture, of heated surface in annular channel, and liquid head driving force for flow in annular channel. The fact that the external parts of the test apparatus were to be glass provided a straight-forward method of measuring wetted area of heated surface and liquid head driving force. It was planned that the heater surface would be visible for visual observation. A graduated scale, appropriately positioned proximate to the visible area of heated surface would permit visual measurement of the wetted length. Similarly, the scale would permit direct visual measurement of the liquid head driving force.

Composite Design, Fabrication and Assembly of Test Section

The test section therefore consists of the following basic elements:

a. Copper heater containing a small electric element

b. Precision glass sleeve forming the outer surface of the narrow channel

c. Instrumentation (described in previous section)

Precision machining of the copper heater was necessary in view of the small gap sizes desired: 0.005- to 0.080-inch Machining of the heater was therefore performed in two steps. The first one, rough machining, brought the heater outside diameter to within about 0.010-inch of the final diameter of the heater. At that point, the wall thermocouples were installed in the heater wall and soldered, and the end plates were also installed and soldered. The second step of machining reduced the outside diameter of the heater to the exact desired diameter. The assembly of the test unit was done with specailly designed flanges. Figures 6 and 7 show an assembled section. Location collars and a specially built tapered gauge were used to insure exact concentricity during assembly. The surface finish of each heater was carefully checked and its roughness was measured with a Profilometer (50). The two plated heaters, heaters no. 9 and 10, were machined like the copper heaters. They were, then, sent out for plating with about 4 mils of nickel and cadmium respectively. The plated surface was finally machined again to the required diameter which removed about 2 mils of the plating. This concept was used in order to insure the same type of surface finish for all the heaters tested.

Another important consideration was the determination of the exact gap size at the liquid nitrogen and neon temperatures. This was accomplished by accurate measurements of the outside diameter of the heater and the inside diameter of the precision Pyrex sleeve at ambient temperature. The best available coefficients of thermal expansion as a function of temperature for the OFHC copper and the Pyrex sleeve (1, 35) were used to calculate the contraction of both materials from ambient to liquid nitrogen and neon temperatures. Detailed calculations show that a contraction of 0.004 inch occurs for both the liquid nitrogen and neon cases. The gap dimension at liquid nitrogen and neon temperature is therefore, the gap size measured at ambient conditions plus the contraction correction of 0.004 inch. Refer to Appendix D for calculations.

Since the tests are to be carried out at cryogenic temperatures, heat leak to the test section is an important factor. Calculations show that the precision glass sleeve offers sufficient resistance to render the heat leak effect negligible. However, it was decided to minimize this effect further by the addition of a second Pyrex pipe around the precision Pyrex pipe, thus forming a vapor barrier.

Auxiliary Equipment

Auxiliary equipment was required in conjunction with the main test section. Figures 11 and 12 are views of two components: dewar assembly and gas recovery bag.

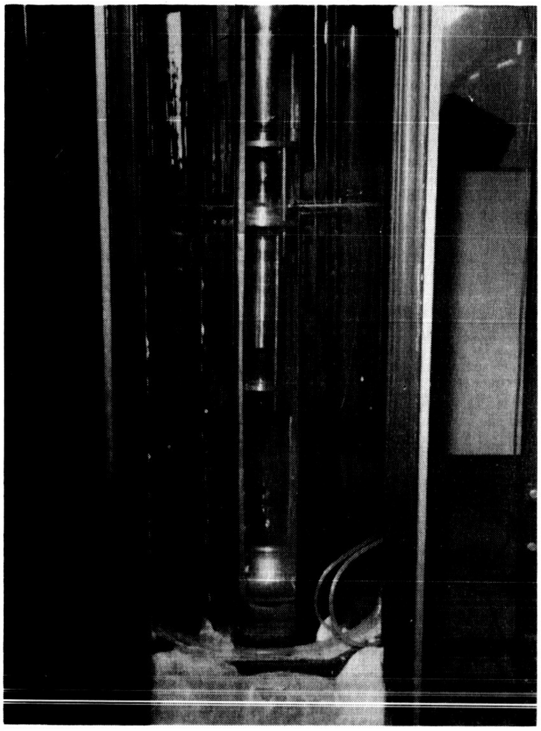

FIGURE 11

PICTURE OF DEWARS' ASSEMBLY

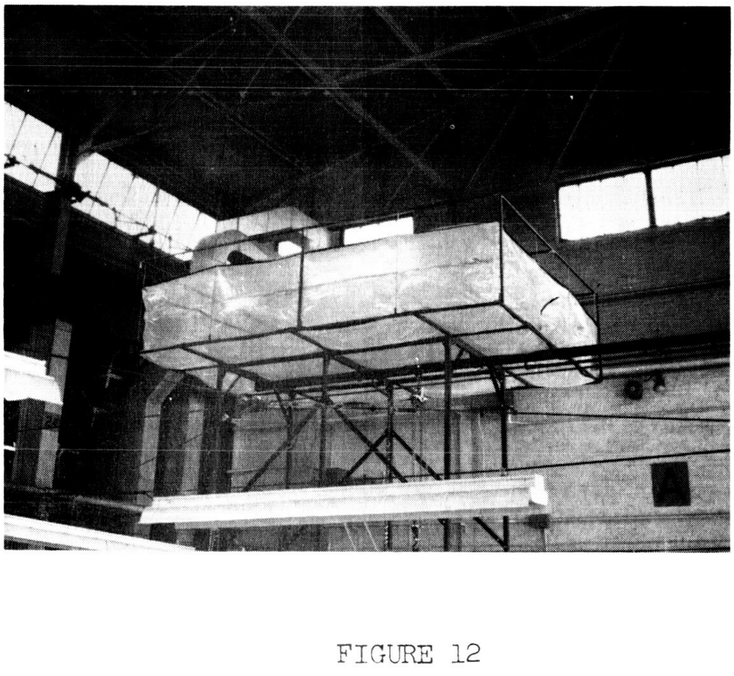

FIGURE 12

PICTURE OF GAS RECOVERY BAG

A description of the auxiliary equipment consisting of the following will be found in Appendix F.

1. Glass dewar assembly
2. Test section structure
3. Gas recovery bag
4. Liquid neon storage and transfer equipment

Experimental Procedure

The experimental program was divided into two parts, the first one related to the study of boiling liquid nitrogen and the second one to the study of boiling liquid neon.

Liquid Nitrogen Boiling Study

Two complete sets of runs were made with each heater: one set of runs under pool boiling conditions and the second one under annular flow boiling conditions.

The test section was assembled and introduced into the glass dewars shown in Figure 11. In the case of pool boiling, the heater was introduced alone without the precision tube glassware forming the annular space. The heater cavity was evacuated and the whole section was then cooled down with liquid nitrogen. The shield section of the dewars assembly was also filled with liquid nitrogen. The heater cavity having a volume of about 500 cc, was filled with about 250 cc of liquid nitrogen. This was accomplished by introducing enough gaseous nitrogen in the heater and condensing it.

After the heater was filled with the desired amount of liquid nitrogen the system was assumed to have reached equilibrium when the heater pressure was below 3 to 4 inches of water for over 15 minutes, with zero heat input to the test section.

A complete series of runs for pool boiling consisted of varying the electrical power input to the heating element from 0 watts to about 400 watts at at least two different submergences, submergence being defined as the depth of the lower edge of the heating surface below the surface of the liquid. A 7 1/2-inch submergence corresponds to 100% submergence since the heaters have a 7 1/2-inch effective heating surface. The following readings were taken for each run: heater pressure, wattage, heater wall temperature measurements, and submergence. A total of 6 heaters were tested under pool boiling conditions: four copper heaters, nos. 12b, 6, 7, and 8; and heaters nos. 9 and 10 which were nickel and cadmium plated respectively. The pool boiling runs were made in order to establish a datum plane for the annular gap boiling studies. The experimental procedure for the annular gap boiling was identical except for the fitting of the heater with the precision glassware that formed the annular gap. Four major gap sizes were tested, namely, 6, 20, 53, and 80 mils measured at liquid nitrogen temperature. Two additional gap widths of 21 and 22 mils were also tested in the case of the nickel plated and cadmium plated heaters respectively. In the case of the annular gap boiling, two submergences were considered: the inner submergence defined as the length of the heater surface which is wetted by the boiling liquid and the outer submergence defined as the depth of the lower edge of the heater relative to the liquid level outside the annulus. Both submergences are identified in Figure 7.

A series of runs for annular gap boiling was similar to the one for pool boiling and consisted of varying the electric power input to the electric element at at least two inner submergences. Heater pressure, wattage, wall temperatures and both inner and outer submergences were measured for each run. The six heaters tested under pool boiling conditions were tested under annular gap boiling conditions.

Liquid Neon Boiling Study

The experimental procedure used for the liquid nitrogen boiling study was also used for the liquid neon boiling study.

Since the heaters were already tested under pool boiling conditions with liquid nitrogen, only heater 12b was similarly tested under pool boiling conditions with liquid neon.

Experimental difficulties were experienced in the case of neon boiling, during the transfer of the liquid neon from storage to the test dewar. The main difficulties were the result of freezing and precipitation as solids of trace quantities of air introduced in the liquid neon during the filling of the inner glass dewar. Solid CO_2 and air had a tendency to plug the narrow annulus. A fine screen was installed at the bottom of the test heater to prevent the occluded solids from entering the annulus. Another difficulty was the frosting of the windows which greatly reduced the visibility of the test section.

A total of five heaters were tested under annular gap boiling conditions at full submergence except for heater 7b which was tested at three different submergences. The five heaters tested consisted of the four copper heaters with 6, 20, 53, and 80 mil gap widths, and the nickel plated heater with a 21 mil gap width.

It should be noted that the heater cavity was filled with 250 cc of liquid neon in the case of the neon boiling study.

Experimental Data

The characteristic dimensions of the six test heaters are summarized in Table I. The physical properties of the two cryogenic fluids tested, nitrogen and neon, are listed in Tables II and III respectively. The experimental data covering all the runs with nitrogen and neon, are tabulated in Tables IV to XXI.

TABLE I

CHARACTERISTIC DIMENSIONS OF TEST SECTIONS

Heater No.	Heater OD - " D_1	Glass Sleeve ID - " D_2	Gap Size at Liq. Ne & N_2 Temp. - " t	Annular Flow Area ft^2 A_t (a)	Equivalent Diameter " D_e (b)	Heat Transfer Area ft^2/in.	Surface Finish RMS "
12b	2.9975	3.0015	0.006	3.916×10^{-4}	0.024	0.06540	9-11
6	2.9695	3.0015	0.020	13.01×10^{-4}	0.080	0.06478	16-20
9	2.9675	3.0015	0.021	13.65×10^{-4}	0.084	0.06474	6-8 (Ni)
10	2.9645	3.0015	0.022	14.12×10^{-4}	0.088	0.06468	8-11 (Cd)
7b	2.9030	3.0015	0.053	34.09×10^{-4}	0.212	0.06333	11-13
8	2.8495	3.0015	0.080	50.99×10^{-4}	0.320	0.06217	13-15

(a) Annular Flow Area: $A_t = \frac{\pi}{4} \frac{(D_2^2 - D_1^2)}{144} = \frac{\pi}{4 \times 144}\left[D_2^2 - (D_2 - 2t)^2\right]$

$$= \frac{\pi}{4 \times 144}\left[D_2^2 - D_2^2 + 4D_2 t - 4t^2\right] = \frac{\pi}{144}\left[D_2 t - t^2\right]$$

TABLE I (CONTINUED)

(b) Equivalent Diameter: $$D_e = \frac{4\ \text{Flow Area}}{\text{Wetted Perimeter}} = \frac{4\ (\pi/4)\ (D_2^{\ 2} - D_1^{\ 2})}{\pi D_1}$$

$$= \frac{(D_1 + 2t + D_1)\ (D_1 + 2t - D_1)}{D_1} = \frac{4\ (D_1 + t)t}{D_1}$$

$$= 4t + \frac{4t^2}{D_1} = 4t$$

since $\frac{4t^2}{D_1} << 4t$

TABLE II

PROPERTIES OF NITROGEN

Liquid at Boiling Point

ρ_L = 50.32 lb/ft^3 (1)

μ_L = 0.385 lb/ft-hr (1)

k_L = 0.0805 Btu/hr-ft-°F (1)

σ = 0.0006 lb/ft (1)

Cp = 0.476 Btu/lb-°F (1)

Pr = 2.275 (1)

λ = 2405 Btu/lb-mole = 86 Btu/lb (1)

Vapor at Boiling Point

ρ_V = 0.2939 lb/ft^3 (1)

μ_V = 0.012 lb/ft-hr (1)

k_V = 0.0043 Btu/hr-ft-°F (1)

Cp = 0.20 Btu/lb-°F (1)

Pr = 0.56 (1)

TABLE III

PROPERTIES OF NEON

Liquid at Boiling Point	Vapor at Boiling Point
ρ_L = 75.2 lb/ft^3 (1)	ρ_V = 0.56 lb/ft^3 (1)
μ_L = 0.714 lb/ft-hr$^{(a)}$ (10,31)	μ_V = 0.0124 lb/ft-hr (34)
k_L = 0.0752 Btu/hr-ft-°F (12)	k_V = 0.0236 Btu/hr-ft-°F (1)
σ = 0.00032 lb/ft (1)	Cp = 0.44 Btu/lb-°F (1)
Cp = 0.427 (1)	
Pr = $Cp\,\mu_L/k_L$ = 4.054	
λ = 748 Btu/lf-mole = 35 Btu/lb (1)	

(a) μ_L estimated as follows:

$$T^* = \frac{k\,T}{\varepsilon}\,,\quad \eta^* = \frac{\eta\sigma^2}{\sqrt{m\,\varepsilon}}\qquad \text{(Ref. 10, 31)}$$

For neon, ε/k = 35.7°K, σ = 2.789A° (31)

Liquid neon temperature = T = 27.3°K

$$\frac{1}{T^*} = \frac{\varepsilon/k}{T} = \frac{35.7}{27.3} = 1.31$$

η^* = 2.3 (Ref. 10, Argon Curve)

$\sqrt{m\varepsilon}$ = 10 (calculated from Ref. 10 curves)

$$\mu_L = = \frac{\eta^*\sqrt{m\varepsilon}}{2} = \frac{2.3 \times 10}{2.789^2} = 2.96 \text{ micro-poises} = 0.714 \text{ lb/ft-hr}$$

TABLE IV

EXPERIMENTAL TEMPERATURE DATA - NITROGEN POOL BOILING HEATER #12b

Run#	Wattage	Heater Pressure	ΔT_t ^oF	ΔT_b - ^oF			
				ΔT_b #1	ΔT_b #2	ΔT_b #3	ΔT_b #5
A-P12b.2	15	3.65"Hg	1.6	0.9	1.4	1.6	1.5
3	25	4.15"Hg	1.8	0.5	1.1	1.5	1.5
4	16	-------	----	0.3	0.9	1.1	1.1
5	40	6.5"Hg	3.0	1.0	1.7	2.4	2.5
6	60	9.2"Hg	4.3	1.5	2.3	3.3	3.1
7	80	12.0"Hg	5.5	1.9	2.7	3.9	4.2
8	120	15.2"Hg	6.7	2.5	3.4	4.8	5.2
9	160	19.4"Hg	8.4	2.8	3.8	5.6	6.1
10	219	28.7"Hg	11.4	4.7	5.0	8.8	9.1
11	219	27.8"Hg	11.0	4.9	5.2	9.0	9.5
12	300	17.5psig	13.0	7.1	7.2	10.8	12.5
14	16	7.1"Hg	3.3	1.1	1.1	2.4	2.6
15	25	10.8"Hg	5.0	2.2	1.8	3.5	4.2
16	40	16.0"Hg	7.0	3.3	2.9	5.1	6.1
17	62	22.6"Hg	9.3	3.7	3.5	6.7	7.9
18	83	29.6"Hg	11.6	4.2	3.9	8.3	9.9
19	122	21.5psig	15.2	5.5	5.0	11.7	13.5
20	163	31.5psig	20.2	6.6	6.3	14.6	17.3
21	218	43.5psig	25.0	8.8	9.3	18.8	21.6
22	278	68.0spig	33.5	10.8	11.2	24.2	27.4

TABLE IV CONTINUED

Run#	Wattage	Heater Pressure	ΔT_t ^oF	$\Delta T_b - {}^oF$			
				$\Delta T_b\#1$	$\Delta T_b\#2$	$\Delta T_b\#3$	$\Delta T_b\#5$
A-P12b-24	16	12.9"Hg	5.8	2.4	2.4	3.8	4.7
25	25	16.8"Hg	7.3	3.3	3.1	5.1	6.0
26	40	26.6"Hg	10.7	4.8	4.5	7.7	8.8
27	63	19.5psig	14.1	6.5	6.6	11.2	12.4
28	80	27.5psig	18.4	8.0	8.4	14.1	15.8
29	123	49.8psig	27.2	3.2	13.5	22.2	24.3
32	25	5.3"Hg	2.4	0.9	1.3	1.8	2.2
33	60	13.3"Hg	6.0	2.3	2.7	4.0	5.0
34	120	25.9"Hg	10.4	3.6	4.2	7.1	8.4
35	181	17.9psig	13.1	4.9	6.0	10.1	11.0
36	240	24.0psig	16.6	7.6	8.4	13.6	14.0
37	320	40.0psig	23.7	10.6	11.0	19.4	19.1

TABLE V

EXPERIMENTAL TEMPERATURE DATA - NITROGEN POOL BOILING HEATER #6

Run#	Wattage	Heater Pressure	ΔT_t °F	ΔT_b - °F ΔT_b#2	 ΔT_b#3	 ΔT_b#5	Remarks
A-P6-1	15	3.40"Hg	1.4	0.5	1.0	1.0	Heater half
2	50	10.6"Hg	4.9	1.6	2.5	3.7	full with
3	100	24.2"Hg	9.8	3.2	2.9	8.2	liquid N_2
4	150	18.6psig	13.5	4.8	5.3	10.8	↓
5	198	27.5psig	18.4	5.1	6.4	15.5	
6	300	46.3psig	26.0	7.5	7.5	22.3	
9	15	7.3"Hg	3.3	2.0	2.1	2.9	
10	50	23.7"Hg	9.7	4.6	5.3	8.6	
11	100	23.0psig	16.0	6.6	8.7	14.1	
12	150	33.2psig	21.0	7.8	8.8	18.5	
13	200	42.6psig	24.6	8.4	9.1	22.3	
14	300	70.0psig	34.7	10.7	11.3		
17	150	25.0psig	17.0	5.4	5.2	11.4	Heater 2/3
18	300	78.0psig	35.6	9.8	8.7	24.3	full with
19	50	23.4"Hg	9.5	2.0	2.1	4.5	liquid N2

TABLE VI

EXPERIMENTAL TEMPERATURE DATA - NITROGEN POOL BOILING HEATER #9 (NICKEL PLATED)

Run#	Wattage	Heater Pressure	ΔT_t °F	ΔT_b - °F		
				ΔT_b#1	ΔT_b#2	ΔT_b#3
A-P9-2	15	4.8"Hg	2.1	.9	.9	1.5
3	25	7.6"Hg	3.6	1.4	1.3	2.2
4	40	12.3"Hg	5.6	2.0	1.9	3.1
5	60	18.5"Hg	7.9	2.8	2.5	4.3
6	80	24.5"Hg	10.0	3.2	2.8	5.3
7	120	37.0"Hg	13.8	3.8	3.2	6.3
8	160	22.5psig	15.8	4.5	3.8	7.4
9	220	32.0psig	20.7	4.8	4.0	8.9
10	300	54.5psig	28.0	5.4	4.6	11.7
11	400	80.5psig	36.2	6.2	5.3	13.9
14	15	9.0"Hg	4.2	1.8	1.8	2.4
15	25	13.4"Hg	6.0	2.3	2.3	3.4
16	40	20.6"Hg	8.7	2.8	2.7	4.8
17	60	30.7"Hg	11.9	3.2	3.2	6.1
18	80	19.6psig	14.1	3.6	3.6	7.3
19	113	24.0psig	16.6	4.5	4.2	9.5
20	155	41.5psig	24.2	-	-	-
21	222	67.5psig	32.8	-	-	-
22	162	43.5psig	25.0	-	-	-

TABLE VII

EXPERIMENTAL TEMPERATURE DATA - NITROGEN POOL BOILING HEATER #10 (CADMIUM PLATED)

Run#	Wattage	Heater Pressure	ΔT_t °F	ΔT_b - °F				
				ΔT_b#1	ΔT_b#2	ΔT_b#3	ΔT_b#4	ΔT_b#6
A-P10-2	60	18.6"Hg	8.0	5.6	5.6	8.2	9.0	12.9
3	120	17.0psig	12.6	9.0	8.0	14.6	15.5	21.6
4	180	27.0psig	18.1	12.7	11.0	20.0	20.6	29.0
5	300	56.0psig	29.4	16.6	12.9	29.7	29.7	42.8
8	60	32.0"Hg	12.4	8.8	7.5	13.1	14.8	20.2
9	120	31.0psig	20.0	12.5	10.0	23.2	24.0	33.4
10	180	50.0psig	27.3	16.8	6.6	31.8	29.2	43.8

TABLE VIII

EXPERIMENTAL TEMPERATURE DATA - NITROGEN POOL BOILING HEATER #7b

Run#	Wattage	Heater Pressure	ΔT_t ^oF	$\Delta T_b - {}^oF$					
				ΔT_b#1	ΔT_b#2	ΔT_b#3	ΔT_b#4	ΔT_b#5	ΔT_b#6
A-P7b-2	15	5.6"Hg	2.5	1.2	1.2	1.4	1.6	1.8	1.8
3	15	9.6"Hg	4.5	2.0	1.9	2.6	3.0	3.1	3.3
4	40	15.6"Hg	6.8	2.8	2.9	3.6	4.2	4.5	4.5
5	40	24.5"Hg	10.0	4.1	4.2	6.0	5.7	7.6	7.6
6	80	31.1"Hg	12.1	4.7	5.0	6.3	7.5	8.5	8.5
7	80	25.4psig	17.4	6.6	7.0	10.5	12.1	13.5	13.5
9	150	29.6psig	19.4	4.9	6.7	9.9	11.2	13.5	14.2
10	221	44.5psig	25.4	6.5	8.0	12.0	14.7	17.3	17.0
11	350	85.0psig	37.4	8.0	9.3	15.8	21.8	25.4	25.2
22	60	15.2"Hg	6.6	3.5	3.1	4.4	3.7	5.5	6.2
23	120	28.2"Hg	11.2	5.4	5.2	7.3	6.6	9.8	10.7
24	180	21.0psig	14.9	7.2	7.4	8.5	9.5	13.3	14.0
25	300	42.0psig	24.4	10.8	9.7	15.9	12.1	21.1	21.3
28	60	27.8"Hg	11.0	5.9	4.3	7.3	5.4	9.3	10.1
29	120	27.0psig	18.0	9.4	6.6	12.3	9.0	15.9	16.9
30	180	43.0psig	24.8	12.9	8.9	17.0	11.8	21.4	23.0

TABLE IX

EXPERIMENTAL TEMPERATURE DATA - NITROGEN POOL BOILING HEATER #8

Run#	Wattage	Heater Pressure	ΔT_t ^oF	ΔT_b - ^oF		
				ΔT_b#1	ΔT_b#2	ΔT_b#3
A-P8-2	50	9.5"Hg	4.4	2.7	3.1	3.8
3	50	17.5"Hg	7.6	4.7	5.3	6.5
4	100	13.7"Hg	6.1	3.8	3.9	5.3
5	100	33.9"Hg	12.9	7.5	8.0	10.2
6	150	21.1"Hg	8.8	8.6	9.0	11.2
7	150	23.0psig	16.0	10.3	10.6	13.9
8	200	28.2"Hg	11.2	6.7	6.7	10.2
9	200	32.0psig	20.4	12.2	12.3	17.4
10	300	24.0psig	16.6	10.6	10.0	14.4
11	400	37.0psig	22.4	12.1	12.2	16.1
12	300	51.3psig	27.8	16.4	15.2	23.9
13	400	66.8psig	32.6	18.6	17.5	25.6

TABLE X

EXPERIMENTAL TEMPERATURE DATA - NITROGEN ANNULAR GAP BOILING HEATER #12b -- 0.006" Gap

Run#	Wattage	Heater Pressure	ΔT_t °F	ΔT_b - °F			
				ΔT_b#1	ΔT_b#2	ΔT_b#3	ΔT_b#5
A-6-2	15	2.6"Hg	1.1	0.8	0.7	1.0	1.1
3	25	3.9"Hg	1.6	1.2	1.1	1.7	1.6
4	40	6.2"Hg	2.8	1.6	1.4	2.3	2.5
5	60	9.4"Hg	4.4	2.3	1.8	3.1	3.5
6	80	13.5"Hg	6.0	2.5	2.3	4.3	4.6
7	120	23.6"Hg	9.7	3.3	3.3	6.7	7.3
8	160	↗	↗	13.6	15.0	25.6	27.3
10	15	2.6"Hg	1.1	1.0	0.8	1.0	1.1
11	25	3.9"Hg	1.6	0.5	0.4	0.7	0.6
12	40	7.0"Hg	3.2	2.0	1.5	2.6	2.7
13	60	10.1"Hg	4.7	2.4	1.9	3.3	3.8
14	80	15.0"Hg	6.6	2.9	2.4	4.6	5.2
15	120	↗	↗	18.5	19.5	25.7	27.7
17	15	3.8"Hg	1.6	0.8	0.8	1.5	1.7
18	25	6.1"Hg	2.8	1.2	1.2	2.3	2.7
19	40	16.0"Hg	7.0	2.8	3.0	5.2	6.5
20	60	↗	↗	8.6	9.9	11.1	13.1
21	130	↗	↗	8.6	9.9	11.1	31.1

TABLE XI

EXPERIMENTAL TEMPERATURE DATA - NITROGEN ANNULAR GAP BOILING HEATER #6 -- 0.020" Gap

Run#	Wattage	Heater Pressure	ΔT_t ^oF	ΔT_b - ^oF ΔT_b#1	ΔT_b#2	ΔT_b#3	ΔT_b#5	ΔT_b#6	Remarks
A-20-2	15	2.1"Hg	0.8	0.7	0.7	1.0	0.8	0.9	Rotameter Connected
3	15	3.5"Hg	1.5	1.1	0.9	2.6	1.4	1.4	
4	15	4.1"Hg	1.8	1.0	1.1	1.4	1.7	1.7	
5	15	6.7"Hg	3.1	2.5	2.4	2.0	2.8	2.9	
6	15	9.4"Hg	4.4	↗	↗	↗	↗	↗	
7	15	11.4"Hg	5.2	↗	↗	↗	↗	↗	
8	15	4.2"Hg	1.8	1.4	1.2	1.5	1.8	1.7	
9	15	4.1"Hg	1.7	1.4	1.2	1.6	1.8	1.8	
10	50	6.5"Hg	3.0	1.3	1.1	1.7	1.7	2.0	
11	50	6.5"Hg	2.9	1.3	1.1	1.7	1.7	1.9	
12	50	11.3"Hg	5.2	2.4	2.5	2.7	2.9	4.0	
13	50	15.7"Hg	6.9	4.2	3.7	3.6	5.4	5.7	
14	50	20.5"Hg	8.6	5.7	5.4	4.7	7.0	7.2	
15	50	21.6"Hg	9.0	6.2	5.9	5.0	7.4	7.7	
16	50	6.5"Hg	3.0	1.6	1.3	2.0	2.0	2.2	
19	49	14.6"Hg	6.5	1.9	1.8	2.6	4.3	5.5	
20	49	14.5"Hg	6.4	1.9	1.8	2.6	4.3	5.2	
21	49	21.3"Hg	9.0	3.7	3.1	3.5	6.9	7.8	
22	49	27.4"Hg	10.9	4.9	4.4	4.3	8.6	9.6	
23	49	25.0psig	17.1	↗	↗	↗	↗	↗	

TABLE XI CONTINUED

Run#	Wattage	Heater Pressure	ΔT_t ^oF	ΔT_b - ^oF $\Delta T_b\#1$	$\Delta T_b\#2$	$\Delta T_b\#3$	$\Delta T_b\#5$	$\Delta T_b\#6$
A-20-26	150	17.9"Hg	7.7	2.5	2.3	4.1	4.6	6.3
27	150	19.6"Hg	8.4	---	---	---	---	---
28	100	12.2"Hg	5.5	1.7	1.5	3.5	3.6	4.6
29	100	12.2"Hg	5.5	---	---	---	---	---
33	15	1.9"Hg	0.8	0.7	0.4	2.7	0.4	0.5
34	15	1.9"Hg	0.8	0.7	0.5	1.8	0.6	0.9
35	14.5	------	---	0.8	0.5	1.9	0.5	1.0
36	14.5	2.4"Hg	1.0	0.6	0.4	1.6	0.5	0.9
37	14.5	3.5"Hg	1.5	0.8	1.7	1.7	1.0	1.1
38	14.5	1.8"Hg	0.7	0.5	0.3	1.4	0.2	0.9
39	14.5	3.4"Hg	1.4	0.7	0.6	1.6	1.0	1.1
40	14.5	1.8"Hg	0.7	0.5	0.4	1.4	0.3	0.9
41	14.5	1.8"Hg	0.8	0.5	0.4	1.3	0.2	0.9
42	50	5.7"Hg	2.6	1.2	1.1	2.3	1.8	2.3
43	50	5.7"Hg	2.5	1.3	1.2	2.6	2.0	2.4
44	50	5.7"Hg	2.5	1.4	1.3	2.4	2.2	2.6
45	50	6.4"Hg	2.9	1.4	1.3	2.6	2.5	2.8
45a	50	10.0"Hg	4.4	3.1	1.9	3.3	3.7	4.3
46	50	14.6"Hg	6.5	3.7	3.6	4.0	5.6	6.1
47	50	9.3"Hg	4.3	1.6	1.6	3.0	3.4	4.1

TABLE XI CONTINUED

Run#	Wattage	Heater Pressure	ΔT_t ^oF	$\Delta T_b - {}^oF$				
				ΔT_b#1	ΔT_b#2	ΔT_b#3	ΔT_b#5	ΔT_b#6
A-20-48	100	10.6"Hg	4.9	1.3	1.2	2.7	2.9	3.9
49	100	11.9"Hg	5.4	2.3	1.9	3.6	3.9	4.8
50	100	11.8"Hg	5.4	1.9	1.6	3.3	3.7	4.6
51	100	12.0"Hg	5.4	2.3	2.0	3.7	2.4	4.9
52	100	15.7"Hg	6.9	3.0	2.5	5.2	5.5	6.3
53	100	-------	---	3.3	2.7	5.2	6.2	7.1
54	100	23.2"Hg	9.6	4.7	4.2	5.4	8.0	9.9
55	150	16.0"Hg	7.0	3.1	2.5	4.2	4.9	6.3
56	150	18.2"Hg	7.8	3.6	2.9	4.6	5.8	7.3
57	150	19.0"Hg	8.1	3.7	2.9	4.6	6.0	7.5
58	150	23.0"Hg	9.5	4.0	3.4	6.1	7.5	8.8
59	200	-------	---	5.4	3.4	5.4	6.6	9.3
60	200	24.8"Hg	10.1	4.4	3.4	5.6	7.0	9.0
61	200	28.4"Hg	11.2	---	---	---	---	---
62	200	26.0"Hg	10.5	4.7	3.7	6.1	9.4	10.1
63	200	29.6"Hg	11.6	4.9	3.7	6.0	10.3	10.9
64	250	-------	-----	6.1	4.4	6.9	10.4	12.0
65	250	16.0psig	12.1	6.0	4.1	6.9	11.3	12.1
66	250	17.4psig	12.9	6.0	4.1	6.8	11.3	12.2
67	250	19.0psig	13.8	6.7	4.6	7.2	12.7	13.5

TABLE XI CONTINUED

Run#	Wattage	Heater Pressure	ΔT_t °F	ΔT_b - °F				
				ΔT_b#1	ΔT_b#2	ΔT_b#3	ΔT_b#5	ΔT_b#6
A-20-68	250	15.8psig	11.9	5.8	4.1	5.9	11.3	11.8
83	300	21.5psig	15.2	6.6	4.6	5.6	13.4	14.7
84	300	22.0psig	15.4	7.0	4.7	6.0	14.0	15.2
85	300	21.5psig	15.2	7.0	4.7	5.9	14.0	14.2
86	300	25.3psig	17.4	↗	5.8	6.6	15.0	16.9
87	350	21.5psig	15.2	↗	↗	↗	↗	↗
88	350	25.8psig	17.4	10.1	6.7	9.2	15.1	16.5
89	350	27.4psig	18.4	10.7	6.8	9.5	16.1	17.0
90	350	27.0psig	18.1	10.6	6.9	9.4	----	16.9

TABLE XII

EXPERIMENTAL TEMPERATURE DATA - NITROGEN ANNULAR GAP BOILING HEATER #9 (NICKEL PLATED) 0.021" GAP

Run#	Wattage	Heater Pressure	ΔT_t °F	ΔT_b - °F		
				ΔT_b#1	ΔT_b#2	ΔT_b#3
A-21-11	80	12.3"Hg	5.7	1.1	0.5	2.6
12	15	2.3"Hg	1.0	0.3	0.8	1.2
13	25	3.5"Hg	1.5	0.6	1.2	1.3
14	40	5.8"Hg	2.6	0.7	1.4	2.3
15	60	9.1"Hg	4.2	0.7	1.6	2.7
16	80	12.7"Hg	5.8	1.1	1.8	3.0
17	122	20.4"Hg	8.8	1.8	1.8	3.0
18	160	29.6"Hg	11.6	2.5	1.2	3.0
19	220	22.8psig	15.9	2.4	2.2	4.4
20	300	35.0psig	21.7	2.9	1.6	6.6
21	400	54.0psig	30.8	4.3	2.4	9.3

TABLE XII CONTINUED

Run#	Wattage	Heater Pressure	ΔT_t ^oF	$\Delta T_b - {}^oF$		
				ΔT_b#1	ΔT_b#2	ΔT_b#3
A-21-26	15	2.0"Hg	0.8	0.5	0.4	0.5
27	25	3.2"Hg	1.3	0.8	0.5	0.8
28	40	5.4"Hg	2.4	1.0	0.7	1.1
29	60	8.8"Hg	4.1	1.4	0.9	1.5
30	80	12.5"Hg	5.6	1.5	1.1	2.2
31	120	19.7"Hg	8.4	1.8	1.2	2.9
32	160	27.9"Hg	11.0	2.6	1.6	4.0
33	222	20.5psig	14.7	3.7	2.3	5.5
34	300	32.5psig	20.7	5.0	3.4	9.4
35	402	54.0psig	28.7	6.3	2.6	12.4

TABLE XIII

EXPERIMENTAL TEMPERATURE DATA - NITROGEN ANNULAR GAP BOILING HEATER #10 (CADMIUM PLATED) 0.022" GAP

Run#	Wattage	Heater Pressure	ΔT_t °F	ΔT_b - °F				
				ΔT_b #1	ΔT_b #2	ΔT_b #3	ΔT_b #4	ΔT_b #6
A-22-2	20	2.8"Hg	1.1	0.6	0.6	0.8	0.7	0.8
3	40	5.6"Hg	2.5	1.1	1.0	1.6	1.4	1.9
4	61	9.1"Hg	4.3	1.4	1.2	2.3	2.2	3.3
5	92	14.7"Hg	6.5	1.9	1.6	3.4	3.4	5.0
6	120	20.1"Hg	8.5	2.6	1.8	4.3	4.3	6.9
7	161	26.6"Hg	10.7	3.4	2.6	5.6	5.5	8.7
8	202	17.3psig	12.9	3.8	2.4	7.1	6.7	11.0
9	250	24.0psig	16.6	4.3	2.6	9.1	8.3	13.8
10	325	35.0psig	21.7	4.2	2.0	11.9	10.6	18.0
11	385	49.0psig	27.0	4.7	2.7	14.9	13.0	22.4
13	42	5.4"Hg	2.4	0.7	0.5	1.3	1.1	2.2
14	101	15.6"Hg	6.9	1.2	0.7	3.0	2.9	5.6
15	165	27.3"Hg	10.9	2.4	1.5	5.1	4.8	9.1
16	245	23.1psig	16.2	3.3	1.6	8.5	7.6	13.8
17	345	47.0psig	26.3	3.8	2.2	14.7	13.1	22.5
19	41	7.2"Hg	3.3	0.3	0.0	1.4	1.0	2.8
20	81	16.0"Hg	7.0	0.8	0.2	2.9	2.4	6.0
21	126	16.0psig	12.1	1.1	0.2	6.3	5.4	11.1
22	79	19.0psig	13.8	1.7	0.8	9.3	8.7	12.5

TABLE XIV

EXPERIMENTAL TEMPERATURE DATA - NITROGEN ANNULAR GAP BOILING HEATER #7b 0.053" GAP

Run#	Wattage	Heater Pressure	ΔT_t °F	ΔT_b - °F					Remarks
				ΔT_b#1	ΔT_b#2	ΔT_b#3	ΔT_b#4	ΔT_b#5	
A-53-2	15	3.3"Hg	1.4	1.1	1.1	1.1	1.2	1.2	15% of surface oxidized
3	40	6.9"Hg	3.2	2.1	2.2	2.2	2.5	2.7	
4	80	14.2"Hg	6.3	3.6	3.9	4.2	4.4	4.7	
5	150	28.8"Hg	11.4	4.8	5.9	6.8	7.9	10.2	
6	200	18.0psig	13.2	5.1	5.9	7.8	9.5	12.0	
7	250	25.5psig	17.4	6.1	6.4	9.3	11.6	14.9	
8	300	33.5psig	21.1	7.1	6.3	10.6	13.4	17.3	
9	400	51.0psig	27.6	8.2	8.0	13.5	17.7	22.8	
10	200	19.5psig	14.1	6.6	7.0	8.9	10.8	12.6	
13	15	2.8"Hg	1.2	1.1	1.1	1.0	1.1	1.9	
14	50	7.8"Hg	4.1	1.7	2.0	2.2	2.6	4.2	
15	150	25.2"Hg	10.2	3.1	4.5	5.2	6.5	9.2	
16	300	31.5psig	20.2	4.5	5.1	8.9	12.0	16.9	
17	400	51.0psig	27.6	5.2	5.5	11.4	15.8	22.4	
18	15	2.8"Hg	1.2	0.2	0.1	0.0	0.3	0.2	
19	15	3.6"Hg	1.5	0.3	0.1	0.3	0.4	9.7	
20	50	11.9"Hg	5.4	1.2	1.5	2.0	2.5	4.2	
21	150	20.0psig	14.4	2.7	3.4	6.6	8.3	12.7	
22	300	63.0psig	31.5	4.3	4.8	13.5	18.2	27.5	
23	400	111.0psig	43.4	4.9	5.5	16.9	22.1	39.5	

TABLE XIV CONTINUED

Run#	Wattage	Heater Pressure	ΔT_t °F	ΔT_b - °F					Remarks
				ΔT_b#1	ΔT_b#2	ΔT_b#3	ΔT_b#4	ΔT_b#5	
A-53-24	15	3.0"Hg	1.2	0.3	0.3	0.5	0.8	4.3	15% of surface oxidized
25	15	7.0"Hg	3.2	1.2	1.1	1.7	2.0	2.8	
26	50	22.4"Hg	9.3	2.5	2.8	9.3	6.1	8.1	
27	150	53.0psig	28.4	5.7	5.7	17.4	19.6	25.5	
30	15	3.1"Hg	1.3	0.7	0.7	0.8	0.9	0.6	Surface completely cleaned
31	40	7.3"Hg	3.4	1.0	1.3	1.4	1.8	2.3	
32	80	15.2"Hg	6.7	2.0	2.5	3.6	3.9	4.9	
33	148	26.6"Hg	10.7	3.3	4.8	5.7	6.3	8.4	
34	220	22.5psig	15.8	4.8	6.5	7.2	10.2	12.5	
35	350	48.5psig	26.8	6.1	7.7	12.2	16.7	20.5	
38	150	69.5psig	4.2	1.4	1.4	1.9	2.6	3.6	
39	120	--------	----	2.3	3.0	3.9	5.4	8.1	
40	120	23.6"Hg	9.7	2.5	3.3	4.3	5.5	8.0	
41	230	21.8psig	15.3	2.8	4.2	5.9	8.3	12.6	
42	370	41.0psig	24.0	5.7	6.3	10.7	15.1	20.3	
44	60	11.0"Hg	5.0	1.8	2.4	2.4	3.0	4.3	
45	25	4.1"Hg	1.8	0.7	0.9	1.0	1.2	1.6	
46	25	------	----	0.6	0.7	1.0	1.0	1.9	
47	40	8.5"Hg	4.0	0.9	1.0	1.3	1.5	2.7	
48	80	19.3"Hg	8.2	1.6	2.0	3.0	3.7	6.8	
49	120	16.5psig	12.4	0.7	1.1	3.6	5.1	9.9	

TABLE XIV CONTINUED

Run#	Wattage	Heater Pressure	ΔT_t $^{\circ}F$	$\Delta T_b - {^{\circ}F}$						Remarks
				ΔT_b#1	ΔT_b#2	ΔT_b#3	ΔT_b#4	ΔT_b#5	ΔT_b#6	
A-53-50	150	20.5psig	14.7	1.0	1.6	4.7	7.6	12.0	—	Surface
51	220	36.0psig	22.0	---	---	9.1	11.9	19.0	—	completely
55	15	7.2"Hg	3.4	1.1	1.9	1.9	2.7	8.9	—	cleaned
56	40	18.4"Hg	7.9	2.2	3.0	4.2	5.5	7.1	—	
A-53a-2	25	4.7"Hg	2.0	0.8	1.0	1.4	1.2	1.7	1.5	
3	61	11.9"Hg	5.4	2.0	2.5	3.4	1.9	4.4	4.6	
4	122	23.3"Hg	9.6	3.7	4.7	6.1	5.7	8.6	8.9	
5	179	15.0psig	11.6	4.7	7.3	8.8	8.9	11.3	11.6	
6	250	26.8psig	18.0	8.3	8.8	12.6	10.7	15.7	16.1	
7	320	40.0psig	23.6	9.2	9.2	15.8	11.1	19.8	19.0	
8	400	56.5psig	29.5	11.1	10.4	19.3	12.8	25.5	23.7	
10	30	5.6"Hg	2.5	0.9	1.1	1.5	1.3	1.8	2.3	
11	70	14.1"Hg	6.3	1.9	2.2	3.3	2.8	4.9	5.7	
12	120	26.8"Hg	10.8	3.4	3.5	5.8	5.0	8.9	9.6	
13	173	20.4psig	14.8	5.1	5.0	9.3	7.4	12.7	13.0	
14	240	30.7psig	19.9	7.3	6.1	12.2	9.6	16.5	16.8	
15	352	55.0psig	28.8	12.2	9.1	18.1	13.0	25.7	24.4	
17	30	8.9"Hg	4.1	0.9	1.1	1.9	0.9	2.5	2.2	
18	71	19.7"Hg	8.4	2.2	2.4	4.0	2.6	6.1	6.0	
19	120	18.5psig	13.6	4.5	3.6	7.7	5.4	11.4	11.4	
20	180	30.6psig	19.8	7.7	6.0	12.2	9.3	16.7	16.4	
21	83	24.5psig	16.9	10.4	5.7	12.0	7.9	14.7	14.3	
22	129	50.5psig	27.5	17.9	10.1	20.1	13.7	24.3	23.8	

TABLE XV

EXPERIMENTAL TEMPERATURE DATA - NITROGEN ANNULAR GAP BOILING HEATER #8 0.080" GAP

Run#	Wattage	Heater Pressure	ΔT_t °F	ΔT_b - °F ΔT_b#1	 ΔT_b#2	 ΔT_b#3	 ΔT_b#4
A-80-13	15	3.4"Hg	1.4	1.1	0.9	1.3	1.1
14	15	3.6"Hg	1.5	1.1	1.0	1.0	1.2
15	15	4.2"Hg	1.8	1.0	1.0	0.8	1.3
16	15	8.0"Hg	3.7	---	2.3	2.3	2.5
17	15	7.0"Hg	3.2	---	2.0	2.2	2.4
18	15	3.6"Hg	1.6	1.1	1.2	1.5	1.2
19	15	3.0"Hg	1.2	1.2	1.2	1.6	1.2
20	15	3.0"Hg	1.3	1.6	1.5	2.0	1.4
22	50	8.2"Hg	3.8	2.9	2.7	3.6	3.1
23	50	9.0"Hg	4.2	2.9	2.8	3.4	3.3
24	50	18.4"Hg	7.9	---	4.7	5.5	6.0
26	100	16.7"Hg	7.3	3.4	4.2	5.2	5.4
27	100	18.2"Hg	7.8	3.9	4.5	5.6	7.0
28	100	36.0"Hg	13.5	4.8	7.3	8.9	10.1
29	50	7.6"Hg	3.6	3.4	3.3	3.9	3.2
30	50	9.0"Hg	4.2	3.3	3.2	3.9	3.3
32	15	3.0"Hg	1.2	2.6	2.2	2.6	1.5
33	15	3.6"Hg	1.5	2.4	2.0	2.5	1.7
34	15	6.7"Hg	3.1	2.6	2.7	3.2	2.8
37	150	25.1"Hg	10.2	3.2	4.7	5.8	7.1

TABLE XV CONTINUED

Run#	Wattage	Heater Pressure	ΔT_t ^oF	ΔT_b - ^oF			
				ΔT_b#1	ΔT_b#2	ΔT_b#3	ΔT_b#4
A-80-38	150	28.3"Hg	11.2	3.4	5.1	6.4	7.8
39	150	28.6psig	18.9	6.6	9.2	10.8	13.3
41	200	32.5"Hg	12.5	4.3	5.7	9.1	10.0
42	199	18.7psig	13.6	4.2	5.5	9.1	10.0
43	199	37.2psig	22.6	9.4	10.4	13.0	15.6
45	250	20.6psig	14.8	4.1	6.5	8.7	10.8
46	250	24.0psig	16.6	4.2	7.1	9.8	11.7
47	250	45.4psig	25.8	---	11.0	14.3	17.7
48	300	26.7psig	18.0	4.6	7.3	10.4	12.4
49	300	27.0psig	18.1	---	7.8	11.3	13.4
50	301	52.0psig	27.9	---	11.5	14.8	19.2
58	100	17.6"Hg	7.6	3.2	3.8	5.2	5.7
59	99	32.1"Hg	12.4	4.0	6.3	7.7	9.2
60	99	16.2"Hg	7.1	3.1	3.6	4.7	5.1
62	400	44.5psig	25.4	---	8.9	13.6	16.2
63	400	51.5psig	27.8	---	8.2	13.2	16.2
64	400	128.5psig	47.0	---	29.2	21.4	---
65	400	123.5psig	46.0	---	---	---	41.2
66	400	59.0psig	30.3	---	---	---	24.4
67	400	57.5psig	30.1	---	12.5	15.1	---

TABLE XVI

EXPERIMENTAL TEMPERATURE DATA - NEON ANNULAR GAP BOILING - 0.006" Gap

Run#	Wattage	Heater Pressure	ΔT_t °F	ΔT_b - °F		
				ΔT_b#1	ΔT_b#3	ΔT_b#5
B-6-2	15	4.0"Hg	.7	0.4	0.4	0.6
3	40	10.2"Hg	1.7	0.4	0.2	0.9
4	80	↗	↗	↗	↗	↗
6	26	6.7"Hg	1.1	0.4	0.8	1.0
7	35	9.5"Hg	1.6	0.5	1.0	1.2
8	46	12.9"Hg	2.1	0.5	1.1	1.3
9	55	↗	↗	↗	↗	↗
10	10	3.8"Hg	.6	0.6	0.2	0.6
11	20	5.8"Hg	1.0	0.9	0.6	1.2
12	50	↗	↗	↗	↗	↗
13	30	31.6"Hg	4.7	4.4	3.3	4.1

TABLE XVII

EXPERIMENTAL TEMPERATURE DATA - NEON ANNULAR GAP BOILING - 0.020" Gap

Run#	Wattage	Heater Pressure	ΔT_t ^oF	ΔT_b - ^oF					
				ΔT_b#1	ΔT_b#2	ΔT_b#3	ΔT_b#4	ΔT_b#5	ΔT_b#6
P-20-6	15	------	---	0.4	0.4	---	---	0.6	---
7	40	15.0"Hg	2.5	0.4	0.6	0.6	0.9	0.9	---
8	15	5.5"Hg	0.9	---	0.6	---	---	0.9	---
9	80	30.5"Hg	4.6	0.9	2.0	1.4	1.8	1.8	0.9
10	150	35.0psig	8.4	1.8	5.2	3.7	4.8	4.4	4.4
11	150	35.0psig	8.4	4.6	7.3	6.5	8.6	11.5	11.6
12	150	35.0psig	8.4	6.3	6.5	8.2	10.2	13.5	11.3
13	150	35.0psig	8.4	5.2	3.8	2.7	3.8	8.2	7.3
14	220	64.2psig	12.4	---	---	---	---	2.4	1.6
20	72	29.5"Hg	4.5	11.0	11.4	13.5	13.5	---	12.8
21	72	29.6"Hg	4.5	11.2	11.6	11.9	12.3	15.5	15.1

TABLE XVIII

EXPERIMENTAL TEMPERATURE DATA - NEON ANNULAR GAP BOILING HEATER #9 (NICKEL PLATED) 0.021" GAP

Run#	Wattage	Heater Pressure	ΔT_t °F	ΔT_b - °F		
				ΔT_b #2	ΔT_b #3	ΔT_b #4
B-21-4	15	14.4"Hg	2.4	0.6	0.4	0.6
5	30	23.5"Hg	3.7	0.6	0.9	0.9
6	50	19.0psig	5.6	0.0	0.6	0.6
9	50	19.1psig	5.7	---	---	0.6
10	80	30.4psig	7.7	---	0.4	1.1
11	121	47.2psig	10.3	0.4	0.8	2.0
12	161	68.0psig	13.1	0.8	1.5	3.0
13	204	90.5psig	15.5	1.3	2.1	2.6

TABLE XIX

EXPERIMENTAL TEMPERATURE DATA - NEON ANNULAR GAP BOILING HEATER #7b 0.053" GAP

Run#	Wattage	Heater Pressure	ΔT_t ^oF	ΔT_b - ^oF				
				ΔT_b#1	ΔT_b#2	ΔT_b#3	ΔT_b#4	ΔT_b#5
B-53-2	15	8.5"Hg	1.4	0.6	0.8	0.8	0.6	0.6
3	40	19.1"Hg	3.1	1.6	2.4	2.2	2.2	2.0
4	80	18.9psig	5.6	2.9	3.7	3.5	3.7	4.4
5	150	38.0psig	8.8	4.4	3.7	4.4	4.8	6.5
6	400	20.2psig	23.6	9.4	5.2	6.9	15.7	19.2
8	250	95.0psig	15.9	10.5	5.4	11.3	10.5	16.1
9	200	66.0psig	12.8	10.7	5.4	10.0	9.0	15.3
10	150	46.0psig	10.0	10.7	5.4	9.4	7.5	13.7

TABLE XX

EXPERIMENTAL TEMPERATURE DATA - NEON ANNULAR GAP BOILING HEATER #8 0.080" GAP

Run#	Wattage	Heater Pressure	ΔT_t ^oF	ΔT_b - ^oF				
				ΔT_b #1	ΔT_b #2	ΔT_b #3	ΔT_b #4	ΔT_b #5
B-80-2	15	9.1"Hg	1.5	---	---	0.4	0.4	0.6
3	40	22.1"Hg	3.6	0.4	0.4	1.0	0.8	1.0
4	80	25.0psig	6.7	0.6	0.6	1.8	1.3	2.0
5	150	54.2psig	11.3	1.3	1.3	2.9	3.1	3.8
6	220	89.0psig	14.9	2.2	2.4	4.2	4.8	5.7
7	220	87.6psig	14.8	2.2	2.6	4.4	5.2	5.7
8	350	179.0psig	22.2	3.3	4.6	6.9	9.0	9.4
10	25	14.4"Hg	2.4	0.4	0.6	0.8	0.8	1.0
11	60	18.0psig	5.4	1.0	1.3	2.0	2.2	2.6
12	100	31.8psig	7.8	1.0	1.6	2.2	2.9	3.5
14	70	21.0psig	5.9	0.6	1.3	1.8	2.4	2.6
15	450	280.0psig	27.2	4.6	6.5	8.6	17.5	13.7

TABLE XXI

EXPERIMENTAL DATA - NEON POOL BOILING HEATER #12b

Run#	Wattage Watts	Submergence "	Q Btu/hr	Q/A_w Btu/hr ft^2	Heater Pressure	ΔT_t °F
B-P12b-2	15	7 1/2	51.2	104.4	6.9"Hg	1.1
3	40	7 1/2	136.5	278.3	11.1"Hg	1.8
4	80	7 1/2	273.0	556.7	20.5"Hg	3.3
5	150	7 1/2	512.0	1044	19.0psig	5.6
6	250	7 1/2	853.3	1740	45.5psig	10.0
7	350	7 1/2	1195	2435	117.0psig	17.7
9	15	3 3/4	51.2	208.7	8.1"Hg	1.3
10	40	3 3/4	136.5	556.5	15.4"Hg	2.5
11	80	3 3/4	273.0	1160	25.4"Hg	4.0
12	150	3 3/4	512.0	2087	21.7psig	6.1
13	250	3 3/4	853.3	3478	47.0psig	10.2
14	350	3 3/4	1195	4870	102.7psig	16.6

Experimental Observations

The design of the experimental section incorporated the concept of visual observation and picture taking of boiling nitrogen and neon in the narrow annuli. Unfortunately, picture taking proved to be extremely difficult on account of the seven glass surfaces between the heater surface and the camera lens. These many surfaces resulted in distortion and glare which prevented good clear pictures. However, in spite of these difficulties several pictures and about 100 to 200 feet of 16 mm movies were sufficiently clear to permit close study of the boiling phenomena.

Visual observation during the runs was possible most of the time. Efforts were made to avoid frosting of the dewar surfaces by proper purging and good sealing of the dewar assembly so that observation would not be hampered by snow or frost. This was not always possible, particularly in the case of the neon boiling experiments where frosting was a serious problem.

It should be noted, that in spite of substantial effort during the machining of the heater surfaces, to have all the surfaces identical, a variation in the surface roughness of 6 to 20 micro-inches RMS between heaters, was measured with a Profilometer. A complete description of the surface finish of each heater is included in Appendix F.

At this time some general observations can be made regarding pool and annular gap boiling, for both nitrogen and neon runs. These observations are very similar to the ones made by other investigators with water and organic chemicals. Two of the most common behaviors reported in the literature were also observed in this study. These are described in paragraphs a and b below.

a. The occurrence of overheated surface at the beginning of some runs where boiling did not start until the surface temperature reached a certain level. The boiling suddenly occurred over the whole surface and the surface temperature was rapidly lowered to its normal level. Whenever this behavior occurred, the heater pressure, which is directly related to the wall temperature, would vary by about 20 to 30 psi representing 4 to 8°F. The sudden boiling was almost explosive in nature and the entire surface was covered with bubbles. This occurred even at low heat fluxes but was more prevelent at the higher heat fluxes.

b. Patch-to-patch boiling occurred frequently at the higher heat fluxes (600 Btu/hr-ft^2). This behavior consisted of having small patches of boiling surface shifting from place to place. It seemed that the whole patch moved from one location to the other. These patches were square in shape having about 1 x 1-inch sides.

Shifting of the boiling patches did not follow any pattern and was completely random.

c. In contrast to the patch-to-patch boiling described above, it also appeared that certain sites once activated with nucleate boiling remained active throughout the run. These active sites which were usually obtained on increasing heat flux remained active even when the heat flux was reduced. The sites were random and usually occurred at different spots from run to run. It appeared that the most permanent sites were the ones obtained during the sudden boiling described in (1) above. When the violent boiling started with an overheated surface many active sites were maintained throughout this particular series of runs.

d. The cadmium plated heater (heater no. 10) had several small patches of copper showing on the surface. Observations during the boiling runs with this heater indicated that the boiling on this heater was of the same nature as the boiling on the other heaters. There was no preferential boiling or lack of it on the copper patches.

e. It was mentioned earlier (p. 59) that experimental difficulties prevented measurement of entrainment. Observations showed that the occurrence of entrainment depended on the outer submergence and heat flux. In general there was no entrainment with an outer submergence of about 6 inches or less at low heat fluxes of the order of 100 - 200 Btu/hr-ft^2. At higher heat fluxes, a lower outer submergence was necessary to prevent entrainment.

Entrainment was easy to observe, since the liquid in the annulus was rather clear except for about 1/2 - 1 inch of cellular type clear foam. This foam was light in texture, consisting of 70-80% void space, and was clearly defined in all cases, except for the heater with the 6 mil gap. With this very narrow gap width, the foam covered 2 to 3 inches of the surface and often consisted of a large bubble flattened between the heater surface and the Pyrex pipe.

Neon entrainment appeared slightly larger than nitrogen entrainment, otherwise the two were very similar.

f. The effect of back pressure resulting from the use of a rotameter to measure boil-off was very noticeable. When the rotameter was connected, the inner submergence was always lower than the outer one, and the foam on top of the liquid was very shallow, about 1/4-inch, and very clearly defined. There never was any entrainment in this case.

When the test section operated as a true thermosyphon reboiler, without a rotameter connection, the inner submergence was always higher than the outer one, and was topped with 1/2 - 1-inch foam made up of larger bubbles than in the previous case.

g. Even though the foam on top of the liquid in the annulus was rather sharply defined, it did fluctuate by about 1/4 to 1/2-inch depending on the heat flux. Measurements of the inner submergence were obtained at the maximum height of the foam throughout the particular run. This therefore gave a maximum wetted surface for each run, resulting in minimum calculated heat flux. Any error resulting from this fluctuation was small at the higher submergences but could be quite significant at the very low inner submergences of 1 to 2 inches. At the 2-inch level an error of 1/4 inch would result in an error of wetted surface calculation of 12 1/2%, while it would be about 3% at the 7-inch level.

h. The pool boiling runs showed about the same type of bubbling as the annular gap boiling. In the case of pool boiling a small crown of liquid surrounded the heater surface at the free liquid surface. The crown about 1/4 to 1/2-inch high acted as a shower around the heater. This was the result of thermal pumping generated by the surface bubbling. In this case calculation of the wetted surface was based on the height of the crown rather than on the height of the liquid free surface.

i. The heater design consisted of a 7 1/2-inch copper surface or copper plated with nickel or cadmium surface with two formica sleeve insulators at both ends of the heater. The formica sleeves were epoxied to the heater and efforts were made to avoid any cracks and/or crevices between the formica and the heater. It was hoped that this area would not offer any areas of preferential boiling. However, boiling did occur preferentially at this location with a ring of bubbles originating at this section between the formica sleeve and the heater element. It was noted that in general a substantial fraction of the boiling took place at the intersection of the formica and the heater with scattered boiling on the surface. However, as the heat flux increased the amount of boiling taking place on the surface increased. It was mentioned earlier that under certain conditions active sites would remain active regardless of the changes in heat fluxes. When this occurred it was noticed that the same heat flux was obtained at the same ΔT whether boiling originated at the formica-heater joint or elsewhere on the surface.

j. There were only two behaviors which occurred exclusively in the case of gap boiling. One of them related to the oscillation of bubbles in the gap. Very tiny bubbles forming on the surface or at the bottom of the heater at the formica joint, appeared to dance in the annulus prior to rising to the surface. This appeared to be a more frequent occurrence with neon boiling than with nitrogen. However, it did very clearly occur with both liquids. The second behavior was of the same nature as the bubble oscillation except that it was more extreme. It was a case of slugging during which the vapor being formed on the surface forced all the liquid downward and the heater was then completely dry for a fraction of a second. Liquid then re-entered the gap and the slugging recurred. This slugging occurred only at high heat fluxes in the order of 1000 Btu/hr-ft^2. It is interesting to note that slugging was not always reproducible even when high heat fluxes were reached. It was noticed that at a given heat flux the driving force was about the same with and without slugging.

k. Preliminary testing performed with a 4-mil gap heater showed that the gap was so small that the heater itself could not be wetted, thus resulting in a very high resistance to heat flow which prevented the reaching of equilibrium conditions. This condition was partially remedied by increasing the gap size to 6 mils, which indicates that a 5 to 6-mil gap is a minimum gap size consistent with annular gap boiling.

l. Maximum heat fluxes were reached with nitrogen only with the 6 mil gap heaters. Whenever a heat flux exceeded 850 Btu/hr-ft^2 the heater temperature kept rising without reaching equilibrium. With neon, maximum heat fluxes were reached with both the 6 mil and 20 mil gap heaters. These were 350 and 1600 Btu/hr-ft^2 for the 6 and 20 mil gap heaters.

m. Liquid neon boiling runs introduced several difficulties which were not experienced with nitrogen. The main difficulty was due to the freezing out of air, and CO_2 impurities and creating a snowy surface on the dewar windows. This made visual observation of the neon runs quite difficult. Furthermore the solid air at times plugged the annulus shut and runs could not be made until the whole section was warmed and the plug thawed. In order to prevent this difficulty a very fine screen was attached to the bottom of the heating section to trap out all the solid CO_2 and air. In spite of the screen, plugging did occur several times and runs had to be repeated. The neon data are much more scattered than the nitrogen data, and it is believed that this scattering may be due to the effect of these solid particles partially plugging the heater or even possibly covering some of the heater surface and therefore changing the available heating surface for boiling. All efforts were made to prevent this from occurring and whenever this effect could be seen on the surface the data were rejected and the runs repeated.

VI. TREATMENT OF EXPERIMENTAL DATA

Pool Boiling

The experimental data for the pool boiling runs consisted of: wattage, heater pressure, electromotive force generated by the wall thermocouples, and heater submergence.

Since the main purpose of the pool boiling runs is to establish a basis for the evaluation of the annular gap boiling, the data are treated in the conventional manner, i.e., relating heat fluxes to driving force, for each heater tested. The calculations involved in the reduction of the pool boiling data are identical to the first steps involved in the calculation of the annular gap boiling data, therefore a complete calculation of a typical annular gap boiling run will also demonstrate the data reduction method for pool boiling. Calculations for run A-6-5 which follow, will suffice.

Annular Gap Boiling

Observation of the annular gap boiling showed the existence of a convective type of heat transfer disturbed by bubbles rising to the surface. Actually, the heater surface was completely covered by a layer of liquid which was interrupted only at the bubble sites. Furthermore, it was noted that the actual bubble site area was a small fraction of the total heating area. It appeared that the only effect of the rising bubbles was to increase the turbulence of the liquid flowing in the annulus.

In view of these observations, it is reasonable to treat the annular gap boiling case in a manner similar to the one used for convective heat transfer. This approach was used by other investigators (49, 52, 56) and was the starting point of most theoretical derivations (9, 27, 62). However, factors affecting bubble formation and behavior should also be considered.

The following factors affecting convective heat transfer, bubble formation and behavior should be considered:

h_b	heat transfer coefficient for boiling
u	fluid velocity
ρ_L	liquid density
ρ_V	vapor density
Cp_L	liquid specific heat
Cp_V	vapor specific heat
D	characteristic dimension
k_L	liquid thermal conductivity
k_V	vapor thermal conductivity
L	wetted length of surface
μ_L	liquid viscosity
μ_V	vapor viscosity
σ	surface tension
K_H	conversion from kinetic energy to heat
g_c	conversion from force to mass
P_V	vapor pressure
λ	latent heat

Since it was observed that heat is transferred through a liquid film, only liquid properties for thermal conductivity, density, and heat capacity should be considered in addition to vapor density, surface tension and the rate of change of vapor pressure which influence bubble formation on growth.

The rate of change of vapor pressure with temperature is defined by the Clausius-Clapeyron equation which approximates to

$$\frac{dP_V}{dT} = \frac{\lambda P_V}{R\ T_2} \qquad (64)$$

Since the vapor pressure is directly related to the boiling temperature, only one of the variables of equation 64 need be considered.

The rate of boil-off is directly related to latent heat and heat input, $W = Q/\lambda$, and W in turn is directly related to the fluid velocity, $u = (W/\rho)/A_t$, therefore only one of the factors u or λ is needed.

The change in specific volumes $\left(\frac{1}{\rho_V} - \frac{1}{\rho_L}\right)$ affects the bubble behavior. This expression can be rewritten as $\left[1/\rho_L\right]\left[(\rho_L/\rho_V) - 1\right]$, and the density ρ_L and dimensionless term $\left[(\rho_L/\rho_V) - 1\right]$ can be considered separately.

A dimensional analysis of all factors mentioned above results in the following dimensionless groups:

Nusselt Number: $$\frac{h_b\ D}{k_L} \tag{65}$$

Reynolds Number: $$\frac{D\ u\ \rho}{\mu_L} = \frac{D\ G}{\mu_L} \tag{66}$$

Prandtl Number: $$\frac{Cp_L\ \mu_L}{k_L} \tag{67}$$

Length to **Characteristic Dimension Ratio:** L/D (68)

Ohnesorge Number: $$\frac{\mu_L{}^2}{\rho_L\ g_c\ D\sigma} \tag{69}$$

$$\frac{\mu_L{}^2}{\rho_L\ g_c\ D^2\ P_V} \tag{70}$$

and generalized equation

$$\frac{h_b\ D}{k_L} = a' \left(\frac{D\ G}{\mu_L}\right)^b \left(\frac{L}{D}\right)^c \left(\frac{Cp_L\ \mu_L}{k_L}\right)^d \left(\frac{\mu_L{}^2}{\rho_L\ g_c\ D\sigma}\right)^e$$

$$\times \left(\frac{\mu_L{}^2}{\rho_L\ g_c\ D^2\ P_V}\right)^f \left(\frac{\rho_L}{\rho_V} - 1\right)^g \tag{71}$$

It should be noted that other relations between σ and P can be obtained such as $(P_V\ D/\sigma)$ which assumes that $e = -f$. The dimensionless group $(P_V\ D/\sigma)$ was actually used by McNelly in his generalized correlation (49).

The present experimental work covering liquid nitrogen and neon only, does not permit determination of the exponents for all the terms of Equation (71). It is proposed to combine all the groups affecting bubble behavior in a new term

$$a = a' \left(\frac{\mu_L^{\,2}}{\rho_L \, g_c \, D \, \sigma} \right)^e \left(\frac{\mu_L^{\,2}}{\rho_L \, g_c \, D^2 \, P_V} \right)^f \left(\frac{\rho_L}{\rho_V} - 1 \right)^g \tag{72}$$

and to modify Equation (71) as follows:

$$\frac{h_b \, D}{k_L} = a \left(\frac{D \, G}{\mu_L} \right)^b \left(\frac{L}{D} \right)^c \left(\frac{Cp_L \, \mu_L}{k_L} \right)^d \tag{73}$$

An additional modification to Equation (73) is necessary, namely, the substitution of a significant dimension for the characteristic length D. The conventional equivalent diameter, D_e, for annular gaps was selected where $D_e = \frac{4 \text{ x flow area}}{\text{wetted perimeter}}$.

The final equation is now:

$$\frac{h_b \, D_e}{k_L} = a \left(\frac{D_e \, G}{\mu_L} \right)^b \left(\frac{L}{D_e} \right)^c \left(\frac{Cp_L \, \mu_L}{k_L} \right)^d \tag{74}$$

This equation includes the most important properties affecting heat transfer, as well as the characteristic dimensions of the annular gap. The coefficient and exponents of this equation can now be calculated from the experimental data obtained in this work.

Since heat transfer coefficients are a derived quantity, it is important to discuss the operations required in the reduction of data.

The experimental data consisted of the following: wattage, heater pressure, electromotive force generated by the wall thermocouples, heater inner and outer submergences, and gap size. Measurements of the surface roughness, and heater plating, if any, were also reported for each series of runs. A complete calculation for run A-6-5 will demonstrate the data reduction method.

Experimental Data - Run A-6-5

Heater 12b, heater OD 2.9975-inches at ambient temperature,

Precision Pyrex sleeve ID 3.0015-inches at ambient temperature

Copper heater - surface roughness as determined by Profilometer measurement: 9-10 micro-inches

Fluid tested: nitrogen

Wattage	Heater Pressure	Outer Submergence	Inner Submergence
60 watts	9.4 " Hg	7 1/2 "	7 1/2 " +

Wall Thermocouples - emf mv

TC #1	TC #2	TC #3	TC #4	TC #5	TC #6
0.086	0.069	0.073	-----	0.059	-----

Gap Size

$$t = \frac{3.0015'' - 2.9975''}{2} + 0.004'' = 0.006''$$

where 0.004" is the correction due to contraction (Calculations for the contraction correction are detailed in Appendix D).

Heat Input: $Q = 3.413$ Btu/watt-hr x 60 watts = 204.8 Btu/hr.

Wetted Area:

$$A_w = \frac{\pi \times 2.9975''}{12} \times \frac{7.5''}{12} = 0.4905 \text{ ft}^2$$

The area A_w, used to calculate heat fluxes was the heater area which was actually wetted by the boiling liquid. As mentioned earlier, the liquid in the annular gap was topped by a well defined foam. The top of the foam was visually measured to ±0.1" and this measurement defined as inner submergence, was used in the calculation of A_w. In the case of fluctuation in the foam level, the maximum wetted height was always measured.

Heat Flux:

$$Q/A_w = \frac{204.8 \text{ Btu/hr}}{0.4905 \text{ ft}^2} = 417.5 \text{ Btu/hr-ft}^2$$

Heat transfer coefficient to the nitrogen vapor phase across a natural convective film, is less than 1 Btu/hr-ft^2-°F. The assumption that all power input to the electric element is dissipated by boiling and transferred through the wetted surface only, results in a negligible error of less than 1%.

In view of the above, it was decided to calculate all heat fluxes on the basis of wetted area only and to ignore the negligible heat transfer from the non-wetted surface. The calculated heat flux was always a minimum value since it was based on a maximum wetted area.

Overall Temperature Driving Force: $\Delta T_t = 4.4^{\circ}F$

The overall temperature driving force is the temperature difference between the temperature of the boiling-condensing nitrogen inside the heater, and the saturation temperature of the liquid nitrogen surrounding the test section. In other words, it is the sum of the temperature drop across the condensing film inside the heater, the copper wall, and the boiling film outside the heater. Since the temperature drop across the heater is in the order of 0.01 and 0.2°F for 50 and 1300 Btu/hr heat input respectively, the wall resistance to heat transfer can be neglected.

ΔT_t is obtained from the heater pressure curves, Figures 13 or 15, which are calculated from vapor pressure data for nitrogen (1). The vapor pressure data for neon (1) have also been reduced in a similar manner, i.e., pressure as a function of temperature difference between the temperature of the boiling-condensing liquid inside the heater and the normal boiling temperature of the liquid surrounding the heater. Figures 13 and 14 represent the neon pressure curves.

Boiling Temperature Driving Force: $\Delta T_b = 2.8^{\circ}F$

The boiling temperature driving force is the temperature drop across the boiling film surrounding the heater, i.e.,

ΔT_b = wall temperature - normal boiling temperature of liquid.

This temperature difference was measured directly by means of wall thermocouples, having their cold junctions immersed in the liquid being tested. A zero point for each thermocouple was

FIGURE 13, HEATER PRESSURE VERSUS TEMPERATURE DIFFERENCE

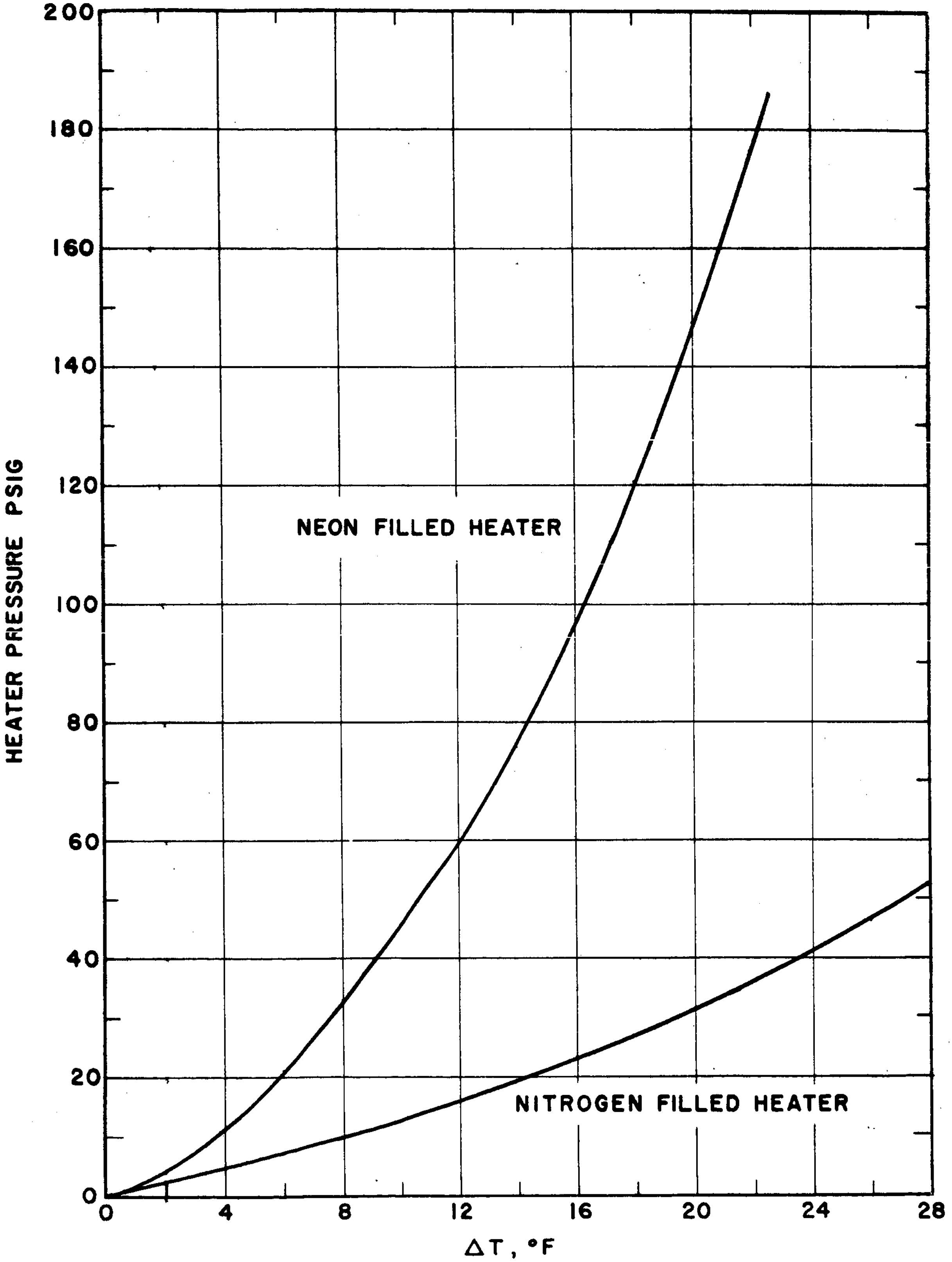

FIGURE 14, HEATER PRESSURE VERSUS TEMPERATURE DIFFERENCE

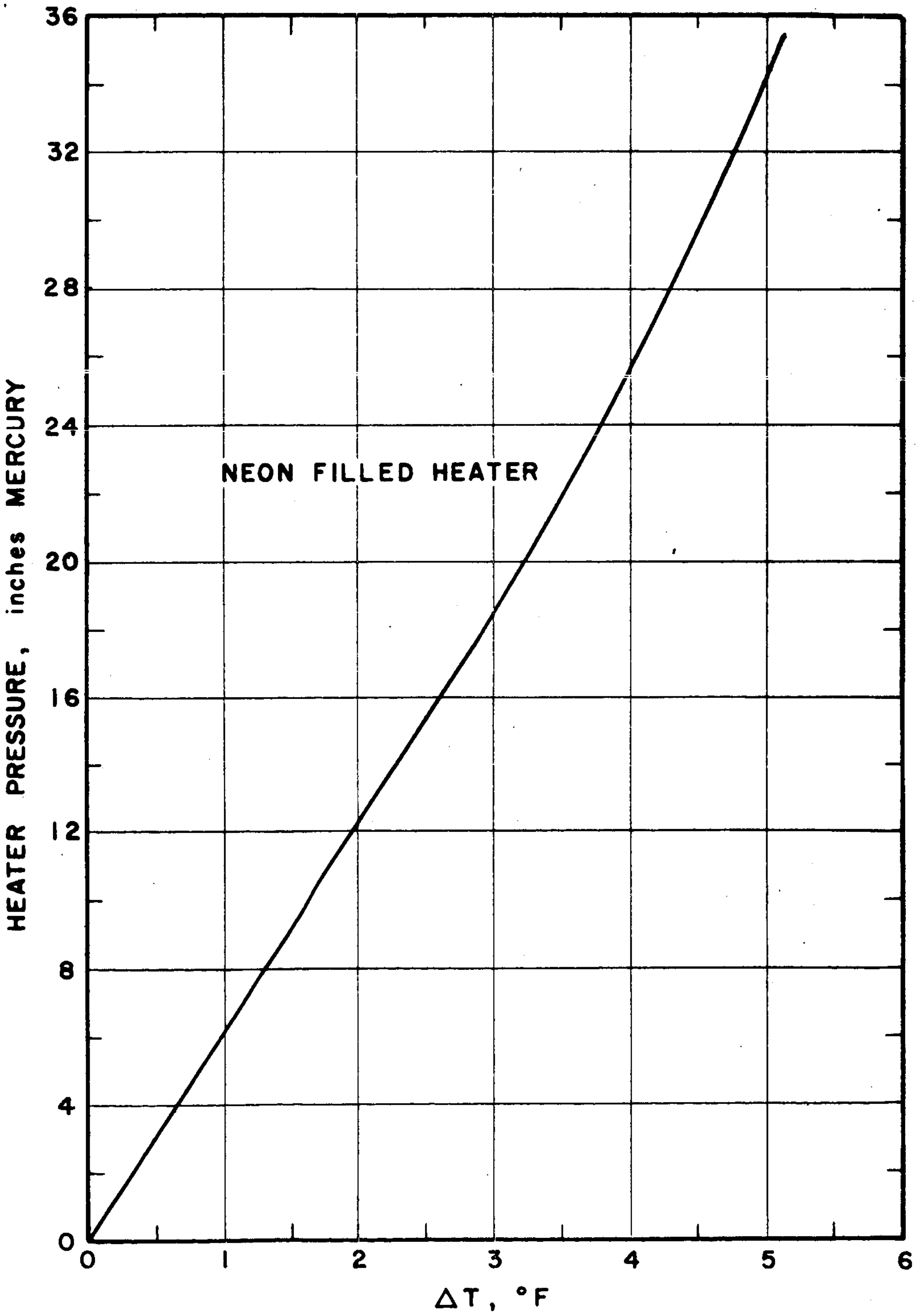

FIGURE 15, HEATER PRESSURE VERSUS TEMPERATURE DIFFERENCE

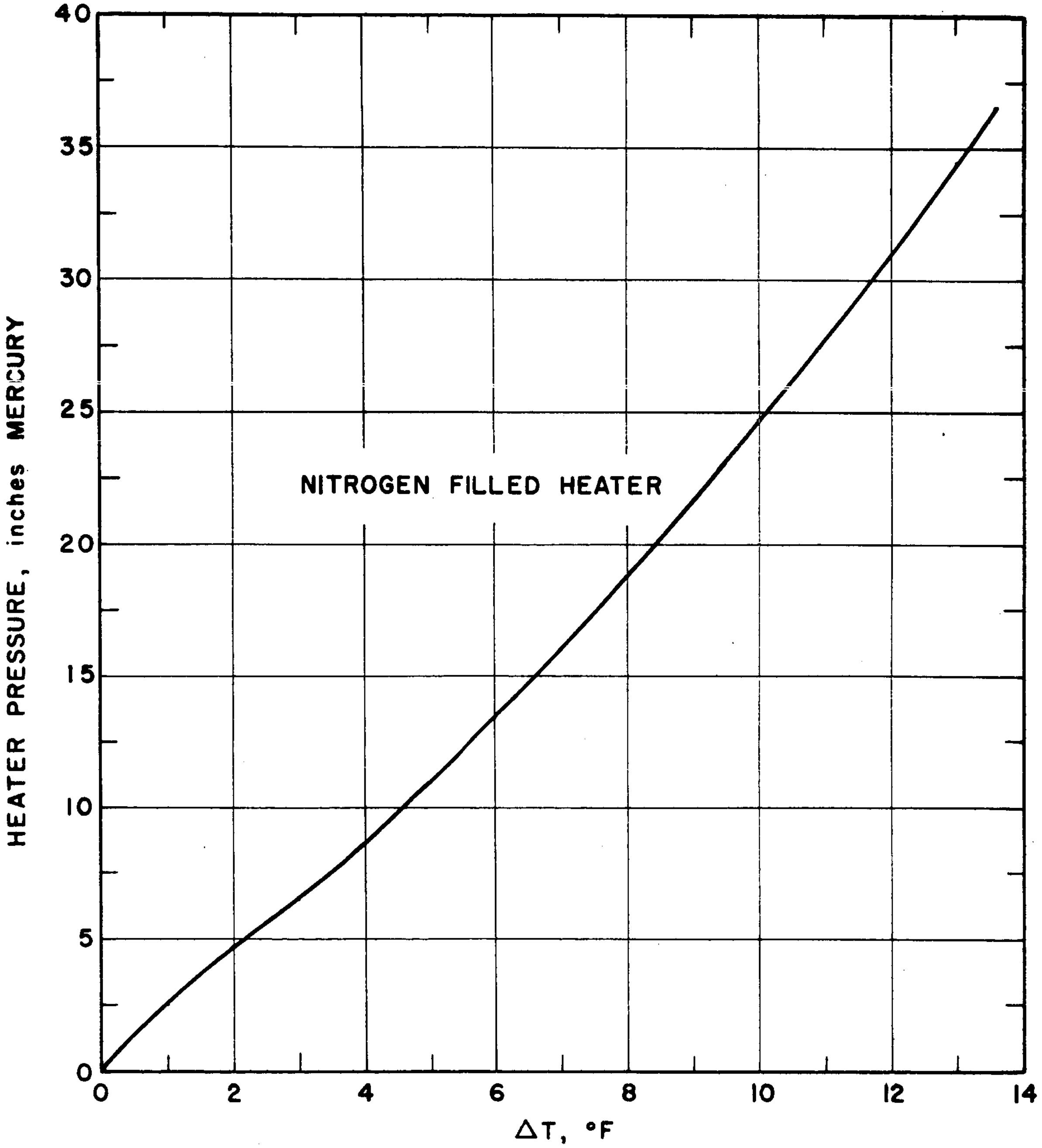

obtained by recording the emf generated by the thermocouples at the condition of no heat input. The difference between the emf recorded for the run and the one obtained at zero power input was the Δ mv used to determine the boiling temperature driving force, ΔT_b. Figures 16 and 17 are emf curves for copper-constantan thermocouples as a function of temperature difference between the hot junction and the cold one immersed in liquid nitrogen and neon respectively. These curves were calculated from the data published by Powell, et.al. (57).

The original intent was to have an isothermal heater. It was expected that the violent boiling occurring inside the heater, and the complete wetting of the inside heater wall resulting from the thermosyphon action would maintain the heater wall at a constant uniform temperature. Indeed, preliminary tests performed with a duplicate thermosyphon heating element in a glass dewar containing liquid nitrogen were successful and proved the feasibility of the concept. However, actual performance of the 3-inch heater showed that the heater wall was not isothermal. This can be seen by examining the boiling temperature driving force profile plotted in Figure 18. This profile, which is typical for most runs, indicates that the temperature at the top of the heater is always highest. This behavior is caused by two types of heat transfer occurring simultaneously inside the heater because of its being only partially filled with liquid.

FIGURE 16, EMF VERSUS TEMPERATURE DIFFERENCE FOR COPPER-CONSTANTAN THERMOCOUPLES

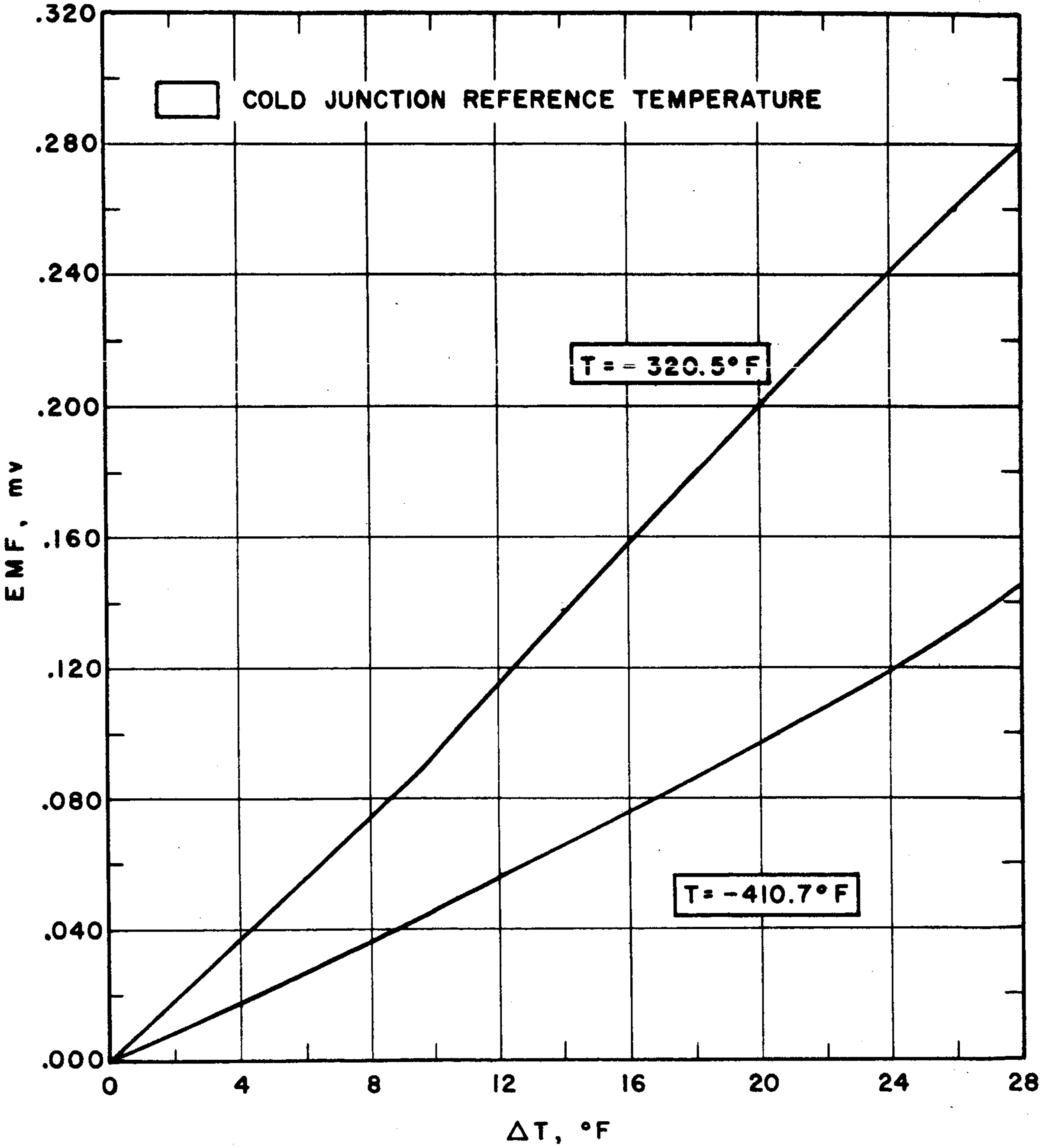

FIGURE 17, E M F VERSUS TEMPERATURE DIFFERENCE FOR COPPER-CONSTANTAN THERMOCOUPLES

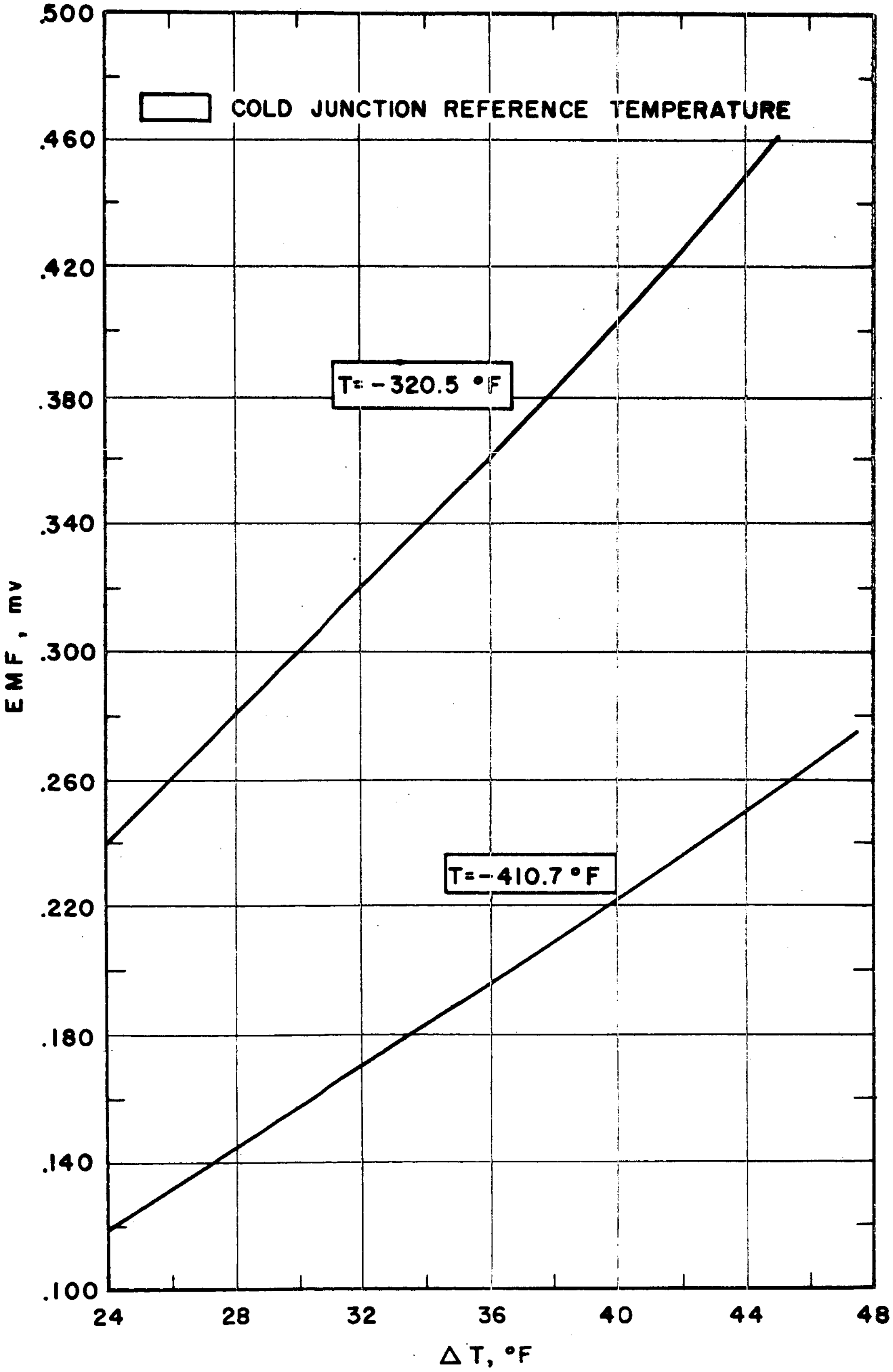

FIGURE 18, TYPICAL HEATER WALL TEMPERATURE BOILING DRIVING FORCE PROFILE

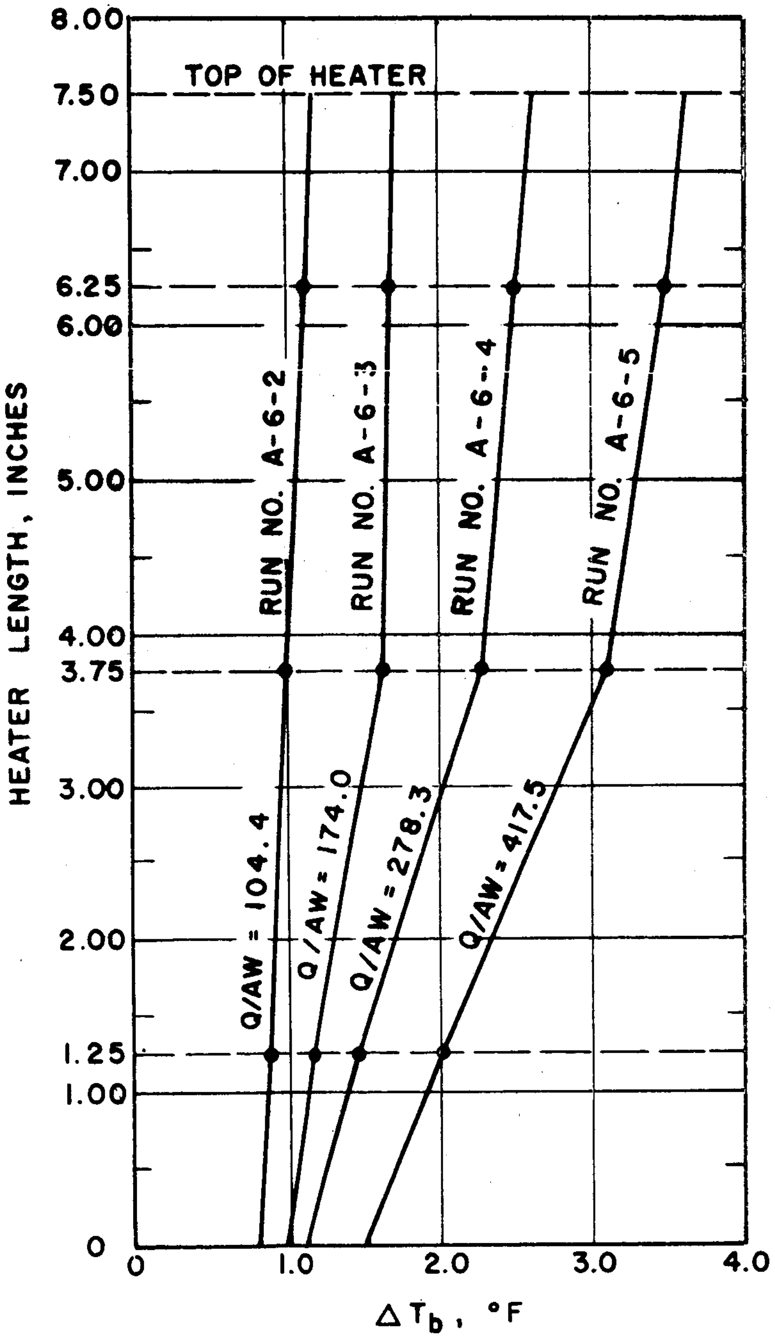

This partial filling was necessary to prevent burnout of the electric element. As a result of this condition, the top half of the heater was subjected to condensation heat transfer, while the lower part was subjected to convective heat transfer. The higher condensing film coefficient at the top resulted in a small inside temperature driving force, while the smaller convective heat transfer coefficient in the lower half caused a larger inside temperature driving force than in the top section. The violent agitation of the boiling-condensing fluid inside the heater, maintained it at a uniform temperature. Similarly, the fluid outside the heater was at constant temperature. This results in a larger boiling temperature driving force at the top of the heater than at its bottom. The several boiling temperature difference profiles of Figure 18 clearly show this behavior.

The explanation that the heater wall temperature profile was the result of the two types of heat transfer coefficient inside the heater has been experimentally verified. Runs A-P6-2, A-P6-4, and A-P6-6 are identical to runs A-P6-19, A-P6-17, and A-P6-18 respectively, except for the amount of liquid inside the heater. The heater was half full with liquid nitrogen during the first three runs and two-thirds full during the last three runs. The overall temperature driving force, being the sum of the individual boiling (external) and condensing (internal) temperature driving forces, is proportional to the internal temperature driving force, when the boiling one is constant. Since the boiling driving force is independent of the internal temperature driving force, it will remain constant when the heat flux is constant. Therefore at a given heat input, one would expect that the heater with condensation over a larger internal surface, would have a lower overall temperature driving force than the one with condensation over a smaller internal surface. This is actually substantiated since the runs with the heater half full of liquid show a substantially lower overall temperature driving force and top boiling temperature driving force than the ones measured for the runs having the heater two-thirds full of liquid. These results are shown in Table V.

It should be noted, that the high thermal conductivity of the copper wall (580 Btu/hr-ft-$^{\circ}$F at -320°F and 695 Btu/hr-ft-$^{\circ}$F at -410°F) has a beneficial effect in reducing the temperature difference along the heater wall.

Since the boiling temperature driving force, ΔT_b, is not constant over the heater length, an average boiling temperature driving force was used in all calculations. This average was obtained by integrating ΔT_b over the wetted wall length.

Boiling Heat Transfer Coefficient:

$$h_b = \frac{(Q/A_w) \text{ Btu/hr-ft}^2}{\Delta T_b \ {}^{\circ}\text{F}} = \frac{417.5}{2.8} = 149.1 \text{ Btu/hr-ft}^2\text{-}{}^{\circ}\text{F}$$

Nitrogen Boil-off:

$$W = \frac{Q \text{ Btu/hr}}{\lambda \text{ Btu/lb}} = \frac{Q \text{ Btu/hr} \times 28 \text{ lb/lb-mole}}{2405 \text{ Btu/lb-mole}}$$

$$= 0.01164 \, Q \text{ lb/hr}$$

$$= 0.01164 \times 204.8 = 2.38 \text{ lb/hr}$$

Runs A-80-5 to A-80-10 were used to establish the validity of determining the rate of boil-off by dividing the electric power input by the fluid latent heat and assuming negligible heat leak to the test section. A rotameter was connected to the 6-inch glass chamber on top of the test heater, and rotameter, temperature of the vapor entering the rotameter, and wattmeter readings were taken simultaneously. Temperature and density correction, $C = \sqrt{\frac{520}{T} \times \frac{28}{29}}$ where T °R is the vapor temperature, were made to the reading of the rotameter scale which was calibrated for air at 60°F.

The results of the flow check are summarized in Table XXII and the comparison between the calculated and measured boil-off rates is shown in Figure 19.

It was assumed that the same relationship existed for the neon runs. Observation of the test section at zero heat input showed no bubble formation for both the nitrogen and neon cases, thus substantiating the assumption of zero heat leak to the test section.

Annular Gap Flow Area:

$$A_t = \frac{\pi}{4} \frac{(D_2^2 - D_1^2)}{144} = \frac{\pi}{144} (D_2 t - t^2) \text{ ft}^2$$

TABLE XXII

COMPARISON BETWEEN CALCULATED AND MEASURED NITROGEN BOIL-OFF

Run No.	Wattage watts	Calculated Boil-Off SCFM (60°F & 1 atm)	Rotameter Reading	Temperature @ Rotameter °F	Measured Boil-Off (60°F & 1 atm)
A-80-5	100	0.91	0.92	60	0.91
A-80-6	200	1.83	1.75	20	1.82
A-80-7	300	2.74	2.50	0	2.65
A-80-9	150	1.36	1.25	10	1.32
A-80-10	250	2.27	2.10	0	2.23

FIGURE 19, COMPARISON BETWEEN MEASURED AND CALCULATED NITROGEN BOIL-OFF

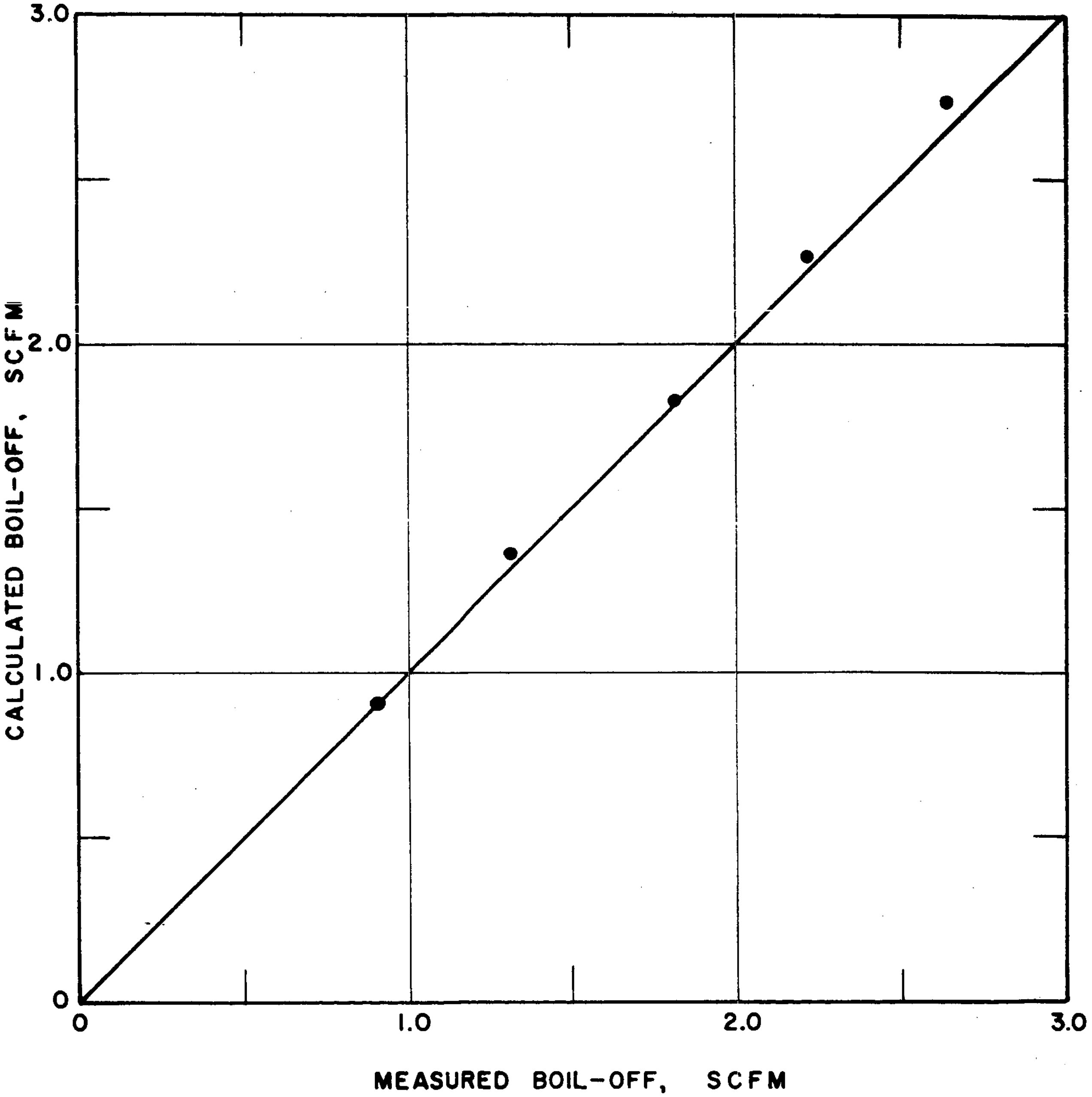

where D_2, D_1, and t are given in inches

$$A_t = \frac{\pi}{144} (3.0015 \times 0.006 - 0.006^2) = 0.0003916 \text{ ft}^2$$

at liquid nitrogen and neon temperatures.

Mass Velocity:

$$G = \frac{W \text{ lb/hr}}{A_t \text{ ft}^2} = \frac{2.38}{0.0003916} = 6078 \text{ lb/hr-ft}^2$$

Equivalent Diameter:

$$D_e = \frac{4 \times \text{Flow Area}}{\text{Wetted Perimeter}} = \frac{4\ (\pi/4)(D_2^2 - D_1^2)}{\pi\ D_1}$$

$$= \frac{(D_1 + 2t + D_1)(D_1 + 2t - D_1)}{D_1} = 4t + \frac{4t^2}{D_1} = 4t$$

since $\frac{4t^2}{D_1} << 4t$

$D_e = 4 \times 0.006 = 0.024$ inches

Nusselt Number:

$$Nu_L = \frac{h_b D_e}{k_L} = \frac{149.1 \times 0.024}{0.0805 \times 12} = 3.70$$

Reynolds Number:

$$Re_L = \frac{D_e G}{\mu_L} = \frac{0.024 \times 6078}{12 \times 0.385} = 31.6$$

Length to Diameter Ratio: $L/D_e = 7.5/0.024 = 313$

The constants used in the reduction of data for the nitrogen and neon runs are summarized in Tables XXIII and XXIV respectively.

TABLE XXIII

CALCULATION CONSTANTS FOR NITROGEN RUNS

Heater No.	D_e inches	$G = W/A_{t_2}$ lb/hr-ft^2	Nu_L $h_b D_e/k_L$	Re_L $D_e G/\mu_L$
12b	0.024	2554 W	0.0248 h_b	0.00519 G
6	0.080	769 W	0.0828 h_b	0.01732 G
9	0.084	733 W	0.0870 h_b	0.01818 G
10	0.088	708 W	0.0911 h_b	0.01905 G
7b	0.212	293.3 W	0.2195 h_b	0.04589 G
8	0.320	196.1 W	0.3313 h_b	0.06926 G

$$W = \frac{Q \text{ Btu/hr}}{\lambda \text{ Btu/lb}} = \frac{Q}{86} = 0.01164\, Q \text{ lb/hr}$$

TABLE XXIV

CALCULATION CONSTANTS FOR NEON RUNS

Heater No.	D_e inches	$G = W/A_{t_2}$ lb/hr-ft^2	Nu_L $h_b D_e/k_L$	Re_L $D_e G/\mu_L$
12b	0.024	2554 W	0.0266 h_b	0.00280 G
6	0.080	769 W	0.0887 h_b	0.00934 G
10	0.088	708 W	0.0975 h_b	0.01027 G
7b	0.212	293.3 W	0.2349 h_b	0.02475 G
8	0.320	196.1 W	0.3546 h_b	0.03735 G

$$W = \frac{Q \text{ Btu/hr}}{\text{Btu/lb}} = \frac{Q}{35} = 0.02698\, Q \text{ lb/hr}$$

VII. RESULTS AND DISCUSSION

Nitrogen Pool Boiling

The nitrogen pool boiling data reduced to heat flux and boiling temperature driving force, are tabulated in Tables XXV to XXX and plotted in Figures 20 to 26.

The data for full submergence case, can be correlated satisfactorily by the equation $Q/A_W = a\ (\Delta T_b)^b$. (75)

The coefficient and exponent of equation 75, for each individual heater, which were obtained by the "method of least squares" with a GE 225 computer (except heater no. 10) are listed in Table XXXI.

It is interesting to note that the exponents vary between 0.99 to 1.50, a value which is substantially lower than the 3 to 4 value suggested by other investigators (15, 43, 47, 62). However, exponents having a value of 0.98 and 0.94 can be calculated for liquid helium and liquid nitrogen respectively from the experimental data presented by Richards et.al. (61) in Figures 2 and 8. Furthermore, the level of heat flux obtained in this study is in excellent agreement with some of the data presented by Richards. For example, at $\Delta T_b = 1.8^oF$, the heat flux equals 174 Btu/hr-ft^2 for heater 12b (run A-P12b-3); and 160 Btu/hr-ft^2 for Haselden and Peters data covered in Figure 8 of Richards' survey.

TABLE XXV

CALCULATED DATA - NITROGEN POOL BOILING HEATER #12b

Run#	Q Btu/hr	Submergence "	Wetted Area ft^2	Q/A_W Btu/hr ft^2	ΔT_t °F	ΔT_b °F	W lb/hr
A-P12b-2	54.6	13 1/2	0.4905	111.3	1.6	1.4	0.636
3	85.3	13 1/2	0.4905	174.0	1.8	1.2	0.993
4	51.2	13 1/2	0.4905	104.3	---	0.9	0.596
5	136.5	13 1/2	0.4905	278.3	3.0	2.1	1.59
6	204.8	13 1/2	0.4905	417.5	4.3	2.8	2.38
7	273.0	13 1/2	0.4905	556.7	5.5	3.4	3.18
8	409.6	13 1/2	0.4905	835.1	6.7	4.3	4.77
9	546.1	13 1/2	0.4905	1113	8.4	5.2	6.36
10	747.4	12 1/2	0.4905	1524	11.4	7.5	8.70
11	747.4	13 1/2	0.4905	1524	11.0	7.7	8.70
12	1024	13 1/2	0.4905	2087	13.0	10.1	11.92
14	54.6	4	0.2616	208.7	3.3	1.4	0.636
15	85.3	4	0.2616	326.1	5.0	2.3	0.993
16	136.5	4	0.2616	526.8	7.0	3.6	1.59

TABLE XXV CONTINUED

Run#	Q Btu/hr	Submergence "	Wetted Area Ft^2	Q/A_w Btu/hr ft^2	ΔT_t ^oF	ΔT_b ^oF	W lb/hr
A-P12b-17	211.6	4	0.2616	808.9	9.3	4.4	2.46
18	283.3	4	0.2616	1083	11.6	5.2	3.30
19	416.4	4	0.2616	1592	15.2	6.8	4.85
20	556.3	4	0.2616	2127	20.2	8.8	6.48
21	744.0	4	0.2616	2844	25.0	13.7	8.66
22	948.8	4	0.2616	3627	33.5	14.7	11.04
24	54.6	1 1/2	0.0981	556.5	5.8	2.0	0.636
25	85.3	1 1/2	0.0981	869.5	7.3	2.7	0.993
26	136.5	1 1/2	0.0981	1391	10.7	4.3	1.59
27	215.0	1 1/2	0.0981	2191	14.1	6.1	2.50
28	273.0	1 1/2	0.0981	2783	18.4	7.4	3.18
29	419.8	1 1/2	0.0981	4279	27.2	12.2	4.89

TABLE XXV CONTINUED

Run#	Q Btu/hr	Submergence "	Wetted Area Ft^2	Q/A_W Btu/hr ft^2	ΔT_t ^oF	ΔT_b ^oF	W lb/hr
A-P12b-32	85.3	7 1/2	0.4905	174.0	2.4	1.7	0.993
33	204.8	7 1/2	0.4905	417.5	6.0	3.8	2.38
34	409.6	7 1/2	0.4905	835.0	10.4	6.4	4.77
35	617.8	7 1/2	0.4905	1259	13.1	8.8	7.19
36	819.1	7 1/2	0.4905	1670	16.6	11.7	9.53
37	1092	7 1/2	0.4905	2270	23.7	16.3	12.71

TABLE XXVI

CALCULATED DATA - NITROGEN POOL BOILING HEATER #6

Run#	Q Btu/hr	Submergence "	Wetted Area Ft^2	Q/A_w Btu/hr ft^2	ΔT_b ^oF	W lb/hr
A-P6-1	51.2	7 1/2	0.4859	105.4	0.7	0.596
2	170.7	7 1/2	0.4859	351.3	2.6	1.99
3	341.3	7 1/2	0.4859	702.4	5.5	3.97
4	512.0	7 1/2	0.4859	1054	7.2	5.96
5	675.8	7 1/2	0.4859	1391	9.4	7.87
6	1024	7 1/2	0.4859	2107	14.9	11.92
9	51.2	3 3/4	0.2429	210.8	2.0	0.596
10	170.7	3 3/4	0.2429	702.6	4.7	1.98
11	341.3	3 3/4	0.2429	1405	7.2	3.97
12	512.0	3 3/4	0.2429	2108	9.6	5.96
13	682.6	3 3/4	0.2429	2810	11.0	7.95
14	1024	3 3/4	0.2429	4214	10.9	11.92
17	512.0	7 1/2	0.4859	1054	7.4	5.96
18	1024	7 1/2	0.4859	2107	16.0	11.92
19	170.7	7 1/2	0.4859	351.3	2.9	1.98

TABLE XXVII

CALCULATED DATA - NITROGEN POOL BOILING HEATER #9 (NICKEL PLATED)

Run#	Q Btu/hr	Submergence "	Wetted Area Ft^2	Q/A_w Btu/hr ft^2	ΔT_b ^oF	W lb/hr
A-P9-2	51.2	7 1/2	0.4856	105.4	1.5	0.596
3	85.3	7 1/2	0.4856	175.7	2.2	0.993
4	136.5	7 1/2	0.4856	281.1	3.1	1.59
5	204.8	7 1/2	0.4856	421.7	4.3	2.38
6	273.0	7 1/2	0.4856	562.3	5.3	3.18
7	409.6	7 1/2	0.4856	843.4	6.3	4.77
8	546.1	7 1/2	0.4856	1125	7.4	6.36
9	750.9	7 1/2	0.4856	1546	8.9	8.74
10	1024	7 1/2	0.4856	2109	11.7	11.92
11	1365	7 1/2	0.4856	2811	13.9	15.89
14	51.2	7 1/2	0.4856	210.9	2.0	0.596
15	85.3	3 3/4	0.2428	351.4	2.6	0.993
16	136.5	3 3/4	0.2428	562.3	3.4	1.59
17	204.8	3 3/4	0.2428	843.4	4.1	2.38
18	273.0	3 3/4	0.2428	1125	4.8	3.18
19	385.7	3 3/4	0.2428	1588	5.6	4.49

TABLE XXVIII

CALCULATED DATA - NITROGEN POOL BOILING HEATER #10 (CADMIUM PLATED)

Run#	Q Btu/hr	Submergence "	Wetted Area Ft^2	Q/A_w Btu/hr ft^2	ΔT_b ^oF	W lb/hr
A-P10-2	204.8	7 1/2	0.4851	422.1	9.1	2.38
3	409.6	7 1/2	0.4851	844.3	15.0	4.77
4	614.3	7 1/2	0.4851	1266	20.2	7.15
5	1024	7 1/2	0.4851	1024	28.6	11.92
8	204.8	3 3/4	0.2426	844.3	9.8	2.38
9	409.6	3 3/4	0.2426	1688	14.5	4.77
10	614.3	3 3/4	0.2426	2532	19.3	7.15

TABLE XXIX

CALCULATED DATA - NITROGEN POOL BOILING HEATER #7b

Run#	Q Btu/hr	Submergence "	Wetted Area Ft^2	Q/A_w Btu/hr ft^2	ΔT_b ^oF	W lb/hr
A-P7b-2	51.2	7 1/2	0.4750	107.8	1.5	0.596
3	51.2	3 3/4	0.2375	215.8	2.1	0.596
4	136.5	7 1/2	0.4750	287.4	3.7	1.59
5	136.5	3 3/4	0.2375	574.7	4.5	1.59
6	273.0	7 1/2	0.4750	574.7	6.7	3.18
7	273.0	3 3/4	0.2375	1149	7.8	3.18
9	512.0	7 1/2	0.4750	1078	9.5	5.96
10	754.3	7 1/2	0.4750	1588	12.1	8.78
11	1195	7 1/2	0.4750	2516	17.2	13.91
22	204.8	7 1/2	0.4750	431.1	4.5	2.38
23	409.6	7 1/2	0.4750	862.2	7.3	4.77
24	614.4	7 1/2	0.4750	1293	9.9	7.15
25	1024	7 1/2	0.4750	2156	15.3	11.92
28	204.8	3 3/4	0.2375	862.2	5.1	2.38
29	409.6	3 3/4	0.2375	1724	8.6	4.77
30	614.4	3 3/4	0.2375	2587	11.6	7.15

TABLE XXX

CALCULATED DATA - NITROGEN POOL BOILING HEATER #8

Run#	Q Btu/hr	Submergence "	Wetted Area Ft^2	Q/A_w Btu/hr ft^2	ΔT_b ^oF	W lb/hr
A-P8-2	170.7	7 1/2	0.4663	366.0	3.3	1.99
3	170.7	3 3/4	0.2331	732.0	4.3	1.99
4	341.3	7 1/2	0.4663	732.0	4.5	3.97
5	341.3	3 3/4	0.2331	1464	6.8	3.97
6	512.0	7 1/2	0.4663	1098	9.2	5.96
7	512.0	3 3/4	0.2331	2196	9.6	5.96
8	682.6	7 1/2	0.4663	1464	10.0	7.95
9	682.6	3 3/4	0.2331	2968	13.8	7.95
10	1024	7 1/2	0.4663	2196	13.6	11.92
11	1365	7 1/2	0.4663	2928	16.2	15.89
12	1024	3 3/4	0.2331	4393	18.1	11.92
13	1365	3 3/4	0.2331	5857	20.6	15.89

FIGURE 26, HEAT FLUX VERSUS TEMPERATURE DRIVING FORCE ($\Delta T_b = T_w - T_{Sat.}$)
NITROGEN POOL BOILING
COPPER HEATER 12 b
O.D. 2.9975" RMS 9-11μ"

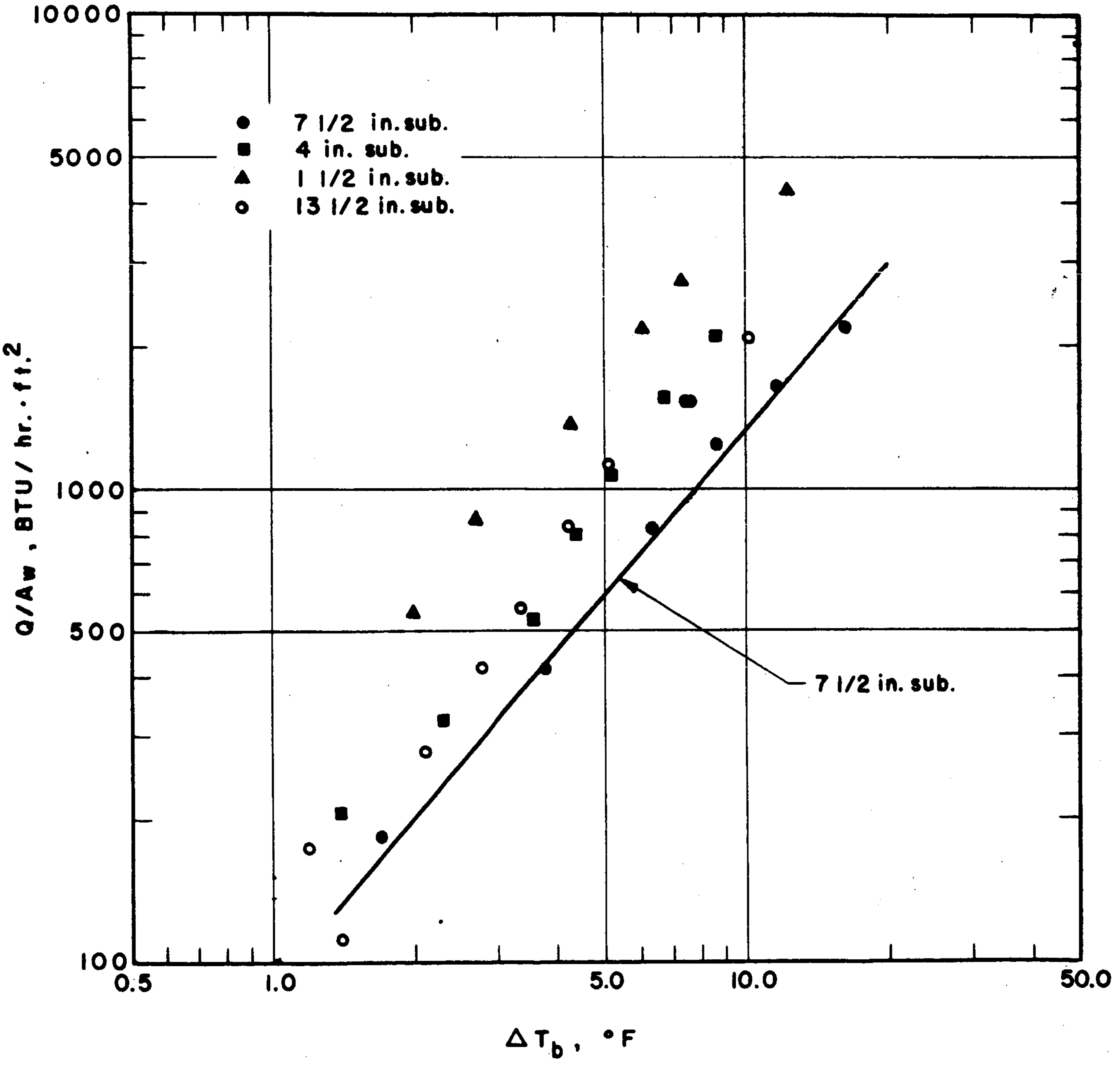

FIGURE 21, HEAT FLUX VERSUS TEMPERATURE DRIVING FORCE ($\Delta T_b = T_w - T_{Sat.}$)
NITROGEN POOL BOILING
COPPER HEATER 6
O.D. 2.9695" RMS 16-20μ"

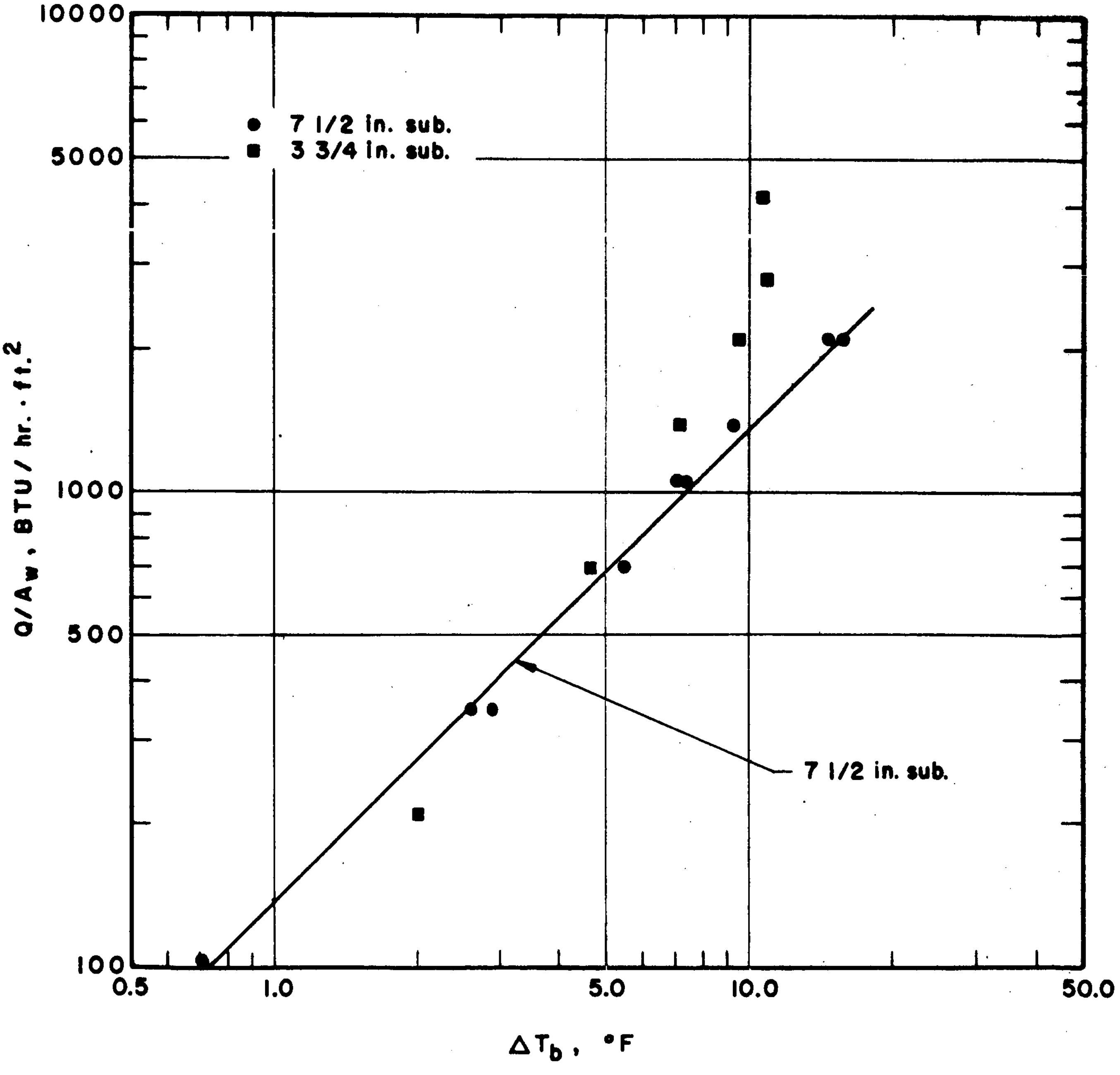

FIGURE 22, HEAT FLUX VERSUS TEMPERATURE DRIVING FORCE ($\Delta T_b = T_w - T_{Sat.}$)
NITROGEN POOL BOILING
NICKEL PLATED COPPER HEATER 9
O.D. 2.9675" RMS 6-8 μ"

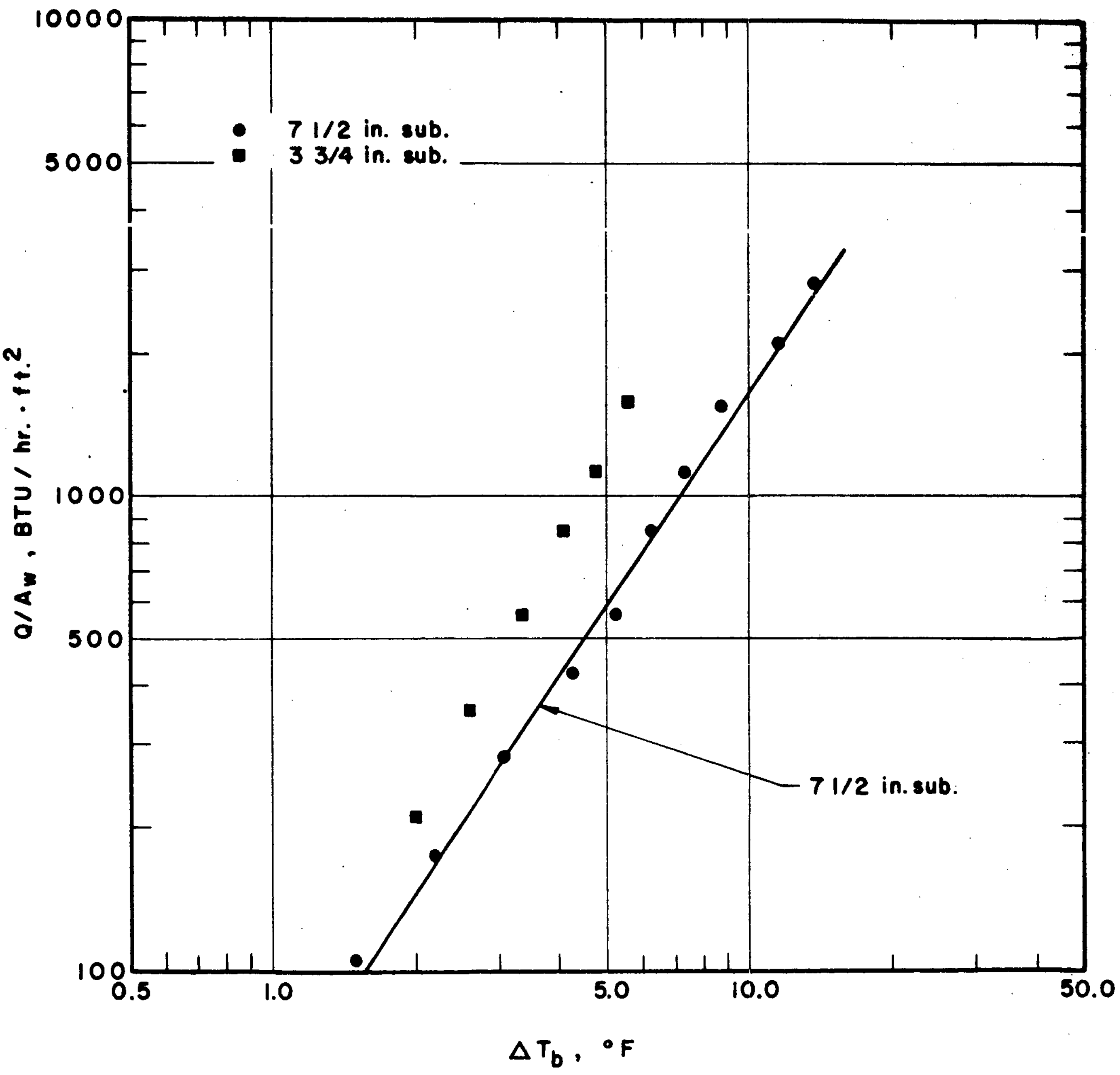

FIGURE 23, HEAT FLUX VERSUS TEMPERATURE DRIVING FORCE ($\Delta T_b = T_w - T_{sat.}$)
NITROGEN POOL BOILING
CADMIUM PLATED COPPER HEATER 10
O.D. 2.9645" RMS 8-11 μ"

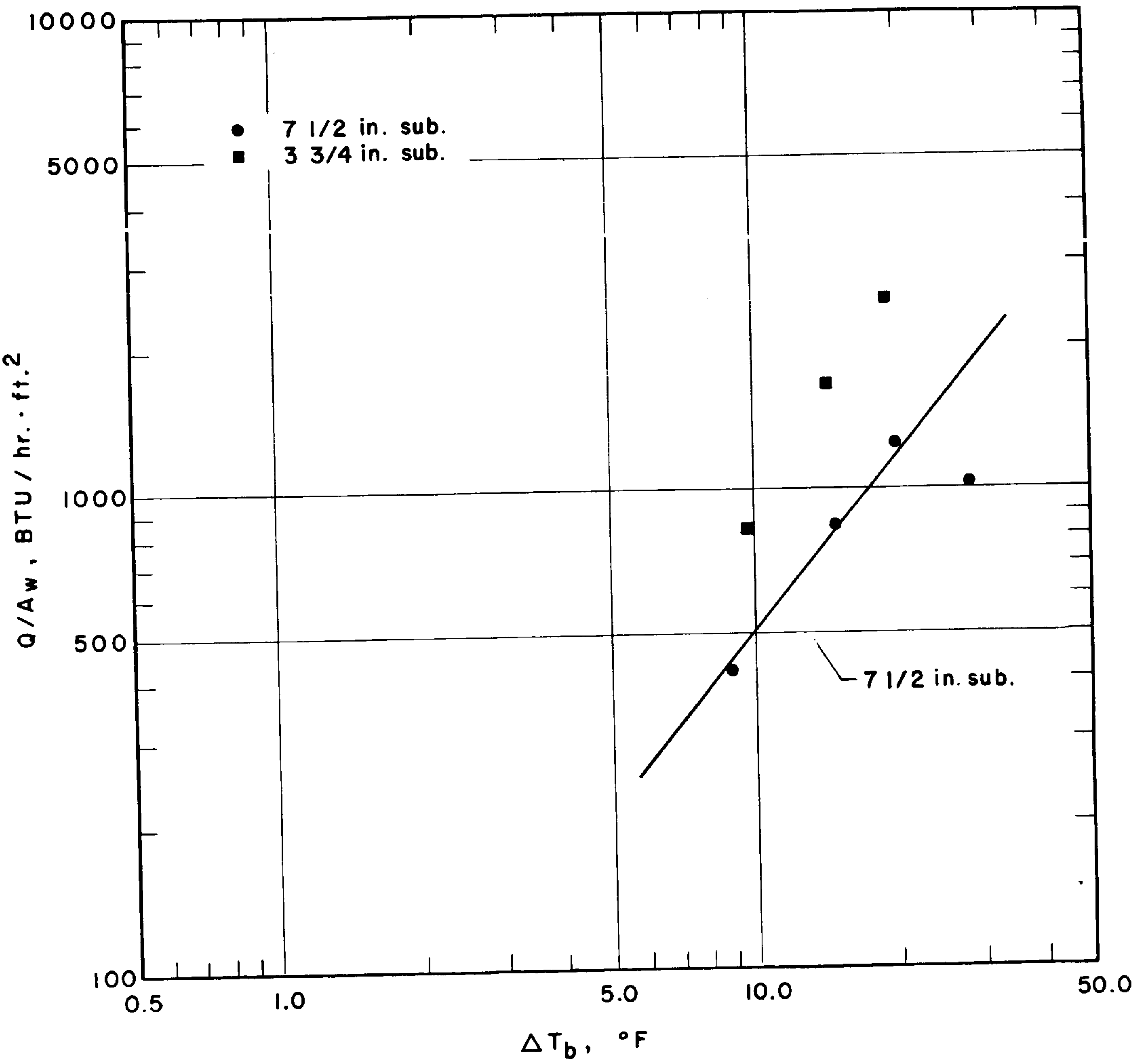

FIGURE 24, HEAT FLUX VERSUS TEMPERATURE DRIVING FORCE ($\Delta T_b = T_w - T_{sat.}$)
NITROGEN POOL BOILING
COPPER HEATER 7b
O.D. 2.9030" RMS 11-13μ"

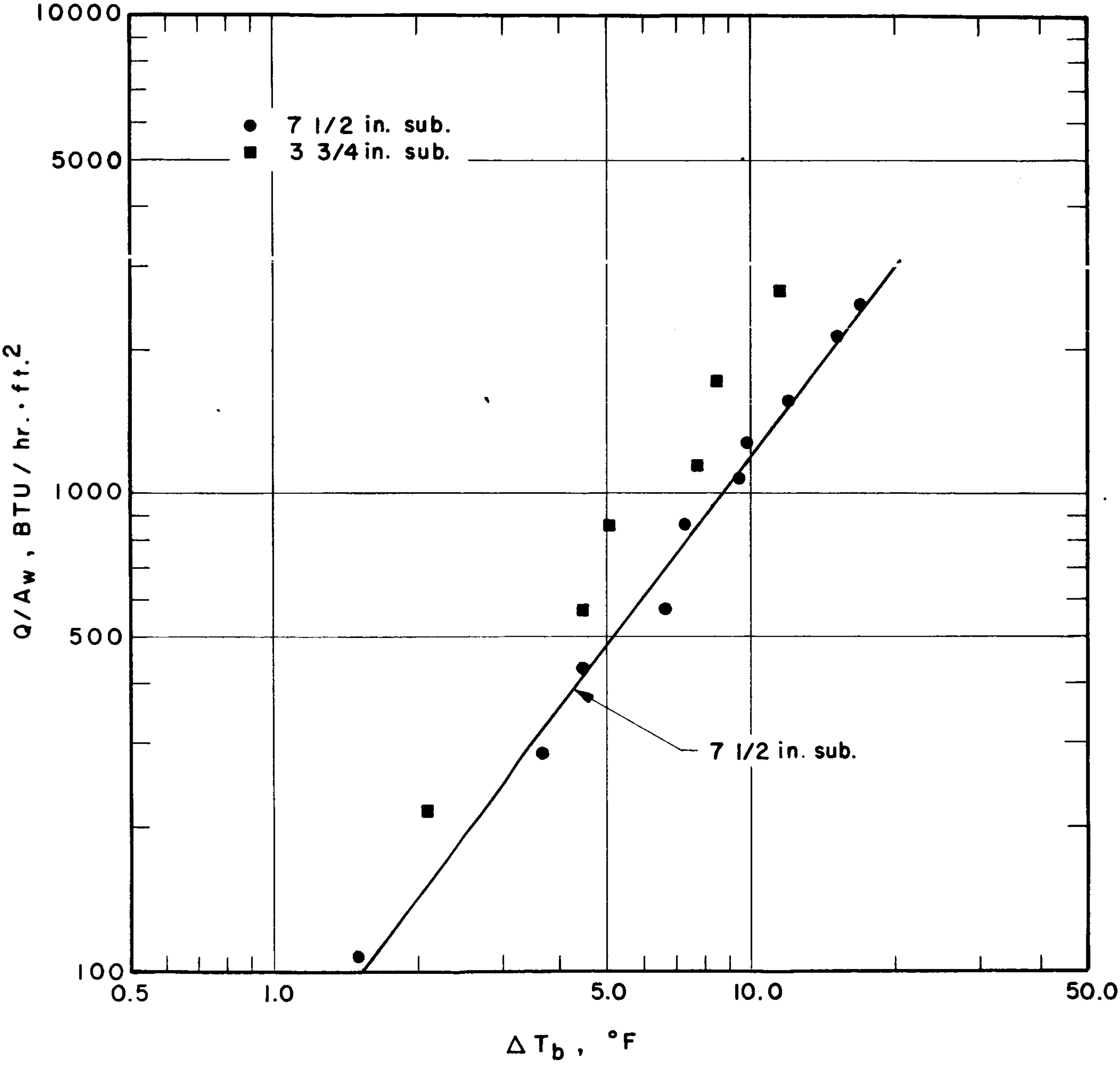

FIGURE 25, HEAT FLUX VERSUS TEMPERATURE
DRIVING FORCE ($\Delta T_b = T_w - T_{Sat.}$)
NITROGEN POOL BOILING
COPPER HEATER 8
O.D. 2.8495" RMS 13-15μ"

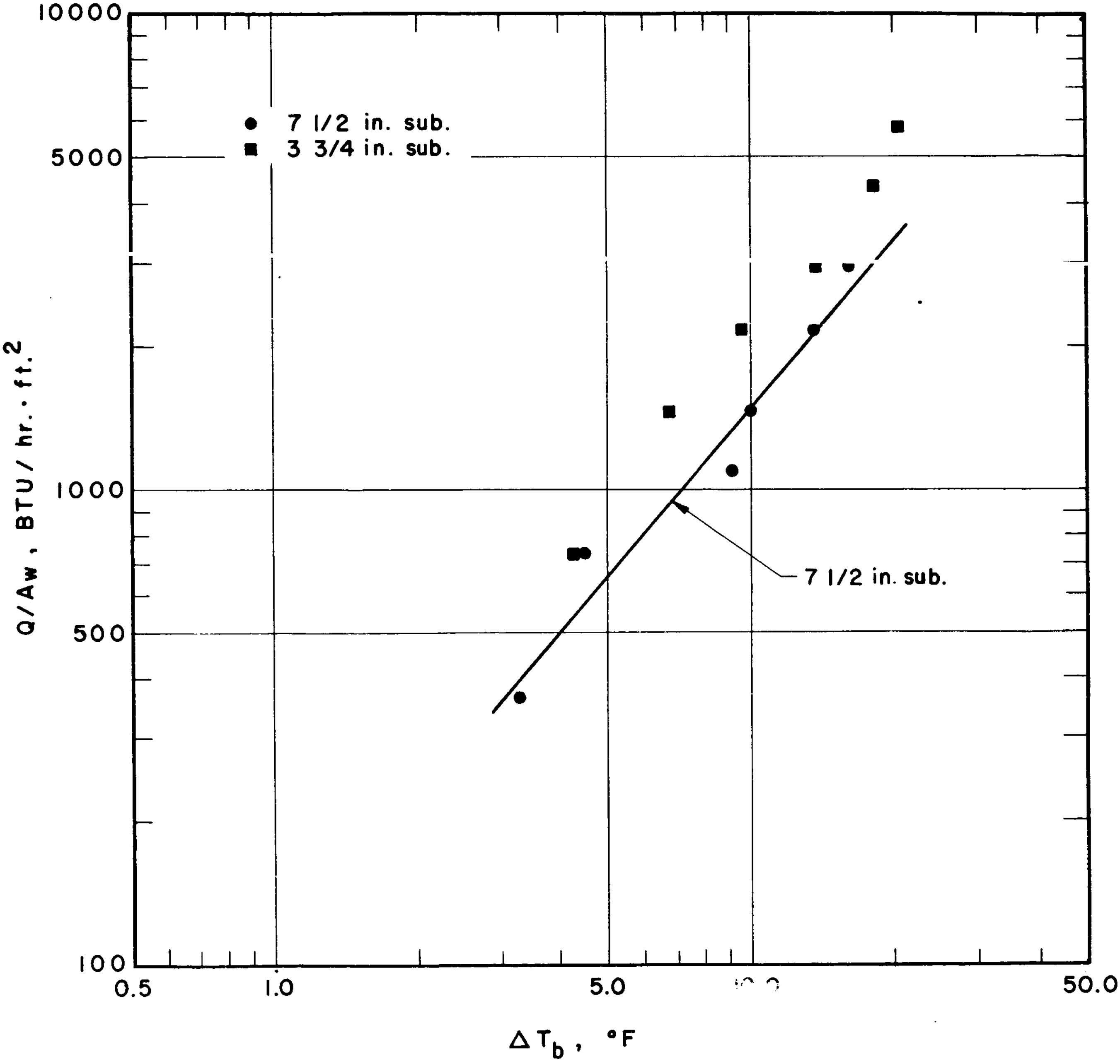

FIGURE 26, HEAT FLUX VERSUS TEMPERATURE DRIVING FORCE ($\Delta T_b = T_w - T_{Sat.}$) NITROGEN POOL BOILING COMPARISON BETWEEN ALL HEATERS AT 7 1/2" SUBMERGENCE

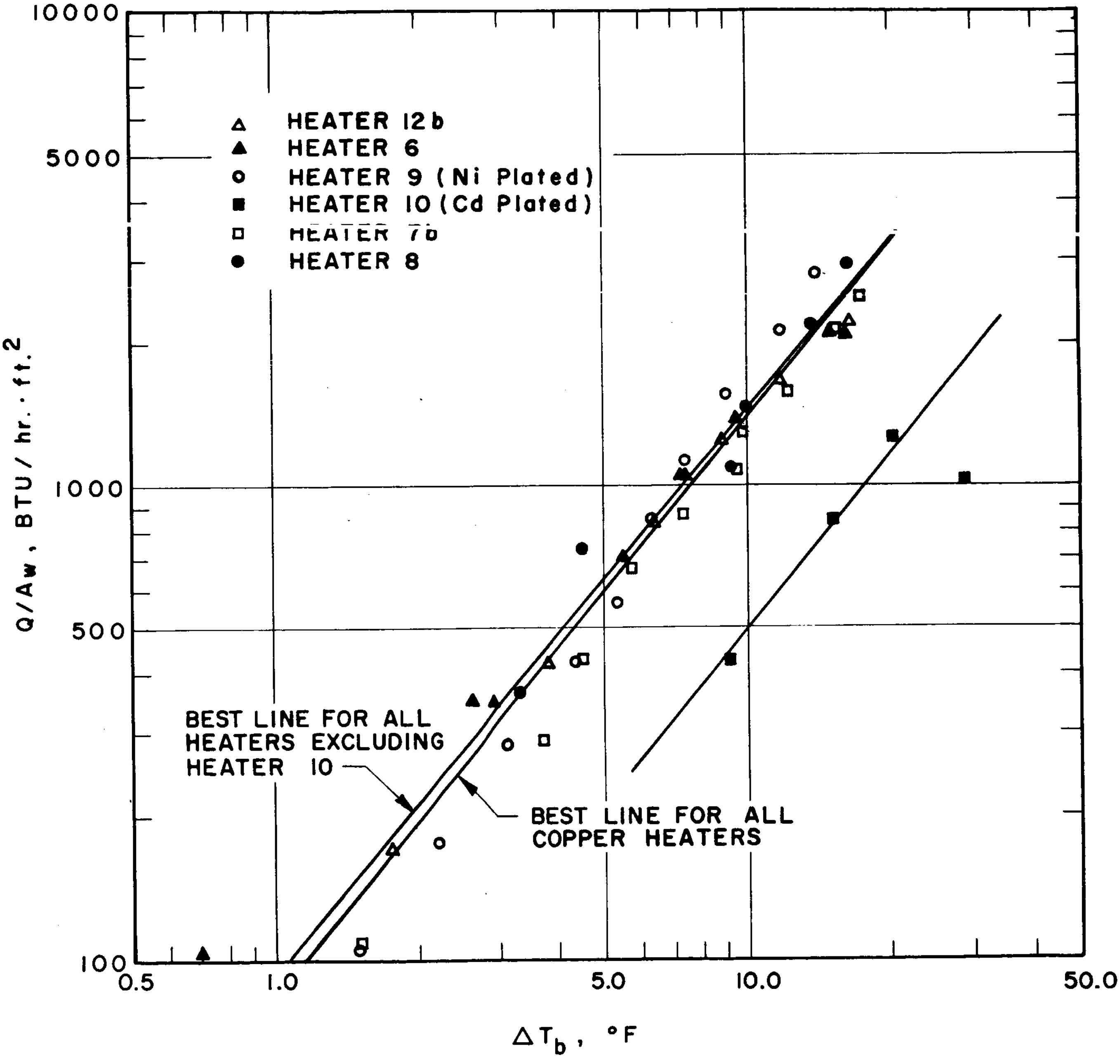

TABLE XXXI

CORRELATION

NITROGEN POOL BOILING

(Full Submergence - 7 1/2-inches)

$$Q/A_w = a\ (\Delta T_b)^b$$

Heater No.	a	b	Average % Deviation
12b	94.0	1.16	4
6	139	0.99	6
9 (Ni)	52.7	1.50	6
10 (Cd)	30.0	1.20	22
7b	57.4	1.32	7
8	98.5	1.18	11
All Cu Heaters	94.7	1.18	14
All Heaters Except Heater No. 10 (Cd)	87.2	1.20	16

The full submergence data for all the copper heaters can be correlated by a single equation with an average percent deviation of 14%.

$$Q/A_w = 94.7\ (\Delta T_b)^{1.18} \tag{76}$$

The average percent deviation is the average of the absolute value of all individual percent deviations calculated from the expression:

$$\frac{\text{observed value} - \text{calculated value}}{\text{observed value}} \times 100.$$

The full submergence data for all the heaters, except heater no. 10 (cadmium plated), can be correlated by the following equation

$$Q/A_w = 87.2\ (\Delta T_b)^{1.20}$$

with an average percent deviation of 16%. The lines for both equations are shown in Figure 26.

There is no apparent reason for the large difference between the results for the cadmium plated heater and those for the other heaters. All the heaters were machine finished in an identical manner using the same tools and the same type Bahr-Manning craucus cloth. Profilometer measurements for surface roughness showed a total range of 6-20 micro-inches for all the six heaters, with a maximum range of 4 micro-inches for each individual heater. This variation in surface roughness is important as shown by the work of Corty and Foust (13), however it does not explain the presents results, since the cadmium plated heater has a roughness which is intermediate between the roughness of the nickel plated and copper heaters.

For the purpose of this study, it will be assumed that all copper heaters are identical, the nickel plated heater similar, and the cadmium plated one different. Since the main purpose of the pool boiling runs was to establish a relationship between heaters, which was done with the full submergence condition, no effort was made to correlate the data obtained at other submergences. These data are reported and plotted together with the full submergence data. Examination of Figures 20 to 25, shows that at a given temperature driving force, the lower the submergence, the higher the heat flux. This can be explained by the appearance of preferential boiling at the joint between the insulation cap and the bottom of the heater. Figures 26a and 26b show this effect.

Examination of the data shows that heat flux decreases with increasing submergence, reaches a minimum at about 100% submergence, and then increases with increasing submergence. Some of the factors that may explain this behavior are surface blanketing with vapor, turbulence, number of bubbling sites, and bubble size. It seems that the blanketing effect is the controlling one for the case of partial and full submergence. The bubbles being formed in the lower part of the heater blanket the upper surface with vapor and reduces its effectiveness. However, when

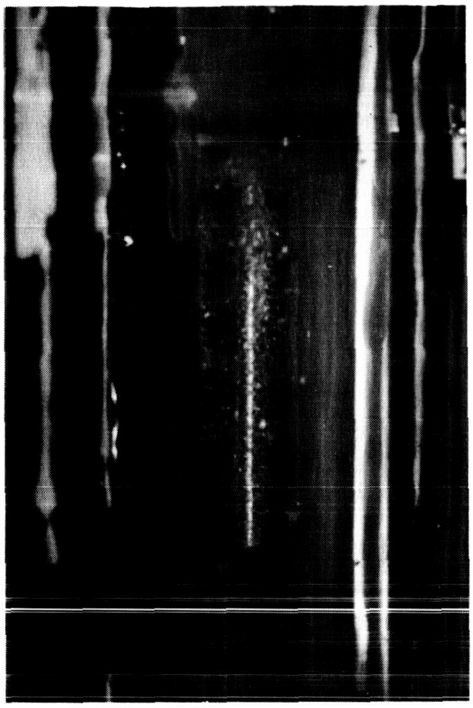

FIGURE 26a

NITROGEN POOL BOILING

FULL SUBMERGENCE

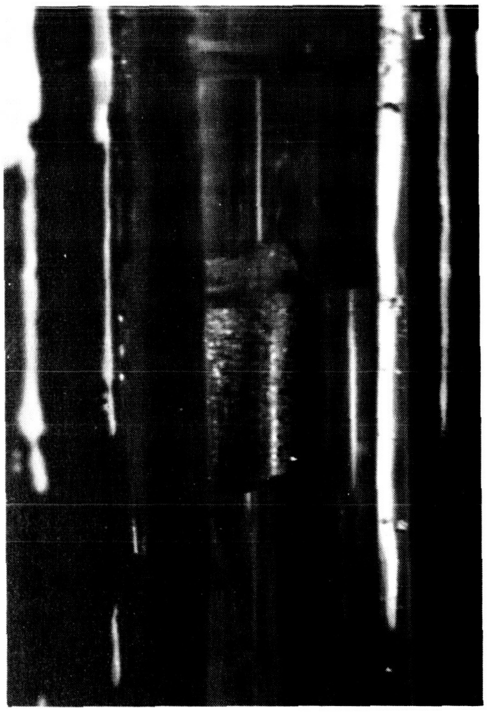

FIGURE 26b

NITROGEN POOL BOILING

HALF SUBMERGENCE

submergence increases beyond the 100% point, the other effects offset the detrimental effect of blanketing and heat flux increases with increasing submergence. It is believed that further study of this problem is necessary to develop a proper understanding of the several effects involved and to establish their magnitude (42).

Neon Pool Boiling

The neon pool boiling data were correlated in the same manner as the nitrogen data except that the overall temperature driving force was used instead of the boiling temperature driving force. For comparison purposes, the nitrogen pool boiling data for heater 12b were also correlated on the basis of overall temperature driving force. The equations for the neon and nitrogen cases are shown in Table XXXII and the two lines are compared in Figure 34.

TABLE XXXII

COMPARISON BETWEEN NITROGEN AND NEON POOL BOILING

(Full Submergence 7 1/2-inches)

Heater 12b

Nitrogen	$Q/A_w = 66.0\ (\Delta T_t)^{1.11}$
Neon	$Q/A_w = 135\ (\Delta T_t)^{1.11}$

Annular Gap Boiling - Nitrogen and Neon

The experimental data for annular gap boiling were reduced to Nusselt and Reynolds numbers using liquid properties and the equivalent diameter for the annulus. The calculated data are presented in Tables XXXIII to XXXVIII for liquid nitrogen and XXXIX to XLIII for liquid neon. These data are presented graphically as heat flux versus boiling temperature driving force, and as Nusselt number versus Reynolds number in Figures 27 to 33, 35 to 51.

The data were correlated by means of Equation (74) which was derived in pages 106-110:

$$\frac{h_b D_e}{k_L} = a \left(\frac{D_e G}{\mu_L}\right)^b \left(\frac{L}{D_e}\right)^c \left(\frac{Cp_L \mu_L}{k_L}\right)^d \qquad (74)$$

or $$Nu_L = a \, (Re_L)^b \, (L/D_e)^c \, (Pr_L)^d$$

The coefficient and exponents were obtained by the method of least squares with a GE computor resulting in the following equation:

$$Nu_L = 150 \, (Re_L)^{0.18} \, (L/D_e)^{-0.82} \, (Pr_L)^{0.95} \qquad (78)$$

which represents all the experimental data with an average percent deviation of 23%. The measured Nusselt numbers are compared with the calculated ones in Figure 52.

TABLE XXXIII

CALCULATED DATA - NITROGEN ANNULAR GAP BOILING HEATER #12b 0.006" GAP

Run#	Q Btu/hr	Outer Sub. "	Max. Inner Sub. "	Wetted Area Ft^2	Q/A_W Btu/hr ft^2	ΔT_b ^oF	h_b Btu/hr ft^2 ^oF	W lb/hr	Nu_L	Re_L	L/De
A-6-2	51.2	7 1/2	7 1/2	.4905	104.4	1.0	104.4	.596	2.59	7.92	313
3	85.3	7 1/2	7 1/2	.4905	174.0	1.5	116.8	.993	2.90	13.2	313
4	136.5	7 1/2	7 1/2	.4905	278.3	2.1	132.5	1.59	3.29	21.1	313
5	204.8	7 1/2	7 1/2	.4905	417.5	2.8	149.1	2.38	3.70	31.6	313
6	273.0	7 1/2	7 1/2	.4905	556.7	3.7	150.5	3.18	3.73	42.2	313
7	409.6	7 1/2	7 1/2	.4905	835.0	5.7	146.5	4.77	3.63	63.3	313
10	51.2	5 1/2	7 1/2	.4905	104.4	1.0	104.4	.596	2.59	7.92	313
12	136.5	5 1/2	7 1/2	.4905	278.3	2.3	121.0	1.59	3.00	21.1	313
13	204.8	5 1/2	7 1/2	.4905	417.5	3.1	134.7	2.38	3.34	31.6	313
14	273.0	5 1/2	7 1/2	.4905	556.7	4.1	135.8	3.18	3.37	42.2	313
17	51.2	2 1/2	7 1/2	.4905	104.4	1.3	80.3	.596	1.99	7.92	313
18	85.3	2 1/2	7 1/2	.4905	174.0	2.1	82.9	.993	2.06	13.2	313
19	136.5	2 1/2	7 1/2	.4905	278.3	4.9	56.8	1.59	1.41	21.1	313

TABLE XXXIV

CALCULATED DATA - NITROGEN ANNULAR GAP BOILING HEATER #6 0.020" GAP

Run#	Q Btu/hr	Outer Sub. "	Max. Inner Sub. "	Wetted Area ft^2	Q/A_W Btu/hr ft^2	ΔT_b °F	h_b Btu/hr ft^2 °F	W lb/hr	Nu_L	Re_L	L/De
A-20- 2	51.2	7 1/2	4 1/2	.2915	175.6	.8	220	.596	18.2	7.95	56.3
3	51.2	6	3	.1943	263.5	1.0	264	.596	21.9	7.95	37.5
4	51.2	5	3	.1943	263.5	1.1	240	.596	19.9	7.95	37.5
5	51.2	4	1 1/2	.0972	526.7	1.1	479	.596	39.7	7.95	18.8
8	51.2	5	2 1/2	.1620	316.0	1.3	243	.596	20.1	7.95	31.3
9	51.2	5	3	.1943	263.5	1.4	188	.596	15.6	7.95	37.5
10	170.7	7 1/2	6	.3887	439.2	1.6	275	1.99	22.8	26.6	75.0
11	170.7	7 1/2	6	.3887	439.2	1.5	293	1.99	24.3	26.6	75.0
12	170.7	6	3	.1943	878.5	2.5	351	1.99	29.1	26.6	37.5
13	170.7	5 1/2	2 1/2	.1620	1054	3.9	270	1.99	22.4	26.6	31.3
14	170.7	4	1 1/2	.0972	1756	3.5	502	1.99	41.6	26.6	18.8
15	170.7	4	1	.0648	2634	5.8	454	1.99	37.6	26.6	12.5

TABLE XXXIV CONTINUED

Run#	Q Btu/hr	Outer Sub. "	Max.Inner Sub. "	Wetted Area ft^2	Q/A_W Btu/hr ft^2	ΔT_b °F	h_b Btu/hr ft^2 °F	W lb/hr	Nu_L	Re_L	L/De
A-20-16	170.7	7 1/2	5 1/2	.3563	479.0	1.7	282	1.99	23.3	26.6	68.8
19	341.3	7 1/2	5	.3239	1054	2.3	458	3.97	37.9	53.0	62.5
20	341.3	7 1/2	5	.3239	1054	2.3	458	3.97	37.9	53.0	62.5
21	341.3	6	2	.1296	2633	3.4	774	3.97	64.1	53.0	25.0
22	341.3	5	2	.1296	2633	4.4	598	3.97	49.5	53.0	25.0
26	512.0	7 1/2	7 1/2	.4859	1054	4.0	264	5.96	21.9	79.5	93.8
28	341.3	6	7 1/2	.4859	702.4	3.0	234	3.97	19.4	53.0	93.8
33	51.2	7 1/2	7 1/2	.4859	105.4	.5	211	.596	17.5	7.95	93.8
34	51.2	6	7 1/2	.4859	105.4	.6	176	.596	14.6	7.95	93.8
35	49.5	5	6 1/2	.4211	117.5	.7	167	.576	13.8	7.69	81.3
36	49.5	4	5	.3239	152.8	.6	255	.576	21.1	7.69	62.5
37	49.5	3	4	.2591	191.0	.9	212	.576	17.6	7.69	50.0
38	49.5	5	6 1/2	.4211	117.5	.5	235	.576	19.5	7.69	81.3

TABLE XXXIV CONTINUED

Run#	Q Btu/hr	Outer Sub. "	Max. Inner Sub. "	Wetted Area ft^2	Q/A_W Btu/hr ft^2	ΔT_b °F	h_b Btu/hr ft^2 °F	W lb/hr	Nu_L	Re_L	L/De
A-20-39	49.5	3	4	.2591	191.0	.9	212	.576	17.6	7.69	50.0
40	49.5	5	6 1/2	.4211	117.5	.5	235	.576	19.5	7.69	81.3
41	49.5	6	7 1/2	.4859	101.9	.5	204	.576	16.9	7.69	93.8
42	170.7	7 1/2	7 1/2	.4859	351.3	1.7	207	1.99	17.1	26.6	93.8
44	170.7	5	7 1/2	.4859	351.3	2.0	176	1.99	14.6	26.6	93.8
45	170.7	4	6 1/2	.4211	405.4	2.1	193	1.98	16.0	26.6	81.3
45a	170.7	3	4 1/2	.2915	585.6	2.8	209	1.98	17.3	26.6	56.3
46	170.7	2	3	.1943	878.5	3.7	237	1.98	19.6	26.6	37.5
47	170.7	3	4 1/2	.2915	585.6	2.1	279	1.98	23.1	26.6	56.3
48	341.3	7 1/2	7 1/2	.4859	702.4	2.4	293	3.97	24.3	53.0	93.8
49	341.3	6	7 1/2	.4859	702.4	3.3	213	3.97	17.6	53.0	93.8
50	341.3	5	7 1/2	.4859	702.4	3.1	227	3.97	18.8	53.0	93.8
51	341.3	4	7	.4535	752.6	3.1	243	3.97	20.1	53.0	87.5

TABLE XXXIV CONTINUED

Run#	Q Btu/hr	Outer Sub. "	Max. Inner Sub. "	Wetted Area ft^2	Q/A_W Btu/hr ft^2	ΔT_b °F	h_b Btu/hr ft^2 °F	W lb/hr	Nu_L	Re_L	L/De
A-20-52	341.3	3	5 1/2	.3563	957.9	4.1	234	3.97	19.4	53.0	68.8
53	341.3	3	5 1/2	.3563	957.9	4.2	228	3.97	18.9	53.0	68.8
54	341.3	2	4	.2591	1317	4.7	280	3.97	23.2	53.0	53.0
55	512.0	7 1/2	7 1/2	.4859	1054	4.2	251	5.96	20.8	79.5	93.8
56	512.0	6	7 1/2	.4859	1054	4.8	220	5.96	18.2	79.5	93.8
57	512.0	5	7 1/2	.4859	1054	4.9	215	5.96	17.8	79.5	93.8
58	512.0	3	6	.3887	1317	5.4	244	5.96	20.2	79.5	75.0
59	683.0	7	7 1/2	.4859	1406	6.0	234	7.95	19.4	106.1	93.8
60	683.0	6	7 1/2	.4859	1406	5.9	238	7.95	19.7	106.1	93.8
62	683.0	5	7 1/2	.4859	1406	6.9	204	7.95	16.9	106.1	93.8
63	683.0	3	5 1/2	.3563	1917	6.4	300	7.95	24.8	106.1	68.8
64	853.0	7 1/2	7 1/2	.4859	1756	8.0	220	9.93	18.2	132.5	93.8

TABLE XXXIV CONTINUED

Run#	Q Btu/hr	Outer Sub. "	Max. Inner Sub. "	Wetted Area ft^2	Q/A_W Btu/hr ft^2	ΔT_b °F	h_b Btu/hr ft^2 °F	W lb/hr	Nu_L	Re_L	L/De
A-20-65	853.0	6	7 1/2	.4859	1756	8.1	217	9.93	18.0	132.5	93.8
66	853.0	5	7 1/2	.4859	1756	8.0	220	9.93	18.2	132.5	93.8
67	853.0	3	6	.3887	2194	8.4	261	9.93	21.6	132.5	75.0
68	853.0	7 1/2	7 1/2	.4859	1756	7.5	234	9.93	19.4	132.5	93.8
83	1024	7 1/2	7 1/2	.4859	2107	8.7	242	11.92	20.0	159.1	93.8
84	1024	6	7 1/2	.4859	2107	9.0	234	11.92	19.4	159.1	93.8
85	1024	5	7 1/2	.4859	2107	8.9	237	11.92	19.6	159.1	93.8
86	1024	3	7	.4535	2258	9.1	248	11.92	20.5	159.1	87.5
88	1195	7 1/2	7 1/2	.4859	2459	11.4	216	13.91	17.9	185.6	93.8
89	1195	6	7 1/2	.4859	2459	11.8	208	13.91	17.2	185.6	93.8
90	1195	5	7 1/2	.4859	2459	12.0	205	13.91	17.0	185.6	93.8

TABLE XXXV

CALCULATED DATA - NITROGEN ANNULAR GAP BOILING HEATER #9 (NICKEL PLATED) 0.021" GAP

Run#	Q Btu/hr	Outer Sub. "	Max. Inner Sub. "	Wetted Area ft^2	Q/A_W Btu/hr ft^2	ΔT_b °F	h_b Btu/hr ft^2 °F	W lb/hr	Nu_L	Re_L	L/De
A-21-11	273.0	7 1/2	7 1/2	.4856	562.3	2.6	216	3.18	18.8	42.3	89.3
12	51.2	7 1/2	7 1/2	.4856	105.4	.7	151	.596	13.1	7.93	89.3
13	85.3	7 1/2	7 1/2	.4856	175.7	1.1	160	.993	13.9	13.2	89.3
14	136.5	7 1/2	7 1/2	.4856	281.1	1.9	148	1.59	12.9	21.1	89.3
15	204.8	7 1/2	7 1/2	.4856	421.7	2.6	162	2.38	14.1	31.7	89.3
16	273.0	7 1/2	7 1/2	.4856	562.3	3.0	187	3.18	16.3	42.3	89.3
17	416.4	7 1/2	7 1/2	.4856	857.5	3.4	252	4.85	21.9	64.6	89.3
18	546.1	7 1/2	7 1/2	.4856	1125	3.0	375	6.36	32.6	84.7	89.3
19	750.9	7 1/2	7 1/2	.4856	1546	4.4	351	8.74	30.5	116.4	89.3
20	1024	7 1/2	7 1/2	.4856	2109	6.6	320	11.92	27.8	158.7	89.3
21	1365	7 1/2	7 1/2	.4856	2811	9.3	302	15.89	26.3	211.5	89.3

TABLE XXXV CONTINUED

Run#	Q Btu/hr	Outer Sub. "	Max. Inner Sub. "	Wetted Area ft^2	Q/A_w Btu/hr ft^2	ΔT_b °F	h_b Btu/hr ft^2	W lb /hr	Nu_L	Re_L	L/De
A-21-26	51.2	5 1/2	5 1/2	.3561	143.7	.5	287	.596	25.0	7.93	65.5
27	85.3	5 1/2	5 1/2	.3561	239.6	.7	342	.993	29.7	13.2	65.5
28	136.5	5 1/2	5 1/2	.3561	383.4	1.0	383	1.59	33.3	21.1	65.5
29	204.8	5 1/2	5 1/2	.3561	575.1	1.4	411	2.38	35.8	31.7	65.5
30	373.0	5 1/2	5 1/2	.3561	766.8	1.8	426	3.18	37.1	42.3	65.5
31	409.6	5 1/2	5 1/2	.3561	1150	2.4	479	4.77	41.7	63.4	65.5
32	546.1	5 1/2	5 1/2	.3561	1534	3.3	465	6.36	40.5	84.7	65.5
33	757.7	5 1/2	5 1/2	.3561	2128	4.5	473	8.82	41.2	117.3	65.5
34	1024	5 1/2	5 1/2	.3561	2875	7.2	399	11.92	34.7	158.7	65.5
35	1372	5 1/2	5 1/2	.3561	3853	9.1	423		36.8	212.3	65.5

TABLE XXXV

CALCULATED DATA - NITROGEN ANNULAR GAP BOILING HEATER #10 (CADMIUM PLATED) 0.022" GAP

Run#	Q Btu/hr	Outer Sub. "	Max. Inner Sub. "	Wetted Area ft^2	Q/A$_W$ Btu/hr ft^2	ΔT_b °F	h_b Btu/hr ft^2 °F	W lb/hr	Nu$_L$	Re$_L$	L/De
A-22- 2	68.3	7 1/2	7 1/2	.4851	140.7	.7	201	.795	18.3	10.7	85.2
3	136.5	7 1/2	7 1/2	.4851	281.4	1.5	188	1.59	17.1	21.5	85.2
4	208.2	7 1/2	7 1/2	.4851	429.2	2.3	187	2.42	17.0	34.2	85.2
5	314.0	7 1/2	7 1/2	.4851	642.0	3.4	189	3.66	17.2	49.3	85.2
6	409.6	7 1/2	7 1/2	.4851	844.3	4.8	176	4.77	16.0	64.4	85.2
7	549.5	7 1/2	7 1/2	.4851	1133	5.8	195	6.40	17.8	86.2	85.2
8	689.4	7 1/2	7 1/2	.4851	1421	6.9	206	8.03	18.8	108.2	85.2
9	853.3	7 1/2	7 1/2	.4851	1759	8.7	202	9.93	18.4	134.0	85.2
10	1109	7 1/2	7 1/2	.4851	2287	11.2	204	12.91	18.6	174.2	85.2
11	1314	7 1/2	7 1/2	.4851	2709	13.2	205	15.30	18.7	206.3	85.2
13	143.3	5 3/4	7 1/2	.4851	295.5	1.1	269	1.67	24.5	22.5	85.2
14	344.7	4 1/2	7 1/2	.4851	710.6	3.2	222	4.01	20.2	54.2	85.2

TABLE XXXVI CONTINUED

Run#	Q Btu/hr	Outer Sub. "	Max. Inner Sub. "	Wetted Area ft^2	Q/A_W Btu/hr ft^2	ΔT_b °F	h_b Btu/hr ft^2 °F	W lb/hr	Nu_L	Re_L	L/De
A-22-15	563.1	4	7 1/2	.4851	1161	5.6	207	6.55	18.9	88.4	85.2
16	836.1	3 1/2	7 1/2	.4851	1724	8.4	205	9.73	18.7	131.3	85.2
17	1177	2 1/2	7 1/2	.4851	2427	12.9	188	13.70	17.1	184.7	85.2
19	139.9	3 3/4	5	.3234	432.7	.8	541	1.63	49.3	22.0	56.8
20	276.5	3	5	.3234	854.8	1.7	503	3.22	45.8	43.5	56.8
21	430.0	2 1/2	5	.3234	1330	3.5	380	5.01	34.6	67.4	56.8
22	269.6	3/4	2	.1294	2084	1.0	2084	3.14	190	42.4	22.7

TABLE XXXVII

CALCULATED DATA - NITROGEN ANNULAR GAP BOILING HEATER #7b - 0.053" GAP

Run#	Q Btu/hr	Outer Sub. "	Max. Inner Sub. "	Wetted Area ft^2	Q/A_W Btu/hr ft^2	ΔT_b °F	h_b Btu/hr ft^2 °F	W lb/hr	Nu_L	Re_L	L/De
A-53- 2	51.2	7 1/2	7 1/2	.4750	107.8	1.1	98	.596	21.5	8.0	35.4
3	136.5	7 1/2	7 1/2	.4750	287.4	2.4	120	1.59	26.3	21.4	35.4
4	273.0	7 1/2	7 1/2	.4750	574.8	4.2	137	3.18	30.1	42.8	35.4
5	512.0	7 1/2	7 1/2	.4750	1078	7.5	144	5.96	31.6	80.1	35.4
6	683.0	7 1/2	7 1/2	.4750	1437	8.6	167	7.95	36.7	107.1	35.4
7	853.0	7 1/2	7 1/2	.4750	1796	10.4	173	9.93	38.0	133.7	35.4
8	1024	7 1/2	7 1/2	.4750	2156	11.8	183	11.92	40.2	160.2	35.4
9	1365	7 1/2	7 1/2	.4750	2874	15.2	189	15.89	41.5	213.8	35.4
10	683.0	7 1/2	7 1/2	.4750	1437	9.8	147	7.95	32.3	107.1	35.4
13	51.2	7 1/2	7 1/2	.4750	107.8	1.1	98	.596	21.5	8.0	35.4
14	170.7	7 1/2	7 1/2	.4750	359.3	2.7	133	1.99	29.2	26.7	35.4
15	512.0	7 1/2	7 1/2	.4750	1078	6.2	174	5.96	38.2	80.1	35.4

TABLE XXXVII CONTINUED

Run#	Q Btu/hr	Outer Sub. "	Max. Inner Sub. "	Wetted Area ft^2	Q/A_w Btu/hr ft^2	ΔT_b °F	h_b Btu/hr ft^2 °F	W lb/hr	Nu_L	Re_L	L/De
A-53-16	1024	7 1/2	7 1/2	.4750	2156	10.4	207	11.92	45.4	160.2	35.4
17	1365	7 1/2	7 1/2	.4750	2874	13.6	211	15.89	46.3	213.8	35.4
20	170.7	4 1/8	5	.3167	539.0	1.9	284	1.99	62.3	26.7	23.6
21	512.0	3 1/2	5	.3167	1617	5.2	311	5.96	68.3	80.1	23.6
22	1024	2 3/4	5	.3167	3233	9.5	340	11.92	74.6	160.2	23.6
23	1365	2 1/2	5	.3167	4310	12.0	359	15.89	78.8	213.8	23.6
24	51.2	7 1/2	7 1/2	.4750	107.8	.7	154	.596	33.8	8.0	35.4
25	51.2	2	2 1/2	.1583	323.4	.9	359	.596	78.8	8.0	11.8
26	170.7	2	2 1/2	.1583	1078	2.5	431	1.99	94.6	26.7	11.8
27	512.0	1 1/2	2 1/2	.1583	3234	5.5	588	5.96	129	80.1	11.8
30	51.2	7 1/2	7 1/2	.4750	107.8	.8	135	.596	29.6	8.0	35.4
31	136.5	7 1/2	7 1/2	.4750	287.4	1.6	180	1.59	39.5	21.4	35.4
32	273.0	7 1/2	7 1/2	.4750	574.8	3.6	160	3.18	35.1	42.8	35.4

TABLE XXXVII CONTINUED

Run#	Q Btu/hr	Outer Sub. "	Max. Inner Sub. "	Wetted Area ft^2	Q/A_w Btu/hr ft^2	ΔT_b °F	h_b Btu/hr ft^2 °F	W lb/hr	Nu_L	Re_L	L/De
A-53-33	505.1	7 1/2	7 1/2	.4750	1063	6.1	174	5.88	38.2	79.2	35.4
34	750.9	7 1/2	7 1/2	.4750	1581	8.9	178	8.74	39.1	117.5	35.4
35	1195	7 1/2	7 1/2	.4750	2515	12.9	195	13.91	42.8	187.2	35.4
38	170.7	7 1/2	7 1/2	.4750	359.3	2.3	156	1.99	34.2	26.7	35.4
39	409.6	7 1/2	7 1/2	.4750	862.3	5.1	169	4.77	37.1	64.4	35.4
40	409.6	7 1/2	7 1/2	.4750	862.3	5.3	163	4.77	35.8	64.4	35.4
41	785.0	7 1/2	7 1/2	.4750	1653	7.4	223	9.14	48.9	122.9	35.4
42	1263	7 1/2	7 1/2	.4750	2659	13.0	205	14.70	45.0	197.6	35.4
44	204.8	7 1/2	7 1/2	.4750	431.1	3.0	144	2.38	31.6	32.0	35.4
45	85.3	7 1/2	7 1/2	.4750	179.6	1.1	163	.993	35.8	13.4	35.4
46	85.3	5	5 1/2	.3483	244.9	.9	272	.993	59.7	13.4	25.9
47	136.5	4 3/4	5 1/2	.3483	391.9	1.3	301	1.59	66.1	21.4	25.9
48	273.0	4	5 1/2	.3483	783.8	2.8	264	3.18	57.9	42.8	25.9
49	409.6	3 1/2	5 1/2	.3483	1176	3.9	302	4.77	66.3	64.4	25.9

TABLE XXXVII CONTINUED

Run#	Q Btu/hr	Outer Sub. "	Max. Inner Sub. "	Wetted Area ft^2	Q/A_W Btu/hr ft^2	ΔT_b °F	h_b Btu/hr ft^2 °F	W lb/hr	Nu_L	Re_L	L/De
A-53-50	512.0	3 1/4	5 1/2	.3483	1470	5.4	272	5.96	59.7	80.1	25.9
51	750.9	3	5 1/2	.3483	2156	10.4	207	8.74	45.4	117.5	25.9
55	51.2	2	2 1/2	.1583	323.4	1.5	216	.596	47.4	8.0	11.8
56	136.5	2	2 1/2	.1583	862.3	2.6	332	1.59	72.9	21.4	11.8
A-53a- 2	85.3		7 1/2	.4750	179.6	1.2	150	.993	32.9	8.87	35.4
3	208.2		7 1/2	.4750	438.0	3.2	137	2.42	30.1	21.6	35.4
4	416.4		7 1/2 + 3/4	.4750	876.6	6.0	146	4.85	32.1	43.3	35.4
5	610.9		7 1/2 + 1	.4750	1286	8.3	155	7.11	34.0	63.5	35.4
6	853.3		7 1/2 + 1 1/4	.4750	1796	11.8	152	9.93	33.4	88.7	35.4
7	1092		7 1/2 + 1 1/2	.4750	2299	13.8	167	12.71	36.7	113.4	35.4

TABLE XXXVII CONTINUED

Run#	Q Btu/hr	Outer Sub. "	Max. Inner Sub. "	Wetted Area ft^2	Q/A_W Btu/hr ft^2	ΔT_b °F	h_b Btu/hr ft^2 °F	W lb/hr	Nu_L	Re_L	L/De
A-53a - 8	1365		7 1/2 + 2 - 2 1/2	.4750	2874	17.0	169	15.89	37.1	141.8	35.4
10	102.4	6 1/4	7 1/2	.4750	215.6	1.4	154	1.19	33.8	10.7	35.4
11	238.9	5 3/8	7 1/2	.4750	503.0	3.4	148	2.78	32.5	24.8	35.4
12	409.6	4 5/8	7 1/2	.4750	862.2	6.0	144	4.77	31.6	42.6	35.4
13	590.4	4	7 1/2	.4750	1243	8.6	145	6.87	31.8	61.2	35.4
14	819.1	3 5/8	7 1/2	.4750	1724	9.5	131	9.53	39.7	85.1	35.4
15	1201	3 1/4	7 1/2	.4750	2529	17.3	146	13.98	32.1	124.7	35.4
17	102.4	3 1/2	4 1/2	.2850	359.3	1.2	299	1.19	65.6	10.7	21.2
18	242.3	3 1/2	5 - 5 1/2	.3483	695.7	3.0	232	2.82	50.9	25.2	25.9
19	409.6	2 3/4 - 3	5 1/2	.3483	1176	5.8	203	4.77	44.6	42.6	25.9
20	614.3	2 1/4 - 2 1/2	5 - 5 1/2	.3483	1764	9.1	194	7.15	42.6	63.9	25.9
21	283.3	1	2 - 2 1/4	.1425	1988	7.1	280	3.30	61.5	29.5	10.6
22	440.3	3/4	1 1/2 - 2	.1267	3475	12.1	287	5.13	63.0	45.9	9.4

TABLE XXXVIII

CALCULATED DATA - NITROGEN ANNULAR GAP BOILING HEATER #8 0.080" GAP

Run#	Q Btu/hr	Outer Sub. "	Max. Inner Sub. "	Wetted Area ft^2	Q/A_w Btu/hr ft^2	ΔT_b °F	h_b Btu/hr ft^2 °F	W lb/hr	Nu_L	Re_L	L/De
A-80-13	51.2	7 1/2	7 1/2	.4663	109.8	1.2	91.5	.596	30.3	8.07	23.4
14	51.2	5 1/2	6	.3730	137.3	1.1	125	.596	41.4	8.07	18.8
15	51.2	4 1/2	5	.3109	164.7	1.0	165	.596	54.7	8.07	15.6
16	51.2	2 1/2	3	.1865	274.5	2.3	119	.596	39.4	8.07	9.38
17	51.2	3	3 1/2	.2176	235.3	2.0	118	.596	39.1	8.07	10.9
18	51.2	5	5 1/2	.3419	149.8	1.3	115	.596	38.1	8.07	17.2
19	51.2	6	6 1/2	.4042	126.7	1.2	106	.596	35.1	8.07	20.3
20	51.2	7 1/2	7 1/2	.4663	109.8	1.3	84.5	.596	28.0	8.07	23.4
22	170.7	7 1/2	7 1/2	.4663	366.1	3.2	114	1.99	37.8	26.9	23.4
23	170.7	5	6	.3730	457.6	3.2	143	1.99	47.4	26.9	18.8
24	170.7	3	4	.2487	686.4	5.2	131	1.99	43.4	26.9	12.5
26	341.3	7 1/2	7 1/2	.4663	731.9	5.1	144	3.97	47.7	53.9	23.4

TABLE XXXVIII CONTINUED

Run#	Q Btu/hr	Outer Sub. "	Max. Inner Sub. "	Wetted Area ft^2	Q/A_w Btu/hr ft^2	ΔT_b °F	h_b Btu/hr ft^2 °F	W lb/hr	Nu_L	Re_L	L/De
A-80-27	341.3	5	7	.4352	784.2	5.4	145	3.97	48.0	53.9	21.8
28	341.3	3	5 1/2	.3419	998.2	7.9	126	3.97	41.7	53.9	17.2
29	170.7	7 1/2	7 1/2	.4663	366.1	3.4	108	1.99	35.8	26.9	23.4
30	170.7	5	6	.3730	457.6	3.5	131	1.99	43.4	26.9	18.8
32	51.2	7 1/2	7 1/2	.4663	109.8	1.2	91.5	.596	30.3	8.07	23.4
33	51.2	5	5 1/2	.3419	149.8	—	—	.596	—	8.07	17.2
34	51.2	3	3 1/2	.2176	235.3	2.7	87.1	.596	28.9	8.07	10.9
37	512.0	7	7 1/2	.4663	1098	6.4	172	5.96	57.0	80.7	23.4
38	512.0	4 1/2	6 1/2	.4042	1267	6.5	195	5.96	64.6	80.7	20.3
39	512.0	2 1/2	4	.2487	2059	7.4	278	5.96	92.1	80.7	12.5
41	683.0	7	7 1/2	.4663	1465	8.6	170	7.95	56.3	108.1	23.4
42	679.0	5	7 1/2	.4663	1465	8.7	167	7.90	55.3	107.4	23.4
43	679.0	2 1/2	4	.2487	2730	11.2	244	7.90	80.8	107.4	12.5
45	853.0	7 1/2	7 1/2	.4663	1829	9.4	195	9.93	64.6	134.7	23.4

TABLE XXXVIII CONTINUED

CALCULATED DATA - NITROGEN ANNULAR GAP BOILING HEATER #8 0.080" GAP

Run#	Q Btu/hr	Outer Sub. "	Max. Inner Sub. "	Wetted Area ft^2	Q/A_w Btu/hr ft^2	ΔT_b °F	h_b Btu/hr ft^2 °F	W lb/hr	Nu_L	Re_L	L/De
A-80-46	853.0	4 1/2	7 1/2	.4663	1829	10.3	178	9.93	59.0	134.7	23.4
47	853.0	2 1/2	4 1/2	.2798	3049	13.0	235	9.93	77.9	134.7	14.1
48	1024	7 1/2	7 1/2	.4663	2196	11.0	200	11.92	66.3	162.1	23.4
49	1024	4 1/2	7 1/2	.4663	2196	12.0	183	11.92	60.6	162.1	23.4
50	1027	2 1/2	4 1/2	.2798	3670	13.5	272	11.95	90.1	162.1	14.1
58	341.3	5	6 1/2	.4041	845	4.9	172	3.97	57.0	53.9	20.3
59	337.9	3	4	.2487	1359	5.9	230	3.93	76.2	53.4	12.5
60	337.9	7 1/2	7 1/2	.4663	725	4.6	158	3.93	52.3	53.4	23.4
62	1365	7 1/2	7 1/2	.4663	2927	14.8	198	15.89	65.6	215.5	23.4
63	1365	4	7 1/2	.4663	2927	14.5	202	15.89	66.9	215.5	23.4
67	1365	3	5 1/2	.3419	3992	16.4	243	15.89	80.5	215.5	17.2

TABLE XXXIX

CALCULATED DATA - NEON ANNULAR GAP BOILING HEATER #12b 0.006" GAP

Run#	Q Btu/hr	Outer Sub. "	Max. Inner Sub. "	Wetted Area ft^2	Q/A$_w$ Btu/hr ft^2	ΔT_b °F	h_b Btu/hr ft^2 °F	W lb/hr	Nu_L	Re_L	L/De
B-6-2	51.2	7 1/2	7 1/2 + 1/4	.4905	104.4	.5	209	1.38	5.56	9.88	313
3	136.5	7 1/2	7 1/2	.4905	278.3	.6	464	3.68	12.3	26.3	313
6	88.7	7 1/2	7 1/2	.4905	180.9	.8	226	2.39	6.01	17.1	313
7	119.5	7 1/2	7 1/2	.4905	243.5	1.0	244	3.22	6.49	23.0	313
8	157.0	7 1/2	7 1/2	.4905	320.1	1.1	291	4.24	7.74	30.3	313
10	34.1	7 1/2	7 1/2	.4905	69.6	.5	139	.920	3.70	6.58	313
11	68.3	7 1/2	7 1/2	.4905	139.2	1.0	139	1.84	3.70	13.2	313

TABLE XL

CALCULATED DATA - NEON ANNULAR GAP BOILING HEATER #6 0.020" GAP

Run#	Q Btu/hr	Outer Sub. "	Max. Inner Sub. "	Wetted Area ft^2	Q/A_W Btu/hr ft^2	ΔT_b °F	h_b Btu/hr ft^2 °F	W lb/hr	Nu_L	Re_L	L/De
B-20-7	136.5	7 1/2	7 1/2	.4859	280.9	.6	468	3.68	41.5	26.4	93.8
9	273.0	7 1/2	7 1/2	.4859	561.8	1.3	432	7.37	38.3	52.9	93.8
10	512.0	7 1/2	7 1/2	.4859	1054	3.8	277	13.81	24.6	99.2	93.8
11	512.0	7 1/2	7 1/2	.4859	1054	8.3	—	13.81	—	99.2	93.8
12	512.0	7 1/2	7 1/2	.4859	1054	9.2	—	13.81	—	99.2	93.8
13	512.0	7 1/2	7 1/2	.4859	1054	5.4	195	13.81	17.3	99.2	93.8
14	750.9	7 1/4	7 1/2	.4859	1545	6.3	245	20.59	21.6	145.4	93.8

TABLE XLI

CALCULATED DATA - NEON ANNULAR GAP BOILING HEATER #9 (NICKEL PLATED) 0.021" GAP

Run#	Q Btu/hr	Outer Sub. "	Max. Inner Sub. "	Wetted Area Ft^2	Q/A_w Btu/hr ft^2	ΔT_b °F	hb Btu/hr ft^2 °F	W lb/hr	NuL	Re_L	L/De
B-21-4	51.2	7 1/2	7 1/2	.4856	105.4	.6	176	1.38	16.4	9.91	89.3
5	102.4	7 1/2	7 1/2	.4856	210.9	.9	234	2.76	21.8	19.8	89.3
6	170.7	7 1/2	7 1/2	.4856	351.4	.6	586	4.61	54.6	33.1	89.3
9	170.7	7 1/2	7 1/2	.4856	351.4	.6	586	4.61	54.6	33.1	89.3
10	273.0	7 1/2	7 1/2	.4856	562.3	1.1	511	7.37	47.6	53.0	89.3
11	413.0	7 1/2	7 1/2	.4856	850.4	2.0	425	11.14	39.6	80.0	89.3
12	549.5	7 1/2	7 1/2	.4856	1132	3.0	377	14.83	35.1	106.5	89.3
13	696.3	7 1/2	7 1/2	.4856	1434	2.6	552	18.79	51.4	135.0	89.3

TABLE XLII

CALCULATED DATA - NEON ANNULAR GAP BOILING HEATER #7b 0.053" GAP

Run#	Q Btu/hr	Outer Sub. "	Max. Inner Sub. "	Wetted Area ft^2	Q/A_w Btu/hr ft^2	ΔT_b °F	h_b Btu/hr ft^2 °F	W lb/hr	Nu_L	Re_L	L/De
B-53- 2	51.2	7 1/2	7 1/2	.4750	107.8	.7	154	1.381	36.2	10.0	35.4
3	136.5	7 1/2	7 1/2	.4750	287.4	2.1	137	3.68	32.2	26.7	35.4
4	273.0	7 1/2	7 1/2	.4750	574.8	3.8	151	7.37	35.5	53.4	35.4
5	512.0	7 1/2	7 1/2	.4750	1078	5.1	211	13.81	49.6	100.0	35.4
6	1365	6 1/2	7 1/2	.4750	2874	13.2	218	36.83	51.2	267.0	35.4
8	853.3	5 1/2	7 1/2	.4750	1796	10.8	166	23.02	39.0	167.0	35.4
9	682.6	4 1/2	7	.4333	1539	9.2	167	18.42	39.2	133.0	33.0
10	512.0	4	6	.3800	1347	7.2	187	13.81	44.0	100.0	28.3

TABLE XLIII

CALCULATED DATA - NEON ANNULAR GAP BOILING HEATER #8 0.080" GAP

Run#	Q Btu/hr	Outer Sub. "	Max. Inner Sub. "	Wetted Area Ft^2	Q/A_w Btu/hr ft^2	ΔT_b °F	h_b Btu/hr ft^2 °F	W lb/hr	Nu_L	Re_L	L/De
B-80-2	51.2	7 1/2	7 1/2	.4663	109.8	0.5	220	1.381	78.1	10.1	23.4
3	136.2	7 1/2	7 1/2	.4663	292.8	.8	366	3.68	130	27.0	23.4
4	273.0	7 1/2	7 1/2	.4663	585.5	1.4	418	7.37	148	54.2	23.4
5	512.0	7 1/2	7 1/2	.4663	1098	3.0	366	13.81	130	101.0	23.4
6	750.9	7 1/2	7 1/2	.4663	1610	4.1	393	20.26	140	148.0	23.4
7	750.9	7 1/2	7 1/2	.4663	1610	4.3	374	20.26	133	148.0	23.4
8	1195	7 1/2	7 1/2	.4663	2562	7.2	356	32.24	126	236.0	23.4
10	85.3	7 1/2	7 1/2	.4663	183.0	.7	251	2.30	92.7	16.9	23.4
11	204.8	7 1/2	7 1/2	.4663	439.2	1.9	231	5.53	82.0	40.4	23.4
12	341.3	7 1/2	7 1/2	.4663	731.9	2.5	293	9.21	104	67.7	23.4
14	238.9	7 1/2	7 1/2	.4663	512.3	1.1	456	6.45	165	47.1	23.4
15	1536	7 1/2	7 1/2	.4663	3294	10.3	320	41.4	114	304.0	23.4

FIGURE 27, HEAT FLUX VERSUS TEMPERATURE DRIVING FORCE ($\Delta T_b = T_w - T_{sat.}$)
NITROGEN ANNULAR GAP BOILING
COPPER HEATER 12 b
GAP DIM. AT LIQ. N_2 TEMP. 6 mils.

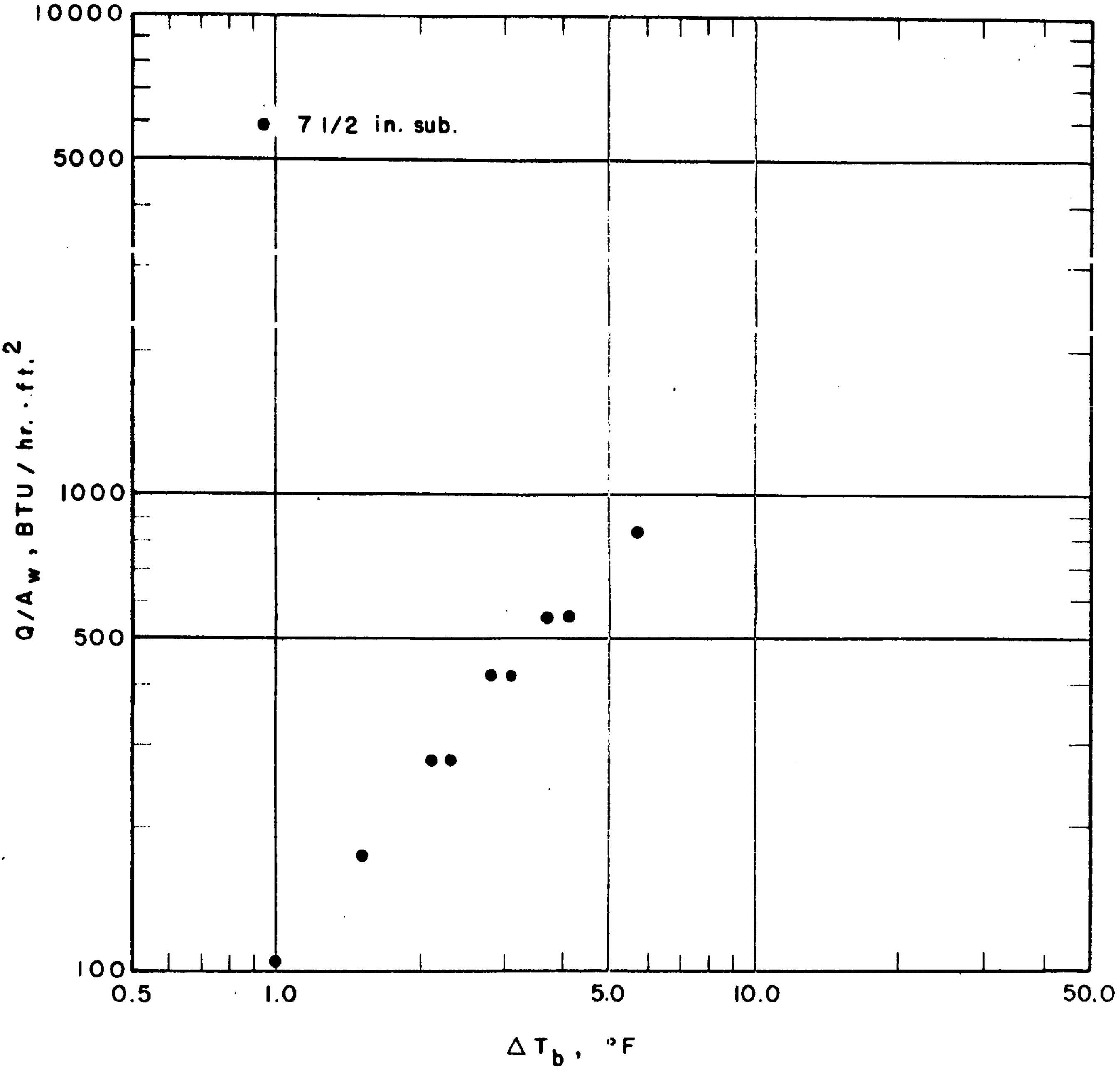

FIGURE 28, HEAT FLUX VERSUS TEMPERATURE DRIVING FORCE ($\Delta T_b = T_w - T_{Sat.}$) NITROGEN ANNULAR GAP BOILING COPPER HEATER 6 GAP DIM. AT LIQ. N_2 TEMP. 20 mils.

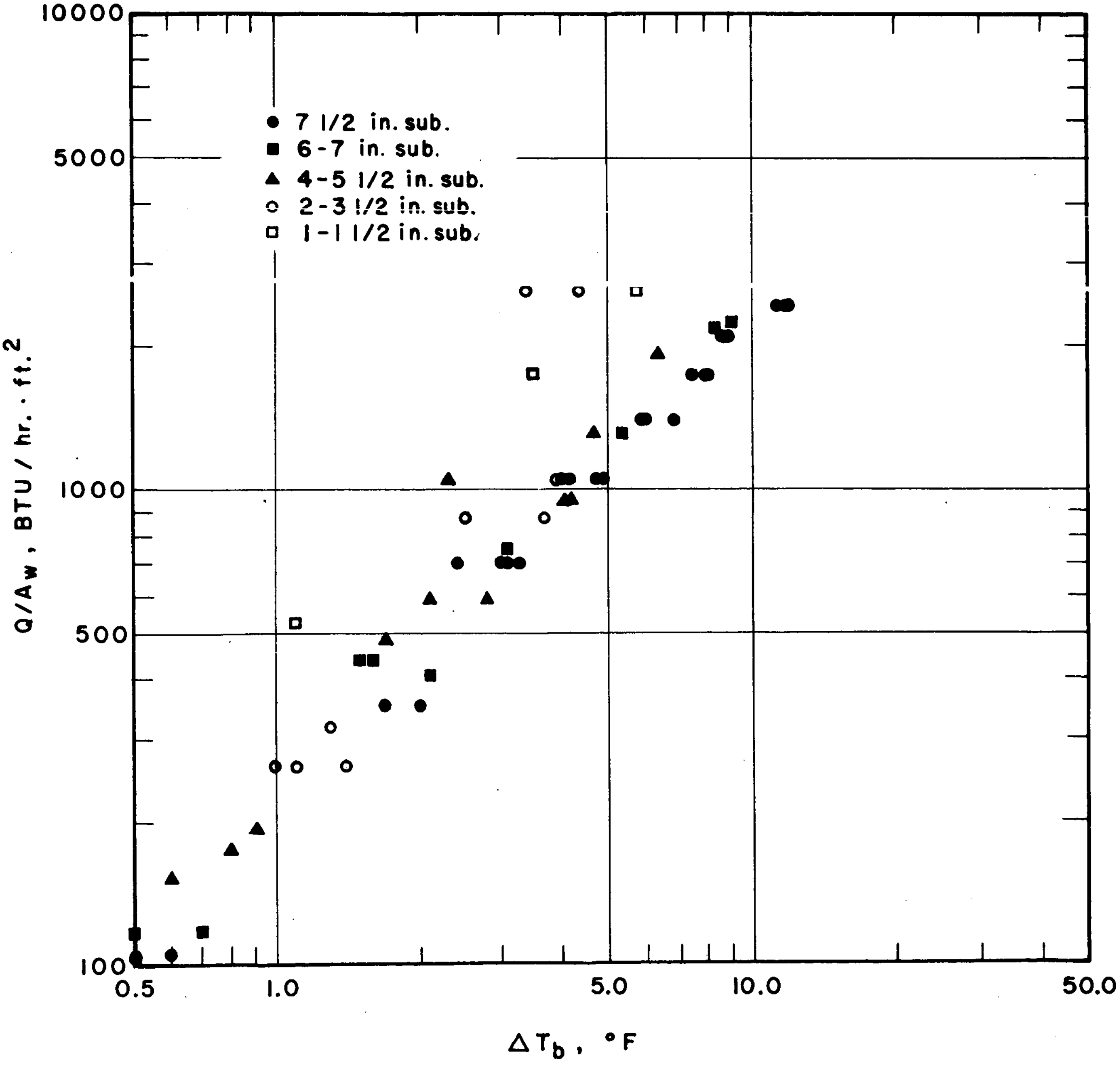

FIGURE 29, HEAT FLUX VERSUS TEMPERATURE DRIVING FORCE ($\Delta T_b = T_w - T_{Sat.}$) NITROGEN ANNULAR GAP BOILING NICKEL PLATED COPPER HEATER 9 GAP DIM. AT LIQ. N_2 TEMP. 21mils.

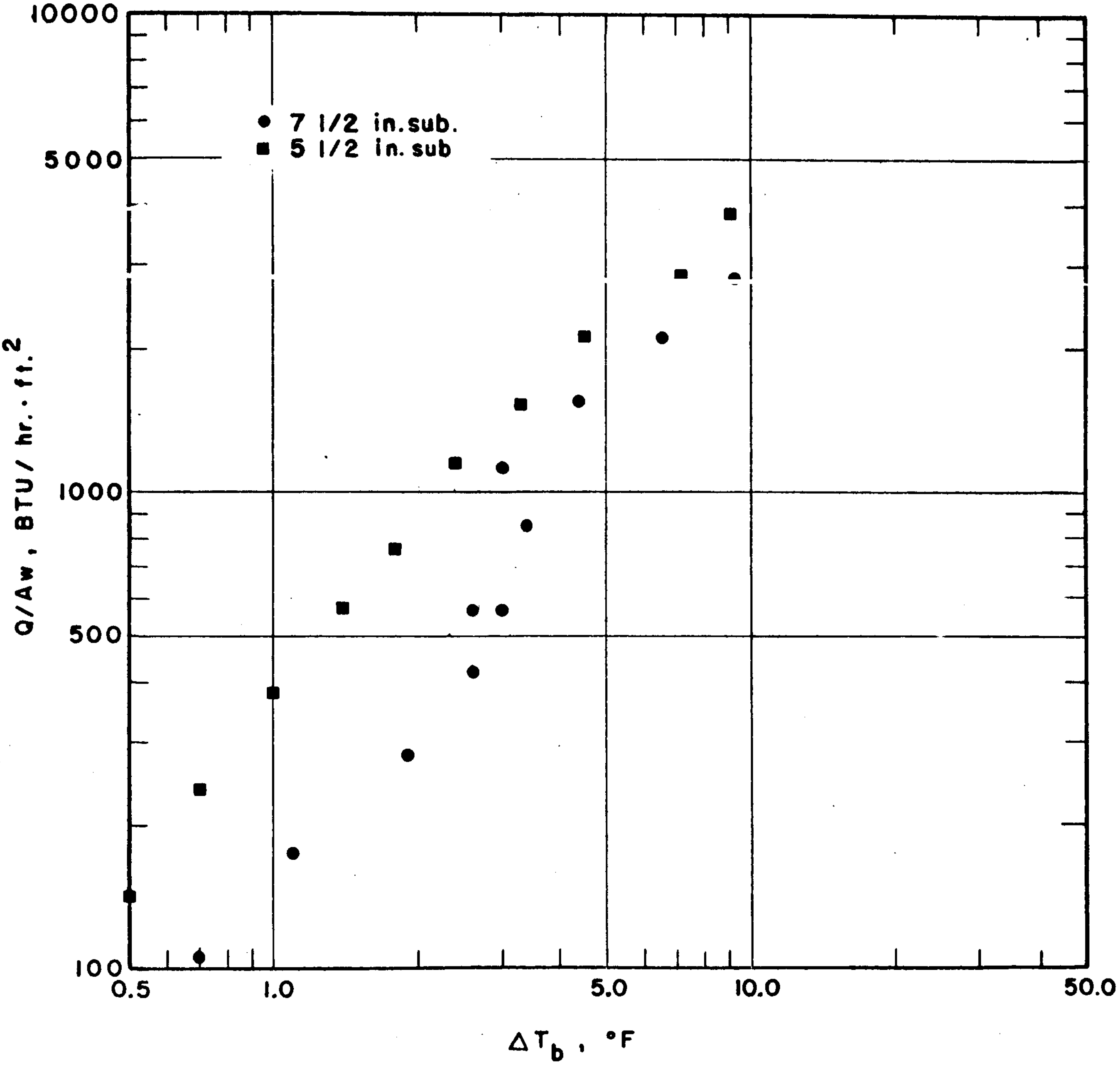

FIGURE 30, HEAT FLUX VERSUS TEMPERATURE DRIVING FORCE ($\Delta T_b = T_w - T_{Sat.}$) NITROGEN ANNULAR GAP BOILING CADMIUM PLATED COPPER HEATER 10 GAP DIM. AT LIQ. N_2 TEMP. 22 mils.

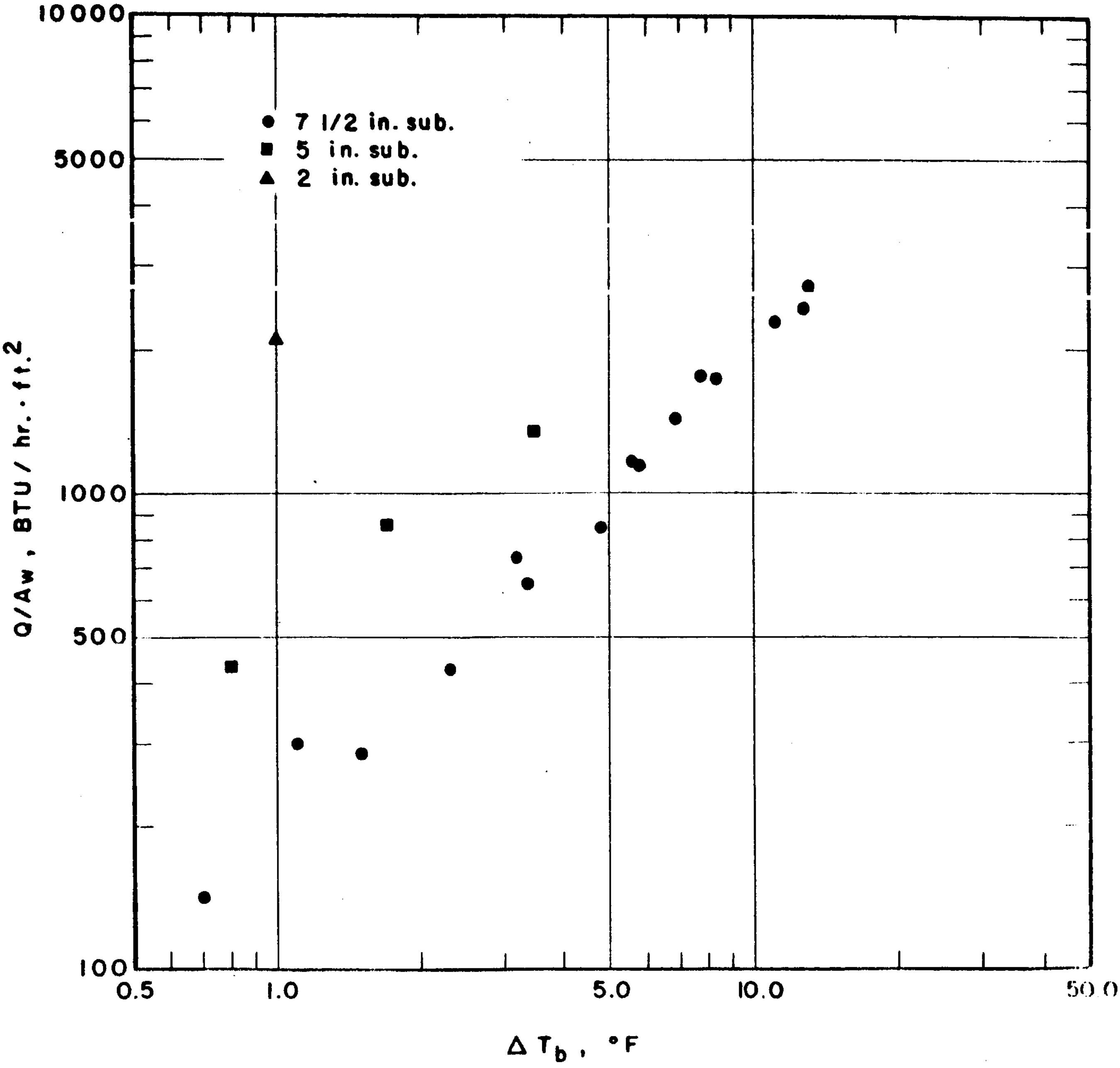

FIGURE 31, HEAT FLUX VERSUS TEMPERATURE DRIVING FORCE ($\Delta T_b = T_w - T_{Sat.}$)
NITROGEN ANNULAR GAP BOILING
COPPER HEATER 7b
GAP DIM. AT LIQ. N_2 TEMP. 53 mils.

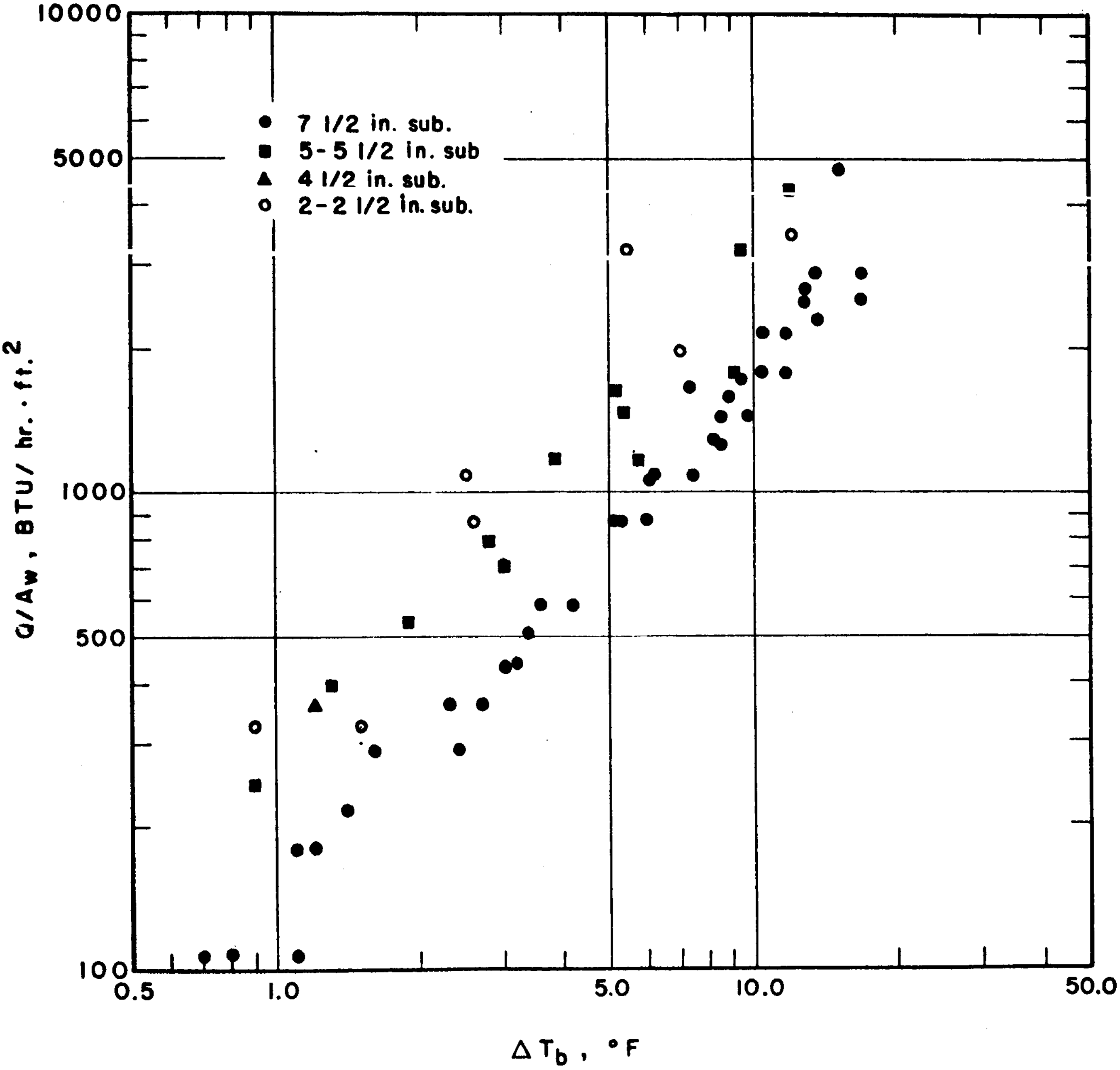

FIGURE 32, HEAT FLUX VERSUS TEMPERATURE DRIVING FORCE ($\Delta T_b = T_w - T_{Sat.}$) NITROGEN ANNULAR GAP BOILING COPPER HEATER 8 GAP DIM. AT LIQ. N_2 TEMP. 80 mils.

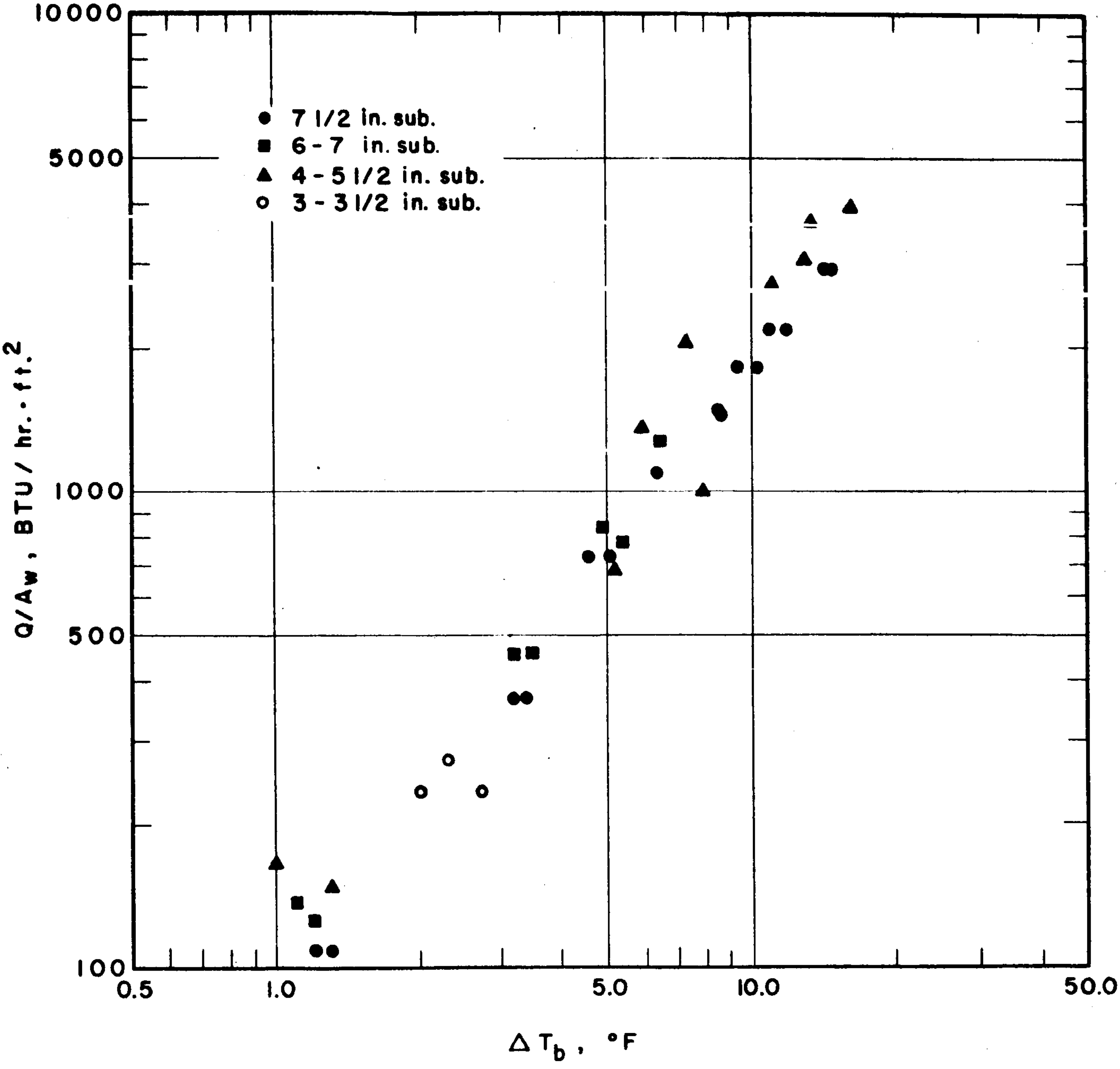

FIGURE 33, HEAT FLUX VERSUS TEMPERATURE DRIVING FORCE ($\Delta T_b = T_w - T_{Sat.}$) NITROGEN ANNULAR GAP BOILING COMPARISON BETWEEN ALL HEATERS AT 7 1/2" INNER SUBMERGENCE

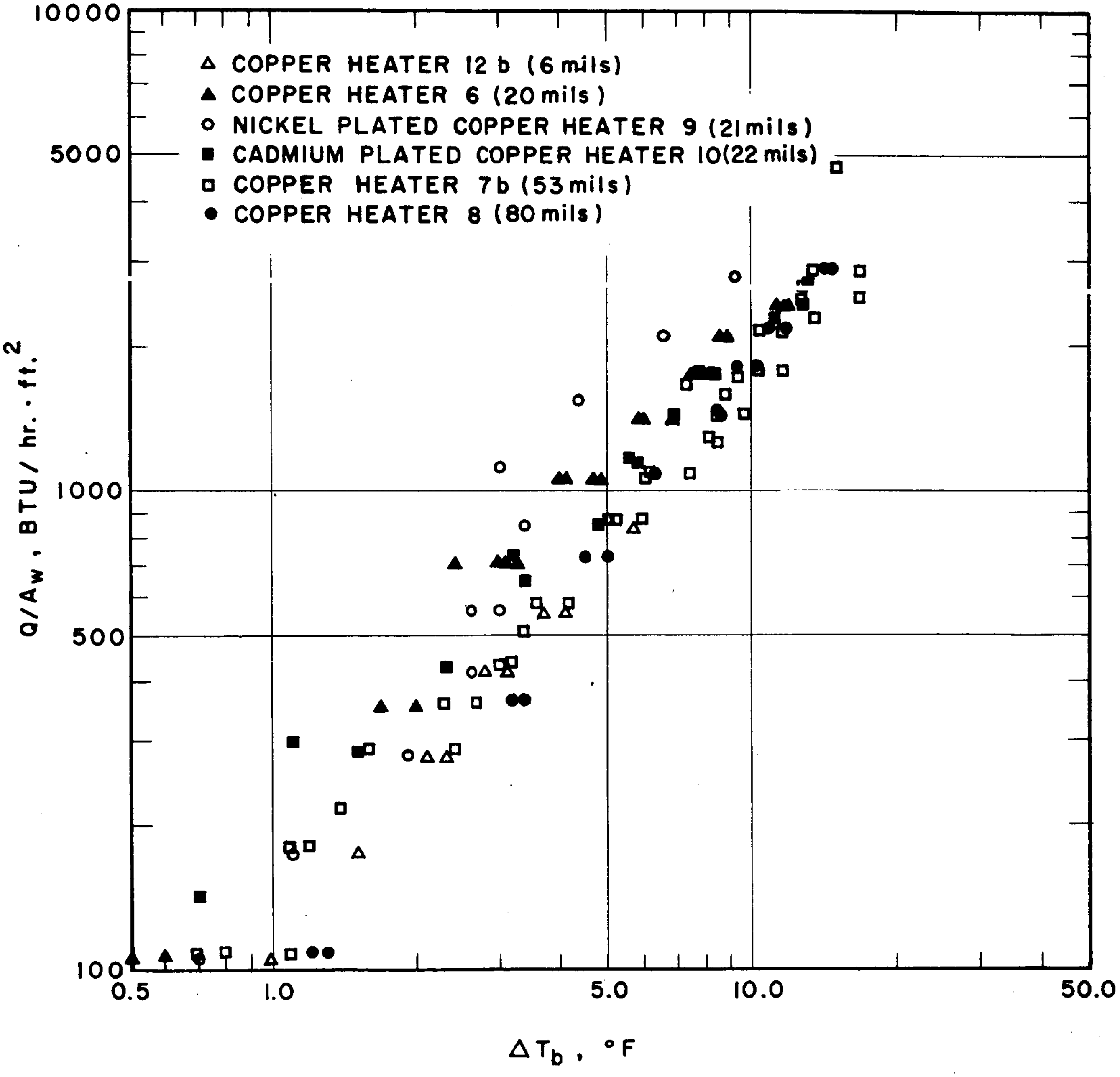

FIGURE 34, COMPARISON BETWEEN NEON AND NITROGEN POOL BOILING HEAT FLUX VERSUS OVERALL TEMPERATURE DRIVING FORCE HEATER 12 b

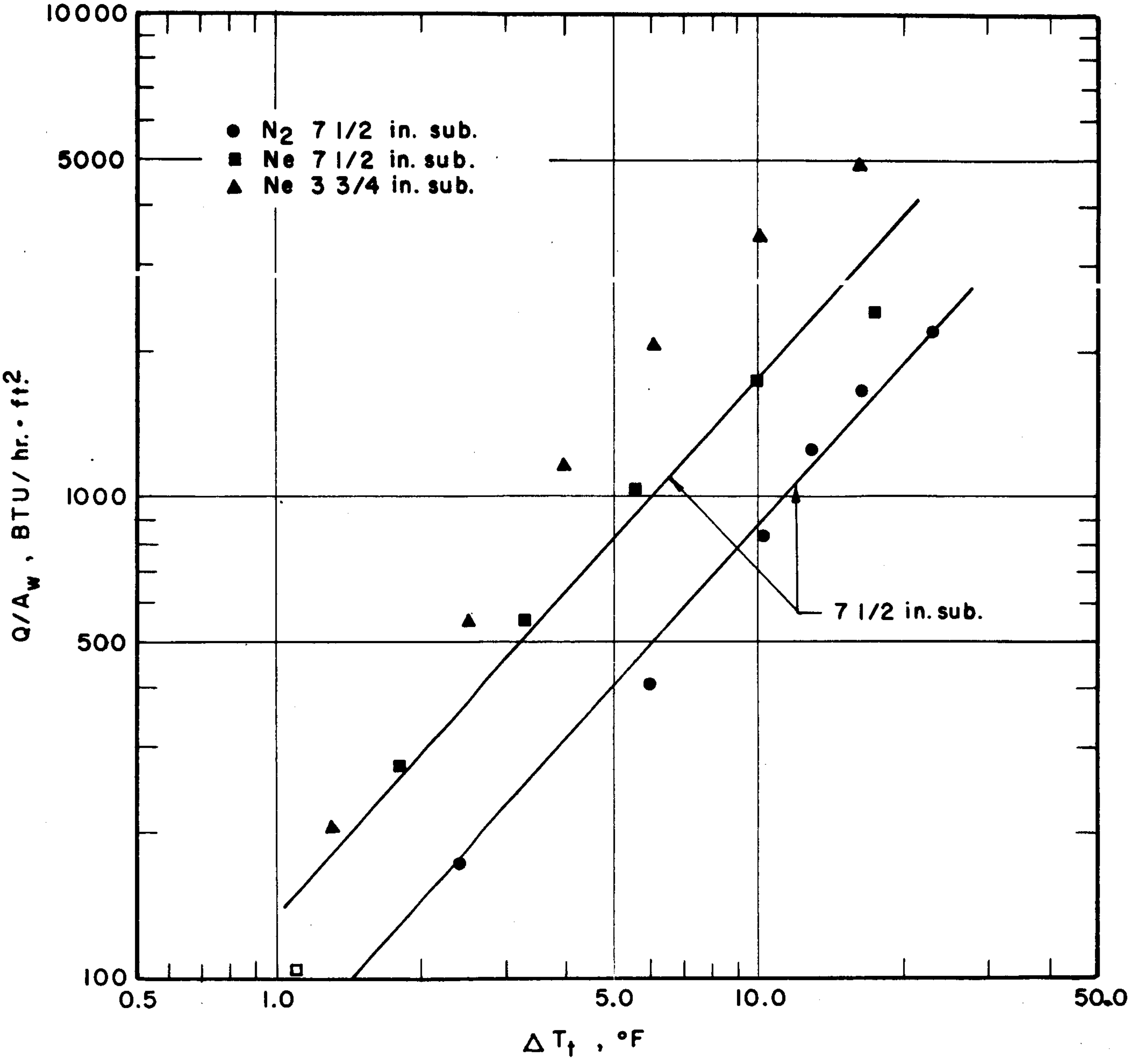

FIGURE 35, HEAT FLUX VERSUS TEMPERATURE DRIVING FORCE ($\Delta T_b = T_w - T_{Sat.}$)
NEON ANNULAR GAP BOILING
COPPER HEATER 12 b
GAP DIM. AT LIQ. NEON TEMP. 6 mils.
7 1/2" INNER SUBMERGENCE

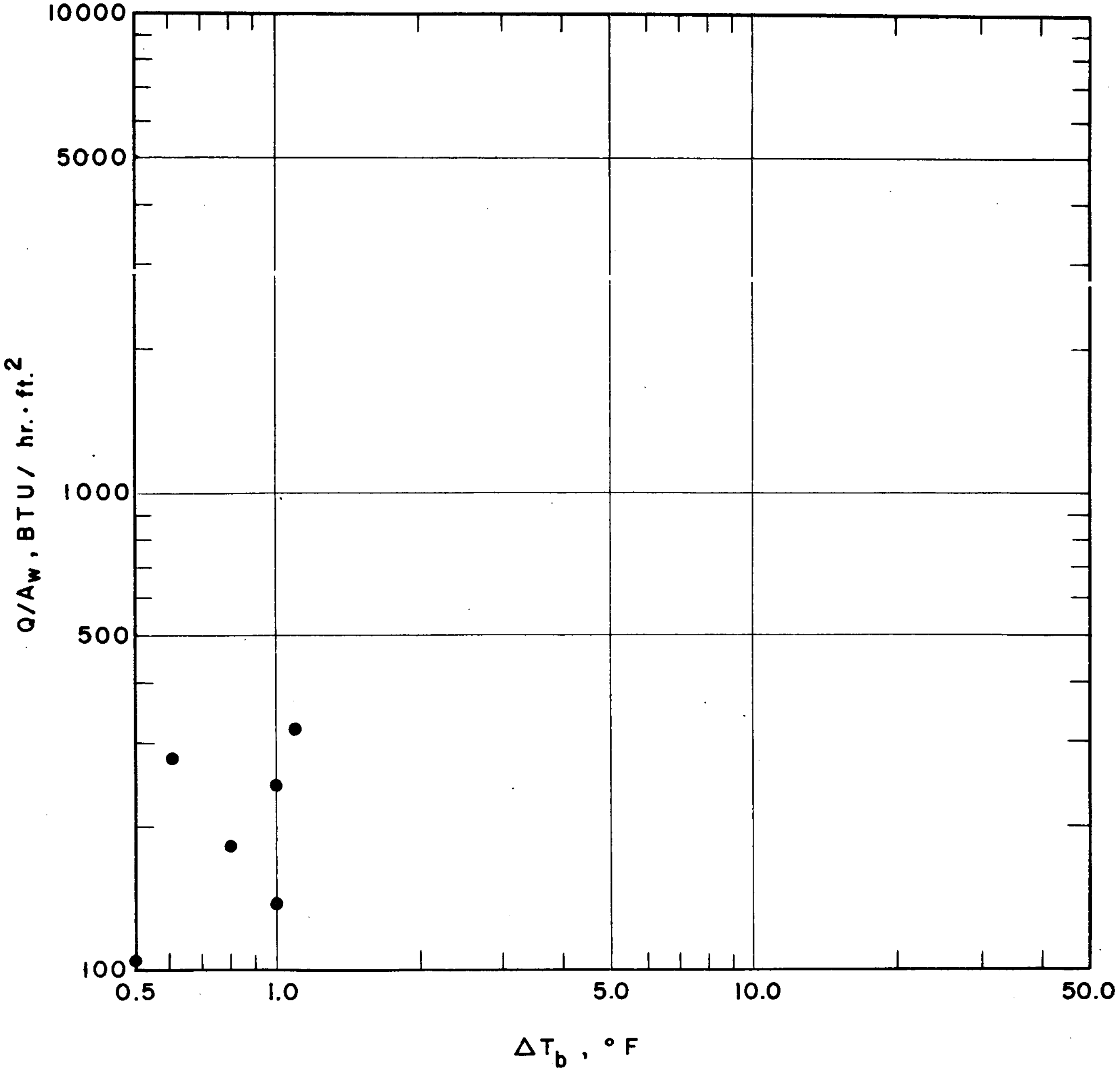

FIGURE 36, HEAT FLUX VERSUS TEMPERATURE DRIVING FORCE ($\Delta T_b = T_w - T_{Sat.}$)
NEON ANNULAR GAP BOILING
COPPER HEATER 6
GAP DIM. AT LIQ. NEON TEMP. 20 mils.
7 1/2" INNER SUBMERGENCE

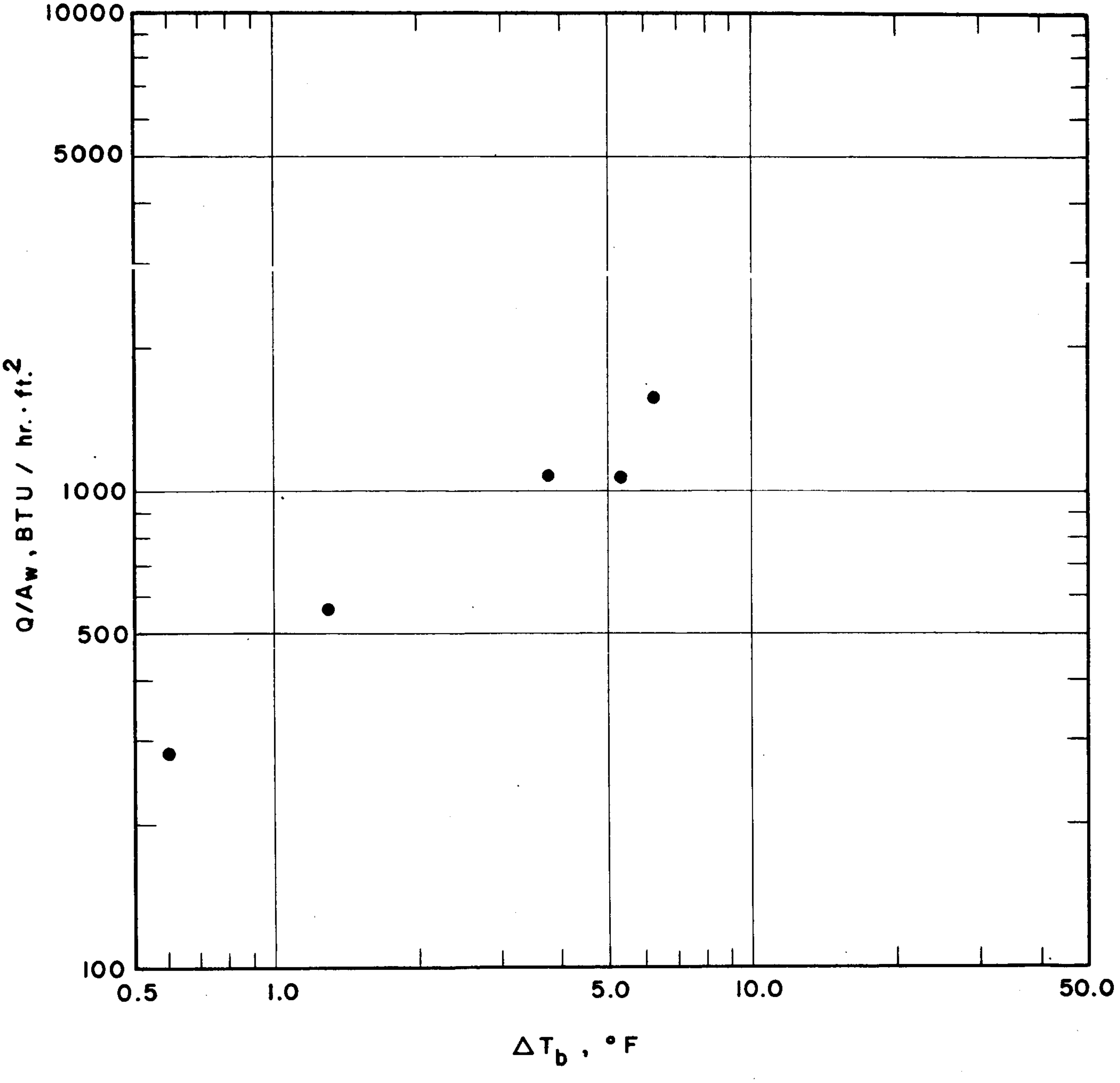

FIGURE 37, HEAT FLUX VERSUS TEMPERATURE DRIVING FORCE ($\Delta T_b = T_w - T_{Sat.}$)
NEON ANNULAR GAP BOILING
NICKEL PLATED COPPER HEATER 9
GAP DIM. AT LIQ. NEON TEMP. 21 mils.
7 1/2" INNER SUBMERGENCE

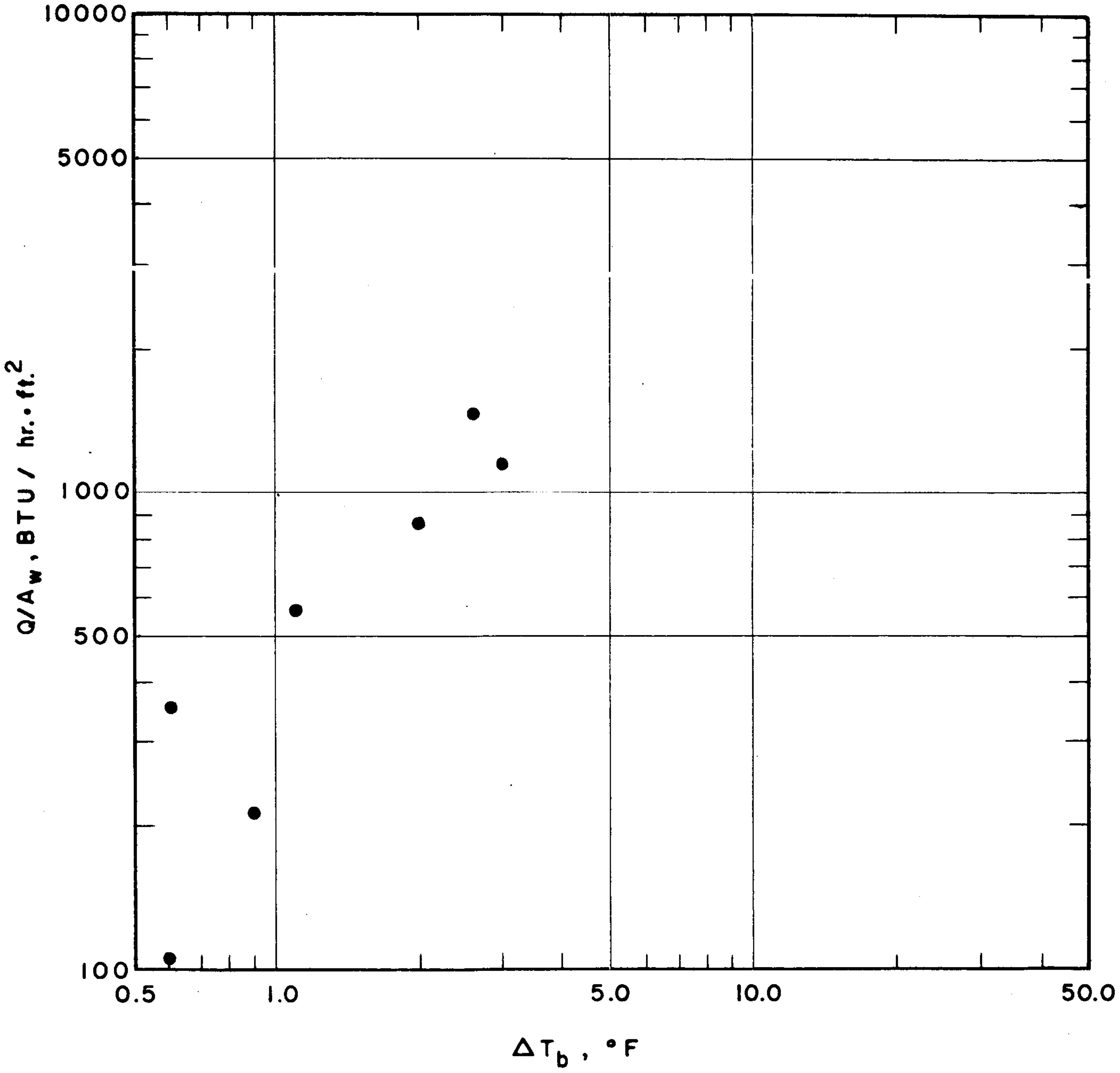

FIGURE 38, HEAT FLUX VERSUS TEMPERATURE DRIVING FORCE ($\Delta T_b = T_w - T_{Sat.}$)
NEON ANNULAR GAP BOILING
COPPER HEATER 7b
GAP DIM. AT LIQ. NEON TEMP. 53 mils.
7 1/2" INNER SUBMERGENCE

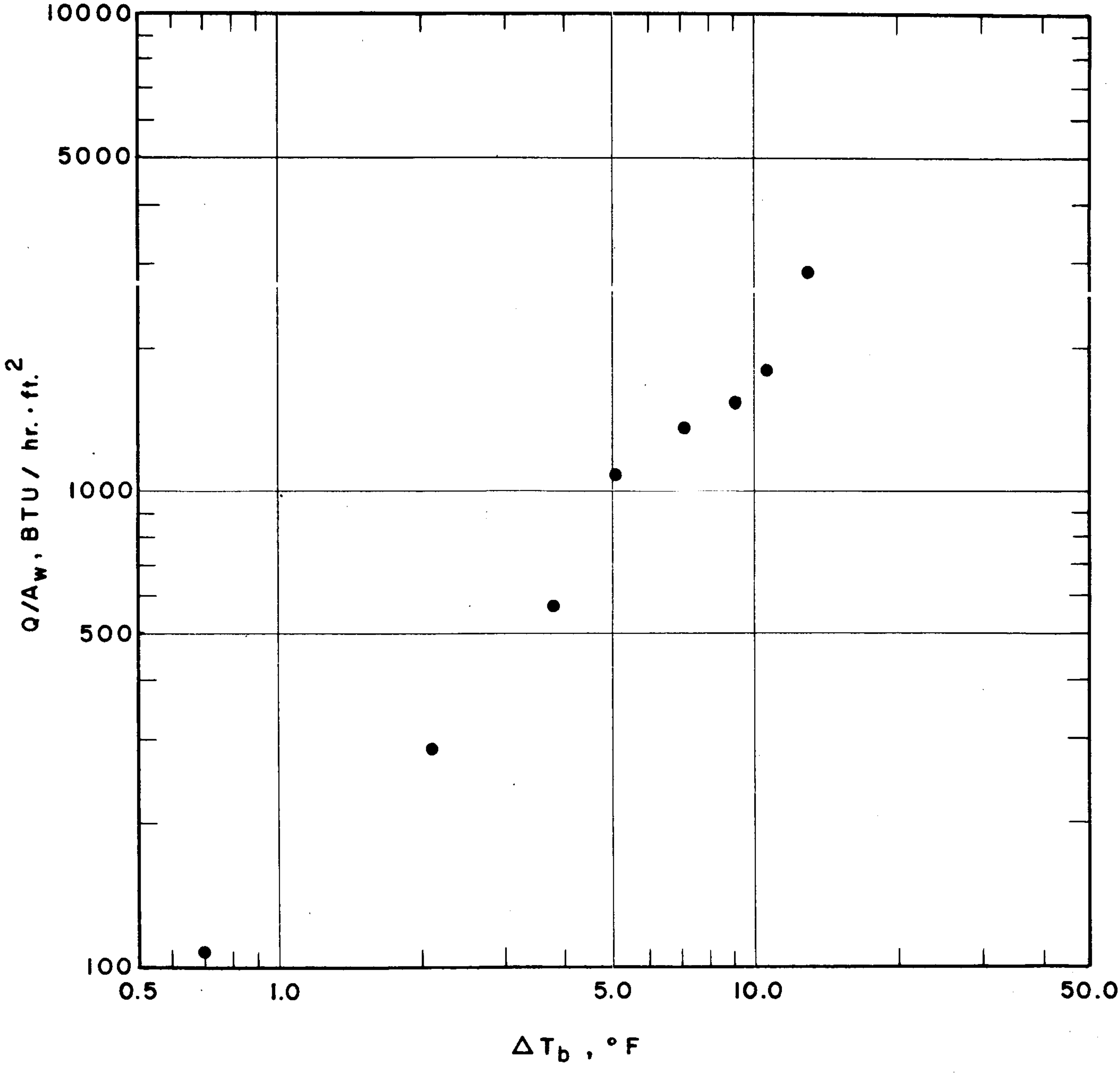

FIGURE 39, HEAT FLUX VERSUS TEMPERATURE DRIVING FORCE ($\Delta T_b = T_w - T_{Sat.}$)
NEON ANNULAR GAP BOILING
COPPER HEATER 8
GAP DIM. AT LIQ. NEON TEMP. 80 mils.
7 1/2" INNER SUBMERGENCE

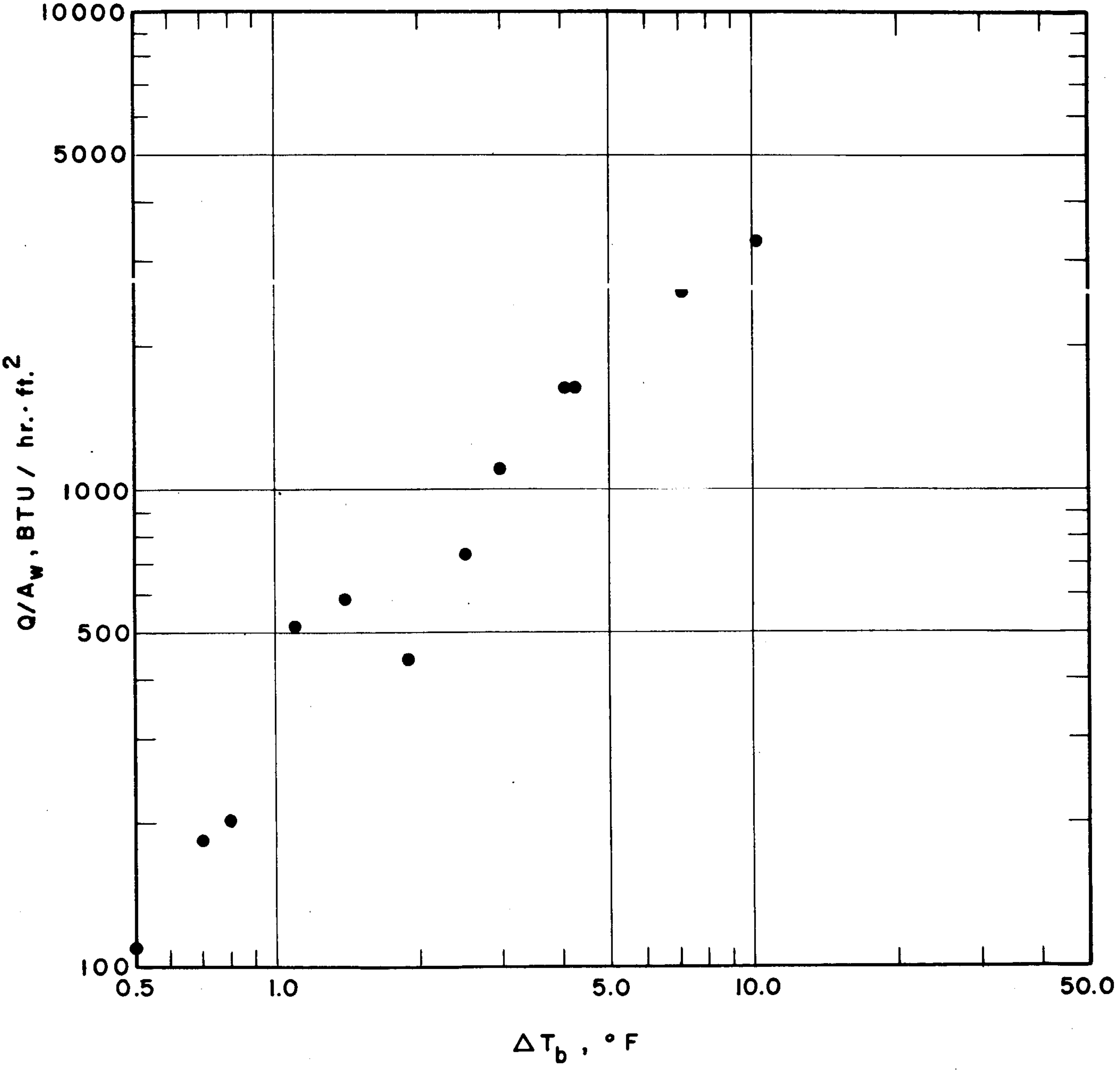

FIGURE 40, HEAT FLUX VERSUS TEMPERATURE DRIVING FORCE ($\Delta T_b = T_w - T_{Sat.}$) NEON ANNULAR GAP BOILING COMPARISON BETWEEN ALL HEATERS AT 7 1/2" INNER SUBMERGENCE

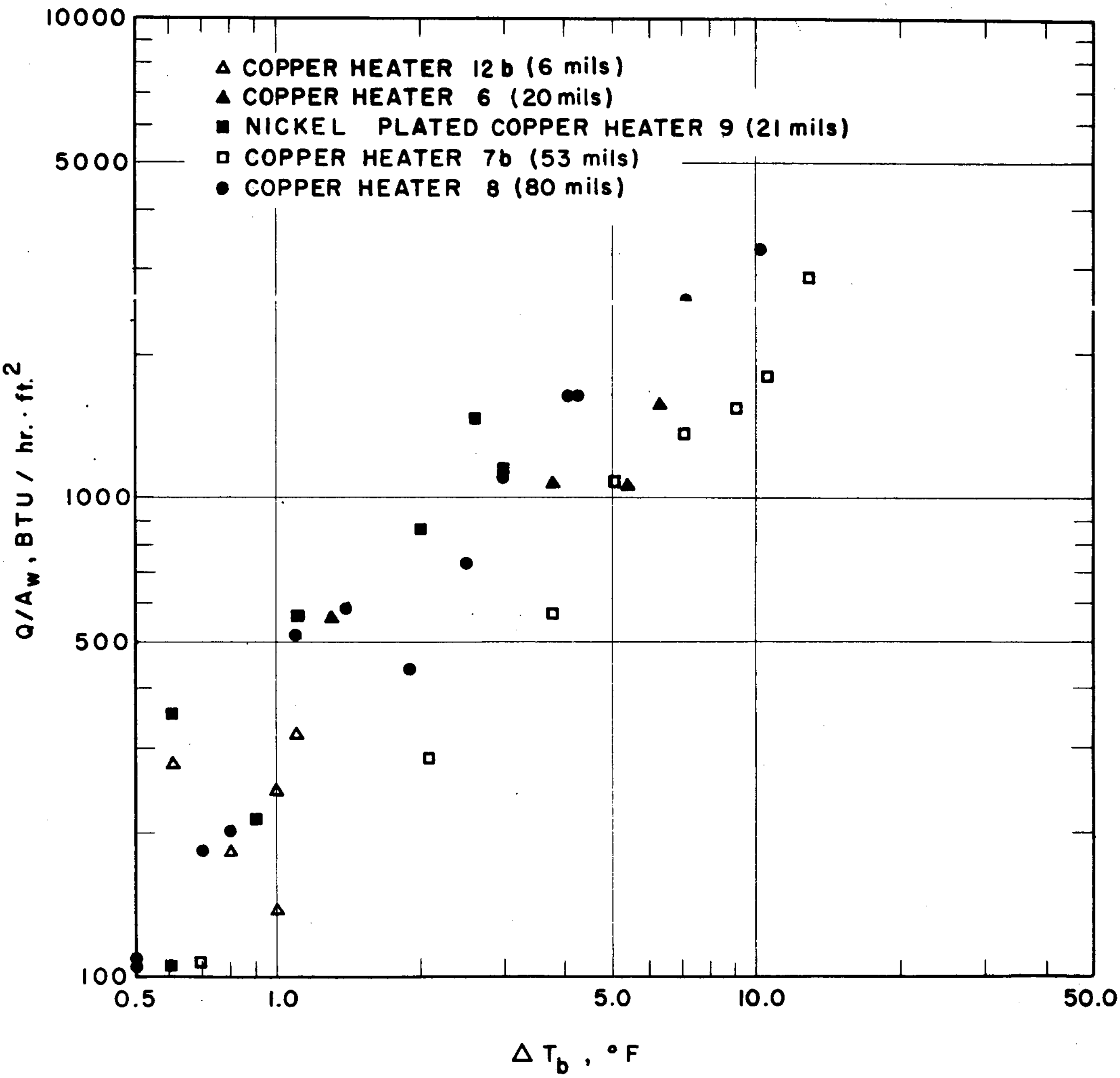

FIGURE 41, NUSSELT NUMBER VERSUS REYNOLDS NUMBER
NITROGEN ANNULAR GAP BOILING
COPPER HEATER 12b, 6 mil GAP

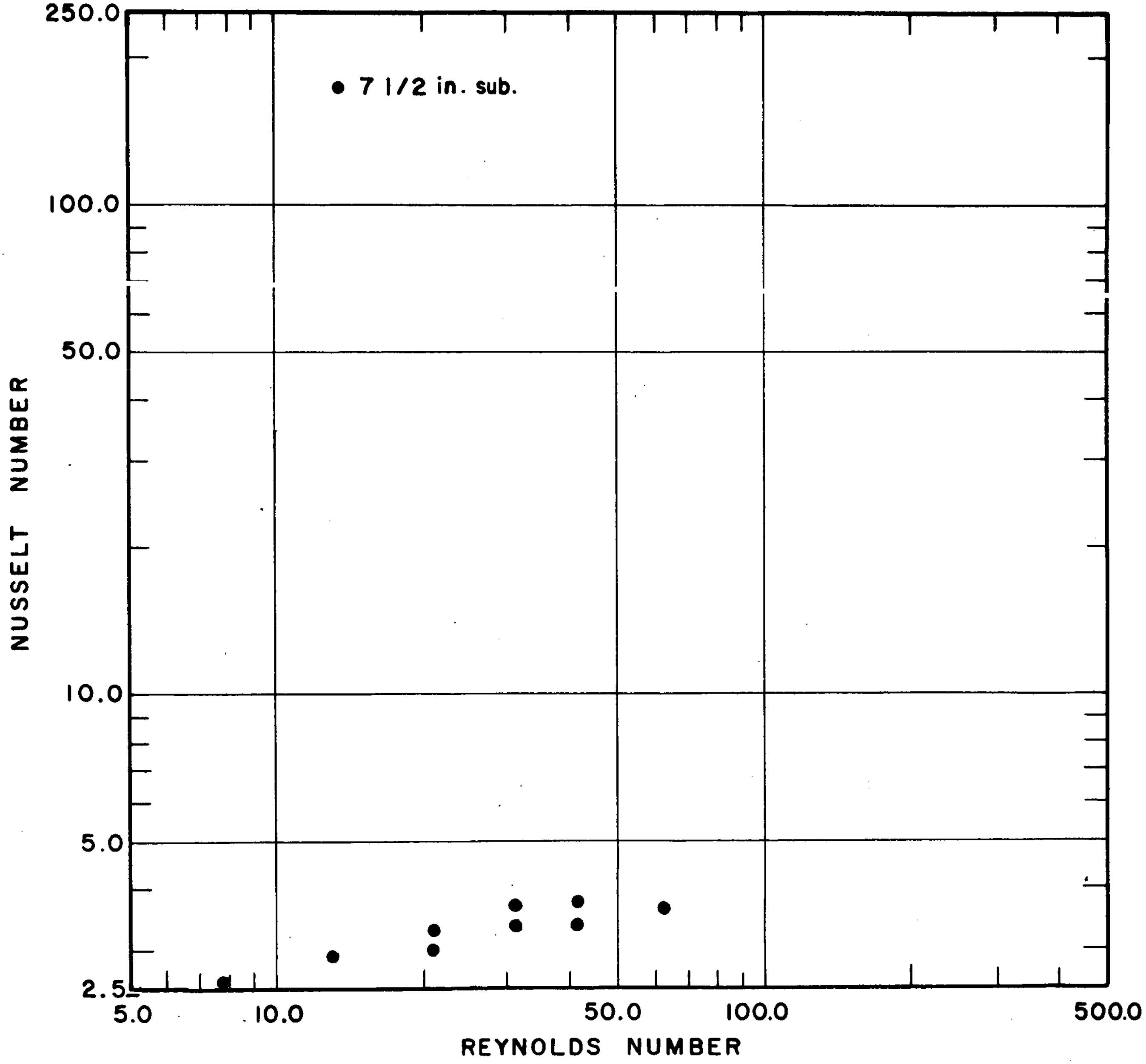

FIGURE 42, NUSSELT NUMBER VERSUS REYNOLDS NUMBER
NITROGEN ANNULAR GAP BOILING
COPPER HEATER 6, 20 mil GAP

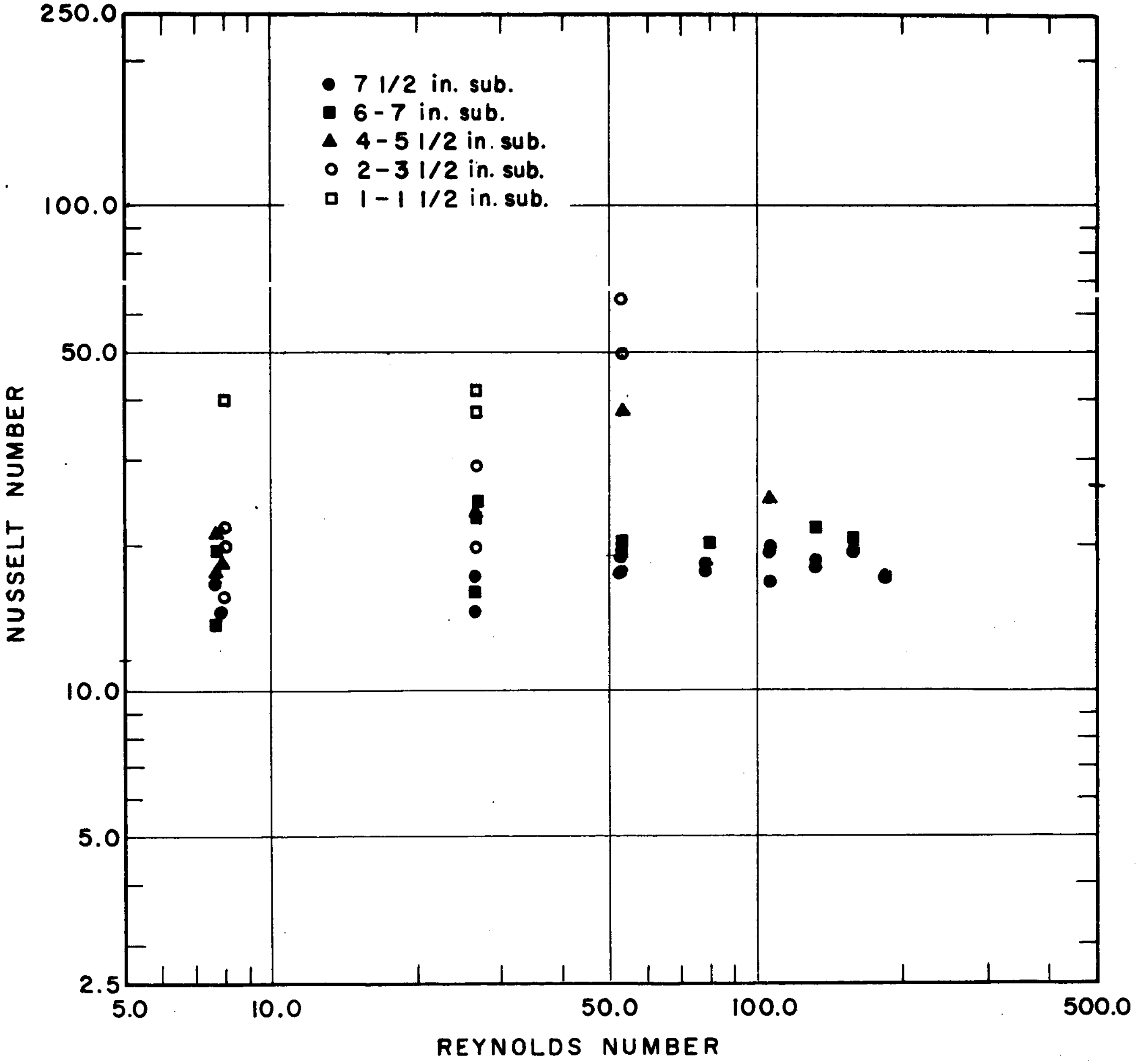

7

FIGURE 43, NUSSELT NUMBER VERSUS REYNOLDS NUMBER
NITROGEN ANNULAR GAP BOILING
NICKEL PLATED COPPER HEATER 9, 21 mil GAP

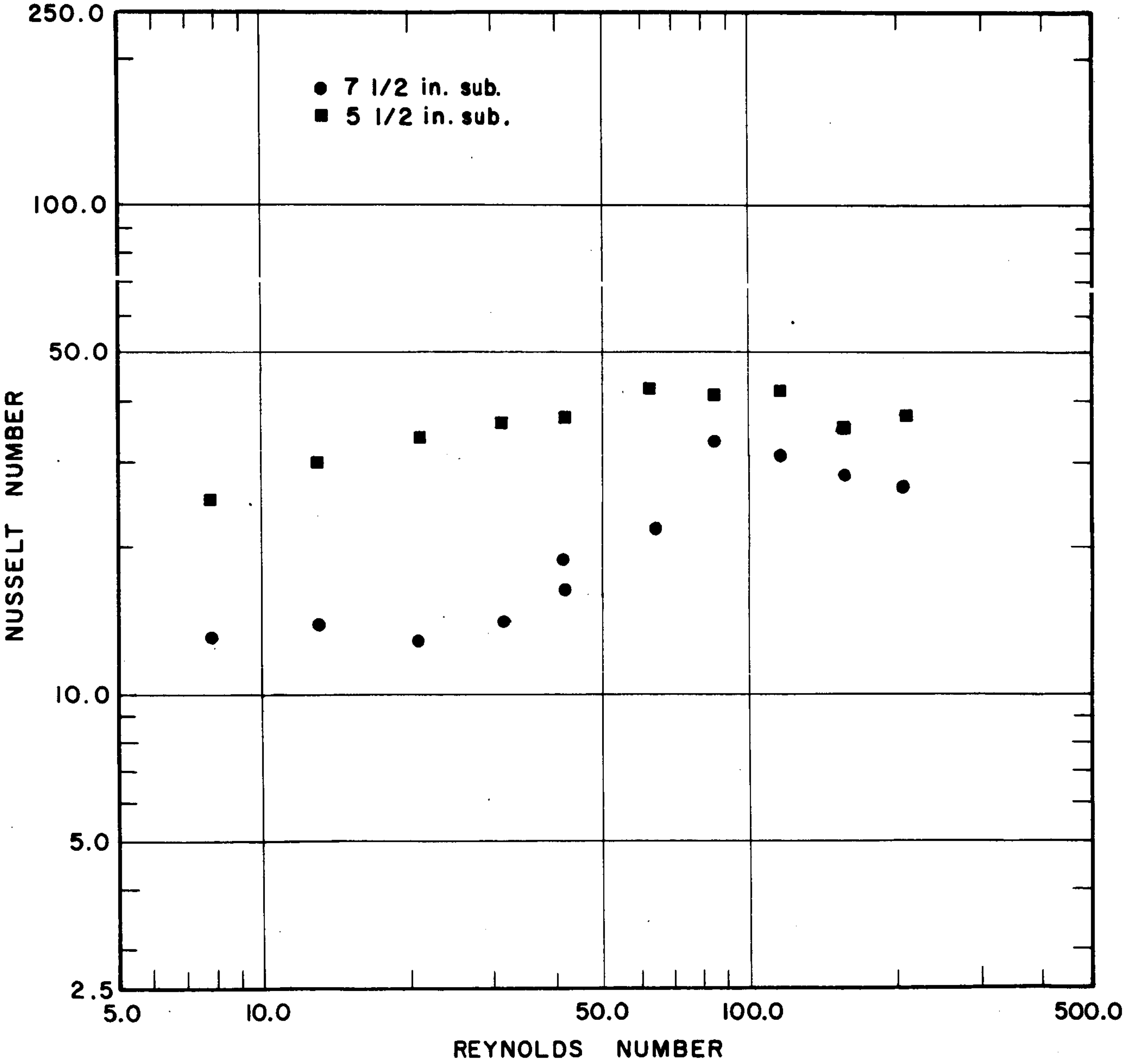

FIGURE 44, NUSSELT NUMBER VERSUS REYNOLDS NUMBER
NITROGEN ANNULAR GAP BOILING
CADMIUM PLATED COPPER HEATER 10, 22 mil GAP

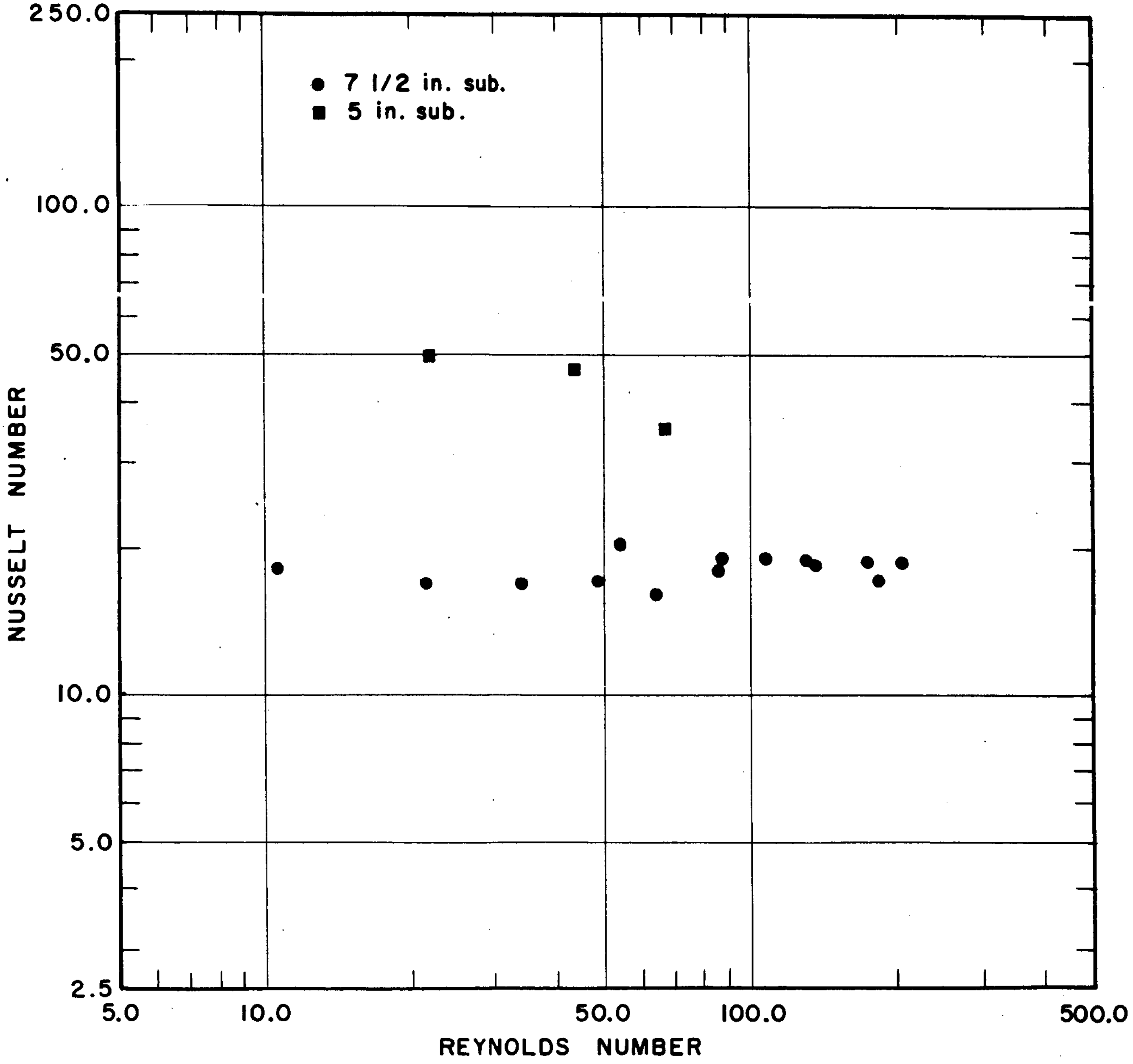

FIGURE 45, NUSSELT NUMBER VERSUS REYNOLDS NUMBER
NITROGEN ANNULAR GAP BOILING
COPPER HEATER 7b, 53 mil GAP

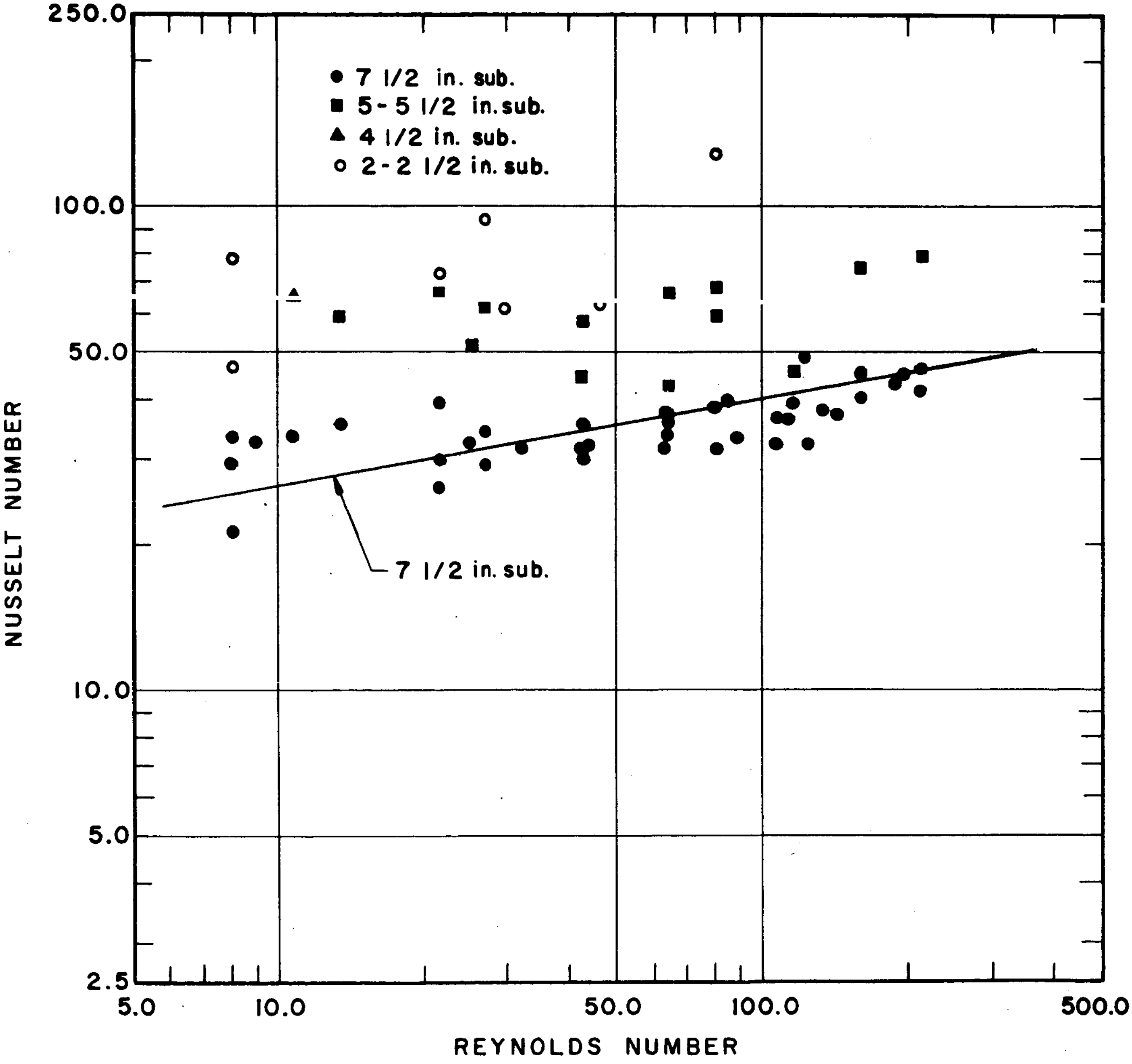

FIGURE 46, NUSSELT NUMBER VERSUS REYNOLDS NUMBER
NITROGEN ANNULAR GAP BOILING
COPPER HEATER 8, 80 mil GAP

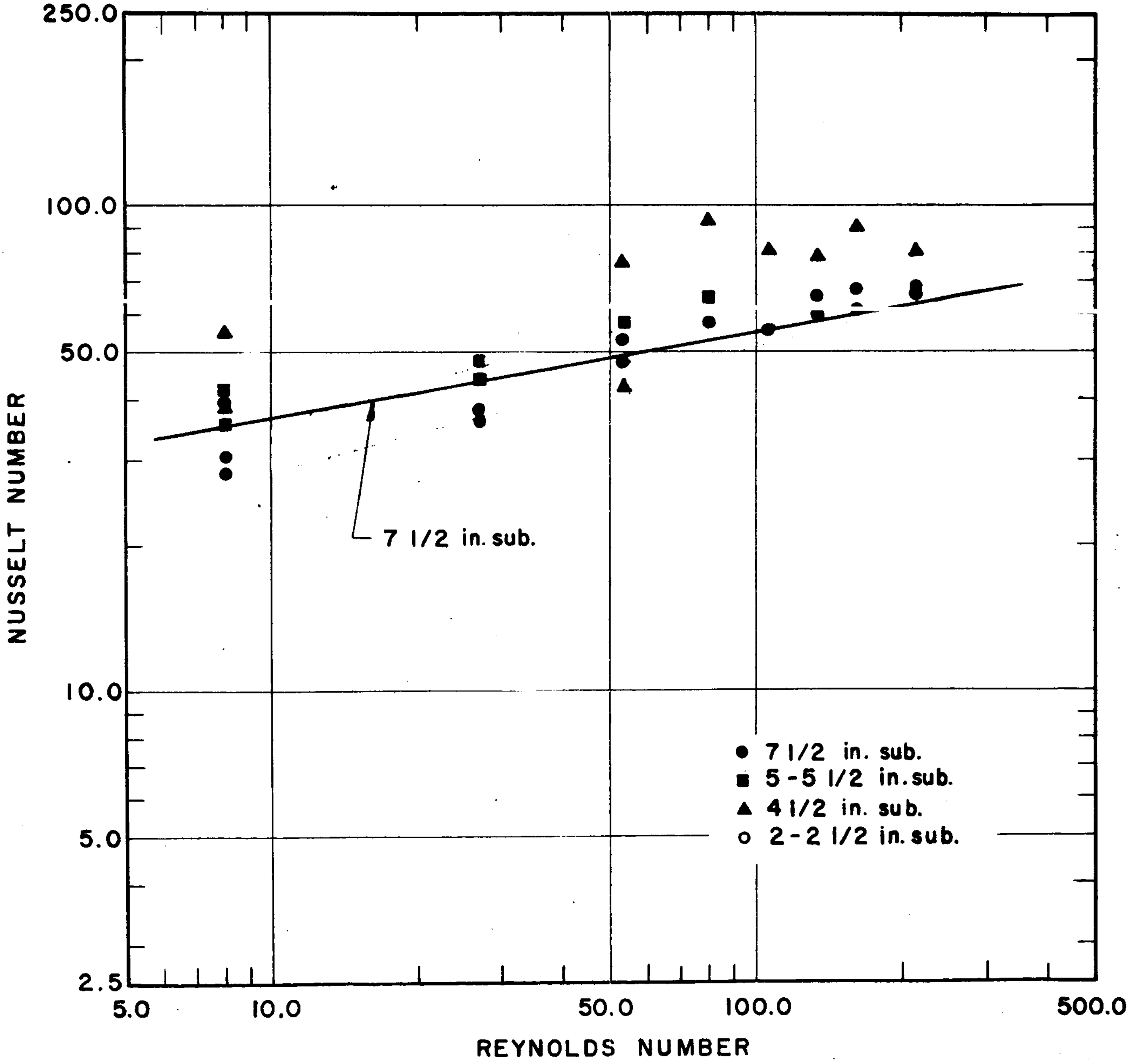

FIGURE 47, NUSSELT NUMBER VERSUS REYNOLDS NUMBER
NEON ANNULAR GAP BOILING
COPPER HEATER 12b, 6mil GAP
7 1/2" INNER SUBMERGENCE

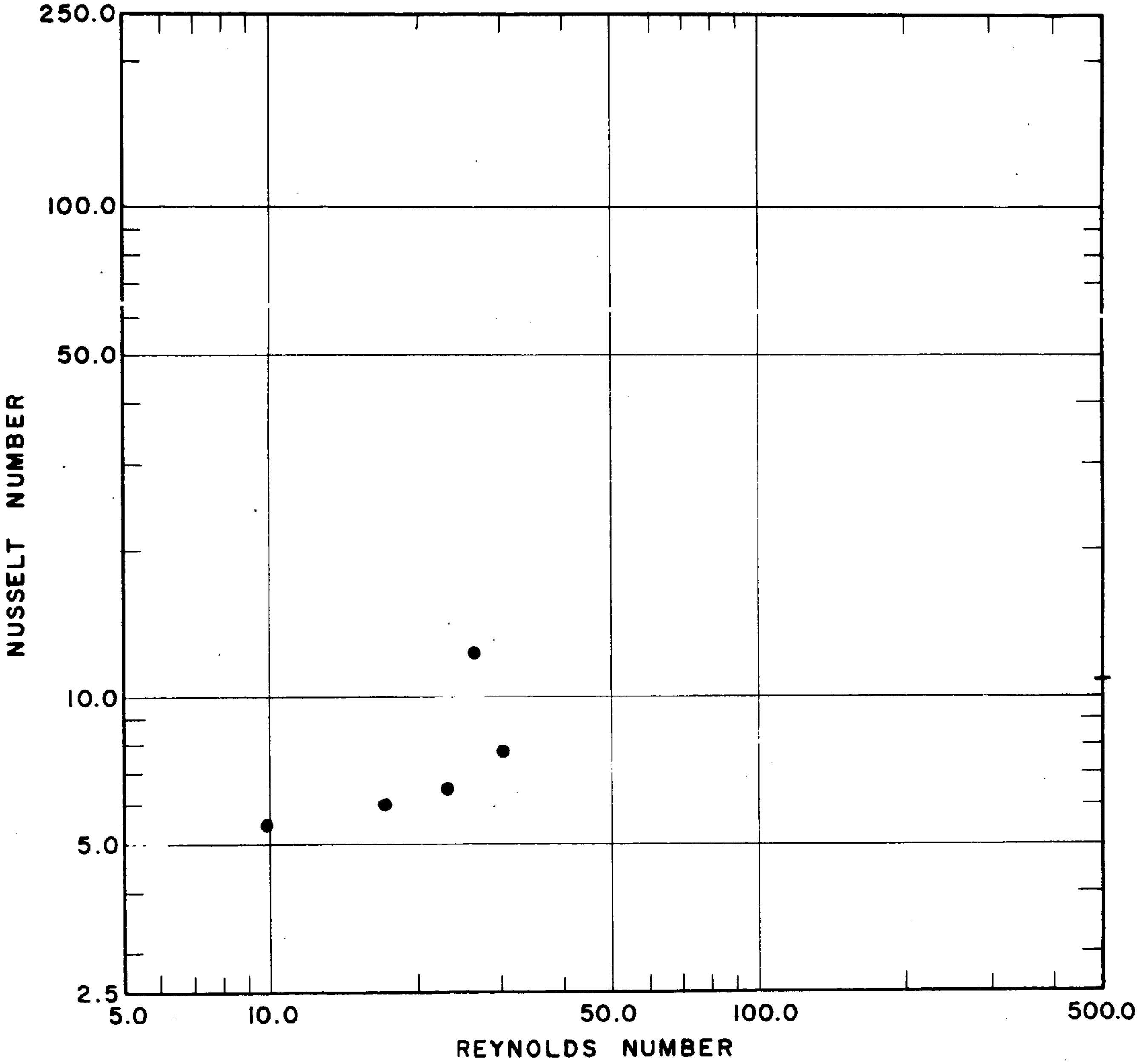

FIGURE 48, NUSSELT NUMBER VERSUS REYNOLDS NUMBER
NEON ANNULAR GAP BOILING
COPPER HEATER 6, 20mil GAP
7 1/2" INNER SUBMERGENCE

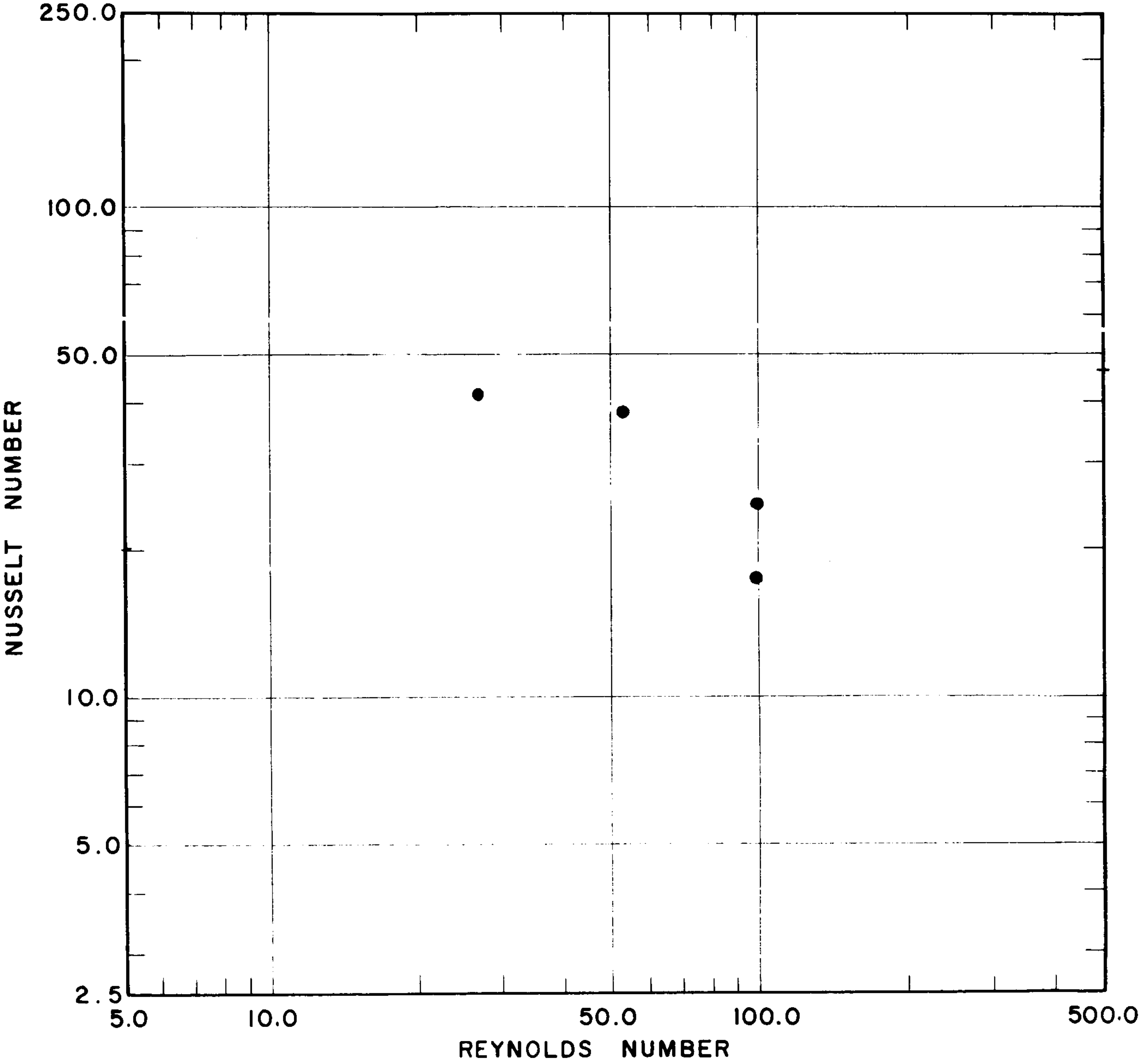

FIGURE 49, NUSSELT NUMBER VERSUS REYNOLDS NUMBER
NEON ANNULAR GAP BOILING
NICKEL PLATED COPPER HEATER 9, 21 mil GAP
7 1/2" INNER SUBMERGENCE

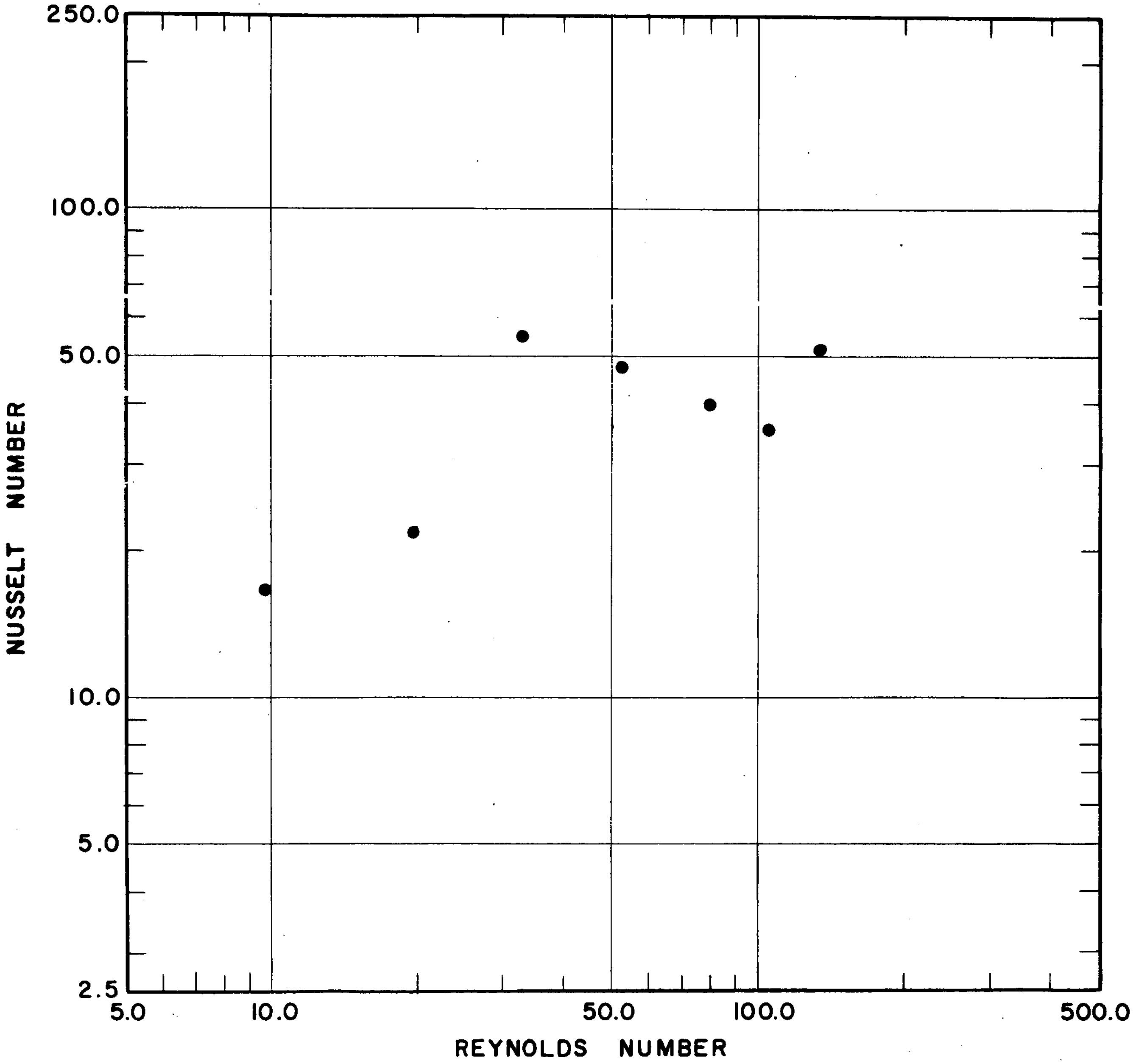

FIGURE 50, NUSSELT NUMBER VERSUS REYNOLDS NUMBER
NEON ANNULAR GAP BOILING
COPPER HEATER 7 b, 53 mil GAP
7 1/2" INNER SUBMERGENCE

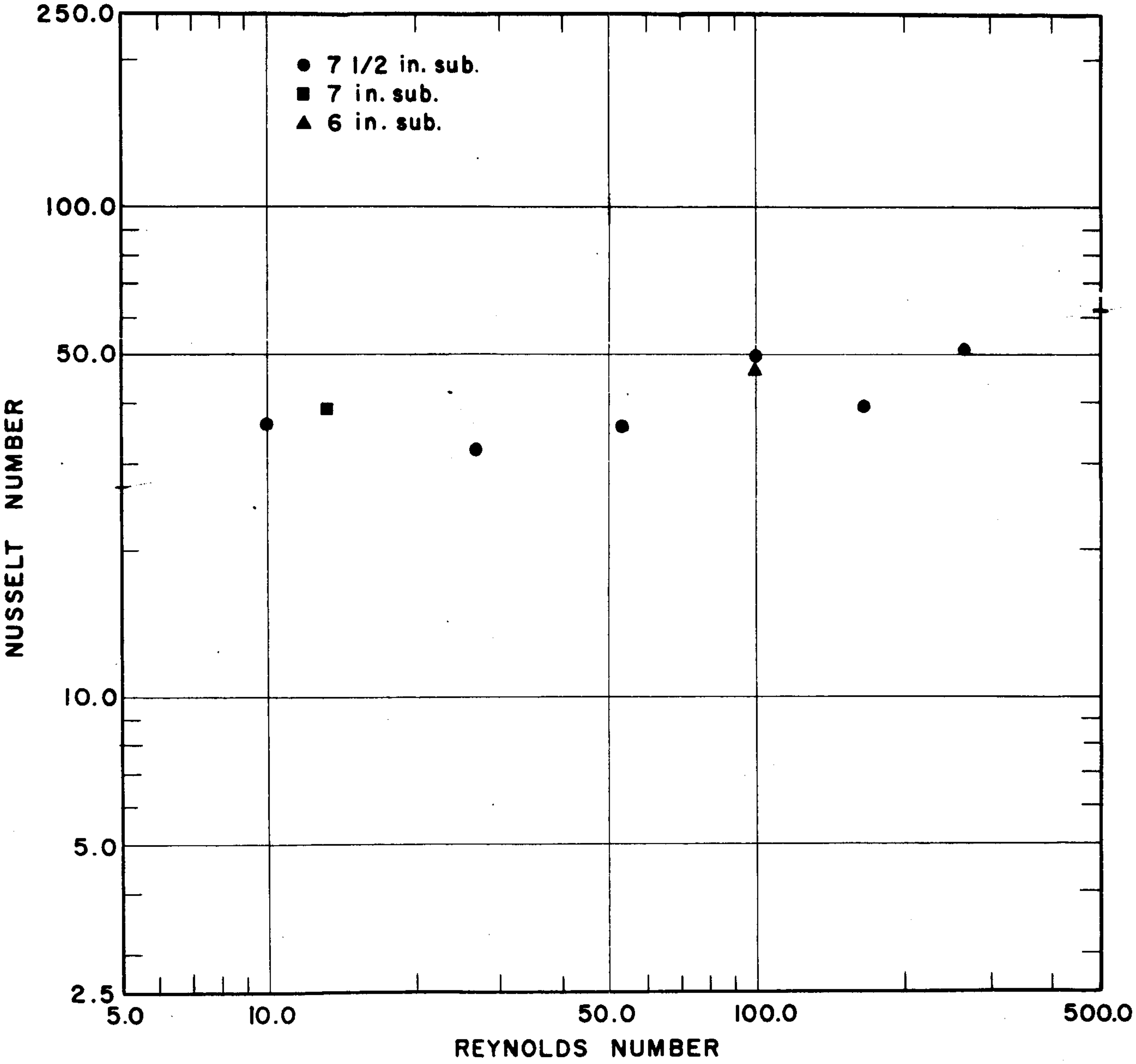

FIGURE 51, NUSSELT NUMBER VERSUS REYNOLDS NUMBER NEON ANNULAR GAP BOILING COPPER HEATER 8 , 80 mil GAP 7 1/2" INNER SUBMERGENCE

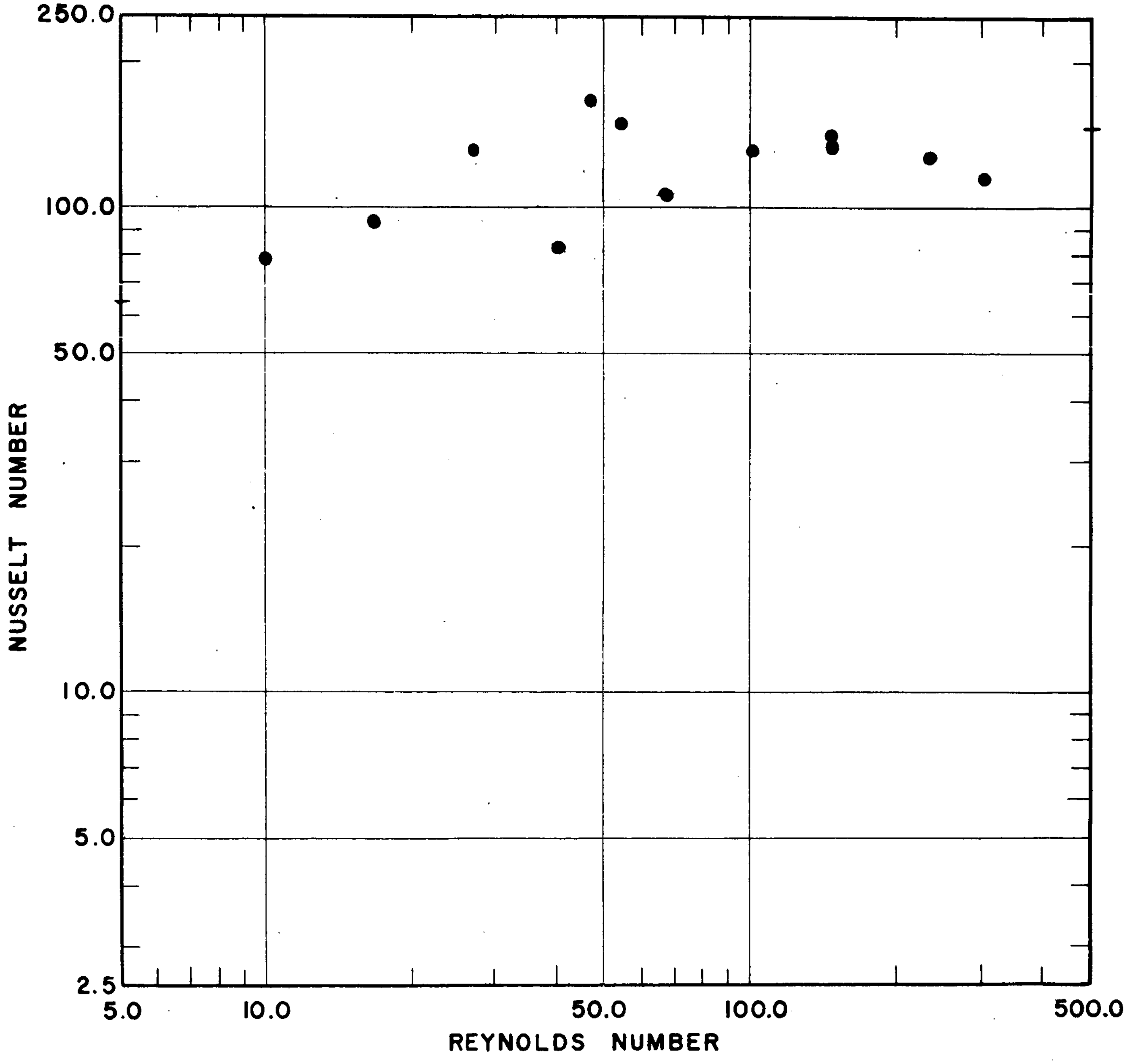

FIGURE 52, COMPARISON BETWEEN MEASURED AND CALCULATED NUSSELT NUMBER FOR ALL NEON AND NITROGEN ANNULAR FLOW BOILING DATA

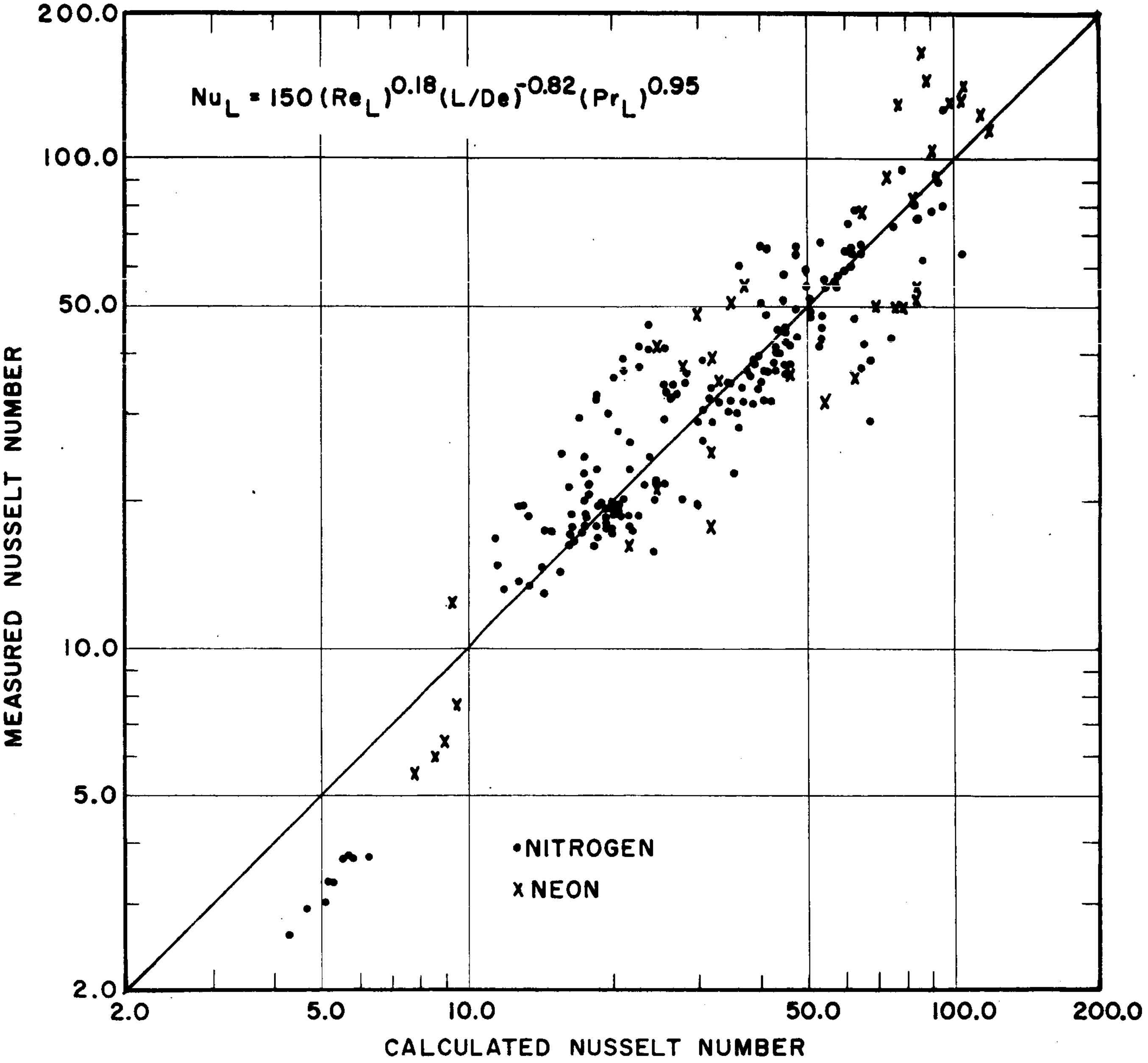

Equations for each individual heater can be easily calculated. For example, equations for annular gap nitrogen boiling at full submergence are:

$$Nu_L = 17.3\ (Re_L)^{0.18} \qquad \text{for 0.053-inch gap} \tag{79}$$

and

$$Nu_L = 24.4\ (Re_L)^{0.18} \qquad \text{for 0.080-inch gap} \tag{80}$$

These equations are shown in Figures 45 and 46 respectively.

The agreement between the correlation and the experimental data is noteworthy in view of the wide range of experimental conditions. The following discussion briefly reviews the effect of the important experimental conditions on the boiling coefficients.

1. Surface Roughness and Finish

The measured root mean square roughness and surface finish appear to have no effect on boiling coefficients in annular gap boiling, at least within the limits of this work. Even the data for the cadmium plated heater are correlated quite well by Equation (78). Based on the pool boiling data, it would have been anticipated that this would not be possible. This apparent independence of annular gap boiling from surface effect has also been observed with respect to surface oxidation. Runs A-53-2 to A-53-27 were made with a copper heater having about 15% of its surface badly oxidized. These runs were repeated with the heater surface completely cleaned and the coefficients calculated from the new data were the same as the ones calculated from the old data.

2. Back Pressure Created by the Rotameter

Runs A-20-2 to A-20-22 were performed with the rotameter line connected to the vapor liquid separator located above the heater section. The effect of the back pressure created by the rotameter on the system was very noticeable. The liquid level inside the annulus was immediately lowered to a point about 1-inch below the outer liquid level. The appearance of the foam was also changed. Its height was reduced from 1 inch or so to about 1/4 inch or less. Entrainment, if any, was completely stopped. Vapor bubbles appear to become smaller. All in all, the back pressure effect on the nature of the gap boiling was significant.

However, in spite of the different appearance of boiling, the heat transfer coefficients calculated for the cases of connected and unconnected rotameter were the same. This suggests that the assumption of convective type heat transfer made in the derivation of Equation (74),

$$Nu_L = a\ (Re_L)^b\ (L/D_e)^c\ (Pr_L)^d\ , \qquad (74)$$

the use of the physical properties for the liquid phase, and the selection of the terms used in the equation are justified.

3. Entrainment

Entrainment occurred when the combination of heat input and outer submergence was sufficient to raise liquid droplets into the entrainment collector. Examination of data taken with and without entrainment shows, that at a given heat flux, the boiling temperature driving force is slightly smaller for the case having entrainment. This is caused by the larger flow existing in the annulus during entrainment resulting in a better performance. The effect, however, was usually small. Differences in temperature driving forces were usually of the order of 0.2-0.4°F at the higher heat fluxes, or the equivalent of 2-3% of the temperature driving force.

4. Length to Diameter Ratio

The L/D_e ratio was varied two ways:

a. by varying the submergence L with a fixed gap size, i.e. a fixed D_e, and

b. by varying the gap size, D_e, for a given submergence.

L/D_e was varied from 9.4 to 313 by means of the two methods a and b.

There is actually a basic difference between methods a and b for varying L/D_e ratios. The heat flux is a function of the submergence L, but is independent of the gap size, or its equivalent diameter D_e. Therefore, when method a is used, a change in L/D_e ratio will result in a change in heat flux even though the heat input to the test heater remains unchanged. This results in a condition of constant boil-off. However, when

L is fixed and D_e is varied, then a change in L/D_e will not affect the heat input, the heat flux, nor the boil-off rate.

In spite of this basic difference between the two ways of varying L/D_e, the data correlates well regardless of how L/D_e was changed.

5. Comparison Between Neon and Nitrogen Boiling

There was no detectable difference between neon and nitrogen, either in pool or in annular gap boiling. Data, however, showed that at a given temperature difference, heat flux for neon was higher than for nitrogen. Figure 34 clearly shows this fact for pool boiling condition. The same conclusion can be reached for annular gap boiling by comparing Figures 33 and 40: at a given ΔT_b, heat fluxes for neon are higher than the ones for nitrogen.

6. Maximum Heat Flux

Maximum heat fluxes due to gap size were experienced in four cases only:

a. 850 Btu/hr-ft^2 at $\Delta T_b = 5.8^\circ F$ for liquid nitrogen flowing in a 6 mil gap heater

b. 350 Btu/hr-ft^2 at $\Delta T_b = 1.1^\circ F$ for liquid neon flowing in a 6 mil gap heater

c. 1600 Btu/hr-ft^2 at $\Delta T_b = 6.5^\circ F$ for liquid neon and a 20 mil gap heater

d. 1600 Btu/hr-ft^2 at $\Delta T_b = 3.0^oF$ for liquid neon and a 21 mil gap heater.

In all other cases, limit on heat flux was the result of heat input limitation rather than gap size effect.

7. Evaluation of the Sydoriak and Roberts Correlation

A comparison between heat fluxes calculated by means of the Sydoriak and Roberts equation and measured ones are summarized in Table XLIV.

It is apparent that the Sydoriak and Roberts equation is not valid for gap sizes larger than 22 mils. The agreement between measured and calculated heat fluxes for nitrogen is better than 2 to 1 for the 20 and 21 mil gap and 2.2 to 1 for the 22 mil gap condition. Comparison could not be made for the 6 mil gap heater nor for neon boiling in view of the reaching of maximum heat fluxes with temperature driving forces smaller than 18^oF.

TABLE XLIV

EVALUATION OF SYDORIAK AND ROBERTS EQUATION

$$Q = A\ L\ (\rho_{V_2}\ \rho_L\ Z_e\ g\ f_2)^{1/2}$$

COMPARISON BETWEEN CALCULATED AND MEASURED HEAT FLUXES

Gap Size inches	Nitrogen		Neon	
	Q/A Calc. Btu/hr-ft^2	Q/A meas. @ 18°F ΔT_b Btu/hr-ft^2	Q/A Calc. Btu/hr-ft^2	Q/A meas. @ 18°F ΔT_b Btu/hr-ft^2
0.006	2110	850 max. reached @ $\Delta T_b = 5.8$°F	1520	350 max. reached @ 1.1°F ΔT_b
0.020	7020	4000	5070	1600 max. reached @ 6.5°F ΔT_b
0.021	7360	6200	5330	1600 max. reached @ 3.0°F ΔT_b
0.022	7630	3500	5510	--------
0.053	18400	3400	13250	3500
0.080	27500	4000	19850	7500

VIII. CONCLUSIONS

An investigation of neon and nitrogen boiling both under pool boiling conditions and in narrow annuli, was completed. The study covered the case of a 7 1/2-inch long vertical heater with a nominal 3-inch outside diameter and gap sizes ranging from 0.006 to 0.080 inch.

The experimental design concept allowed for visual observation simultaneously with data collection, which made it possible to relate data directly to behavior.

The following equation correlating the nitrogen pool boiling data for all heaters, except the cadmium plated one, with an average percent deviation of ±16% was obtained:

$$Q/A_w = 87.2\,(\Delta T_b)^{1.20} \tag{77}$$

A generalized equation for annular gap boiling was derived on the assumption of convective type heat transfer. The concept of equivalent diameter was used to modify the characteristic dimension in the Nusselt and Reynolds numbers.

The following equation correlated all annular gap boiling data obtained with nitrogen and neon with an average percent deviation of ±23%.

$$\frac{h_b\, D_e}{k_L} = 150 \left(\frac{D_e\, G}{\mu_L}\right)^{0.18} \left(\frac{L}{D_e}\right)^{-0.82} \left(\frac{Cp_L\, \mu_L}{k_L}\right)^{0.95} \tag{78}$$

The validity of the correlation over the wide range of parameters involved in the experimental work substantiates the assumptions made and concepts involved in the derivation of the equation.

However, caution should be exercised in the use of Equation (78) outside the range of the experimental work. It is believed that while this equation would be satisfactory for cryogenic fluids in general, certain size limitations should be considered, namely, vertical height less than 15 inches and annular gap sizes in the order of 0.006 to 0.080 inch. It should be noted, however, that this range of gap sizes effectively covers the practical range for narrow annuli. The lower limit of 0.006 inch is very nearly a practical minimum. A gap size exceeding the upper limit of 0.080 inch will result in a condition equivalent to pool boiling.

IX. NOMENCLATURE

Symbol	Meaning	Equation Where Used
a,a'	Constant	15,35,71,72,73,74,75
∂	Constant in Forster-Zuber equation = 0.0015	1
a	Local micro-area of heat transfer surface, ft^2	10,11
A	Surface area, ft^2	1,21,26,37,40,44,48, 49,50,51,52
A, A_t	Cross sectional area of annular gap, ft^2	13, Table I
A_b	Buffle surface area	47,52
$A_{b,i}$	Bubble surface area at heated surface before bubble departure, ft^2	50
A_w	Test section, wetted effective heat transfer area, ft^2	75,76,77
b	Constant	5,15,35,71,73,74,75
B_L	Coefficient defined by equations 50 and 51	51,52
c	Constant	71,73,74
c,Cp,C	Specific heat, Btu/lb-°F	1,42
C_1, C_2 C_3, C_4	Constants	16,17,19,21
C_L, Cp_L	Heat capacity of liquid, Btu/lb-°F	24,26,27,31,33,34,36, 38,40,41,44,46,47,50, 51,53,56,58,73,74,78
C_{L_w}	Specific heat of liquid at wall temperature, Btu/lb-°F	54
Cp	Specific heat of liquid, k cal/kg/grad.	5
Cp_V	Specific heat of vapor, Btu/lb-°F	page 107

Symbol	Meaning	Equation Where Used
d	Constant	71,73,74
d, D	Characteristic dimension, ft	42,65,66,68,69,70, 71,72,73
D	Diameter, ft	59,62,63
D	Outside diameter of tube, ft	2,53
D_b	Bubble diameter, ft	16,17,18,19,22
D_e	Equivalent diameter	12,74,78
D_1	Test heater outside diameter, in.	Table I
D_2	Precision Pyrex pipe, inside diameter, in.	Table I
e, f	Constant	71,72
f	Frequency, hr^{-1}	16,18,19,48,49
f_2	Mass fraction vapor in the fluid leaving heater	13
F	Reynolds number factor, $(Re/Re_L)^{0.8}$	62,63
g	Constant	71,72
g	Acceleration of gravity, 4.17×10^8 ft/hr^2	2,17,19,21,23,26,27
g	Acceleration of gravity, 32.2 ft/sec^2	13
g_c	Gravitational constant	56,58,69,70,71,72
g_o	Conversion factor, lb-mass x ft/(lb-force x hr^2)	17,19,21,23,26
G	Mass flow velocity, $lb/hr\text{-}ft^2$	62,66,71,73,74,78
h	Two-phase heat transfer coefficient, $Btu/hr\text{-}ft^2\text{-}^\circ F$	55
h	Individual heat transfer coefficient, $Btu/hr\text{-}ft^2\text{-}^\circ F$	3,22,23,26,27,41,53
h_b	Boiling heat transfer coefficient, $Btu/hr\text{-}ft^2\text{-}^\circ F$	42,65,71,73,74,78
h_{co}	Film coefficient of heat transfer, if there were no radiation, $Btu/hr\text{-}ft^2\text{-}^\circ F$	2
h_{fg}	Latent heat of vaporization, Btu/lb	46,47,48,49
h_{mac}	Macro-convective heat transfer coefficient	55,59,63

h_{mic}	Micro-convective heat transfer coefficient	55,56,58
H	Heat flux, Btu/hr-ft^2	42
I	Mechanical equivalent of heat, kgr/kcal, used in definition of p' and T_s	5,6
k	Thermal conductivity, Btu/hr-ft-°F	1,2,42
k	Thermal conductivity of two-phase fluid	59,61
k	Boltzman constant	Table III, 37
k_L	Thermal conductivity of liquid, Btu/hr-ft-°F	22,23,24,26,27,40, 41,44,47,50,51,53, 56,58,61,63,65,67, 71,73,74,78
k_V	Thermal conductivity of vapor, Btu/hr-ft-°F	Page 107
k_H	Conversion from kinetic energy to heat	Page 107
K	Activation constant	Page 11
L	Latent heat of vaporization, Btu/hr	1,13,29,30,42
L_w	Latent heat of vaporization at wall temperature, Btu/lb	54
L	Wetted length of surface	12,68,71,73,74,78
m	Constant	1
m	Mass of particle	Table III
M	Molecular weight of liquid	11
n	Constant	1
n	Number of nucleating points per unit area, ft^{-2}	18,19
n	Number of points of origin of bubble columns per ft^2 of heating surface	48,49

Symbol	Meaning	Equation Where Used
N	Local population of active sites on area a, ft^{-2}	10,11
$\bar{N}$	Average population of active sites on area A, ft^{-2}	10,11
N*	Avogadro's number	11
N_o	Constant	11
Nu	Nusselt number: h D/k	15,22,23,25,35,37,39
Nu_f	Nusselt number at film conditions	12
Nu_L	Nusselt number based on liquid properties	74,78,79,80
$\left(\frac{Nu_{calc}}{Nu_{exp}}\right)_f$	Ratio of calculated to experimental Nusselt number at the mean film conditions	4
p'	$\frac{r\, I \gamma' \gamma''}{T_s (\gamma' - \gamma'')}$	5
p_v	Pressure of the vapor in a bubble, lb/ft^2	11,28,29,30,38,41
p_∞	Saturation pressure of a flat liquid surface, lb/ft^2	11,28,38,41
P	Absolute pressure, lb/ft^2	43
P_c	Pressure inside the bubble, lb/ft^2	14
P_R	Reduced pressure	54
Pr	Prandtl number, Cp /k	15,35,39,59,60
Pr_f	Prandtl number based on film properties	12
Pr	Prandtl number of vapor	2
Pr	Prandtl number of the two-phase fluid	59,60
Pr_L	Prandtl number based on liquid properties	24,25,78,60,63
P_s	Absolute pressure at saturation temperature, lb/ft^2	14
Pu(Na)	A probability that a random local area a has a population N	10
P_V	Liquid vapor pressure	64,70,71,72

Symbol	Meaning	Equation Where Used
q	Heat transfer rate, Btu/hr	20,21,26,37,40
q	Heat flux, kcal/m^2hr	5,6
$\bar{q}$	Heat flux, Btu/hr-ft^2	54
q_b	Heat transfer rate from liquid to vapor bubble, Btu/hr	47,52
Q	Heat transfer rate, Btu/hr	1,44,48,50,51,52, 75,76,77
Q	Heat transfer rate, Btu/sec	13
Q_b	Heat carried away by the bubbles, Btu/hr	49
r	Radius ratio: R/R_o	31
r_1	Radius ratio: R_1/R_o	31
r, R	Bubble radius, ft	14,28,32,33,34,36, 37,38,43,46,47,49
r	Latent heat of vaporization in $p' = \frac{r\, I\, \gamma'\, \gamma''}{T_s\, (\gamma' - \gamma'')}$, kcal/kg	5
R	Gas constant, ft/°R	11,30,64
Re	Reynolds number for the two-phase fluid	59,62
Re	Reynolds number $D u \rho/\mu$	15,19,21,25,35,36,39
Re_f	Reynolds number at film condition	12
Re_L	Reynolds number based on liquid properties	62,63,78,79,80
R_i	Bubble radius at heating surface when first formed, ft	50
R_o	Radius of nucleus, ft	31,32
R_s	Bubble radius at edge of superheated layer, ft	48,50
S	Suppression factor: $(\Delta T_e/\Delta T)^{0.99}$ which is modified to $S = (\Delta T_e/\Delta T)^{0.24} (\Delta P_e/\Delta P)^{0.75}$	57,58

Symbol	Meaning	Equation Where Used
t	Time variable, hr	46,47
t	Test section gap size at liquid nitrogen and neon temperature, in.	Table I
T	Absolute temperature, °R	29,30,46,47,64
T	Absolute temperature, °K	Table III
T_1	Absolute temperature of liquid, °K	1
T_o	Temperature of superheated liquid, °F	32
T_s	Temperature of solid surface, °F	33
T_s	Temperature of saturation in $\frac{r\ I\ \gamma'\ \gamma''}{T_s(\gamma' - \gamma'')}$	6
$T_s; T_{sat}$	Saturation temperature, °R	44,45,46,47,50
T_v	Temperature inside a bubble, °F	32
T_w	Temperature of heating surface, °R	50,54
T_w	Absolute temperature of wall or heating surface, °K	1,11
T_∞	Saturation temperature of a liquid flat surface at the existing pressure, °F	32
T*	Reduced temperature	Table III
u	Velocity	66
V	Velocity, ft/hr	18,19
w	Mass flow rate, lb/hr	20
$\dot{w}_g$	Mass flow rate gas, lb/hr, used in χ_{tt}	4
$\dot{w}_1$	Mass flow rate liquid, lb/hr, used in χ_{tt}	4

Symbol	Meaning	Equation Where Used
z	Weight fraction liquid	62
z_e	Hydrostatic head, ft	13
α	Constant	15
α, α_L	Thermal diffusivity of liquid, ft^2/hr	1,31,33,34,36,38 40,64
β	Contact angle measured through the liquid	17,19,21,23,26,27
β	Pr/Pr_L	60
γ	k/k_L	61
γ'	Specific weight of the liquid, kgr/m^3	5
γ''	Specific weight of the saturated vapor, kgr/m^3	5
δ	$\left(\frac{\sigma}{\gamma' - \gamma''}\right)^{1/2}$ derived from bubble diameter $do = 20\theta\left(\frac{\sigma}{\gamma' - \gamma''}\right)^{1/2}$	5
Δp	$p_v - p_\infty$, lb/ft^2	40
Δp	Vapor pressure difference corresponding to the superheat temperature, lb/ft^2	1,57,58
ΔP	$P_w - P_s$, lb/ft^2	54
ΔP_e	Effective value of ΔP	56,57
Δt	Temperature difference between hot surface and liquid at its boiling point, °F	2,3
ΔT	Temperature driving force, $T_L - T_v$ for homogeneous case, $T_s - T_\infty$ for heterogeneous case, °F	27,31,33,34,36,37,38, 40,41,53
ΔT	Temperature difference, °K	1
$\Delta T, \Delta T_b$	Boiling temperature driving force, $T_w - T_s$, °F	51,57,58,75,76,77
ΔT_e	Effective value of ΔT	56,57
ΔT_t	Overall temperature driving force	Table XXXII
ΔV	Difference between specific volume of vapor and liquid	29

Symbol	Meaning	Equation Where Used
ε	Parameter in intermolecular potential function	Table III
η	Viscosity	6, Table III
η^*	Reduced viscosity: $\frac{\eta\sigma^2}{\sqrt{m\,\varepsilon}}$	Table III
θ	Time, hr	28,31,33,34,36
θ	Contact angle	5
λ	Latent heat of vaporization, Btu/lb	20,21,26,27,31,33, 34,36,38,40,41,56, 58,64
λ	Thermal conductivity, kcal/m/hr/grad	5
λ'	Difference in heat content between vapor at its arithmetic average temperature and liquid at its boiling point, Btu/lb	2
μ	Viscosity, lb/ft-hr	1,42
μ_L	Viscosity of liquid, lb/ft-hr	19,21,24,26,27,36,40 41,53,56,58,62,66,67, 69,70,71,72,73,74,78 Table III
μ_{L_w}	Viscosity of liquid at wall temperature,lb/ft-hr	54
μ_V	Viscosity of vapor, lb/ft-hr, used in χ_{tt}	4
ρ	Density, lb/ft^3	66
ρ, ρ_V	Density of vapor, lb/ft^3	1,17,19,21,23,26,27,28, 31,33,34,36,40,41,42,44, 45,46,47,48,49,50,51,71, 72
ρ_L	Density of liquid, lb/ft^3	1,11,13,17,19,21,23,26, 27,31,33,34,36,38,40, 41,42,44,45,46,47,50, 51,53,56,58,69,70,71,72
ρ_{L_w}	Density of liquid at wall temperature, lb/ft^3	54

Symbol	Meaning	Equation Where Used
ρ_{V2}	Exit vapor density, lb/ft^3	13
ρ_{V_w}	Density of vapor at wall temperature, lb/ft^3	54
σ	Surface tension kg/m	5
σ	Surface tension, lb/ft	1,11,14,17,19,21,23, 26,27,28,38,40,41,42, 43,50,51,53,56,58,69, 71,72
σ	Parameter in intermolecular potential function	Table III
ϕ	Correction term = $\frac{(2 - \text{Cos}\,\beta)(1 + \text{Cos}\,\beta)^2}{4}$	11
$\chi_{tt,f}$	Martinelli two-phase parameter, gas phase evaluated at film temperature $\chi_{tt} = \left(\frac{\dot{w}_l}{\dot{w}_g}\right)^{0.9} \left(\frac{\mu_L}{\mu_V}\right)^{0.1} \left(\frac{\rho_V}{\rho_L}\right)^{0.5}$	4

X. BIBLIOGRAPHY

1. Air Products and Chemicals, Inc., Allentown, Pennsylvania, Technical Data Book.
2. ASME Boiler and Pressure Vessel Code, Section VIII - Unfired Pressure Vessels, 1959 ed., 1959.
3. ASTM, 1955 Book of ASTM Standards, Part 2, Non-Ferrous Metals, ASTM, Philadelphia, Pennsylvania, 1955, pp. 132-135.
4. Asch, Victor, Chemical Engineering, 70, 125-128, (April 29, 1963).
5. Berenson, P. J., Int. J. Heat Mass Transfer, 5, 985-999, (1962).
6. Bonilla, C. F., J. J. Grady, and G. W. Avery, AIChE, Preprint No. 32, Sixth National Heat Transfer Meeting, AIChE-ASME, Boston, August 11-14, 1963.
7. Bromley, L. A., Chemical Engineering Progress, 46, No. 5, 221-227, (May 1950).
8. Cichelli, M. T., and C. F. Bonilla, Trans. Amer. Inst. Chem. Eng., 41, 755-787, (1945).
9. Chen, J. C., ASME Paper No. 63-HT-34, Sixth National Heat Transfer Meeting, AIChE-ASME, Boston, August 11-14, 1963.
10. Cini-Castagnoli, G., G. Pizzella, and F. P. Ricci, il Nuovo Cimento, XI, No. 3, pp. 466-467. **(February 1, 1939)**
11. Class, C. R., J. R. DeHaan, M. Piccone, and R. B. Cost, Beechcraft R & D Engineering Report No. 6154, October 1958.
12. Cook, G. A., Argon, Helium and the Rare Gases, I, Interscience Publishers, New York, 1961.
13. Corty, Claude, and A. S. Foust, C.E.P. Symposium Series, 51, No. 17, 1-12, (1955).

14. Cryder, D. S., and A. C. Finalborgo, Trans. Amer. Inst. Chem. Eng., 33, 346-363, (1937).

15. Cryder, D. S., and E. R. Gilliland, I & EC, 24, 1382-1387, (1932).

16. Danilova, G. N., and V. K. Belsky, Journal of Refrigeration, 5, No. 5, 120-121, (September/October 1962).

17. Dengler, C. E., and J. M. Addoms, C.E.P. Symposium, 18, 52, Heat Transfer, Louisville, Kentucky, (1956).

18. Drayer, D. E., and K. D. Timmerhaus, Advances in Cryogenic Engineering, K. D. Timmerhaus, ed., Vol. 7, Plenum Press, New York, 1962, pp. 401-412.

19. Drew, T. B., and A. C. Mueller, Trans. Amer. Inst. Chem. Eng., 33, 449-471, (1937).

20. Engelberg-Forster, Kurt, and R. Greif, Journal of Heat Transfer, 81, 43-53, (1959).

21. Forster, H. K., and N. Zuber, AIChE Journal, 1, No. r, 531-535, (1955).

22. Gaertner, R. F., C.E.P. Symposium Series, 59, No. 41, 52-61.

23. Gambill, W. R., British Chemical Engineering, 8, No. 2, 93-98, (February 1963).

24. von Glahn, U. H., and J. P. Lewis, Advances in Cryogenic Engineering, K.D. Timmerhaus, ed., Vol. 5, Plenum Press, New York, 1960, pp. 262-268.

25. Griffith, Peter, and J. D. Wallis, C.E.P. Symposium Series, Heat Transfer Conf., Storrs, Conn., 49-63, (1959).

26. Grilly, E. R., Cryogenics, (U.K.), 2, No. 4, 226-229, (June 1962).

27. Guter, M., Trans. Inst. Chem. Eng., 29, (1949).

28. Hanson, W. B., and R. J. Richards, "Heat Transfer to Boiling Liquefied Gases," N.B.S. Cryogenic Eng. Lab., Laboratory Note Project No. 8629, File No. 65-1, March 7, 1956.

29. Haselden, G. G., and J. I. Peters, Inst. Chem. Eng., London, (1949).

30. Haselden, G. G., and S. Prosad, Trans. Inst. Chem. Eng., (London) 27, 195-200, (1949).

31. Hirschfelder, J. O., C. F. Curtis, and R. B. Bird, Molecular Theory of Gases and Liquids, John Wiley & Sons, New York, 1954.

32. Hendricks, R. C., R. W. Graham, Y. Y. Hsu, and A. A. Madeiros, ARS Journal, 32, 244-252, (February 1962).

33. Hughmark, G. A., Int. J. Heat Transfer, 5, 667-672, (1962).

34. Johnson, V. J., "A Compendium of the Properties of Materials at Low Temperature (Phase I) Part I. Properties of Fluids," N.B.S. WADD Report 60-56 Part I, October 1960.

35. Johnson, V. J., "A Compendium of the Properties of Materials at Low Temperatures (Phase I) Part I. Properties of Solids," U.S. Dept. of Commerce, N.B.S. WADD Tech. Report 60-56 Part II, October 1960.

36. Jiji, L. M., and J. A. Clark, ASME Paper No. 62-WA-202, Annual Meeting, New York, November 25-30, 1962.

37. Kapinos, V. M., and N. I. Nikitenko, Int. J. Heat Mass Transfer, 6, 271-276, (1963).

38. Kutateladze, S. S., "Heat Transfer in Condensation and Boiling," AEC Translation Series - 2nd ed., AEC-tr-3770, 1952.

39. Kutateladze, S. S., "Problems of Heat Transfer During a Change of State: A Collection of Articles," AEC Translation Series, AEC-tr-3405, 1953.

40. Lang, C., Trans. Inst. Eng. Shipbuilders, Scot., 32, 279-295, (1888).

41. Lapin, A., "Joule-Thomson Neon Liquefier", Presented at the semi-Annual Meeting of American Society of Heating, Refrigerating and Air Conditioning Engineers, Feb. 11-14, 1963, pp. 2-12, "The Role Cryogenics is Playing in Expanding Mechanical Engineering", published by ASHRAE.

42. Lapin, A., L. A. Wenzel, and H. C. Totten, "Study of Nitrogen and Neon Pool Boiling on a Short Vertical Pipe", AIChE Journal 11, No. 2 (Mar. 1965).

43. Laurence, J. C., G. V. Brown, J. M. Geist, and K. Zeitz, "A Large Liquid-Neon-Cooled Electromagnet," Prepared for International Conference on High Intensity Magnetic Fields, Cambridge, Mass., November 1-3, 1961.

44. Leidenfrost, J. G., "De aquae communis nonnullis qualitatibus tractatus," Duisburg, (1756).

45. Levy, S., Journal of Heat Transfer, 81, 37-42, (February 1959).

46. Lukomskii, S. M., Bull. Acad. Sci., V.R.S.S., Classe Sci. Tech., 1946, 175-3-66, C.A. 41:335 9b.

47. McAdams, W. H., Heat Transmission, 3rd ed., McGraw-Hill Book Co. Inc., New York, 1954, pp. 370-374.

48. McFadden, P. W., and P. Grassmann, Int. J. Heat Mass Transfer, 5, 169-173, (1962).

49. McNelly, M. J., J. Imperial College Chem. Eng. Soc., 7, 18-34, (1953).

50. Micrometrical Manufacturing Co., "Technical Bulletin on Surface Measurement".

51. Monroe, A. G., H. A. S. Bristow, and J. E. Newell, Journal of Applied Chemistry, 2, 613-624, (November 1952).

52. Neusen, K. F., G. J. Kangas, and N. C. Sher, C.E.P. Symposium Series, 59, No. 41, 185-192.

53. Nukiyama, S. J., Soc. Mech. Eng. (Japan), 37, 367-374, S53-54, (1934).

54. Nusselt, W. Z., Ver Deut. Ing., 60, 541-569, (1916).

55. Piret, E. L., and H. S. Isbin, Chemical Engineering Progress, 50, No. 6, 305-311, (1954).

56. Polomik, E. E., S. Levy, and S. G. Sawochka, "Heat Transfer Coefficients with annular flow during 'one-through' boiling of water to 100% quality at 800, 1100 and 1400 psi," GEAP-3703, Atomic Power Equipment Dept., G. E. Co., San Jose, California, May 1961.

57. Powell, R. L., M. D. Bunch, and R. J. Corruccini, Cryogenics, 1, No. 3, 1-12, (1961).

58. Rabin, I. A., R. T. Beaubonef, and G. Commerford, AIChE Report No. 28, Sixth National Heat Transfer Conference, AIChE-ASME, Boston, August 11-14, 1963.

59. Reeber, M. D., Journal of Applied Physics, 34, No. 3, 481-483, (March 1963).

60. Richards, R. J., R. F. Robbins, R. B. Jacobs, and D. C. Holten, Advances in Cryogenic Engineering, Vol. 3, K. D. Timmerhaus, ed., Plenum Press, New York, 1960, pp. 375-389.

61. Richards, R. J., W. G. Steward, and R. B. Jacobs, "A Survey of the Literature on Heat Transfer from Solid Surfaces to Cryogenic Fluids", N.B.S. TN 122, PB 161623, Bureau of Standards, Washington 25, D. C. (October 1961).

62. Rohsenow, W. M., Trans. Amer. Inst. Mech. Eng., 74, 338-352, 969-996, (1952).

63. Rohsenow, W. M., Heat Transfer Symposium Series, U. of Mich., 101, (1952).

64. Ruzicka, J., Institut International du Froid-Annexe 1958-4, Supplement au Bulletin de l'Institut du Froid, 47-52.

65. Schweppe, J. L, and A. S. Foust, C.E.P. Symposium Series, Heat Transfer, 49, No. 5, 77-89, (1953).

66. Sydoriak, S. G., and T. R. Roberts, Journal of Applied Physics, 28, No. 2, 143-148, (February 1957).

67. Weil, L., and A. Lacaze, Compte, Rendu, 230-186, (1950).

68. Weil, L., and A. Lacaze, J. de Phys. Rad., 12, 890, (1951).

69. Westwater, J. W., Advances in Cryogenic Engineering, I, T. B. Drew and J. W. Hoopes, Jr. ed., Academic Press, New York, 1956, pp. 2-76.

70. Zuber, N., Int. J. Heat Mass Transfer, 6, 53-78, (1963).

71. Zuber, N., and E. Fried, "Two-Phase Flow and Boiling Heat Transfer to Cryogenic Liquids," ARS - Propellants, Combustion and Liquid Rockets Conference, Palm Beach, Florida, April 26-28, 1961, pp. 1709-61.

72. Zuber, N., and E. Fried, ARS Journal, 32, 1332-1341, (September 1962).

XI. APPENDIXES

APPENDIX A

CALCULATION OF NEON BOIL OFF RATE FOR PRELIMINARY DESIGN OF TEST SECTION

The neon boil off rate calculation incorporates the following:

1. heated surface 10 inches long, 4 inches diameter
2. assumption that maximum heat flux in annular boiling is 10% burn-out heat flux for pool boiling (66)
3. prediction of pool boiling burn out by Forster-Zuber correlation (20)

$$(q/A)_{max} = C \rho_V \lambda \left[\sigma g \left(\frac{\rho_L - \rho_V}{\rho_{V}^{2}}\right) g_o\right]^{\frac{1}{4}}$$

$(q/A)_{max}$ = burn out heat flux, pool boiling

$C = 0.131$, empirical coefficient

$\rho_L = 75.35 \frac{lb.}{ft.^3}$, liquid neon density

$\rho_V = \rho_o \frac{To}{T}$, gaseous neon density

$\rho_o = 0.0522 \frac{lb.}{ft^3}$, std. gaseous neon density

$To = 530^oR$, std. temp.

$T = 50^oR$, gasous neon temp. at boil off

$\therefore \quad \rho_V = 0.554$ lb./ft.^{3}

$g = 32.17$ ft/sec^2, gravitational acceleration

$g_o = 32.17 \frac{lb.m\ ft.}{lb.\ F\ sec^2}$, gravitational constant

$\sigma = 0.00036 \frac{lb.\ F}{ft.}$ surface tension of liquid neon at N.B.P.

$\lambda = 37.05 \frac{BTU}{lb.m}$, latent heat of vaporization at neon N.B.P.

Substituting and solving,

$(q/a)_{\text{max pool boiling}} = 29{,}100 \frac{BTU}{ft^2\ hr}$, and

$(q/A)_{\text{max annular boiling}} = 2{,}910 \frac{BTU}{ft^2\ hr}$.

Consider heated surface, A, as

$$A = \frac{10 \text{ in} \times \pi\, 4 \text{ in.} \times \text{ft}^2}{144 \text{ in}^2}$$

$$= 0.872 \text{ ft}^2$$

Solving from (q/A) max and A,

$$q = 2{,}910 \frac{\text{BTU}}{\text{hr ft}^2} \times 0.872 \text{ ft}^2$$

$$q = 2{,}545 \frac{\text{BTU}}{\text{hr}}.$$

Boiling rate w is then determined, knowing volume latent heat λvol.

$$w = \frac{q}{\lambda \text{vol}} \quad , \qquad \text{where } \lambda \text{ vol} = 98.8 \text{ Btu/lt}$$

$$w = \frac{2{,}545 \text{ BTU/hr}}{98.8 \text{ BTU/lt}}$$

$$= 25.8 \text{ lt/hr}$$

Recalculation using 7 1/2 inch length and 3 in. diameter heater yields a maximum boil-off rate

$$w = 14.5 \text{ lt/hr}$$

Assuming that the average heat flux for a complete run will approximate 40% of the maximum heat flux, average boil-off is then estimated to be:

$$W_{avg} = 0.40 \times 14.5 = 5.8 \text{ lt/hr}$$

APPENDIX B

CALCULATIONS FOR INVAR PRESSURE VESSEL IN TEST SECTION DESIGN

Preliminary conditions used in the design calculations of the pressure vessel:

1. heating surface, 7 1/2 inches long, 3 inches nominal outside diameter
2. 400 psia max operating pressure at -410°F. (400 psia is approximately critical pressure of neon)

A.S.M.E. Boiler and Pressure Vessel Code information:

$$t = \frac{PR}{SE-0.6P}$$

t = design thickness

P = 400 psia, operating pressure

R = 1.5 inches, vessel radius

S = 15,000 psia (approx Factor of Safety, 5, based on 75,000 tensile strength)

E = 1 , joint efficiency of seamless tube

$$t = \frac{400 \times 1.5}{15{,}000 - 240} \text{ inches}$$

$$= \frac{600}{14{,}760} \text{ inches}$$

$$= 0.0407 \text{ inches}$$

Heat transfer characteristics calculated for invar pressure vessel:

1. wall thickness taken as 0.250 inches, surface area 7 1/2 length, 3π inches circumferential length.
2. average heat flux of 1,455 BTU/hr ft^2
3. thermal conductivity at liquid neon temperatures 1.5 BTU/hr ft°R (24% Ni Stainless Steel) (Ref. 36)
4. assume inner and outer surface temperatures are the same as the respective fluid saturation temperatures

Conduction heat transfer formulation:

$$q/A = k \frac{\Delta T}{t}$$

t = 0.250 in. thickness

k = 1.5 BTU/hr ft R, thermal conductivity (36)

q/A = 1,455 BTU/hr ft^2, heat flux

Solving for the temperature difference ΔT

$$\Delta T = \frac{1{,}455 \times 0.250}{1.5 \times 12} \, ^{\circ}R$$

$$\Delta T = 20.2^{\circ}R$$

APPENDIX C

CALCULATIONS FOR OFHC COPPER PRESSURE VESSELS IN TEST SECTION

Preliminary dimensions of pressure vessel:

1. heating surface 7 1/2 inches long, 3 inches nominal outside diameter
2. 400 psia max operating pressure at -410°F (400 psia approximately critical pressure of neon)

A.S.M.E. Boiler and Pressure Vessel Code Information

$$t = \frac{PR}{SE-0.6P}$$

t = design thickness

P = 400 psia, operating pressure

R = 1.5 inches, vessel radius

S = 6,000 psia, A.S.M.E. Boiler and Pressure Vessel Code Material Specification SB-75

$$t = \frac{400 \times 1.5}{6000-240} \text{ inches}$$

$$= \frac{600}{5760} \text{ inches}$$

$$= 0.102 \text{ inches}$$

Calculation of deflection for outer surface of copper pressure vessel using wall thickness of 0.125 in. and thick walled cylinder formula

$$U_O = \frac{1+\nu}{E}\left(1 + \frac{R_I^2}{R_O^2 - R_I^2}\right)R_O P$$

$\nu = 0.33$ Poisson ratio for copper

$R_O = 1.5$ inches, outside diameter

$R_I = 1.375$ inches, inside diameter

E = 17,000,000 psia, modulus of elasticity

P = 400 psia, internal pressure

U_o = deflection of outer surface in radial direction

$$U_o = \frac{1.33}{17{,}000{,}000}\left(1 + \frac{1.89}{2.25-1.89}\right) 1.5 \times 400 \text{ inches}$$

$$= \frac{1.33\ (6.29)\ 1.5 \times 400}{17{,}000{,}000} \text{ inches}$$

$$= 0.000294 \text{ inch}$$

Error involved for operation with 0.0050 inches gap at two pressure levels, 0 psig and 400 psig

1. P = 0 psig

   $U_o = 0$

   gap = 0.0050

2. P = 400 psig

   U_o = 0.0003 inches

   gap = 0.0047 inches

Error of difference

$$\frac{0.0050 - 0.0047}{0.0047} = 6.4\%$$

APPENDIX D

CALCULATION OF CONTRACTION CHARACTERISTIC OF TEST SECTION MATERIALS

In general, thermal contraction of a material is accounted for in the formula

$$L_{\Delta T} = L_o (1 + \alpha \Delta T)$$

where L_o = original length at temperature T_o

$L_{\Delta T}$ = length after temperature change from T_o to T or $\Delta T = (T - T_o)$

α = average coefficient of linear thermal expansion for temperature change ΔT.

For the large temperature change experienced by the test section, it is erroneous to consider an average coefficient of linear thermal expansion. Instead, a temperature dependency of the coefficient should be considered. Including the temperature dependency of the coefficient in a formulation for contraction is accomplished by using a stepwise calculation. The stepwise calculation assumes a constant value of the expansion coefficient over a small temperature change, the total temperature change of concern being the sum of the small step changes.

Let $L_{\Delta T total}$ and L_o be the final and initial length respectively. A calculated length for a small temperature change ΔT_n would be represented by L_n. Noting this then, the formulation is as follows:

$$L_1 = L_o (1 + \alpha_1 \Delta T_1)$$

$$L_2 = L_1 (1 + \alpha_2 \Delta T_2) = L_o (1 + \alpha_1 \Delta T_1)(1 + \alpha_2 \Delta T_2)$$

or $$L_n = L_o (1 + \alpha_1 \Delta T_1)(1 + \alpha_2 \Delta T_2) \ldots\ldots (1 + \alpha_n \Delta T_n).$$

The nth temperature change step would end at T_n such that $T_n = T_f$,

where $\Delta T_{total} = T_f - T_o = \Sigma \Delta T_n$,

Thus, when $T_n = T_f$, L_n corresponds to $L_{\Delta T_{total}}$, and the formulation is then $L_{\Delta T_{total}} = L_o\,(1 + \alpha_1\;\Delta T_1)\;(1 + \alpha_2 \Delta T_2)\;\ldots\ldots(1 + \alpha_n \Delta T_n)$.

A stepwise calculation of coefficients of thermal expansion of Pyrex glass and copper for temperature changes of ambient temperature to liquid nitrogen and liquid neon temperatures is made. Graphical representation of the stepwise breakdown is presented in Figure 53.

Stepwise Calculation of Contractraction Characteristic for Copper.

Step n	T_n (°F)	ΔT_n (°F)	$\alpha_n \times 10^6$(in.°F/in.)	$1 + \alpha_n \Delta T_n$
0	70	0		
1	-28	-98	9.1	0.99911
2	-152	-124	8.5	0.99895
3	-252	-100	7.5	0.99925
4	-292	-40	6.25	0.99975
5	-320.5	-28.5	5.0	0.99986
6	-353	-32	3.25	0.99989
7	-410.7	-57.7	1.25	0.99993

For the liquid nitrogen temperature level

$$L_{\Delta T_{total}} = L_o\,(1 + \alpha_1 \Delta T_1)\;\ldots\ldots(1 + \alpha_n \Delta T_n),\; n = 5$$

$$= L_o\,(0.99695)$$

For the liquid neon temperature level

$$L_{\Delta T_{total}} = L_o(1 + \alpha_1 \Delta T_1)\;\ldots\ldots(1 + \alpha_n \Delta T_n),\; n = 7$$

$$= L_o(0.99674)$$

Nominal diameter (L_o) of copper being 3.0 inches, nominal contraction will then be:

$$L_{Cu,\,N_2} = 3.0000\;(0.99695 - 1.00000)\text{ in.}$$

$$= -0.00915\text{ in.}$$

$$L_{Cu,\,Ne} = 3.000\;(0.99674 - 1.00000)\text{ in.}$$

$$= -0.00978\text{ in.}$$

FIGURE D.1, COEFFICIENT OF LINEAR THERMAL EXPANSION FOR COPPER AND PYREX

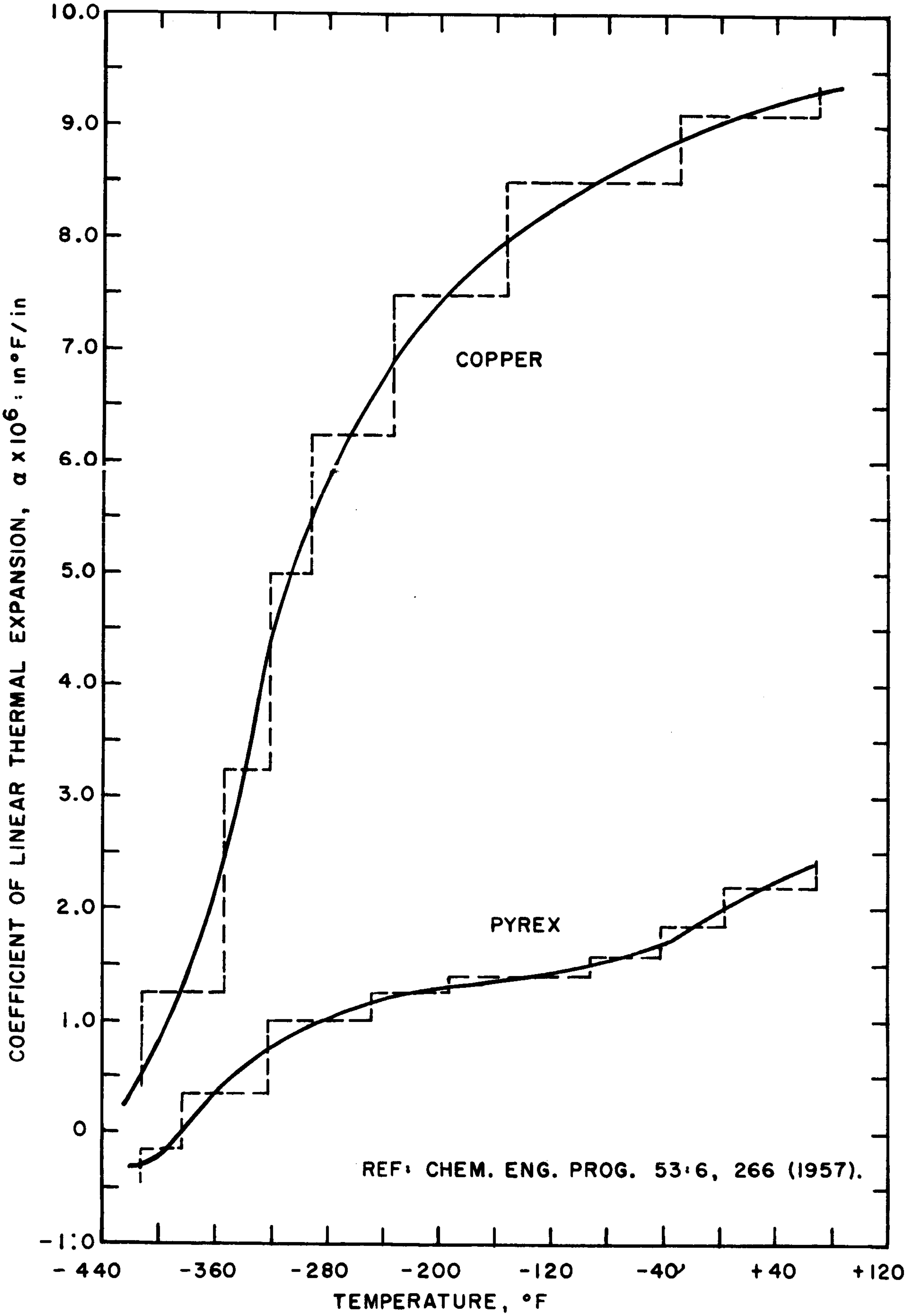

Stepwise Calculation of Contraction Characteristics for Pyrex

Step n	T_n (°F)	ΔT_n (°F)	$\alpha_n \times 10^6$ (in.°F/in.)	$1 + \alpha_n \Delta T_n$
0	70	60		
1	4	-66	2.20	0.99985
2	-43	-47	1.85	0.99991
3	-92	-49	1.58	0.99992
4	-192	-100	1.40	0.99986
5	-248	-56	1.25	0.99993
6	-320.5	-72.5	1.00	0.99993
7	-383.0	-62.5	0.40	0.99997
8	-410.7	-27.7	-0.15	1.00000

For the liquid nitrogen temperature level:

$$L_{\Delta T_{total}} = L_o (1 + \alpha_1 \Delta T_1) \ldots\ldots (1 + \alpha_n \Delta T_n), \; n = 6.$$

$$= L_n (0.99940)$$

For the liquid neon temperature level:

$$L_{\Delta T_{total}} = L_o (1 + \alpha_1 \Delta T_1) \ldots\ldots (1 + \alpha_n \Delta T_n), \; n = 8$$

$$= L_o (0.99937)$$

Nominal diameter (L_o) of Pyrex being 3.0 inches, nominal contraction will then be:

$$\Delta L_{(Pyrex,\ N_2)} = 3.0000 \ (0.99940 - 1.00000) \text{ in.}$$

$$= -0.00180 \text{ in.}$$

$$\Delta L_{(Pyrex,\ Ne)} = 3.0000 \ (0.99937 - 1.00000) \text{ in.}$$

$$= -0.00189 \text{ in.}$$

Net Total Differential Contraction is calculated to be:

for liquid nitrogen

$$\Delta L_{Net,\ N_2} = \Delta L_{(Pyrex,\ N_2)} - \Delta L_{(Cu,\ N_2)}$$

$$= (-0.00180 + 0.00915) \text{ in.}$$

$$= 0.00735 \text{ in.}$$

and for liquid neon

$$\Delta L_{\text{Net, Ne}} = \Delta L_{(\text{Pyrex, Ne})} - \Delta L_{(\text{Cu, Ne})}$$

$$= (-0.00189 \quad 0.00978) \text{ in.}$$

$$= 0.00789 \text{ in.}$$

Net Differential Annular Gap, Contraction used in data calculations:

for liquid nitrogen

$$\Delta_{N_2} = 1/2 \, \Delta L_{\text{Net, } N_2}$$

$$= 0.00368 \text{ in.} = 0.004 \text{ in.}$$

for liquid neon

$$\Delta_{Ne} = 1/2 \, \Delta L_{\text{Net. Ne}}$$

$$= 0.00395 \text{ in.} = 0.004 \text{ in.}$$

APPENDIX E

Test Section Auxiliary Equipment

The auxiliary equipment required to complement the test heater assembly consisted of the following.

1. Test Section Dewars:

   Since visual observation was one of the basic concepts for the boiling study, it was necessary to use glass dewars to contain the boiling liquid and the test heater. In order to minimize heat leak to the system, a set of two silvered glass dewars with four windows was specified and manufactured by H. S. Martin and Sons, Evanston, Illinois. The specifications for the set were:

   Inner dewar:

   outer wall 10 1/4" ±1/8" OD x 1/9" thick
   inner wall 9 1/8" ±1/8" OD x 1/4" thick
   evacuated length 54"
   pipe flange, standard 9" glass pipe flange with 12" length of pipe attached to the top of the dewar
   evacuated section silvered except for four windows 4" wide, full dewar length, and located every 90°

   Outer dewar:

   outer wall 14 ±1/8" OD x 5/16" thick
   inner wall 12 1/2" ±1/8" OD x 5/16" thick
   evacuated length 48"

pipe flange, standard 12" glass pipe flange with 12" length
of pipe attached to top of dewar

evacuated section silvered, except for four windows 4" wide,
full dewar length, and located every 90°

The dewar set was "hung" in appropriate collars held by a frame. Styrofoam was used to protect the bottom sections of the two dewars and to act as locating spacers. Figure 11 is a picture of the dewars assembly.

2. Gas Recovery Bag:

In view of the high cost of neon, it was necessary to provide a means to recover the neon boil-off. A rectangular shaped polyethylene gas bag, 3' x 9' x 12', was connected to the inner dewar by means of a 1 5/8" copper line. A frame allowing the bag to "breathe" was designed and constructed. Figure 12 is a picture of the inflated bag.

3. Test Section Structure:

Because of the length of the dewar set, a large tower-like structure was designed for the experimental setup. The frame, 4' x 8' x 16' in size, provided support for the respective outer dewar and inner dewar collars such that the mouth of the inner dewar was located 7' above the floor. To permit ease of access, a floor was fabricated within the tower framework 7' above the floor. This then provided entrance to the inner dewar through a "hole in the floor." An overhead winch was provided to move the test section in and out of its operating position inside the inner dewar.

The tower also supported a shatterproof glass enclosure around the outer dewar to protect it from accidental contact and to prevent possible violent implosion of the glassware.

4. Liquid Neon Storage and Transfer Equipment:

The neon liquefaction plant was operated in a batch type process, each batch consisting of approximately 20-25 liters of liquid. Several 25 liter standard liquid nitrogen shielded dewars were used for neon storage.

Transfer of liquid neon from the neon plant to the 25 liter dewars and from the 25 liter dewars to the test section dewar was accomplished through a commercially available vacuum insulated flexible transfer line.

APPENDIX F

Examination of Test Heater Surfaces

All heaters were machined, finished, and polished in a similar manner. They all appeared identical, except for a few minor faults that generally affected less than 5% of the total surface. A close examination of each heater was made to determine the type and extent of these faults.

The results of each examination are briefly summarized below.

Heater 6

1. OFHC copper
2. Highly polished with regular polishing scratches around circumference
3. Six thermocouple indication points in each of two longitudinal lines 180° apart
4. Multiple longitudinal scratches of zero apparent depth around 120° of circumference
5. Surface roughness - 16-20 micro-inches RMS

Heater 7b

1. OFHC copper
2. Regularly polished, highly burnished
3. Six thermocouple indication points
4. Longitudinal spotty corrosion spots 1 inch from one line of thermocouples - zero depth

5. Wide scratches in three areas around periphery 1/3 length of cylinder - zero apparent depth
6. Isolated scratches of 1/16-1/4 inch length, usually longitudinal randomly oriented around periphery
7. Surface roughness 11-13 micro-inches RMS

Heater 8

1. OFHC copper
2. Regular circular machine indications resulting in a highly burnished surface
3. Six thermocouple indication points
4. Two longitudinal areas of corrosion attack (zero apparent depth) 1/4" wide at 110° to each other along complete length, with stain marks (slight color difference) at top and bottom
5. Checkerboard imprints (zero apparent depth) 2 1/4" x 3/4", 2 1/2" and 4" from top
6. One z-shaped scratch at midpoint, zero apparent depth
7. Surface roughness 13-15 micro-inches RMS

Heater 9

1. Nickel plated OFHC copper
2. Extremely high polish with regular circumferential burnishing
3. Six thermocouple indication points
4. Slight discoloration over 10% of surface
5. Isolated pitting (25 to 50 points) over 3/4 of surface

6. Slight, almost invisible, longitudinal scratches, zero depth, over entire surface
7. One area 1/4 x 1" in middlepoint looking like corrosion in alligator pattern (cause unknown)
8. Surface roughness 6-8 micro-inches RMS

Heater 10

1. Cadmium plated OFHC copper
2. Highly polished surface with irregular burnish marks
3. Six thermocouple indication points
4. Three areas, (approximately 1/2 x 3/4"), 3/4" from top land, at 120°, with copper showing
5. Approximately 1/16" over 1/2 circumference at top land with copper showing
6. One area, about 3/4 x 3/4", 1/2" from bottom with copper showing
7. Copper showing for 1/16" at lower land
8. Longitudinal scratches over 1/2 to 1 1/2" of circumference
9. Pitting over 3" of circumference for middle 80%
10. Surface roughness 8-11 micro-inches RMS

Heater 12b

1. Electrolytic tough pitch copper (almost identical to OFHC)
2. Highly polished with irregular polishing scratches around circumference
3. Six thermocouple indication points
4. Six gross (approximately 0.005" deep) irregularities, longitudinal alignment 1/4 to 1/2" long

5. Tear marks visible all over under 48X, but not 1X magnification

6. Surface roughness 9-11 micro-inches RMS